

INVESTIGATION OF MODELING STRATEGIES FOR
SLENDER LIGHTLY REINFORCED CONCRETE SHEAR WALLS

A Research Report

presented to

the Faculty of California Polytechnic State University,

San Luis Obispo

In Partial Fulfillment

of the Requirements for the Degree

Master of Science in in Architectural Engineering

by

Tracy Destiny Doan & Jenna Marie Williams

August 2020

© 2020

Tracy Destiny Doan and Jenna Marie Williams

ALL RIGHTS RESERVED

COMMITTEE MEMBERSHIP

TITLE: Investigation of Modeling Strategies for Slender
Lightly Reinforced Concrete Shear Walls

AUTHORS: Tracy Destiny Doan & Jenna Marie Williams

DATE SUBMITTED: August 2020

COMMITTEE CHAIR: Anahid Behrouzi, Ph.D.
Assistant Professor of Architectural Engineering

COMMITTEE MEMBER: Peter Laursen, Ph.D., P.E.
Professor of Architectural Engineering

COMMITTEE MEMBER: Cole McDaniel, Ph.D., P.E.
Professor of Architectural Engineering

ABSTRACT

INVESTIGATION OF MODELING STRATEGIES FOR SLENDER LIGHTLY REINFORCED CONCRETE SHEAR WALLS

Tracy Destiny Doan and Jenna Marie Williams

A large number of pre-1980's non-ductile reinforced concrete (RC) structures in California utilizing RC shear walls to resist seismic lateral forces have been identified as deficient by industry practitioners. These non-ductile wall systems are typically lightly reinforced and lack adequate boundary element detailing. Analytical studies suggest these walls are susceptible to brittle, compression-controlled failure modes due to damage from concrete crushing and bar buckling. Furthermore, poor behavior of lightly reinforced concrete walls was observed in many recent earthquakes, for example in Chile (1985), New Zealand (2010/2011) and Mexico (2017). This has generated concern among engineers in high seismic regions around the globe.

This research report provides a comprehensive analysis of academic and industry standards for analyzing lightly reinforced concrete shear walls with low axial loads and no boundary elements. First, a comparison of two recent experimental testing programs of non-ductile concrete shear walls by de Sevilla et. al. [11] and Lu et. al. [24] is provided. Next, simplified pushover analyses by Priestley [32] and ASCE 41-17 [4] are compared to the experimental testing results of the above-mentioned test programs. After creating a basis for quick, simple predictions, the authors pursued defining the necessary modeling and analysis parameters to create a sophisticated computer simulated model in PERFORM-3D [9]. A parametric study was utilized to create final calibrations on static pushover analyses and cyclic load analyses of each test wall. PERFORM-3D modeling recommendations are provided to give industry practitioners a starting point for modeling non-ductile concrete walls. Finally, the report ends on small academic and industry studies that will support future design-build-test preparations for large-scale testing at Cal Poly San Luis Obispo.

ACKNOWLEDGMENTS

We would like to extend our gratitude to the faculty, friends, and family who have contributed to our successes during our undergraduate and graduate studies. This research project would not have been possible without the unwavering support of the following people.

The ARCE faculty have provided us an education that was instrumental to the creation of this research report. Dr. Anahid Behrouzi, our co-advisor and professor, inspired us to share our research and gave us multiple opportunities to practice communication of engineering topics. Dr. Peter Laursen, our co-advisor and professor, imparted invaluable knowledge of the academic and industry norms related to our research studies and taught us the value of continuous investigation during research. Dr. Cole McDaniel, our graduate advisor and professor, gave us mindful advice as we navigated our research timeline and as we juggled the transition to online learning in March. Dr. Allen Estes, our ARCE Department head, was an avid supporter of our research whenever we presented it, from the ARCE advisory board meeting to the CSU student research competition. Brent Nuttall, our professor, graciously lent us his past projects to contribute a significant amount of data to our industry survey. In addition to the abovementioned professors, we would like to thank all ARCE faculty for being the educators that shaped our views of the built-environment world.

We would also like to extend our appreciation to the help we received outside of the ARCE department. Andrew Kline and his CM student team began extremely helpful coordination efforts for the next design-build-test of a lightly reinforced concrete shear wall at Cal Poly. CAED support shop staff, Dave Kempken and Vince Pauschek, allowed us to utilize High Bay and the concrete yard for material testing this year and large-scale experimental testing the prior year.

Many ARCE alumni who now serve as impactful industry members have been integral to this research report. Garrett Hagen was our PERFORM-3D expert as we learned an unfamiliar software program with limited resources. Margaux Burkholder helped us navigate our industry survey and

more importantly she became a female structural engineer role model to us. Jerry Luong and Rory de Sevilla, predecessors to our research work, provided numerous words of wisdom and encouragement throughout the year. Additionally, thank you to all the industry practitioners who donated their time to participating in our industry survey on lightly reinforced concrete shear walls.

While many of our supporters guided us in ARCE endeavors, we are without a doubt most grateful to our friends who taught us there is more to life than just work. The humor, happiness, generosity, and shared struggles that our friends shared with us every single day in the ARCE labs were absolutely priceless. We would like to especially acknowledge our close friend, Anisha Datta, who has been our exuberant and rooted supporter throughout our research project.

Tracy would like to thank her family for being one of her biggest support systems throughout this project along with Jenna. Their sacrifices did not go unnoticed and she thrives to work hard to repay every ounce of their love. A second family to Tracy was her work family from Innovative Structural Engineering, who provided unwavering faith in her ability since her first day as an intern there and welcome her future there with open arms. The third family for Tracy was her best friends John, Wood and Vince, who provided endless advice and support through every single step of this project and never once let her feel alone. These support systems made her who she is today, and she could not have done it without them.

Jenna would like to thank Cal Poly SWE, EERI, SESH, and SEAOC for instilling in her a strong passion to serve others first. More importantly, these organizations provided her with long-lasting friendships that make her a better person. Jenna would also like to thank her family for their unconditional love and support. With every high and low that life threw at her, Jenna's parents were always there for her. They always believed in Jenna's ability to pick herself back up and recover from any obstacle. Jenna's newly awarded undergraduate and graduate degrees belong to her parents. Without her mom and dad's faith, Jenna would never have dreamed this was possible.

TABLE OF CONTENTS

TABLE OF CONTENTS	vi
LIST OF TABLES	xiii
LIST OF FIGURES	xv
LIST OF TERMS	xviii
1.0 INTRODUCTION	1
1.1 Experimental Testing of Lightly Reinforced Concrete Shear Walls.....	2
1.2 Experimental Testing of Lightly Reinforced Concrete Shear Walls.....	3
2.0 LITERATURE REVIEW	4
2.1 Experimental Testing of Lightly Reinforced Concrete Shear Walls.....	4
2.1.1 De Sevilla et. al.....	5
2.1.2 Lu et. al	6
2.2 Simplified Pushover Analyses.....	7
2.2.1 Priestley	7
2.2.2 ASCE 41-17	8
2.3 PERFORM-3D	9
2.3.1 Modeling.....	9
2.3.1.1 Graham Powell	9
2.3.1.2 Lowes et. al.....	10
2.3.2 Material Models	10
2.3.2.1 Concrete Compression Model (Mander et. al)	11
2.3.2.2 Concrete Compression and Tension Model (Scott et. al).....	11
2.3.2.3 Concrete Tension Model (Hwang and Rizkalla).....	12
2.3.2.4 Rebar without Strength Loss Model (Lowes et. al)	13
2.3.2.5 Rebar with Strength Loss Model (Menegotto and Pinto)	13

2.3.3 Limit States	14
2.3.3.1 Material Behavior Limit States (Behrouzi)	14
2.3.3.2 Code Limit States (ASCE 41-17).....	15
2.3.3.3 Ultimate Deformation Limit States (Park)	15
2.4 Industry Survey.....	16
2.4.1 Seymour et. al	16
2.5 Summary	17
3.0 EXPERIMENTAL TESTING COMPARISON	18
3.1 Physical Wall Attributes.....	18
3.2 Observed Crack Patterns	19
3.3 Global Hystereses.....	20
3.4 Strain Distributions.....	22
3.5 Summary of Findings	24
4.0 SIMPLIFIED PUSHOVER ANALYSES	26
4.1 Strategies.....	26
4.1.1 Priestley Method	26
4.1.2 ASCE 41-17 Method.....	28
4.1.3 Plastic Hinge Length Calculation	29
4.2 Comparison of Results	29
5.0 PERFORM-3D: PHASE 1.....	33
5.1 PERFORM-3D Modeling Phase.....	35
5.1.1 Nodes.....	35
5.1.2 Material Models	35
2.3.2.1 Inelastic Concrete Material.....	36
2.3.2.2 Inelastic Steel Material	38
2.3.2.3 Elastic Concrete Material.....	40

2.3.2.4 Elastic Deformation Gages.....	40
5.1.3 Cross Sections.....	41
5.1.4 Compound Sections.....	43
5.1.5 Elements.....	43
5.1.6 Load Patterns.....	44
5.1.7 Drifts.....	45
5.1.8 Structure Sections.....	45
5.1.9 Limit States.....	46
5.2 PERFORM-3D Analysis Phase.....	47
5.2.1 Load Case Definitions.....	47
5.2.2 Analysis Series.....	49
5.2.3 Results.....	49
5.3 Modeling Summary.....	47
6.0 PERFORM-3D ANALYSIS: PHASE 2.....	51
6.1 Modeling Calibration.....	51
6.1.1 Static Pushover Analysis.....	51
6.1.1.1 Varying Mesh Investigation.....	52
6.1.1.2 7x7 Mesh Model with Varying Material Model Investigation.....	54
6.1.1.3 Strength Loss Rebar Model Investigation.....	55
6.1.1.4 Total Strength Loss at X Investigation.....	56
6.1.1.5 P-Delta Investigation.....	57
6.1.1.6 Strain Limit Investigation.....	59
6.1.2 Cyclic Load Analysis.....	60
6.1.2.1 7x7 Mesh with Varying Material Model Investigation.....	60
6.1.2.2 Concrete Tension Model Investigation.....	61
6.1.2.3 Rebar Cyclic Degradation Investigation.....	63

6.1.2.4 Stiffness Factors Investigation.....	64
6.1.2.5 Strength Loss Interaction Investigation.....	65
6.1.2.6 Strain Limit Investigation	66
6.1.3 Final Calibrated Models Comparison	67
6.2 Modeling Validation.....	68
6.2.1 Strategy Verification with de Sevilla et. al Wall W1	69
6.2.2 Strategy Verification with Lu et. al Wall C2 and C3	70
6.2.2.1 Wall C2	70
6.2.2.2 Wall C3	72
6.3 Modeling Recommendations	73
7.0 WALL MODELING STRATEGY RESULTS.....	75
7.1 Comparison of Results	75
7.1.1 Wall W1	78
7.1.2 Wall C1	78
7.1.3 Wall C2	79
7.1.4 Wall C3	79
7.2 Analysis of Effectiveness	80
7.2.1 Priestley	80
7.2.2 ASCE 41-17	81
7.2.3 PERFORM-3D.....	81
7.3 Methodology Recommendations.....	81
8.0 DESIGN-BUILD-TEST PREPARATIONS.....	83
8.1 Reinforced Concrete Shear Wall Behavior Studies.....	83
8.1.1 Flexural Capacity of Walls	83
8.1.1.1 Flexural Strength Calculation.....	84
8.1.1.2 Percent Relative Contribution to Variance	85

8.1.1.3 Results	86
8.1.2 Fault Tree Analysis of Wall Failure Mechanisms	87
8.1.2.1 Analysis Method.....	87
8.1.2.2 Results	88
8.2 Industry Survey.....	90
8.2.1 Survey Implementation	90
8.2.1.1 Survey Goals	90
8.2.1.2 Survey Questions	90
8.2.1.3 Survey Distribution.....	92
8.2.2 Survey Results	93
8.2.2.1 Building Demographics.....	93
8.2.2.2 Concrete Properties and Wall Geometry	94
8.2.2.3 Rebar Properties	95
8.2.2.4 Analysis Method.....	96
8.2.2.5 Retrofit Solution.....	97
8.3 Future Design-Build-Test Recommendations	98
9.0 REFERENCES	99
APPENDICES	
A. PERFORM-3D.....	103
A.1 Phase 1	103
A.2 Phase 2	109
B. REINFORCED CONCRETE SHEAR WALL BEHAVIOR STUDIES	137
B.1 Flexural Capacity of Walls.....	137
B.1.1 Matlab Input.....	137
B.1.1 Matlab Output.....	140
B.2 Fault Tree Analysis of Wall Failure Mechanisms	141

C. INDUSTRY SURVEY	144
C.1 Letter of Investigation	144
C.2 Short Form Survey	145
C.3 Long Form Survey	153

LIST OF TABLES

Table 2.1: Estimated Number of pre-1980s Non-Ductile Concrete Buildings by City.....	17
Table 3.1: Comparison of Physical Properties.....	19
Table 3.2: Comparison of Loading, Experimental Observations, and Failure Modes	19
Table 4.1: Plastic Hinge Length Comparison.....	29
Table 4.2: W1, C1-C3 Quantitative Modeling Accuracy.....	31
Table 5.1: Parametric Study Model Matrix.....	34
Table 5.2: Stress-Strain Values for Concrete Material Models.....	37
Table 5.3: Stress-Strain Values and Cyclic Degradation Values for Concrete Tension Material Models.....	38
Table 5.4: Stress-Strain Values for Rebar Material Models.....	39
Table 5.5: Gravity and Lateral Nodal Loads.....	44
Table 5.6: Axial Strain Limits.....	47
Table 5.7: Rotational Limits.....	47
Table 5.8: Cyclic Load Cases.....	48
Table 6.1: All 7x7 Mesh Models	54
Table 6.2: Tension Models Quantitative Modeling Accuracy	62
Table 6.3: Static Pushover and Cyclic Load Analyses Comparisons.....	67
Table 6.4: W1 Static Pushover and Cyclic Load Analyses Comparisons	69
Table 6.5: C2 Static Pushover and Cyclic Load Analyses Comparisons	71
Table 6.6: C3 Static Pushover and Cyclic Load Analyses Comparisons	73
Table 7.1: W1, C1-C3 Quantitative Modeling Accuracy.....	76
Table 7.2: Qualitative Accuracy for Wall W1 and C1.....	80
Table 7.3: Methodology Effectiveness for Wall W1 and C1.....	82
Table 8.1: Summarized Dimension and Material Properties of Test Specimens.....	85

Table 8.2: Differentials of Random Variables.....	86
Table 8.3: Percent Relative Contribution to Variance of Random Variables.....	86
Table 8.4: Survey Responses by City.....	92
Table 8.5: Reinforcement Specifications.....	95

LIST OF FIGURES

Figure 2.1: de Sevilla et. al. and Lu et. al. Experimental Test Set-Up.....	5
Figure 2.2: Priestley Moment-Curvature Relation and Force-Displacement Relation.....	7
Figure 2.3: ASCE 41-17 Force-Deformation Relation and Plastic Hinge Rotation.....	8
Figure 2.4: Mander et. al Constitutive Concrete Model.....	11
Figure 2.5: Scott et. al Constitutive Concrete Model.....	12
Figure 2.6: Hwang and Rizkalla Concrete Tension Model.....	12
Figure 2.7: Typical Stress-Strain Envelope for Reinforcing Steel based on Lowes et. al.....	13
Figure 2.8: Menegotto and Pinto Constitutive Rebar Model.....	14
Figure 3.1: Wall Test Specimens W1 and C1-C3.....	18
Figure 3.2: Observed Crack Patterns.....	20
Figure 3.3: Experimental Hysteretic Curves	21
Figure 3.4: Experimental Hysteretic Backbone Curves	21
Figure 3.5: Horizontal Strain Profile for Push and Pull of Wall W1.....	22
Figure 3.6: Vertical Strain Profile for Wall W1.....	22
Figure 3.7: Wall C1-C3 Vertical Strain Profiles.....	24
Figure 4.1: Wall C1 Priestley Moment-Curvature Relationship.....	27
Figure 4.2: Wall C1 Priestley Force-Displacement Relationship.....	27
Figure 4.3: Wall C1 ASCE 41-17 Force-Displacement Relationship.....	28
Figure 4.4: Simplified Pushover Analyses Comparison.....	30
Figure 5.1: Material Model Stress-Strain Definitions.....	35
Figure 5.2: Concrete Material Model Mander et. al. and Scott et. al.....	37
Figure 5.3: Concrete Material Model with Tension.....	38
Figure 5.4: Rebar Strength Loss Model and No Strength Loss Model.....	39
Figure 5.5: Deformation Gage Locations.....	41

Figure 5.6: Wall C1 Cross Section.....	41
Figure 5.7: Cross Section Drawing for 7, 3, and 1 Horizontal Mesh.....	42
Figure 5.8: Element Orientation.....	43
Figure 5.9: Elevation View of Gravity and Lateral Loading for 7x7 Mesh.....	44
Figure 5.10: Drift Visualization.....	45
Figure 5.11: PERFORM-3D Structural Section Cut.....	46
Figure 5.12: Cyclic Load Cases Visualization.....	48
Figure 6.1: Mesh Variations	52
Figure 6.2: Varying Vertical Mesh	53
Figure 6.3: Varying Horizontal Mesh	53
Figure 6.4: 7x7 Mesh Models for Static Pushover Analysis	54
Figure 6.5: Model 33 Strength Loss Rebar Model Investigation.....	55
Figure 6.6: Model 33 Strength Loss Rebar Model Investigation.....	55
Figure 6.7: Model 33 Total Strength Loss at X Investigation	56
Figure 6.8: Model 33 P-Delta Investigation.....	57
Figure 6.9: Experimental Test Set-Up for C1-C3 and W1.....	58
Figure 6.10: P-delta Demonstration for C1-C3 and W1	58
Figure 6.11: Model 33 Strain Limit Investigation	59
Figure 6.12: 7x7 Mesh Models for Cyclic Load Analysis.....	60
Figure 6.13: Model 33 Tensile Strength Investigation Complete Hysteresis and Zoom View	62
Figure 6.14: Model 33 with Tensile Strength at 20% of Modulus of Rupture.....	62
Figure 6.15: Rebar Cyclic Degradation Factor Investigation	63
Figure 6.16: Model 33 Stiffness Factors Investigation	64
Figure 6.17: Model 33 Strength Loss Interaction Investigation	65
Figure 6.18: Static Pushover and Cyclic Load Strain Limit Comparison	66
Figure 6.19: Static Pushover and Cyclic Load Analyses Comparisons.....	67

Figure 6.20: W1 Static Pushover Analysis Results.....	69
Figure 6.21: W1 Cyclic Load Analysis Results	69
Figure 6.22: C2 Static Pushover Analysis Results	71
Figure 6.23: C2 Cyclic Load Analysis Results.....	71
Figure 6.24: C3 Static Pushover Analysis Results.....	72
Figure 6.25: C3 Cyclic Load Analysis Results	72
Figure 7.1: Comparison of Wall Modeling Strategies.....	77
Figure 8.1: Fault Analysis Tree Stem.....	87
Figure 8.2: Fault Tree Analysis Flexural Compression Branch.....	88
Figure 8.3: Survey Flowchart.....	91
Figure 8.4: Year Built.....	93
Figure 8.5: Building Sector.....	93
Figure 8.6: Wall Characteristics.....	94
Figure 8.7: Reinforcement Characteristics.....	95
Figure 8.8: Analysis Trigger.....	96
Figure 8.9: Analysis Method.....	96
Figure 8.10: Retrofit Solution Pursued.....	97
Figure 8.11: Retrofit Solution Decision Factor.....	97

LIST OF TERMS

β_1	=	ratio of depth of rectangular stress block to the depth to the neutral axis
δ	=	percent drift
Δ_{cr}	=	displacement at concrete cracking
Δ'_y	=	displacement at first global yield
Δ_y	=	(per Priestley) displacement at nominal capacity
Δ_u	=	displacement at ultimate capacity
ϵ_{cu}	=	ultimate concrete compressive strain
ϵ_r^2	=	rupture strain
ϵ_{sp}	=	spalling strain
ϵ_y	=	yield strain
ϕ'_y	=	curvature at nominal capacity
ϕ_y	=	(per Priestley) curvature at ultimate capacity
ρ_a	=	axial load ratio
ρ_h	=	horizontal reinforcement ratio
ρ_l	=	vertical reinforcement ratio
σ_r^2	=	ultimate strength
σ_y	=	yield strength
θ	=	rotation over the plastic hinge region
A_g	=	gross area of the wall
A_s	=	area of steel reinforcement
c	=	distance from extreme compression fiber to neutral axis

E_c	=	modulus of elasticity
E_t	=	tensile modulus of elasticity
F_{cr}	=	force at concrete cracking
F_n	=	force at nominal capacity
F_u	=	force at ultimate capacity
F_y	=	force at first global yield
f'_c	=	concrete compressive strength
f'_{cc}	=	confined concrete compressive strength
f_r	=	modulus of rupture
f_u	=	rebar ultimate tensile strength
f_y	=	rebar tensile strength
G_c	=	shear modulus
h	=	total wall thickness
k	=	a ratio of ultimate to yield rebar strain
L_c	=	length from the critical section to the point of contraflexure in the wall
L_p	=	plastic hinge length
L_{sp}	=	strain penetration length
L_w	=	wall length
M_n	=	moment at nominal capacity
M_u	=	moment at ultimate capacity
N_u	=	design axial load
P	=	axial load

V = lateral load

CHAPTER 1

INTRODUCTION

Recent earthquakes in Chile (1985), New Zealand (2010/2011), and Mexico (2017) have shown the poor performance of non-ductile concrete shear walls. These walls consist of light reinforcement ratios, low axial load ratios, and lack adequate boundary element detailing—all of which lead to atypical issues with drift capacity, instead of strength. Lightly reinforced concrete shear walls have proven to be susceptible to brittle, compression-controlled failures from concrete crushing and bar buckling. This damage not only produces loss of structure, but it also leads to loss of homes, workspaces, and everything that creates a community. The above-mentioned earthquakes are precedent for the destruction that could be faced in high seismic regions around the globe. In California, a large number of pre-1980's non-ductile reinforced concrete structures have been identified as deficient by industry practitioners.

This research report dissects the analyses methods that industry practitioners are currently pursuing to analyze and retrofit lightly reinforced concrete shear walls with concern for stiffness, strength, and ductility. Past experimental test results are compared against predictions obtained from simplified pushover analyses and sophisticated computer simulation models to determine how accurate industry practitioners can be in determining the global behavior of the wall. The authors provide recommendations on how industry practitioners could improve their results, as well as incentivize the necessity of future experimental testing on lightly reinforced concrete shear walls.

1.1 Document Summary

Below is a summary of this research report by chapter and appendix.

Chapter 2, Literature Review, provides information on the existing research regarding experimental testing of lightly reinforced concrete shear walls, simplified pushover analysis methods, PERFORM-3D modeling and analysis, and building inventory surveys.

Chapter 3, Experimental Testing Comparison, provides a comparison of the large-scale experimental tests by de Sevilla et. al. [11] and Lu et. al. [24] on lightly reinforced concrete shear walls by analyzing the physical wall attributes, observed crack patterns, and global hysteresees.

Chapter 4, Simplified Pushover Analyses, provides the implementation and comparison of two simplified pushover analyses, Priestley [32] and ASCE 41-17 [4], to the existing experimental testing results from de Sevilla et. al and Lu et. al.

Chapter 5, PERFORM-3D: Phase 1, describes the authors' modeling and analysis assumptions in PERFORM-3D to create a parametric study of 36 models with varying horizontal and vertical element meshes and varying concrete and rebar nonlinear material models.

Chapter 6, PERFORM-3D: Phase 2, describes the process taken to narrow down the parametric study to a singular model and to determine final calibrations for a static pushover analysis and cyclic load analysis. The authors validated the wall modeling techniques with three more wall simulations and provided modeling recommendations for industry practitioners.

Chapter 7, Wall Modeling Strategy Results, provides a summary of the simplified pushover analyses results in Chapter 4 and the final PERFORM-3D results in Chapter 6 to compare and analyze the effectiveness of each method. Methodology recommendations are provided for academia and industry.

Chapter 8, Design-Build-Test Preparations, describes the steps taken by the authors to prepare for a large-scale physical test of a lightly reinforced concrete shear wall in the Cal Poly High Bay. Independent studies on flexural wall capacity and wall failure mechanisms as well as an industry survey to current practitioners provided the authors with the parameters to consider in the next experimental test at Cal Poly.

Chapter 9, References, provides a list of the authors' resources in producing the research on the above-mentioned topics.

Appendices A, B, C provide graphics and extensive data on the Chapter 6 and 7 PERFORM-3D simulations (Appendix A), the Chapter 8 independent studies (Appendix B), and the Chapter 9 industry survey (Appendix C).

1.2 Contributions

This research report was produced by Tracy Destiny Doan and Jenna Marie Williams, with their individual contributions described here. Tracy was chief contributor to Chapter 3, Section 5.1, Section 6.2, Section 7.1, Section 8.1.1 and Appendix B.1. Jenna was chief contributor to Chapter 4, Section 5.2 and 5.3, Section 6.3, Section 7.2 and 7.3, Section 8.1.2 and Appendix B.2. Chapter 2 was a joint effort by the authors, with work divided by the literature reviews that were relevant to each author's chief contributions described above. Section 6.1 was a joint effort by the researchers, each of whom individually took on three static pushover investigations and three cyclic load investigations. Sections 8.2 and 8.3 were a joint effort by the authors to provide survey implementation and results that were integrated. Chapter 9, Appendix A, and Appendix C were assembled jointly by both researchers.

CHAPTER 2

LITERATURE REVIEW

This chapter summarizes the sources utilized for determining the direction of investigation for this project. Section 2.1 describes the past experimental tests of lightly reinforced concrete shear walls used for comparison, predictions, and computer simulation modeling conducted in the remainder of this report. Section 2.2 outlines the simplified pushover analyses pursued in Chapter 4. Section 2.3 provides a brief overview of the resources used to determine proper modeling techniques and limit state applications for PERFORM-3D shear wall modeling in Chapter 5 and Chapter 6. Section 2.4 describes a past survey of nonductile concrete buildings in California that proves relevant to the design-build-test preparations pursued in Chapter 8.

2.1 Experimental Testing of Lightly Reinforced Concrete Shear Walls

Lightly reinforced concrete walls performed poorly in the 1985 Chile and 2010/2011 New Zealand earthquake. Unlike how the industry predicted, these walls exhibited few significant crack planes with concentrated damage and multiple bar fractures. Several test experiments were conducted, such as ones by de Sevilla et. al [11] and Lu et. al [24], shown in Figure 2.1, which observed and determined the true failure modes of these walls. This section addresses the findings of the two experimental tests. Comparisons of specimen properties, observed crack patterns, and global hystereses can be found in Chapter 3.

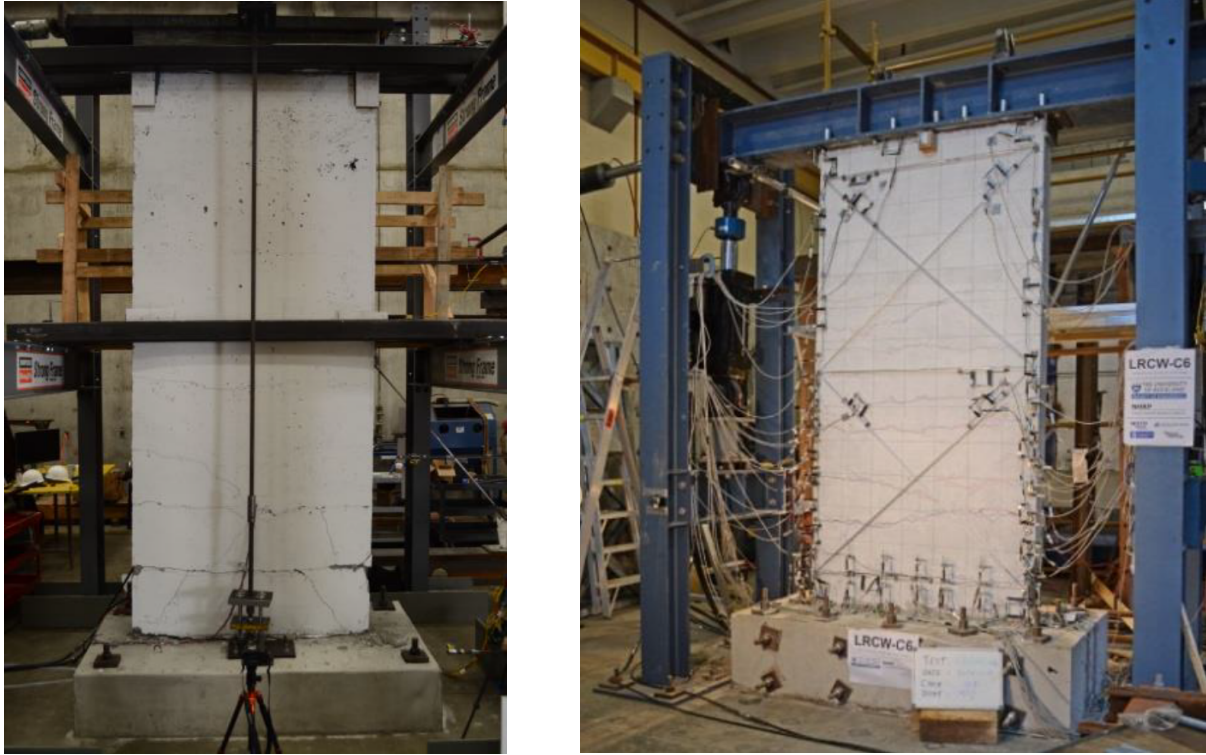


Figure 2.1 – Experimental Test Set-Up for de Sevilla et. al. [11] (left) and Lu et. al. [24] (right)

2.1.1 de Sevilla et. al.

The primary objective of the experimental wall test by de Sevilla et. al. [11] was to understand the different failure mechanisms of pre-1980s lightly reinforced non-ductile concrete walls, due to concerns of sudden catastrophic flexural-compression wall failures. This research stemmed from a limited number of experimental tests that examine the response of these walls.

The experimental testing of a baseline wall fulfilled the criteria of being lightly reinforced, slender, planar, and having no boundary elements. This wall was designed from a sample 1958 reinforced concrete shear wall building. The cross-sectional aspect ratio was 12 and a shear span ratio of ≥ 2.0 to achieve a flexure-dominated response. The longitudinal reinforcement ratio was $\rho_l = \rho_h = 0.37\%$, with longitudinal rebar embedded in the 15-in deep foundation and horizontal bars are lap-spliced 12-in. in the wall end zones with open u-bars.

Lateral loading of the wall consisted of a force control load before yield, and displacement control load after yield. The maximum actuator stroke in the pull direction was about -1.67% drift. When the wall strength decreased by 30% the test was terminated, and the wall proceeded to experience significant base rotation at the foundation with no additional changes in behavior. De Sevilla et. al. anticipated that if the wall test had continued with two-cycle sets, not including the monotonic push, the drift capacity of the wall would be between 2 to 3% drift rather than 3.3%. Overall, the primary wall failure was determined to be due to multiple rebar fractures. There was minor crushing of the concrete at the base with only two longitudinal bars showed slight signs of buckling. The wall also experienced significant base rotation. All the compression related damages were deemed insignificant to the overall wall failures.

2.1.2 Lu et. al.

Lu et al. [24] investigated the behavior and crack patterns associated with lightly reinforced concrete walls that had the minimum vertical reinforcement limits set by the New Zealand Concrete Structures Standard, NZS 3101:2006 [38]. Prior experimental tests by Hidalgo et al. [15], Greifenhagen and Lestuzzi [13] and Deng et al. [12] were designed to explore if a low reinforcement ratio would lead to well-distributed cracks in the plastic hinge region. However, all these walls included concentrated vertical reinforcement in the wall end zones that would lead to desired secondary cracking and high axial loads, the latter of which are not typical of New Zealand structures.

The Lu et al. test program was created to address the need for more experimental data on flexure-dominated lightly reinforced concrete shear walls with low axial loads. The test program consisted of six half-scale reinforced concrete walls with limited ductile detailing and minimum reinforcement requirements per NZS 3101:2006 [38]. Though six walls were tested (C1-C6), the results of specimens C1-C3 are of interest to this paper. Test walls C1-C3 had identical vertical reinforcement ratio, $\rho_v = 0.53\%$, identical axial load ratio, $\rho_a = 3.5\%$ and varying shear span ratios of 2, 4, and 6, respectively. The varying shear span ratios

were achieved on three walls of the same height by applying a moment at the tops of walls C2 and C3 in addition to the lateral load.

The testing protocol consisted of a force-controlled cyclic loading protocol up to the theoretical cracking moment of each wall followed by displacement-controlled loading to 2.5% lateral drift. Walls C1-C3 failed due to flexural tension—rebar fracture and minimal concrete crushing—at 2.5% drift.

2.2 Simplified Pushover Analyses

2.2.1 Priestley

The authors used Priestley [32] as a grounded, theoretical simplified pushover analysis for the sake of comparison against more commonly utilized methods in the structural engineering industry. The simplified pushover analysis procedure by Priestley proposes direct displacement-based design as an alternative to the more commonly used force-based design. This method requires a moment-curvature analysis with a plastic hinge implementation to produce an accurate force-displacement curve.

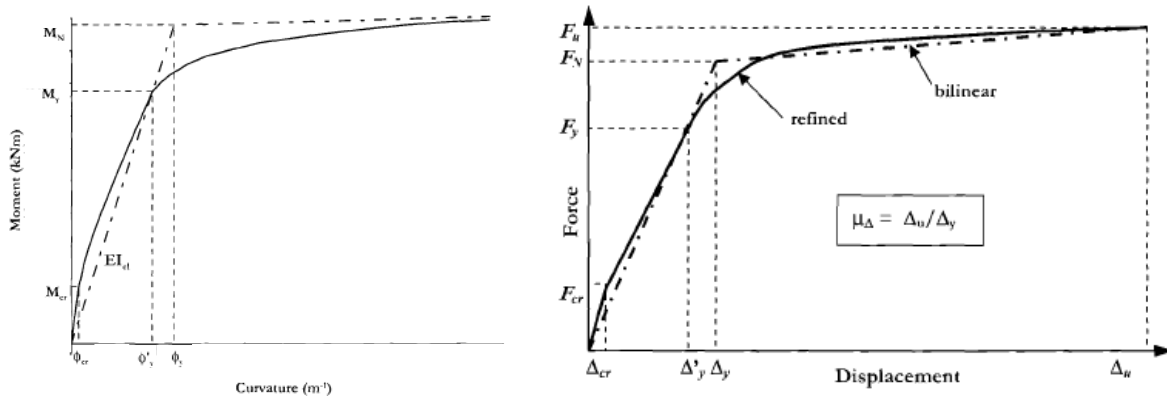


Figure 2.2 – Priestley Moment-Curvature Relation and Force-Displacement Relation [32]

The moment-curvature is idealized as a bilinear relationship with two limit states: nominal capacity (ϕ'_y , M_n) and ultimate capacity (ϕ_y , M_u) shown in Figure 2.2. The first line to nominal capacity is considered the “elastic” branch, followed by the second line from nominal capacity to ultimate capacity that serves as the

“plastic” branch. The corresponding force-displacement curve shown in Figure 2.2 consists of four limit states: concrete cracking (Δ_{cr}, F_{cr}), first global yield (Δ'_y, F_y), nominal capacity (Δ_y, F_n) and ultimate capacity (Δ_u, F_u). The latter two states depend on the plastic hinge length and concrete strains of 0.003 and 0.005 in the extreme compression fiber of the wall, respectively.

2.2.2 ASCE 41-17

The ASCE 41-17 Seismic Evaluation and Evaluation of Existing Buildings [4], provided an industry standard for performing a simplified pushover analysis on reinforced concrete structural walls controlled by flexure. ASCE 41-17 defines concrete structural walls as deformation-controlled, with the acceptable displacement criteria at expected strength levels defined in Table 10-19 for low axial and low reinforcement ratio concrete shear walls. Shown in Figure 2.3, plastic hinge rotations (a) and (b) and residual strength ratio (c) are utilized to create the force-displacement curve with four points: effective yield (A), ultimate strength (B), initial loss of resistance (C), and final loss of resistance (D). Initial loading of the component leads to point A, followed by strain hardening from point A to point B (nominal strength). The initial loss of resistance (C) leads to reduced resistance, and eventual failure at point D (considered the wall ultimate drift capacity). To consider the inelastic behavior of a structural wall under a monotonic nonlinear static load, ASCE 41-17 suggests considering the x-axis of the force-deformation relation as the rotation over the plastic hinging region shown in Figure 2.3.

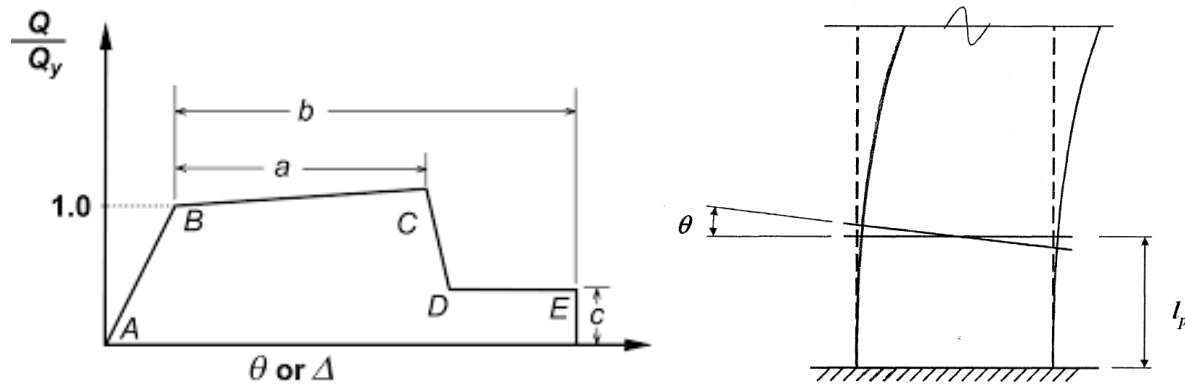


Figure 2.3 – ASCE 41-17 Force-Deformation Relation and Plastic Hinge Rotation [4]

2.3 PERFORM 3-D

2.3.1 Modeling

This section describes the measures the authors took to educate themselves on common and current modeling and calibration techniques for concrete shear walls in PERFORM-3D that extended past the PERFORM-3D manual by Computers and Structures Inc. [9].

2.3.1.1 Powell

The authors followed the assessment for the nonlinear analysis and performance of 3D structures on PERFORM-3D by Powell et. al. [31]. The steel material defined was “Inelastic Steel Material, Non-Buckling”, used for all steel fibers in the wall cross section. For concrete, “Inelastic Concrete Material” was recommended for the unconfined concrete since the walls have no boundary elements. The walls were required to remain elastic in shear, so they were assigned under “Elastic Shear Material for a Wall”, where the material strength is $10\sqrt{f'_c}$. This stress is used to define the shear strength of the wall.

There were two types of fiber sections that Powell et. al. specified, “Fixed Size” and “Auto Size”. For the Fixed Size section, the area and location must be specified for each fiber. This type of section required determining the exact location of the reinforcement to accurately capture the cross-sectional geometry of the wall. For an Auto Size section, only the numbers of steel and concrete fibers needed to be specified, PERFORM-3D calculated the fiber areas and location while assuming equal size fibers so there would be uniform reinforcement across the full cross-section width. This also allowed for the concrete areas to be made smaller towards the outer edges of a wall to allow concrete crushing to occur.

2.3.1.2 Lowes et. al

Lowes et. al [21] recommendations were pursued by the authors to model the nonlinear response of reinforced concrete walls. Shear wall elements were recommended by Lowes et. al as they are intended to represent the nonlinear response of concrete walls subjected to lateral loading, and to simulate nonlinear flexural and shear responses. Each element is a 4-node macro-element with three rotational and three translational degrees of freedom.

Meshing was another parameter Lowes et. al recommended to thoroughly investigate. The PERFORM-3D shear wall element simulates constant curvature and a linear strain distribution along the length of the wall, which is contradictory to experimental wall tests [21]. These strain profiles suggested the need for elements along the length of the wall to simulate a multilinear strain distribution, which necessitates the use of fiber-type section model where the cross section into a series of unconfined and confined concrete fibers overlaid with steel fiber. Lowes et. al recommended a one-dimensional nonlinear stress-strain material response model to be assigned to the unconfined concrete and reinforcing steel. As for the vertical mesh refinement, this is necessary to verify that a converged solution is achieved. Lowes et. al concluded that while vertical mesh refinement has minimal impact on simulated stiffness and strength of cyclic response, the mesh size does impact simulated deformation capacity.

2.3.2 Material Models

This section describes the concrete and rebar material models considered in Chapter 5 and Chapter 6 for the PERFORM-3D modeling and calibration phases. It was important that the authors investigate popular material models that as well as emerging stress-strain relationships that were specific to PERFORM-3D.

2.3.2.1 Concrete Compression Model (Mander et. al.)

Mander et. al. [25] proposed a unified stress-strain model for confined and unconfined concrete with various geometries of transverse reinforcement, as presented in Figure 2.4. The stress-strain model is based on an equation from Popovics [30] considering slow strain rate and monotonic loading. In the stress-strain definition for the cover concrete, the falling branch is assumed to be linear and reaches zero stress at the spalling strain, ϵ_{sp} . The ultimate concrete compressive strain of a section, ϵ_{cu} , where first hoop fracture occurs, may be determined by tracing the work done on the concrete and longitudinal steel when deformed in compression. This generated a constitutive model, which involved a specified ultimate strength surface for multiaxial compressive stresses was used to determine the confined concrete compressive strength, f'_{cc} . The Mander assumes the envelope to the cyclic loading stress-strain response was formed by the monotonic loading stress-strain curve.

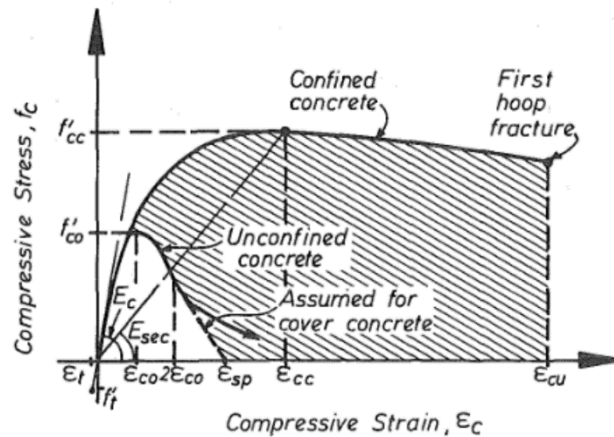


Figure 2.4 – Mander et. al Constitutive Concrete Model [25]

2.3.2.2 Concrete Compression and Tension Model (Scott et. al)

Scott et al. [6] proposed a modified Kent and Park [18] uniaxial concrete fiber model that consists of a monotonic envelope curve shown in Figure 2.5. Where the rising curvilinear relationship to maximum compressive stress is developed from the modulus of elasticity, E_c . Thereafter the stress-strain curve is defined by a falling linear relationship to the minimum stress defined by the ultimate crushing strength of

the unconfined concrete, ϵ_{cu} . The strain at tension peak strength is determined along the slope of the modulus of elasticity, E_c , at the confined concrete tensile strength determined by material testing. The tensile modulus of elasticity, E_t , defines the ultimate tensile strain in the concrete material model.

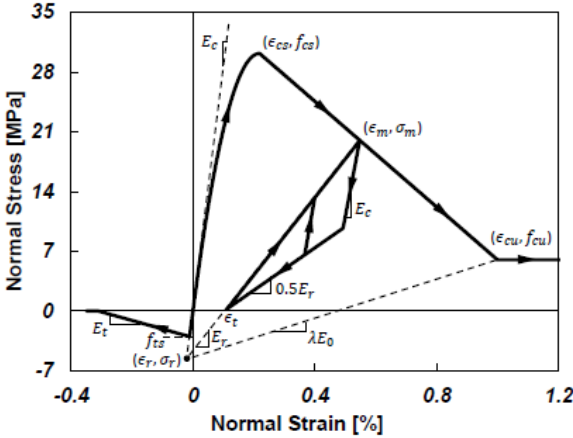


Figure 2.5 – Scott et. al Constitutive Concrete Model [6]

2.3.2.3 Concrete Tension Model (Hwang and Rizkalla)

The concrete tension model proposed by Hwang and Rizkalla [17] is shown in Figure 2.6. The elastic-plastic-softening constitutive relationship assumes a linear relationship, E_c , to the tensile cracking strength determined from a split cylinder strength test, and an exponential relationship after concrete cracking. Tests of uniaxially and biaxially loaded concrete members proved the proposed model, regardless of concrete strength or modulus of elasticity.

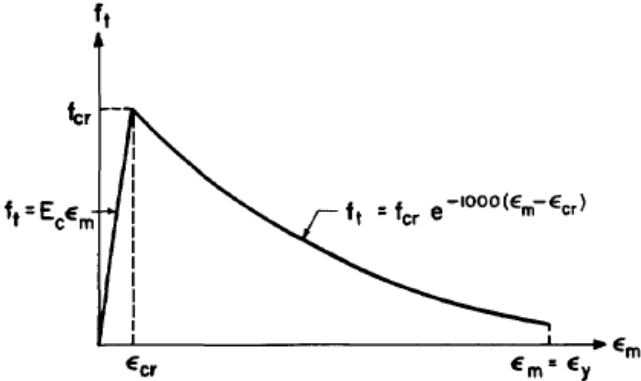


Figure 2.6 – Hwang and Rizkalla Concrete Tension Model [17]

2.3.2.4 Steel Rebar without Strength Loss Model (Lowe et al.)

Lowe et al. [21] provided recommendations on defining the reinforcing steel stress-strain models assigned to web and boundary element steel fibers in a PERFORM-3D wall model. Specifically, the PERFORM-3D “Inelastic Non-buckling Steel” model was employed. Measured stress material properties were used to define the YULRX envelope, which was used to generate the stress-strain envelope for steel tension and compression. An elastic shear material was used where shear stiffness was defined per ATC 72-1 [3].

As shown in Figure 2.6, four critical points, YULRX, were defined on the Lowe et al model for reinforcing steel. The steel experienced elastic behavior prior to the first point which consists of the steel yield stress and strain. The second point consists of the ultimate stress of the steel where the model plateau proceeded until it reached fracture. Strain hardening was not well defined by the available data so a hardening modulus equal to 1.5% of the elastic modulus was assumed. The typical stress strain envelope for reinforcing steel presented by Lowe et al is plotted in Figure 2.7.

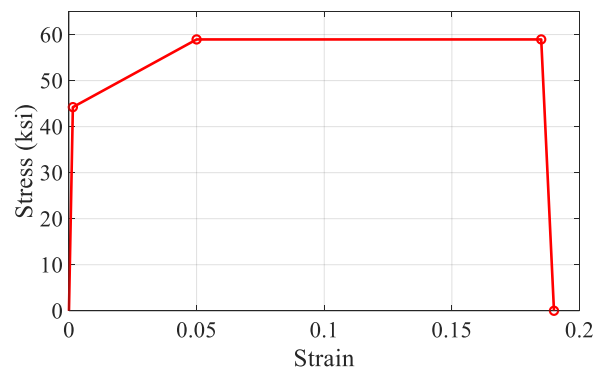


Figure 2.7 –Typical Stress-Strain Envelope for Reinforcing Steel based on Lowe et al. [21]

2.3.2.5 Rebar with Strength Loss Model (Menegotto and Pinto)

Menegotto and Pinto [26] provided a constitutive tensile model of steel reinforcement that captures strain hardening and nonlinear hysteretic behavior. The yield strength, σ_y , is determined by experimental testing, with the rising slope defined by the modulus of elasticity to reach the yield strain, ϵ_y . Following yield, the

steel undergoes a linear strain hardening relationship to reach the ultimate capacity defined by the ultimate strength, σ_r^2 , and rupture strain, ϵ_r^2 , from experimental testing. Subsequent cyclic loading branches with strain reversal considerations are shown in Figure 2.8.

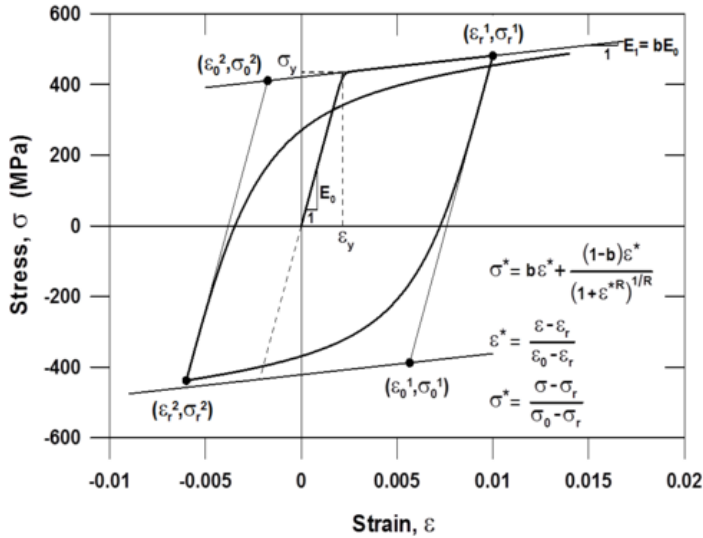


Figure 2.8 – Menegotto and Pinto Constitutive Rebar Model [26]

2.3.3 Limit States

2.3.3.1 Material Behavior Limit States (Behrouzi)

Material limit states to determine drift capacity were defined by Behrouzi [5] in a computational investigation of slender concrete walls in ATENA-3D. The set of simplified predetermined conditions were (1) concrete crushing when the concrete principal stress drops by 30% from peak, (2) rebar fracture when the tensile strain exceeded 33% of the fracture strain measured in experimental material testing and (3) strength loss when the global strength of the wall decreased by 20%. This set of three conditions were used to determine one of three failure modes: buckling-rupture, crushing-buckling, or shear-compression. These recommendations were utilized to set material limit states that were implemented in PERFORM-3D analysis and post-processing codes described in Chapters 6 and 7.

2.3.3.2 Code Limit States (ASCE 41-17)

In addition to simplified pushover analysis guidance, ASCE 41-17 [4] defined the material and rotational limit states allowed for concrete shear wall performance. Usable strain limits are defined in Section 10.3.3.1 for deformation and force-controlled loading on unconfined elements to calculate moment and axial strength at extreme compression and tension fibers of the wall cross section. The limits state that the concrete fiber strain cannot not exceed 0.002 in compression and 0.005 for tension, and the steel fibers cannot exceed 0.02 in compression and 0.05 in tension. Rotational limits are defined in Table 10-19 as the allowable plastic hinge rotation (a and b) and the residual strength ratio (c) for flexure controlled concrete shear walls depending on the reinforcement ratio, axial and lateral loads, and the boundary element conditions. These rotation limits were used to describe when the Immediate Occupancy, Life Safety, and Collapse Prevention allowable designs were reached on a force-displacement curve. Immediate Occupancy Structural Performance is defined when a structure maintains its pre-earthquake strength and stiffness. Life Safety Structural Performance is defined when a structure has damaged components but retains a margin of safety against a partial or total collapse. Collapse Prevention is defined when a structure has damaged components but does not retain a margin of safety against collapse.

2.3.3.3 Ultimate Deformation Limit States (Park)

To determine the ultimate deformation and global failure of a wall, the authors considered recommendations from Park [29] for the maximum displacement of concrete shear walls under displacement-controlled cyclic load protocols. Typical definitions of ultimate displacement are provided by Park as based on: (1) a limiting compression strain, (2) the peak load, (3) when the load carrying capacity has been reduced by 20%, and (4) rebar fracture or buckling. Park describes that 20% post-peak strength loss (option 3) is most appropriate because structures typically will have some capacity for deformation after peak load. Additionally, large scale testing of reinforced concrete shear walls has shown that ultimate deformation will not necessarily correspond to a specified concrete compressive strain [29]. Therefore, ultimate deformation at 20% post-

peak strength loss will be utilized in Chapter 5 and Chapter 6 to predict the ultimate capacity and displacement in PERFORM-3D analyses.

2.4 Industry Survey

To provide the authors with a basis for previous non-ductile concrete building surveys, the following section describes a study that provides insight on the number of buildings this project's work will affect.

2.4.1 Seymour et. al

Seymour et. al [33] performed a non-ductile concrete building inventory supported by the Pacific Earthquake Engineering Research (PEER) Center and Earthquake Engineering Research Institute (EERI). This survey estimated the total number of non-ductile concrete buildings and identification of the high risk buildings in California. Google Earth, Sanborn Maps, and field work contributed to the survey of 30 Californian cities in Table 2.1 performed by volunteers consisting of practicing structural engineers. For the surveyed cities shown in Table 2.1, 7,600 buildings were categorized as non-ductile concrete buildings built before 1980. This survey led to the current estimate of 40,000 non-ductile concrete buildings in all of California—350 cities [33]. This non-ductile concrete building inventory combined with related research allowed for the identification of older concrete buildings at risk for damage and collapse during the next earthquake. Once identified, appropriate actions can be taken to either demolish the building or retrofit policy can be developed and implemented to meet modern seismic code standards.

Table 2.1 – Estimated Number of pre-1980s Non-Ductile Concrete Buildings by City [33]

City	Population	Estimated # of Buildings
Emeryville	6,882	44
Fairfax	7,319	18
Piedmont	10,952	8
Solana Beach	12,979	3
Mill Valley	13,600	13
Albany	16,444	36
Millbrae	20,718	52
El Cerrito	23,171	22
Calabasas	23,652	2
Eureka	25,579	10
Burlingame	27,380	240
Novato	50,335	18
San Rafael	55,716	53
Alameda	70,576	150
Napa	74,782	14
San Leandro	78,178	43
Santa Monica	91,124	70
Daly City	100,339	30
Berkeley	100,744	275
Fullerton	132,787	60
Santa Rosa	154,212	55
San Bernardino	205,010	5
Glendale	207,157	160
Riverside	290,086	6
Oakland	395,274	1300
Long Beach	492,912	400
San Francisco	739,426	3000
Los Angeles	4,018,080	1500

2.5 Summary

The above-described literature review prepared the authors for the research pursued in the following chapters. Past experimental tests of lightly reinforced concrete shear walls provided data for post-testing comparison analysis and computer simulation modeling. Simplified pushover analyses methods were utilized as comparisons to computer simulation models prepared by the authors. PERFORM-3D and computer modeling limit state resources were supportive in the authors' PERFORM-3D explorations. And finally, the survey of nonductile concrete buildings provided relevant data on design-build-test preparations for future researchers.

CHAPTER 3

EXPERIMENTAL TESTING COMPARISON

The de Sevilla et. al. [11] and the Lu et. al. [24] experimental test walls are representative of walls that structural engineers have encountered in existing concrete shear wall buildings: low longitudinal and transverse reinforcement ratios, low axial loads, and a lack of boundary elements. This chapter will discuss the de Sevilla et. al. wall W1 and the Lu et. al walls C1-C3 in terms of physical attributes, observed crack patterns, global hysteresis, and strain profiles.

3.1 Physical Wall Attributes

The geometric and material properties of each wall are shown in Table 3.1 and design drawings are shown in Figure 3.1. It is noted that C1-C3 were of the same physical dimension. The variable shear span to depth ratio was achieved by superimposed moments on C2-C3. All walls were subjected to cyclical loading with the only difference being that W1 underwent an additional high drift monotonic push.

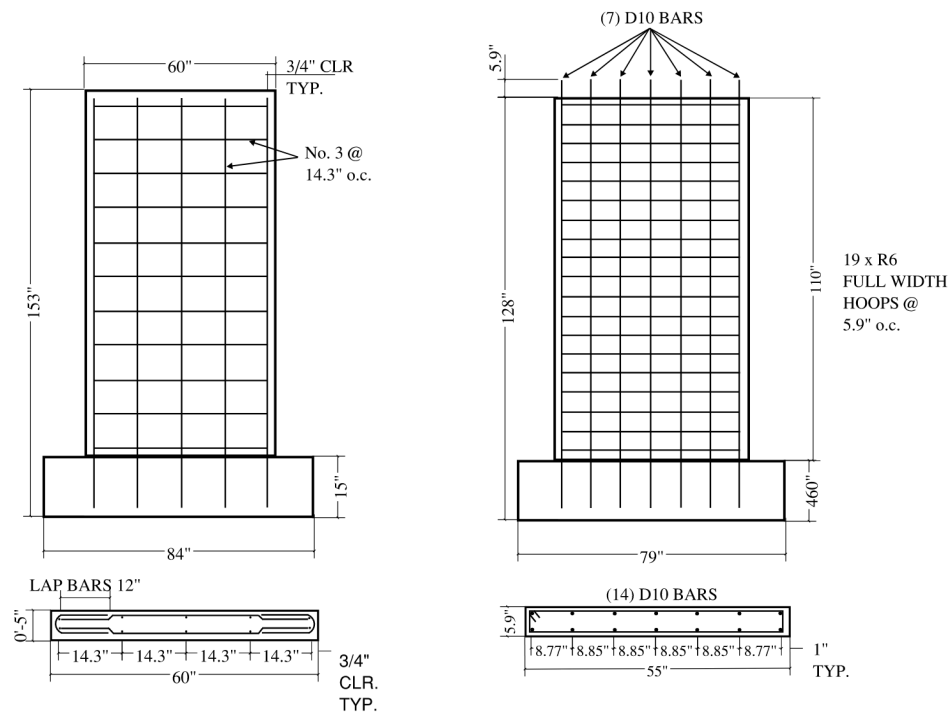


Figure 3.1 – Wall Test Specimens (left) W1 and (right) C1-C3

Table 3.1 – Comparison of Physical Properties

Author	Wall	Length (in)	Height (in)	Thickness (in)	f _c (ksi)	f _y (ksi)	Reinf. Steel Ratio	Axial Load Ratio	Shear Span to Thickness Ratio
de Sevilla et al.	W1	60	153	5	3.80	54.0	0.37%	3.50%	2
Lu et al.	C1	55	110	5.91	5.84	43.5	0.53%	3.50%	2
	C2	55	110	5.91	5.00	43.5	0.53%	3.50%	4
	C3	55	110	5.91	5.25	43.5	0.53%	3.50%	6

1 in = 2.54 cm; 1 ksi = 6.89 MPa

Table 3.2 – Comparison of Loading, Experimental Observations, and Failure Modes

Author	Wall	Applied M _{max} (k-ft)	Applied F _{max} (k)	First Cracking (% drift)	Rebar Buckling (% drift)	Concrete Crushing (% drift)	Rebar Fracture (% drift)	Drift Capacity (%)	Failure Mode
de Sevilla et al.	W1	268	21	0.20%	NA	NA	1.67%	1.67%	FT
Lu et al.	C1	486	39	0.20%	1.50%	2.00%	2.50%	2.50%	FT
	C2	499	20	0.06%	1.50%	2.00%	2.50%	2.50%	FT
	C3	475	13	0.16%	1.50%	2.00%	2.50%	2.50%	FT

1 k = 4.45 KN; 1 ft = 30.48 cm; FT = flexural tension; NA = minimal observations of the state achieved

A cyclical loading protocol was applied in each scenario and produced similar results shown in Table 3.2. Industry practitioners would have expected the walls to fail in flexural compression (concrete crushing and rebar buckling) because they would design the concrete to fail first. However, each of the walls in the above-mentioned tests failed in flexural tension (rebar fracturing), indicating that industry practitioners may not be accurately evaluating existing walls and pursuing the proper retrofit.

3.2 Observed Crack Patterns

The observed crack pattern was a strong indication of flexural tension behavior and failure, as shown in Figure 3.2. Large, main flexural cracks formed at the base of each wall, extending up the wall height in relation to the shear span to depth ratio, respectively. Although C2-C3 had similar applied loads as C1, in terms of base moment, they experienced more significant cracking due to additional applied moments. However, concrete crushing was limited in all tests due to flexural cracking and rebar yielding in the concrete, which did not compromise the concrete compression zones in reverse cycles.

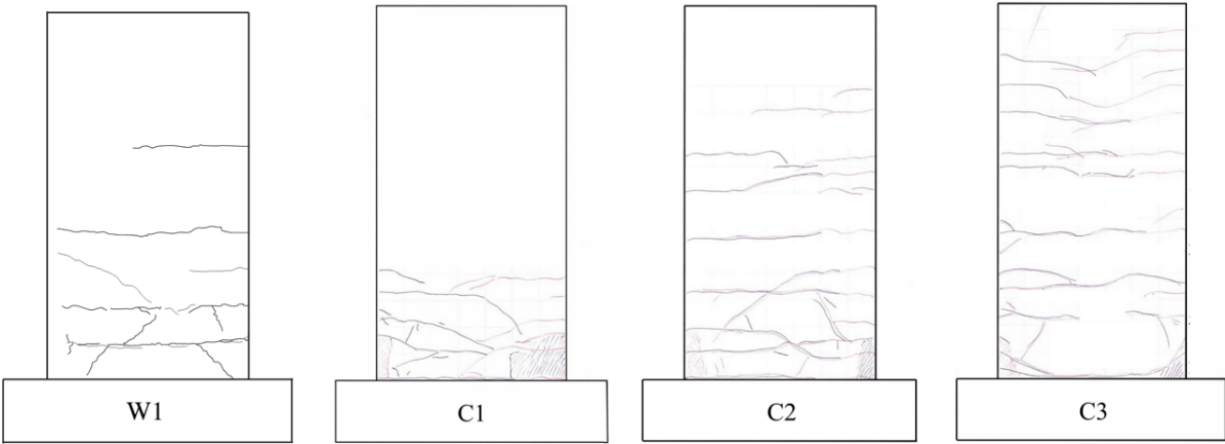


Figure 3.2 – Observed Crack Patterns

3.3 Global Hysteresees

The global hysteresis plots for the walls revealed the overall behavior in terms of the strength, stiffness degradation and energy loss, shown in Figure 3.3. The base moments were normalized by the nominal flexural strength of each wall calculated per ACI 318 [1]. All walls were subjected to cyclical excursions twice to each desired drift level. The differences in their peak loads and corresponding drifts were due to walls C1-C3 being subjected to higher base moments than wall W1, attributable to a higher reinforcement ratio. Wall C2-C3 were subjected to an additional superimposed moment to mimic a multi-story wall, resulting in higher shear span ratios and propagation of flexural cracks further up the height of the wall. Wall W1 was cycled to peak drift extended beyond that of the C1-C3 walls. All walls showed similar hysteretic behavior and minimal base sliding. Experimental peak envelope curves were generated from the backbone of the hysteretic loops for the push direction, shown in Figure 3.4. These envelopes were utilized for later comparisons to the simplified pushover analyses in Chapter 4 and to the PERFORM-3D results in Chapter 6 and Chapter 7.

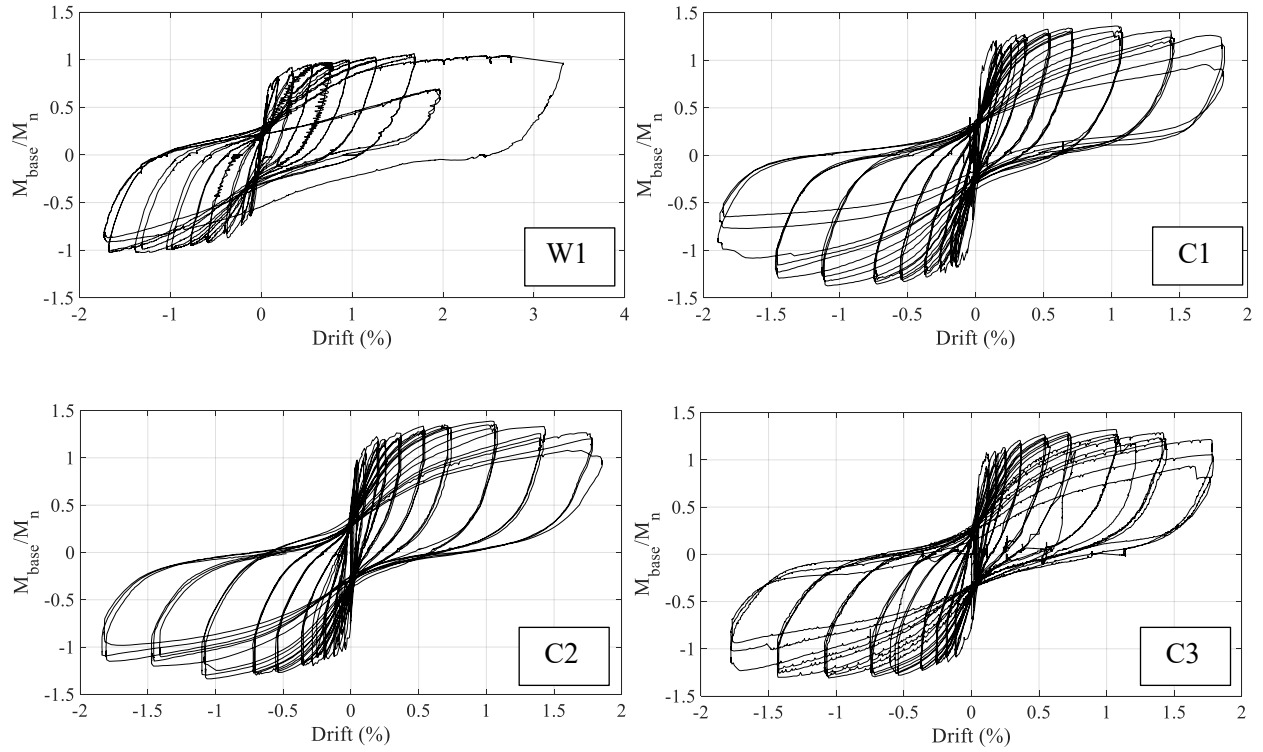


Figure 3.3 – Experimental Hysteretic Curves

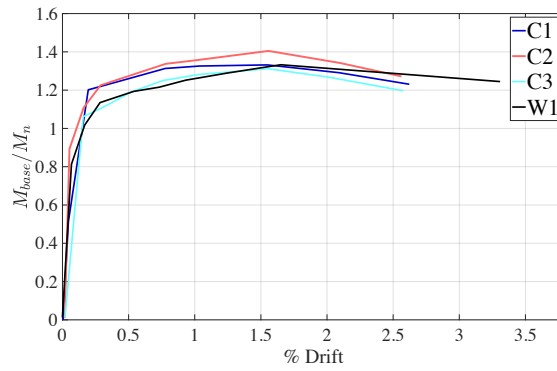


Figure 3.4 – Experimental Hysteretic Backbone Curves

3.4 Strain Distributions

De Sevilla et al. [11] strain profiles along the base of the wall for push and pull are shown in Figure 3.5, and curvature profiles along the height of the wall are shown in Figure 3.6. As expected, the wall experienced extreme strains at the ends of the wall for both the push and pull horizontal strain profiles. For the push profile, the wall reached zero strains at about $0.83L_w$ along the cross-section length. For the pull profile, the wall reached zero strains at around $0.17L_w$, which means 83% of the wall length remained from the opposite end. The two plots showed a near symmetry between the two horizontal profiles, specifically at the boundary length of 17% of the wall length where both plots crossed zero strain.

The de Sevilla et al. vertical strain profile indicated the wall experiencing major strain concentration at the base and seemed to gradually decrease between 10 and 50 inches shown in Figure 3.6. There were no strain gages applied above $0.4H_w$, so the strain is assumed to be zero from there up the remaining height of the wall. The significant strain concentrations are at the very base of the wall to $0.07H_w$. These concentrations inform the location of major flexural cracks and possibly the centroid of the plastic hinge zone.

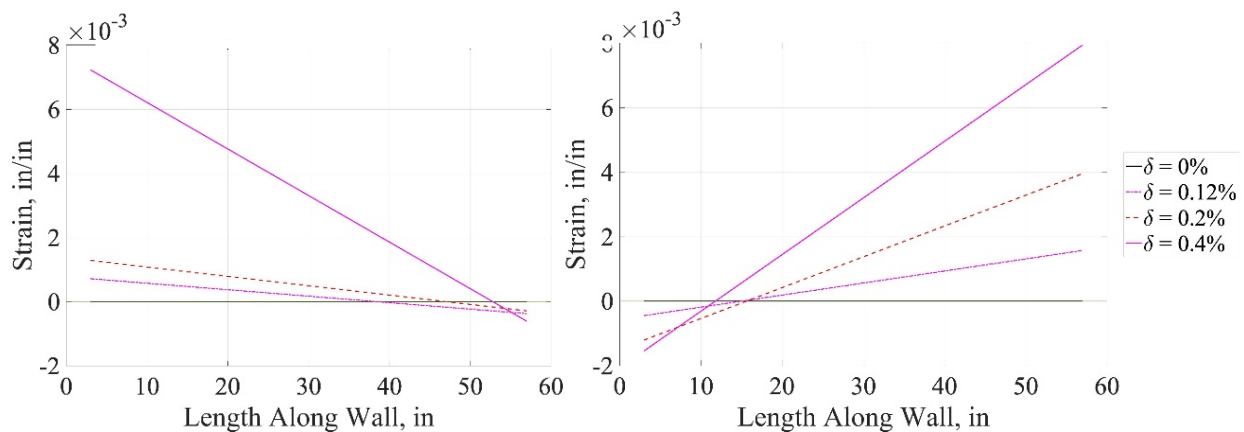


Figure 3.5 – Horizontal Strain Profile for (left) Push and (right) Pull of Wall W1 [11]

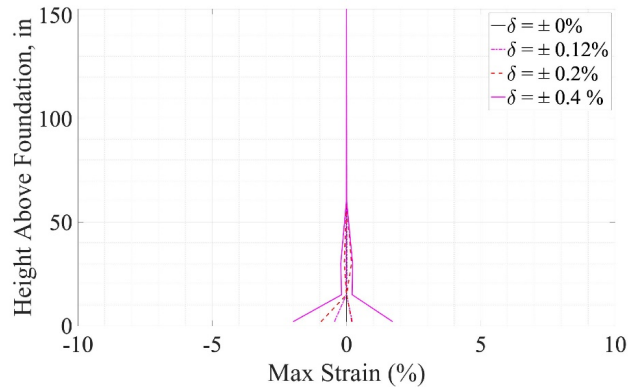


Figure 3.6 – Vertical Strain Profile for Wall W1 [11]

The vertical strain profiles in Figure 3.7 from Lu et. al. [24] depicted the average tensile strains measured along the vertical reinforcement up the height of each wall. The strains were obtained by dividing the readings from the strain gages that were welded to the vertical reinforcement by the respective gage length, which is $0.05H_w$ for C1-C3. The reinforcement strains for these walls varied significantly along the wall height with large inelastic strain concentrations at cracked locations. Similar to W1, the crack locations appeared to be at the base of the wall for all three walls which shows that there were concentrated inelastic deformation at 1-2 flexural cracks.

The superimposed moments on C2 and C3, to implement the effect of a taller wall and generating an increase in the shear span, created drastic changes between the strain profiles for the three walls. C1 exhibited significantly high strain at the base, but going up the wall height, past $0.29H_w$ there was little to no strain. C2, simulating twice the height of C1, seemed to be divided into three major strain concentration areas specifically at the base, $0.25H_w$, and at $0.43H_w$. C3 simulating three times the height of C1, had four distinct area of strain concentration at the base, $0.18H_w$, $0.29H_w$, and $0.43H_w$. This shows the vertical reinforcement yielded over a larger length of the wall height as the effective shear span increased.

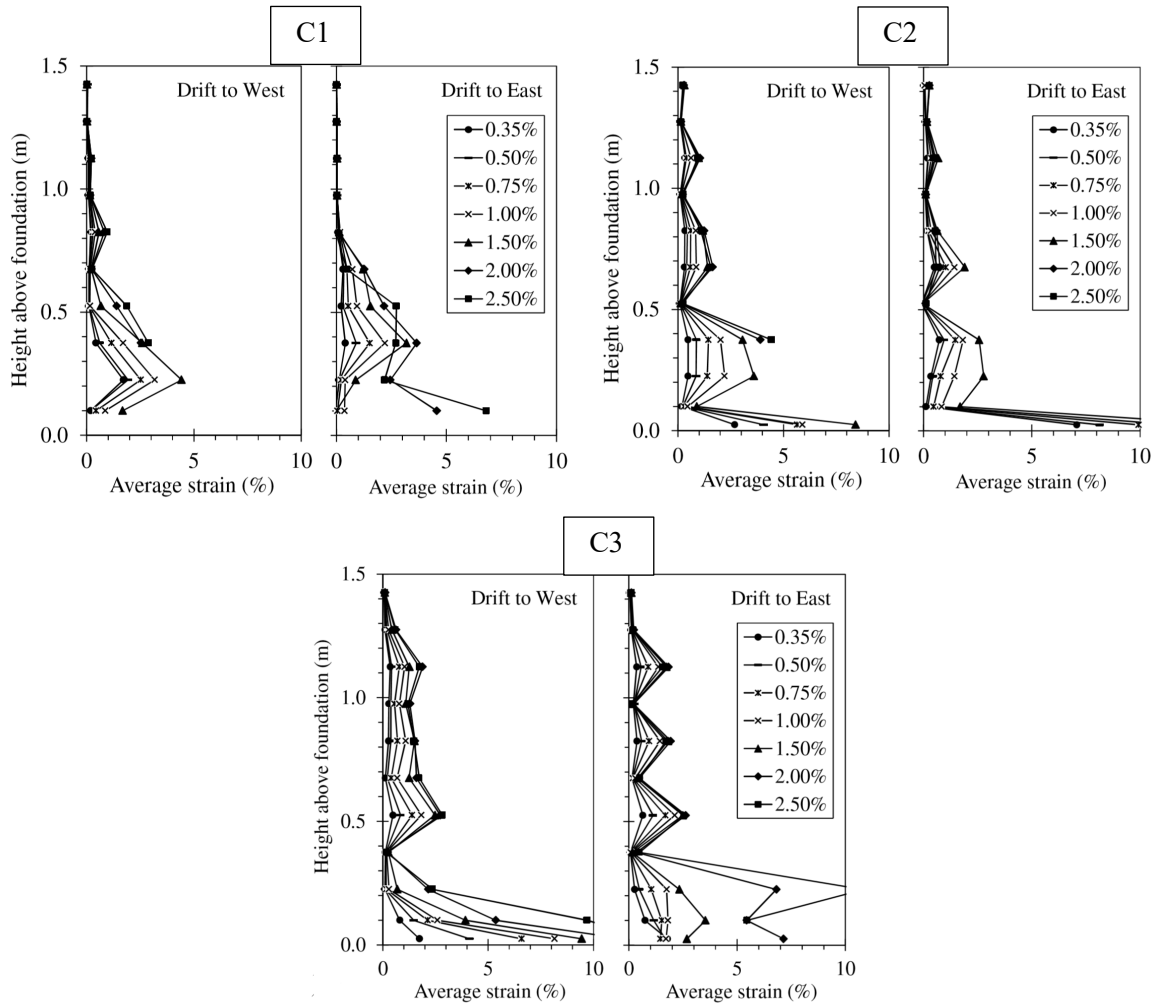


Figure 3.7 – Wall C1-C3 Vertical Strain Profiles [24]

3.5 Summary of Findings

Direct comparisons between C1 by Lu et. al [24] and W1 by De Sevilla et. al [11] were made from the similarities of the physical attributes, observed crack patterns, global hysteresis, and strain profiles of each wall. These walls experienced significant cracking at the base with little to no cracking higher up the wall height. Experimental peak envelope curves for C1-C3 walls indicated to be at a normalized strength of 1.3 times the nominal moment, while W1 at 1 time the nominal moment. The vertical strain profiles depicted significant strain concentrations at the base and decreased up the wall height to $0.83H_w$ for W1 and $0.85H_w$ for C1 until zero strain was reached.

While C2 and C3 were not directly comparable to C1 and W1, the experiments were conducted to represent walls that are twice and three times the height of C1, respectively, with superimposed moments applied during the experimental test through the use of two vertical actuators. The difference between C2-C3, in comparison to C1 and W1, was prominent in significant propagation of flexural cracks further up the height of the wall due to the higher shear span ratios. Another difference from C1 and W1 was the more defined vertical strain concentrations up the height of walls C2 and C3. The authors proceeded with using C1 as an initial model through software analysis to calibrate to the experimental test data since the loading protocol had consistent 2-cycle set and no superimposed moment.

CHAPTER 4

SIMPLIFIED PUSHOVER ANALYSES

4.1 Strategies

Two simplified pushover methods were pursued to evaluate prediction accuracy of the methods to the experimental testing results from W1 and C1-C3. The Priestley [32] method was chosen to represent a classic textbook approach used in academia and research. The ASCE 41-17 [4] method was chosen to represent the practitioner approach commonly utilized in the structural engineering industry to evaluate existing concrete structural walls.

4.1.1 Priestley Method

To properly follow the Priestley [32] guidelines, the authors performed a moment-curvature analysis and defined a plastic hinge length to produce a force-displacement curve. Moment-curvature analysis shown in Figure 4.1 was executed using XTRACT [8], a sectional analysis software that allows the user to input material properties and material models. The stress-strain relationship of the concrete was defined using an unconfined Mander [25] model, where the ultimate concrete strain is 0.005. The steel reinforcement was defined using a bilinearization with strain hardening model.

The moments, curvatures, steel strains, and concrete strains were extracted from XTRACT to identify four points of interest in the moment-curvature response: cracked moment, yield capacity, nominal capacity, and ultimate capacity. A bilinearization of the moment-curvature relationship can be idealized as shown for wall C1 in Figure 4.1 using nominal capacity (ϕ'_y, M_n) and ultimate capacity (ϕ_y, M_u). Nominal capacity is defined when the steel first yields and ultimate capacity is defined where the maximum moment is reached in XTRACT.

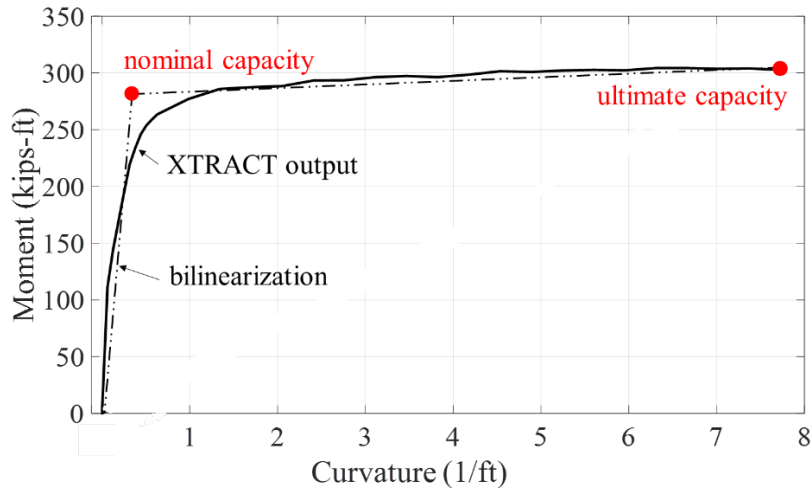


Figure 4.1 – Wall C1 Priestley Moment-Curvature Relationship

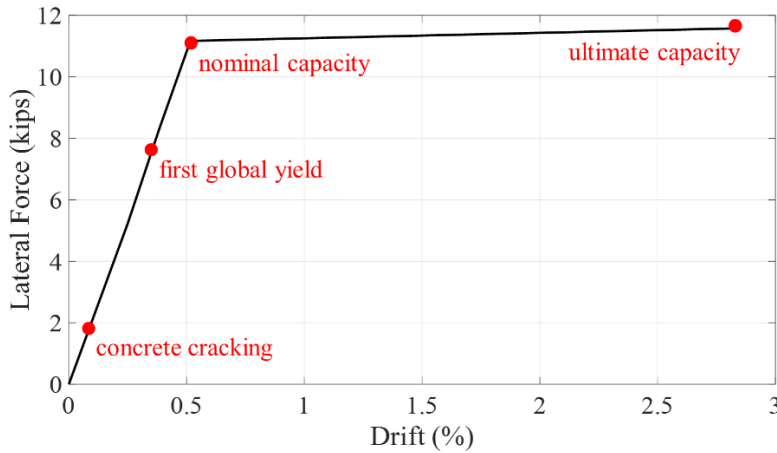


Figure 4.2 – Wall C1 Priestley Force-Displacement Relationship

The force-displacement relationships were developed with four limit states: concrete cracking (Δ_{cr} , F_{cr}), first global yield (Δ'_y , F_y), nominal capacity (Δ_y , F_n) and ultimate capacity (Δ_u , F_u). The latter two states depend on the plastic hinge length, accounting for additional displacement resulting from strain penetration into the foundation. The results of this method produced a nearly bilinear force displacement relationship with an initial stiffness to nominal capacity at a peak concrete strain of 0.003 and final stiffness to ultimate capacity shown in Figure 4.2 for wall C1. It is important to note that the Priestley method is intended for creating a conservative pushover curve for design purposes. Therefore, Priestley suggests a factor of 1.3-

1.6 should be applied to the calculated ultimate displacement to match experimental results. The authors chose to use a factor of 1.5 to all ultimate drift calculations to provide consistency across all walls.

4.1.2 ASCE 41-17 Method

The ASCE 41-17 [4] simplified pushover analysis was performed by creating a generalized force-displacement relationship from four points shown in Figure 4.3: effective yield (A), ultimate strength (B), initial loss of resistance (C), and final loss of resistance (D). The relative locations of these states were characterized by nonlinear modeling parameters and acceptance criteria in Table 10-19 of ASCE 41-17 [4]. Plastic hinge rotations (a and b) and a residual strength ratio (c) are determined by the wall reinforcement ratio, axial and shear demand, and boundary confinement. For walls such as W1 and C1-C3 that have low axial loads, low reinforcement ratios, and no boundary elements, Table 10-19 shows that $a = 0.008$, $b = 0.015$, and $c = 0.6$. The full wall height was utilized to determine the yield displacement and all nonlinear displacement behavior was determined by an effective height that accounted for the plastic hinge length of the wall. ASCE 41-17 suggests that for one story walls that the plastic hinge length be considered less than 50% of the wall length. The plastic hinge length was considered as 25% of the wall length per industry recommendations [14] for a shear wall design where flexure dominates inelastic response.

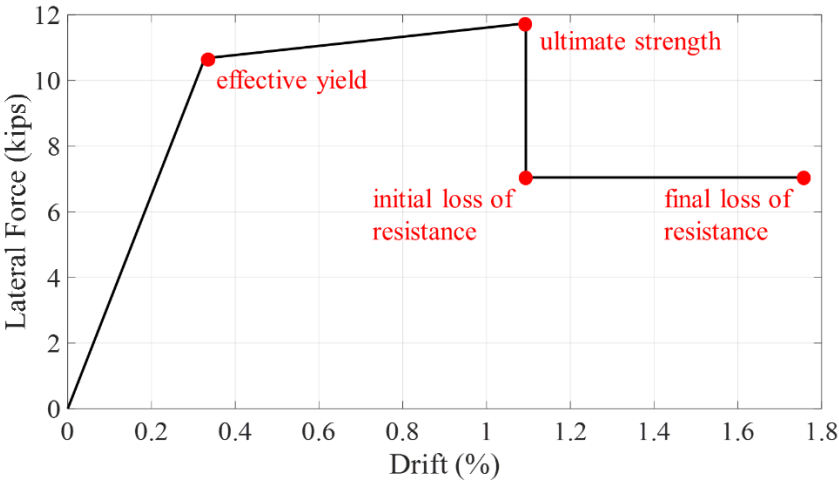


Figure 4.3 – Wall C1 ASCE 41-17 Force-Displacement Relationship

4.1.3 Plastic Hinge Length Calculation

A comparison of the plastic hinge calculation for Priestley [32] and ASCE 41-17 [4] is shown in Table 4.1. The variability in plastic hinge length definition and calculation between each simplified pushover method is indicative of how the wall behavior is being captured. The Priestley plastic hinge length is representative of the length that the simulated wall behaves inelastically, from nominal capacity to ultimate capacity. The plastic hinge length is defined by k , a ratio of ultimate to yield rebar strain, L_c , the length from the critical section to the point of contraflexure in the wall, and L_{sp} , the strain penetration length. The ASCE 41-17 gives the plastic hinge length in relation to L_w , the wall length, and operates with a plastic hinge rotation capacity that is used to calculate the ultimate displacement capacity.

Table 4.1 – Plastic Hinge Length Comparison

Method	Definition (in)	W1 (in)	C1 (in)	C2 (in)	C3 (in)
Priestley	$L_p = 0.08H + 0.1L_w + L_{sp}$	21.28	16.87	25.67	34.47
ASCE 41-17	$L_p = L_w/4$	15.00	13.75	13.75	13.75

4.2 Comparison of Results

Comparison of the Priestley and ASCE 41-17 simplified pushover methods to the experimental testing backbone provided insight on the reliability of each technique. Table 4.2a-d includes ratios of the analytical to experimental values for walls W1 and C1-C3. Initial stiffness was calculated as the slope to the yield point. The ultimate drift was quantified as the final drift for each pushover curve. The peak moment is considered the highest strength capacity reached on the pushover curve. Qualitative conclusions are visualized in Figure 4.4 that are considerate of each wall's quantitative modeling accuracy results.

The quantitative and qualitative results provided conclusions on the effectiveness of each simplified pushover analysis for an industry practitioner. The following summaries of each method were created to provide guidance on the use of each method and urges industry members to consider using a sophisticated nonlinear modeling program instead to gain insight on the true strength, stiffness, and ultimate displacement capacity that can be considered for lightly reinforced concrete shear walls.

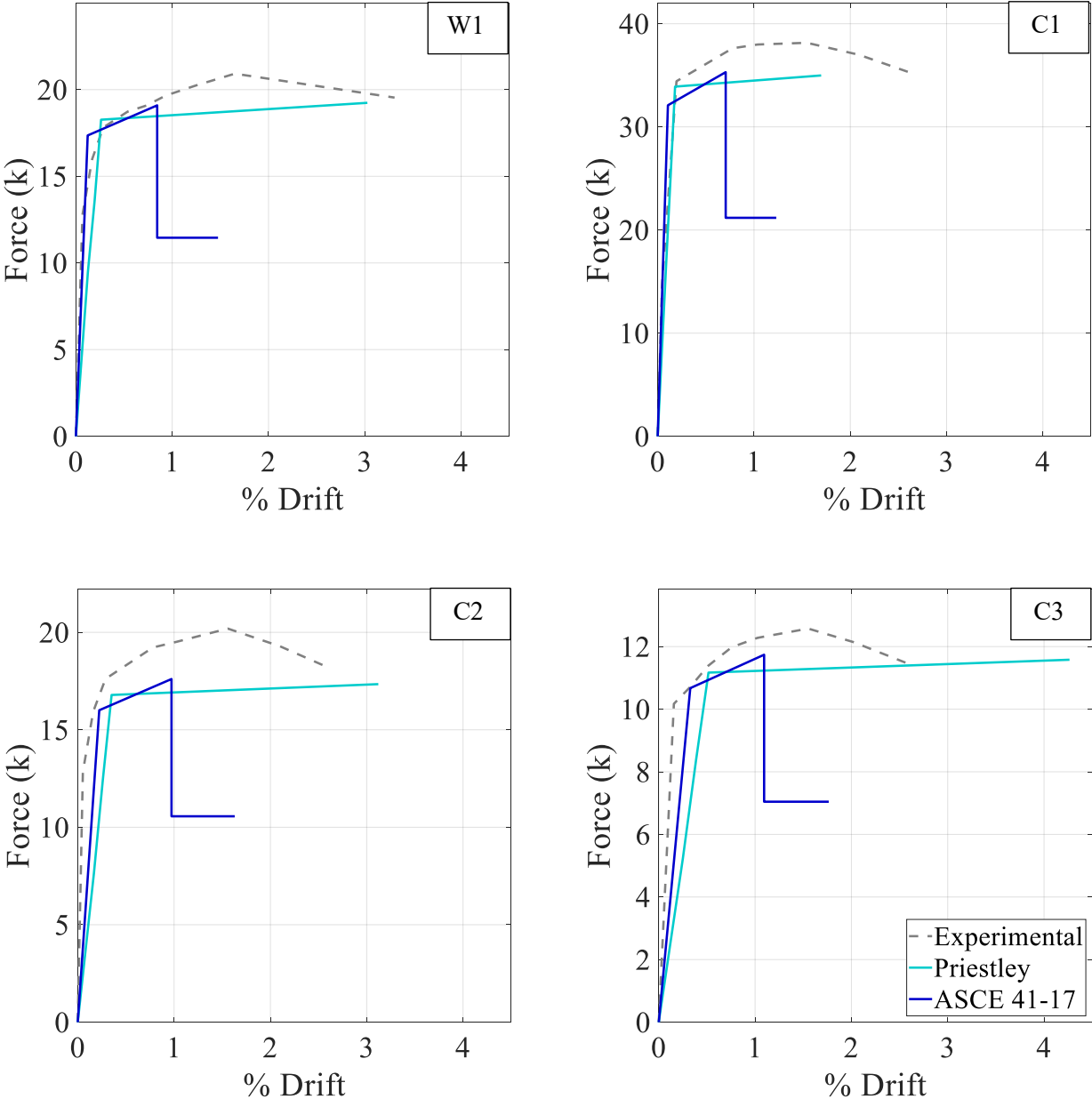


Figure 4.4 – Simplified Pushover Analyses Comparison

Table 4.2a – W1 Quantitative Modeling Accuracy

Method	Initial Stiffness	Nominal Strength	Yield Drift	Yield Moment	Ultimate Drift	Peak Moment	Legend (% error)
Priestley	1.13	1.02	1.16	0.85	0.91	0.92	>1 overestimate
ASCE 41-17	2.29	0.97	0.73	1.09	0.45	0.91	<1 underestimate

Table 4.2b – C1 Quantitative Modeling Accuracy

Method	Initial Stiffness	Nominal Strength	Yield Drift	Yield Moment	Ultimate Drift	Peak Moment	Legend (% error)
Priestley	1.06	0.98	1.16	1.01	0.65	0.92	>1 overestimate
ASCE 41-17	1.71	0.93	0.93	1.30	0.47	0.93	<1 underestimate

Table 4.2c – C2 Quantitative Modeling Accuracy

Model	Initial Stiffness	Nominal Strength	Yield Drift	Yield Moment	Ultimate Drift	Peak Moment	Legend (% error)
Priestley	0.20	0.95	1.63	0.78	1.22	0.95	>1 overestimate
ASCE 41-17	0.30	0.91	1.40	1.00	0.64	0.96	<1 underestimate

Table 4.2d – C3 Quantitative Modeling Accuracy

Model	Initial Stiffness	Nominal Strength	Yield Drift	Yield Moment	Ultimate Drift	Peak Moment	Legend (% error)
Priestley	0.33	0.93	2.46	0.82	1.65	0.92	>1 overestimate
ASCE 41-17	0.50	0.89	2.09	1.05	0.68	0.93	<1 underestimate

The simplified pushover analysis following Priestley [32] guidelines produced a bilinearization that mimicked the experimental curvilinear pushover behavior. The nominal strength, yield moment, and peak moment were relatively accurate—conclusively trustworthy. However, it was difficult to find conclusive results for the accuracy of the initial stiffness and drifts for the set of walls. The authors believe that the plastic hinge length calculation and the defined maximum concrete strain, both of which Priestley calibrates for ductile walls, were accountable for the variation in ultimate deformation results. In addition, moment curvature analyses ignore shear and sliding failure, so even if the primary failure mechanism was flexural failure for each wall, the results are not capturing the shear and sliding failure contributions. The variety of accuracy in calculating stiffness and ductility for each wall draws concern for how this method should be used. Although a relatively straightforward approach to creating a force-displacement relationship,

a phenomenologically based method like this would require a calibration with respect to the wall type investigated herein to adhere to plan check approval.

If the industry practitioner's primary objective is to evaluate the expected strength of a wall, using the ASCE 41-17 [4] simplified pushover method is a good choice. However, similarly to the Priestley method, there were large discrepancies in calculating initial stiffness and drifts dependent on the wall in question. The most recognizable and consistent among these inaccuracies was that the ASCE 41-17 grossly underestimates the drift capacity. Given that industry practitioners are currently not predicting the correct failure mode of these walls, this codified process is possibly incorrect for lightly reinforced concrete shear walls. Although some may consider it conservative, this underestimation means industry practitioners could be dismissing lightly reinforced concrete shear walls as irreparable or vulnerable due to their ASCE 41-17 calculated lack of ductility.

The authors have identified that the popular simplified pushover analyses above are inconsistent for predicting stiffness and ductility for an experimental test. Although accurate for predicting strength, the abovementioned issues combined with an inability to capture cyclic degradation and energy dissipation that occurs in a cyclic load cycle make simplified pushover analyses true to their name—simple. Industry practitioners are urged by the authors to explore in-depth nonlinear modeling strategies described in Chapters 5 and 6 that include material degradation and subject to repeated cycles of lateral loading.

CHAPTER 5

PERFORM-3D ANALYSIS: PHASE 1

The simplified pushover analyses explored in the previous chapter described common academic and industry standards for quick estimation of concrete shear wall strength, stiffness, and displacement capacity. However, industry practitioners would prefer to have a sophisticated computer model that can expand their ability to consider a multitude of parameters in the nonlinear analysis of slender concrete shear walls. The authors chose to pursue computer simulation modeling with PERFORM-3D. After achieving proficiency in modeling set up, the authors pursued a parametric study to calibrate the necessary inputs for an accurate PERFORM-3D model of the nonlinear behavior of slender reinforced concrete shear walls.

The parametric study required modeling of 36 independent PERFORM-3D models to achieve a properly calibrated model. The authors explored variations of four parameters: horizontal meshing, vertical meshing, concrete material modeling, and rebar material modeling. Horizontal meshing and vertical meshing variations were utilized to determine element size recommendations. Concrete material modeling variations explored the validity of including tension strength and rebar material modeling explored the impact of including material strength loss. Table 5.1 outlines the model variations undertaken by the parametric study described in this chapter.

Table 5.1 – Parametric Study Model Matrix

Model No.	Horizontal Mesh	Vertical Mesh	Concrete Tension?	Rebar Strength-loss?
1	1	1	✓	✓
2			✓	
3				✓
4				
5		3	✓	✓
6			✓	
7				✓
8				
9		7	✓	✓
10			✓	
11				✓
12				
13	3	1	✓	✓
14			✓	
15				✓
16				
17		3	✓	✓
18			✓	
19				✓
20				
21		7	✓	✓
22			✓	
23				✓
24				
25	7	1	✓	✓
26			✓	
27				✓
28				
29		3	✓	✓
30			✓	
31				✓
32				
33		7	✓	✓
34			✓	
35				✓
36				

5.1 PERFORM-3D Modeling Phase

This section describes the modeling steps taken to create the models in Table 5.1. All models utilized the same modeling strategies to define material models, cross sections, and elements. Screenshots of the PERFORM-3D modules can be found in Appendix A.1.

5.1.1 Nodes

The first step to modeling on PERFORM-3D is to define nodes. Nodes allow users to generate a grid system to model the layout of the walls. Nodes are identified by their coordinates, which the axes of the coordinate system are H1, H2 and V. To draw, move, or duplicate a node, coordinates of that node must be specified. The node layouts were different for each mesh configuration as described in Table 5.1. First, the four exterior corner nodes are assigned to the extents of the wall. Then, the interior node spacing was calculated per the mesh configuration and was replicated throughout the wall length and height.

5.1.2 Material Models

To generate the wall's nonlinear properties, the authors implemented material models for concrete and steel reinforcement. These material models required definitions of stress and strain at each critical point of analysis, as shown in Figure 5.1.

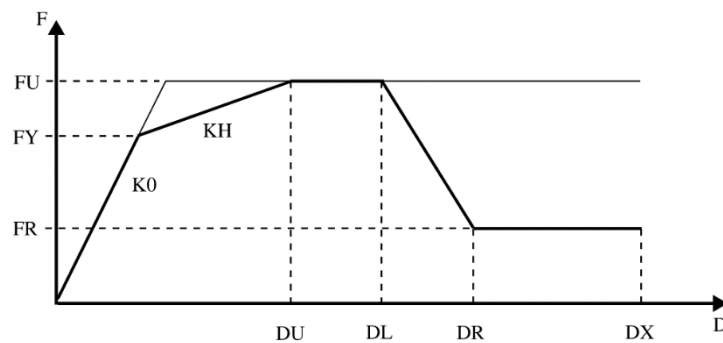


Figure 5.1 – Material Model Stress-Strain Definitions [9]

The yield stress (FY) and the ultimate stress (FU) were defined per the material's specified strength. The stress after strength-loss (FR) for each material can be defined based on residual strength remained in the material after strength-loss. The strain corresponding to each stress described above is DU, DL, DR, and DX. DU is the peak strain at the ultimate stress, ϵ_o , for each model, a common strain at the intersection of initial tangent and plastic unloading slopes. DX is the final strain the material can reach. The strength-loss portion of the material model are defined by DL and DR. DL, by PERFORM-3D's definition, must be at least 1% higher than DU to define the extent of the plateau and the point before strength loss. Material properties were defined in the "Component Properties" tab to generate material models that can be assigned to the wall cross section as fibers. The authors were mainly interested in creating models for inelastic materials with a trilinear relationship that included strength-loss, strain capacities, and cyclic degradation.

5.1.2.1 Inelastic Concrete Material

Two concrete material models by Mander et. al [25] and Scott et al. [6] were explored in the parametric study. Specific stress and strain values defined for both models are displayed in Table 5.2. The yield (FY) and ultimate (FU) stresses corresponded to the material properties, which for both concrete models, were based on the specified compressive strength of concrete. The strain definitions (DU, DL, DR, DX) were highly dependent on the material constitutive models which were used to calculate the defining points for the PERFORM-3D model displayed in Figure 5.2.

DR is the point of strength loss and the main difference between the concrete models. Scott et al. defined DR as being between the strain corresponding to the stress equal to 50% of the maximum concrete strength for unconfined concrete and for confined concrete. Mander et al. defined DR as 95% of the strain at which cover concrete is considered to have completely spalled and ceased to carry any stress. Cyclic degradation for compression strain were implemented per Lowes et. al [21] recommendations for the material model for nonlinear response, YULRX. This nonlinear response model was used for both concrete and reinforcement's definition for cyclic degradation. After a preliminary analysis between the two concrete

models, the authors noticed no significant differences between the strength and initial stiffness of the wall. Since the Mander et. al model is more commonly used in the industry, the authors proceeded the study with this model.

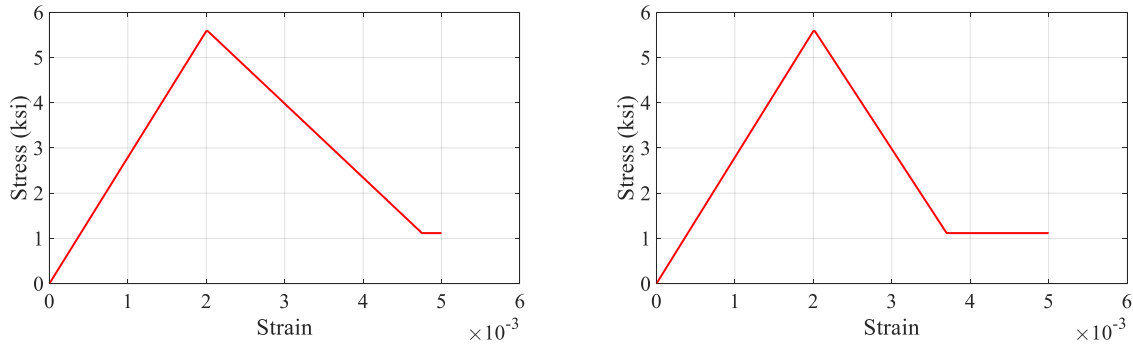


Figure 5.2 – Concrete Material Model (left) Mander et. al [25] and (right) Scott et. al [6]

Table 5.2 – Stress-Strain Values for Concrete Material Models

Model Name	Basic Relationship				Strength Loss			
	E (ksi)	FY (ksi)	FU (ksi)	DU	DX	DL	DR	FR/FU
Mander et. al	3770	4.19	5.58	0.002	0.005	0.00202	0.00475	0.2
Scott et. al	3770	4.19	5.58	0.002	0.005	0.00202	0.0037	0.2

Additionally, the authors explored the effect of including tension in the concrete. The concrete tension model by Hwang and Rizkalla [17] was implemented for the tension side of the Mander et al. model, shown in Figure 5.3. The ultimate tensile stress for concrete cracking of the wall came from Lu et. al [24] tension material test. An exponential relationship was assumed after concrete cracking per the Hwang and Rizkalla’s equation utilizing the strain at yield and at cracking, which were obtained from material testing as well. Stress strain definitions for the tension side of the concrete model are displayed in Table 5.3.

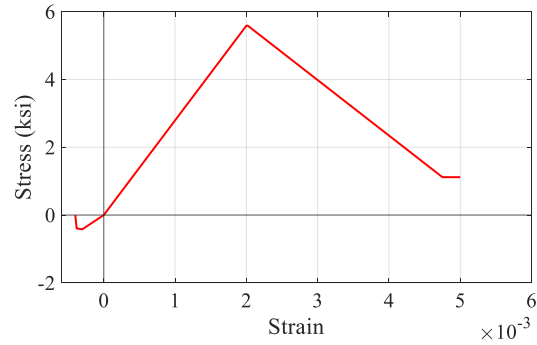


Figure 5.3 – Concrete Material Model with Tension

Table 5.3a – Stress-Strain Values for Concrete Tension Material Models

Model Name	Basic Relationship				Strength Loss		
	FY (ksi)	FU (ksi)	DU	DX	DL	DR	FR/FU
Mander Tension	0.397	0.418	0.0003	0.00207	0.000303	0.00195	0.05

Table 5.3b – Cyclic Degradation Values for Concrete Tension Material Models [25]

Model Name	Cyclic Degradation				
	Y	U	L	R	X
Mander Tension	1	0.4	0.4	0.1	0.1

5.1.2.2 Inelastic Steel Material

Two reinforcement models were implemented in this parametric study, rebar with strength-loss and rebar without strength-loss, shown in Figure 5.4. The basis for the strength loss rebar model came from Menegotto and Pinto [26] and the no strength loss rebar model came from Lowes et. al [21]. The steel reinforcement can show strength loss in tension due to the weakening from prior buckling in the compression cycle and the steel strain forms concentrated concrete cracks, thus localized high strain. The difference between the implemented stress and strain values are displayed in Table 5.4a-c.

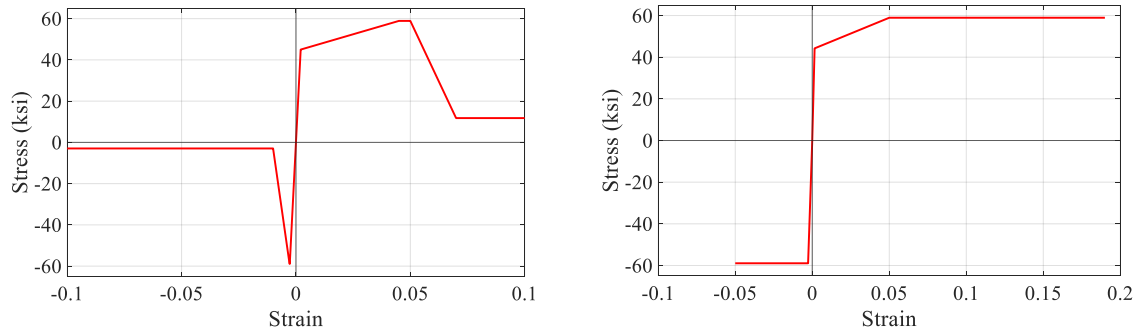


Figure 5.4 – Rebar (left) Strength Loss Model and (right) No Strength Loss Model

Table 5.4a – Stress-Strain Values for Rebar Material Models (Basic Relationship)

Model Name	Basic Relationship								
	Compression					Tension			
	E (ksi)	FY (ksi)	FU (ksi)	DU	DX	FY (ksi)	FU (ksi)	DU	DX
Rebar with Strength-Loss	29000	45	58.9	0.0027	0.1	45	58.9	0.045	0.1
Rebar No Strength-Loss	29000	45	58.9	0.0027	0.05	45	58.9	0.05	0.19

Table 5.4b – Stress-Strain Values for Rebar Material Models (Strength Loss)

Model Name	Strength Loss					
	Compression			Tension		
	DL	DR	FR/FU	DL	DR	FR/FU
Rebar with Strength-Loss	0.00273	0.0475	0.05	0.0455	0.095	0.2

Table 5.4c – Stress-Strain Values for Rebar Material Models (Cyclic Degradation)

Model Name	Cyclic Degradation				
	Y	U	L	R	X
Rebar with Strength-Loss	1	0.4	0.4	0.1	0.1

The strength loss rebar model utilized the same yield stress (FY) and ultimate stress (FU) for the tension side and the compression of the rebar. The strains, however, varied between the tension and compression side. The peak compression strains at ultimate stress (DU) aligned with the concrete strain capacity while the tension strains aligned with the steel capacity. The final stress (DX) extended to the same point on both side per the recommendation of industry advisor Garrett Hagen [14]. The stresses correlated with strength

loss (DL and DR) were determined per PERFORM-3D's minimum allowable value of DL being 1% higher than DU, DR being 95% of DX.

After reaching the ultimate stress (FU), the no strength loss rebar model maintained this value until total loss of strength. This stress-strain model was distinctive from the strength loss rebar model because the stresses were slightly higher for tension but lower for compression. This model did not have DL and DR defined as it did not lose strength on either the tension or compression side.

5.1.2.3 Elastic Concrete Material

An elastic shear material was utilized to describe the shear properties of the concrete wall models. The shear modulus, G_c , was defined according to ACI 318 [1] as $0.4E_c$, where E_c is the modulus of elasticity. The shear stiffness was taken as $0.1G_cA_g$ per ATC 72-1 [3] recommendations where A_g is the gross area of the wall.

5.1.2.4 Elastic Deformation Gages

Deformation gages were implemented in the PERFORM-3D models to monitor the global behavior of the wall, as shown in Figure 5.5. Two-node axial strain gages with intermediate node generation were placed on each end of the wall to monitor the maximum tensile and compressive axial strains. A four-node shear strain gage was connected to the top and bottom corner nodes of the model to monitor the lateral displacement of the wall. A four-node rotational gage, attached similarly to the shear strain gage, was utilized to monitor the global rotation of the wall. All deformation gages were set for different performance level capacities. These capacities were later coincided with limit states to provide insight on when each performance level was reached in a static pushover analysis of the wall.

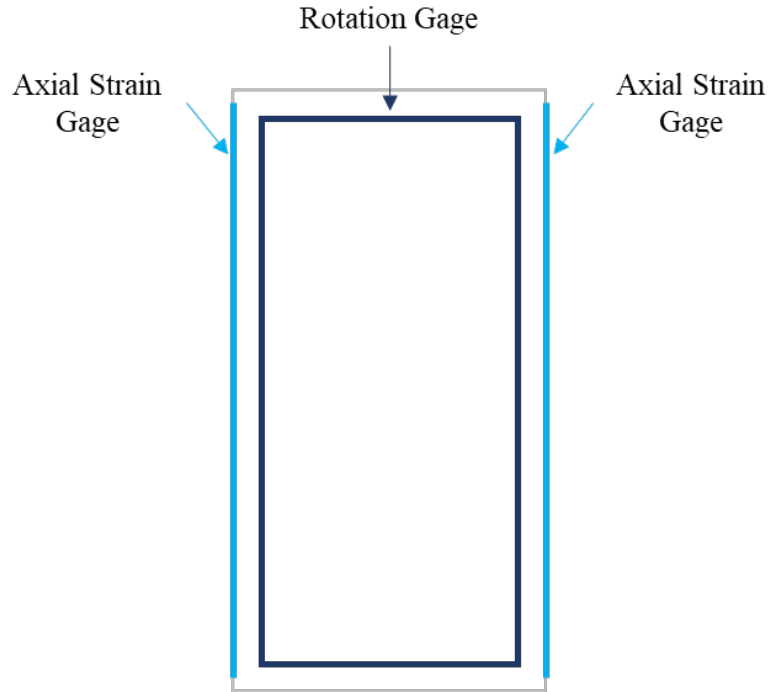


Figure 5.5 – Deformation Gage Locations

5.1.3 Cross Sections

The fiber section was specified to accurately represent the geometry and material configuration of the walls. The “Fixed Size” section option required determining the exact location of the material fibers within the wall to capture the cross-sectional geometry. Each wall cross section was constructed according to the placement of the original experimental wall’s vertical reinforcement per Figure 5.6. There were two types of structural fibers used, “Inelastic 1D Concrete Material” and “Inelastic Non-buckling Steel Material”.

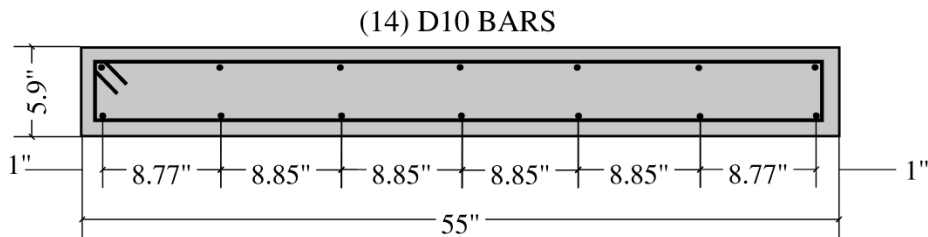


Figure 5.6 – Wall C1 Cross Section

The cross-section for the 7 horizontal mesh model was broken into nearly equal segments. PERFORM-3D is unable to specify more than one row of reinforcement; therefore, rebar was idealized to be one bar at the center of each cross-section segment as shown in Figure 5.7a. The exception was the outer most segments where steel was at a specified distance from the cover. The area and coordinate of each structural fiber used was specified. To allow PERFORM-3D to consider axial bending of the material, a small, negligent value for the steel coordinate. The coordinate position was considered from the center of each cross section. The area referred to the cross-sectional area of each fiber while “T-Draw” referred to the thickness of the fiber; a “T-Draw” of zero was used for circular reinforcing steel. Similarly, the 3 and 1 horizontal mesh were created and are shown in Figure 5.7b and 5.7c.

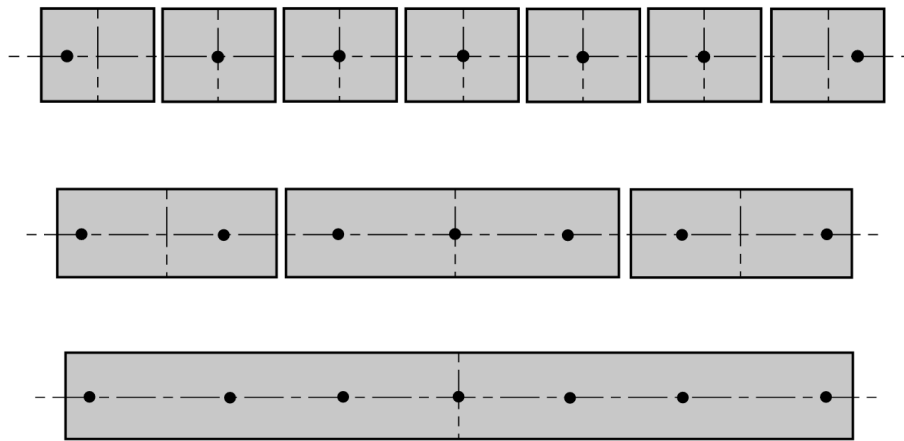


Figure 5.7 – Cross Section Drawing for (a) 7, (b) 3, and (c) 1 Horizontal Mesh

An important addition to the cross section set up was the inclusion of monitored fibers. PERFORM-3D allows for the user to track the strain in fibers. In this case, the extreme concrete and tension fibers in each cross section were chosen as monitored fibers. The strain-displacement results were post-processed to determine when strain limits from Section 5.1.9 were reached.

5.1.4 Compound Sections

“Shear Wall Compound Components” were made up of the wall cross sections, basic and/or strength section components. These compound components were intended for modeling relatively slender walls that takes into considerations the shear force and axial bending action along the vertical direction. For the primary bending behavior, fiber wall cross section must be chosen. The transverse direction was assumed to be a secondary direction similar to beams and columns with the behavior for this mode is out of plane bending which is assumed to be elastic. An effective thickness and elastic modulus must be specified for the secondary behavior as well.

5.1.5 Elements

Elements are created from the nodes set up in Section 5.1.1 and are assigned the shear wall compound component from Section 5.1.4. Shear wall elements act essentially as beams with bending, axial and shear deformations. Following element assignment, local axis orientations are given to the shear wall elements, shown in Figure 5.8. For the modeling of this wall, Axis 3 is the transverse direction in which the element behaves elastically.

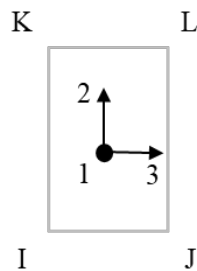


Figure 5.8– Element Orientation

5.1.6 Load Patterns

Load definition involved two steps: load set up in the modeling phase and load pattern assignment in the analysis phase. Three load patterns can be used to construct load cases for static analyses: nodal load patterns, element load patterns, and self-weight patterns. Two nodal patterns, dead load and lateral load, were applied directly to the top nodes of the wall. The dead load applied to the wall was determined from self-weight and axial load on C1 for a total of 67.5 kips distributed along the top nodes of the wall per the tributary width of each node. The lateral load was applied as a unit load distributed across the top nodes. The distribution is mesh dependent and shown in Figure 5.9 for a 7x7 mesh wall model. Since the nodal loadings are dependent on the number of horizontal meshes, the loadings of each mesh for gravity and lateral loads are displayed in Table 5.5.

Table 5.5 – Gravity and Lateral Nodal Loads

Nodal Loads			
Horizontal Mesh	Node ID	Gravity Load (k)	Lateral Load (k)
7 Mesh	N1	3.674	0.125
	N2	8.952	
	N3	10.556	
3 Mesh	N4	8.740	0.250
	N5	25.010	
1 Mesh	N6	33.750	0.500

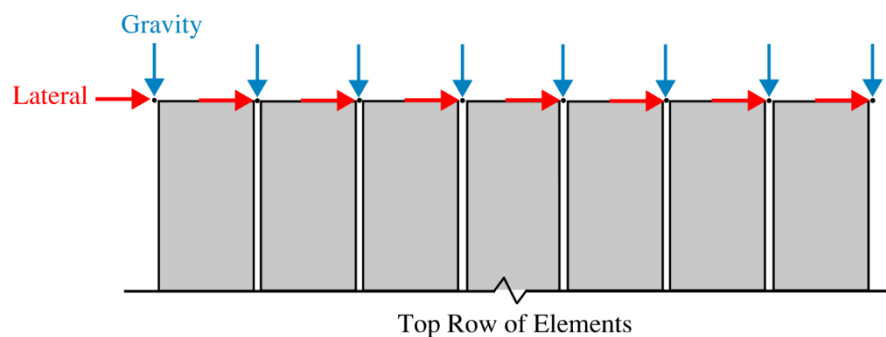


Figure 5.9 –Elevation View of Gravity and Lateral Loading for 7x7 Mesh

5.1.7 Drifts

The two reference nodes selected to calculate global wall drift are shown in Figure 5.10. The drift value would be the top node (roof) displacement divided by the wall height, which is the average drift over all stories. A drift direction was chosen and specified to be used as the reference drift in the analysis phase.



Figure 5.10 – Drift Visualization

5.1.8 Structure Sections

A “Structural Section” is a plane which cuts through all or part of the wall and is described using the IJ, KL, IK, or JL side for a 4-node element, as shown in Figure 5.8. The section for the C1 wall was cut slightly above the base, shown in Figure 5.11, and was used as the critical section for assessing force-displacement response of the wall.

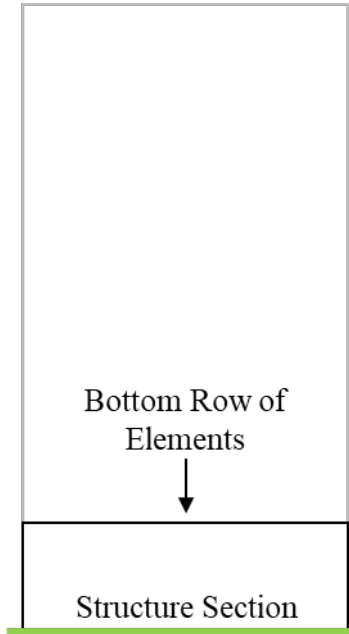


Figure 5.11 – PERFORM-3D Structural Section Cut

5.1.9 Limit States

Limit states were used to describe the behavior of the wall throughout the nonlinear analysis. The monitored fibers described in Section 5.1.3 were used to monitor the extreme rebar and concrete material strains for reaching limit states related to the material behaviors described below.

Material Behavior Strain Limits:

- *Concrete Cracking* was defined at the peak tensile strength of concrete.
- *Concrete Crushing* was defined when the concrete compressive fiber strain reached 0.003.
- *Rebar Fracture* was defined at the maximum tensile strain of the rebar.
- *Rebar Buckling* was defined at the maximum compressive strength of the rebar.

The deformation gages described in Section 5.1.2.4 were used to monitor the global behavior of the wall as it relates to the strain and rotation limits set by ASCE 41-17 Section 10.3.3.1 [4], shown in Table 5.6 and Table 5.7. In addition to material and rotational limits, a global wall failure limit was set at 20% post-peak strength loss, recommended by Park [29].

Table 5.6 – Axial Strain Limits

Strain Limit	Limit Behavior
0.002	Concrete Compression
0.05	Rebar Tension
0.02	Rebar Compression

Table 5.7 – Rotational Limits

Rot. Limit	Limit Behavior
0.002	Immediate Occupancy
0.008	Life Safety
0.015	Collapse Prevention

5.2 PERFORM-3D Analysis Phase

After completing the modeling phase, the lateral load cases were defined in the analysis phase as a static pushover and displacement-controlled cyclic load analysis series. The static pushover analysis was conducted past failure to 10% drift to capture all applicable limit states including 20% post peak strength loss. The displacement-controlled cyclic load analysis followed the test protocol from Lu et al. [24] to produce a force-displacement hysteresis that was comparable to the experimental testing results. Screenshots of the PERFORM-3D modules for each analysis phase section can be found in Appendix A.1.

5.2.1 Load Case Definitions

PERFORM-3D required load cases for the gravity load, static pushover load, and each of the cyclic load cases. The gravity load case was considered a linear analysis and defined by adding the gravity load described in Section 5.1.6 to the load pattern list. The static pushover case was defined according to the recommendations of Powell et. al [31] with the lateral load from Section 5.1.6 added to the load pattern list.

The displacement-controlled cyclic load analysis required the creation of 19 unique load cases shown in Table 5.8 to represent the displacement-controlled protocol specified by Lu et. al [24] and using Powell et. al [31] recommendations for the static pushover case. However, the displacement pattern was reflected by either a positive push or negative pull drift definition using “d along H1”, shown in Figure 5.12. To reflect the increasing displacement, the maximum allowable drift was set equal to the drift required to go from the previous displaced position to the current displaced position. For example, an excursion from -0.25% drift to 0.25% drift, the maximum allowable drift was set to 0.5%. All drifts are defined in Section 5.1.7.



Figure 5.12 – Cyclic Load Cases Visualization

Table 5.8 – Cyclic Load Cases

Target Drift (%)	Max Allowable Drift	d along H1
0.2	0.002	1
-0.2	0.004	-1
0.25	0.0045	1
-0.25	0.005	-1
0.35	0.006	1
-0.35	0.007	-1
0.5	0.0085	1
-0.5	0.01	-1
0.75	0.0125	1
-0.75	0.015	-1
1	0.0175	1
-1	0.02	-1
1.5	0.025	1
-1.5	0.03	-1
2	0.035	1
-2	0.04	-1
2.5	0.045	1
-2.5	0.05	-1
0	0.025	1

5.2.2 Analysis Series

After creating the load cases, two analysis series were created: the static pushover series and displacement controlled cyclic series. The series were set with a general load sequence to allow load cases to be completed sequentially. Each series was first initiated by the gravity load case, followed by the static pushover load case and cyclic load cases, respectively. No P-Delta effects were considered for this parametric study, but its impact was later analyzed in Chapter 6.

5.2.3 Results

Force-displacement results from the static pushover series were available in the General Pushover Plot, with the limit states shown with markers. The cyclic load series force-displacement results were available by viewing the Time Histories results for the structure section defined in Section 5.1.8 as were the strain-displacement relationships of the extreme compression and tension fibers for a single shear wall element. All force-displacement relationships and strain-displacement relationships were saved in text files and post-processed in MATLAB.

5.3 Modeling Summary

Using PERFORM-3D, the authors modeled 36 unique combinations of C1 wall by Lu et. al [24], consisting of four parameters: horizontal meshing, vertical meshing, concrete material modeling, and rebar material modeling, as described in Table 5.1. The process started with generating nodal coordinates to configure the wall dimensions. Then, material models were defined. Since PERFORM-3D only allow users to specify a certain number of points to describe material response, these points were used to define peak, strength-loss, and ultimate stress-strain relationships. Two concrete models with the compression model based on Mander et. al [25] and the tension model based on Hwang and Rizkalla [17] were implemented. Two rebar models were also investigated: a strength-loss model based on Menegotto and Pinto [26] and a no strength-loss model by Lowes et. al [21]. Once material models were established, an elastic shear material was utilized

to describe the shear properties. Three types of deformation gages were placed on the wall: axial, shear, and rotational gages. These were used to monitor strains, lateral displacement, and global rotations, respectively.

Next, the authors assigned horizontal and vertical meshes, which divided the wall cross-section into combinations of one, three, and seven regions. Then, shear wall compound components were established to assign to each element in the wall, followed by the assignment of orientation. Loadings such as gravity, lateral, and drift were specified to simulate the experimental loading protocol. Force-displacement response was analyzed for the critical section of the wall including performance limit states.

PERFORM-3D modeling results were compared to the experimental and assessed for accuracy in strength, stiffness, ductility, energy dissipation, and cyclic degradation. The findings and final model calibrations are discussed in Chapter 6.

CHAPTER 6

PERFORM-3D ANALYSIS: PHASE 2

The previous chapter on PERFORM-3D analysis provided a basis for the modeling steps taken to create a set of 36 models of wall C1 from Lu et. al. [24] that varied in horizontal and vertical mesh as well as in concrete and rebar material models. This chapter describes the findings and final calibrations taken on wall C1 in the static pushover and cyclic load analyses. For the static pushover analysis, there were investigations into the meshing, limit states, strength loss, total strength loss at X, and P-delta effects. For the cyclic load analysis, there were investigations into the meshing, concrete tension model, rebar cyclic degradation, stiffness factors, strength loss interaction, and strain limits. After completing calibrations on wall C1, the modeling strategies were validated using wall C2, C3, and W1.

6.1 Modeling Calibration

All model calibrations on wall C1 were completed independently before choosing to move forward with a value for any given study parameter as final calibration factor. The authors ensured that all calibrations remained independent before exploring the combined effects that can occur.

6.1.1 Static Pushover Analysis

A static pushover analysis was completed on PERFORM-3D for each model described in Table 5.1 and results can be found in Appendix A.2. The global force and displacements, global rotations, and extreme compression and tension fiber strains were analyzed to finalize the wall C1 model for the static pushover analysis.

6.1.1.1 Varying Mesh Investigation

The first investigation was to determine the horizontal and vertical mesh that would achieve accurate initial stiffness and ultimate strength. Figure 6.1 demonstrates the various mesh patterns pursued in the parametric study described in Chapter 5. When exploring the effects of varying vertical mesh on a constant horizontal mesh, as shown in Figure 6.2, the solution converges on the experimental results at a 7x7 mesh. Similarly, when exploring the effects of a varying horizontal mesh on a constant vertical mesh, as shown in Figure 6.3, the solution converges on the experimental results at a 7x7 mesh. To avoid mesh dependency, the authors acknowledged that the 7x7 mesh could be creating the most accurate element aspect ratio for the shear span ratio of wall C1. At this time, it was decided to pursue all 7x7 mesh models with varying material models to narrow the investigations for wall C1.

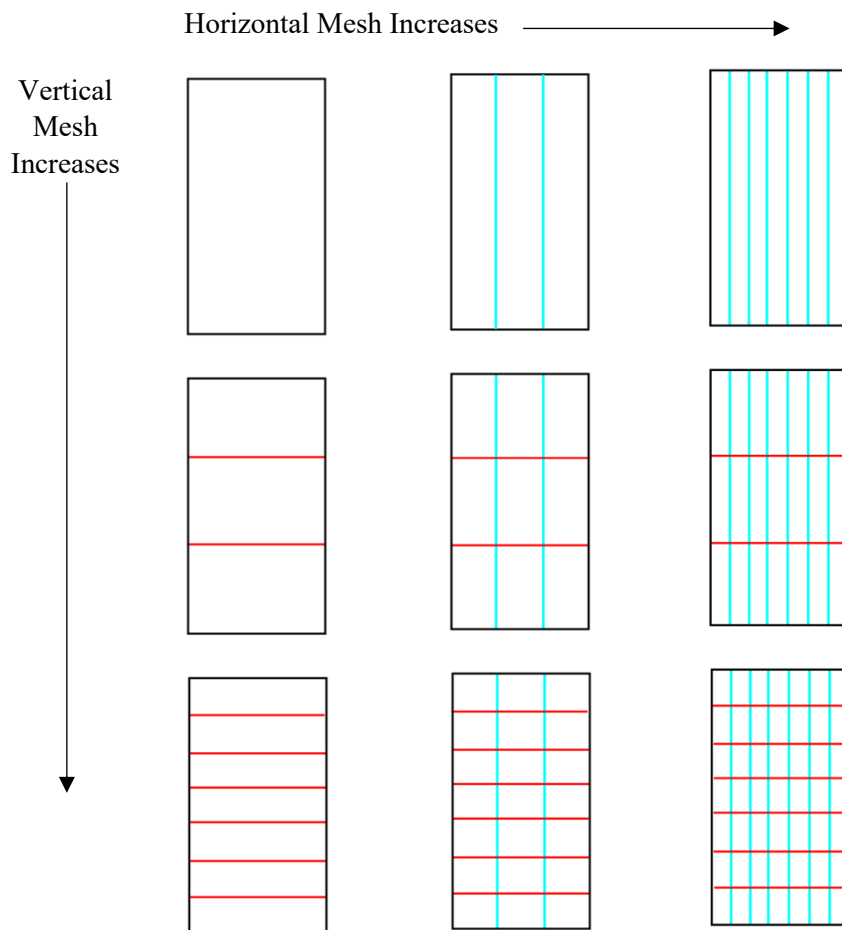


Figure 6.1 – Mesh Variations

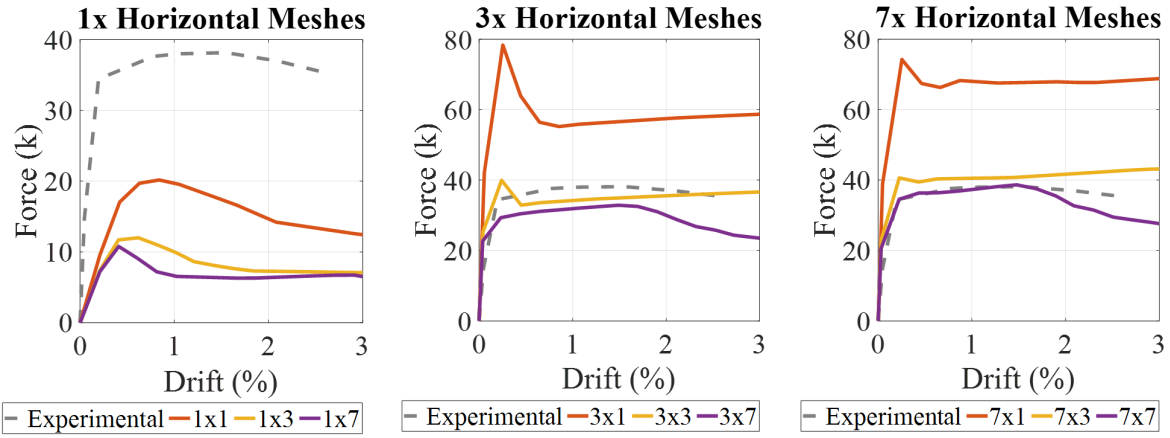


Figure 6.2 – Varying Vertical Mesh

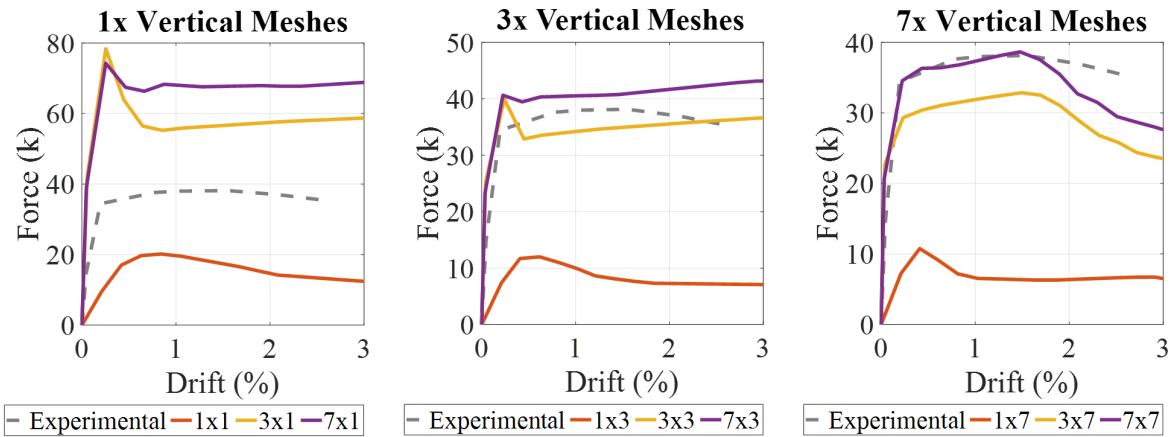


Figure 6.3 – Varying Horizontal Mesh

6.1.1.2 7x7 Mesh Model with Varying Material Model Investigation

After determining the 7x7 mesh models should be pursued, the study was narrowed to the four 7x7 mesh models with varying concrete and rebar material model combinations, Models 33-36, shown in Figure 6.4.

The respective material models utilized in each model are identified in Table 6.1 from Table 5.1.

Table 6.1 – All 7x7 Mesh Models

	Rebar w/ Strength Loss	Rebar w/o Strength Loss
Concrete w/Tension	Model 33	Model 34
Concrete w/o Tension	Model 35	Model 36

The models that had the rebar without strength loss model never degraded or experienced significant global strength loss. For this reason, Model 34 and Model 36 were removed from the static pushover study. The models that had the rebar with strength loss model yielded better results in predicting the ultimate drift at 20% post-peak strength loss. For final calibrations, the authors moved forward with Model 33 because the initial stiffness and strength were better matched to the experimental results.

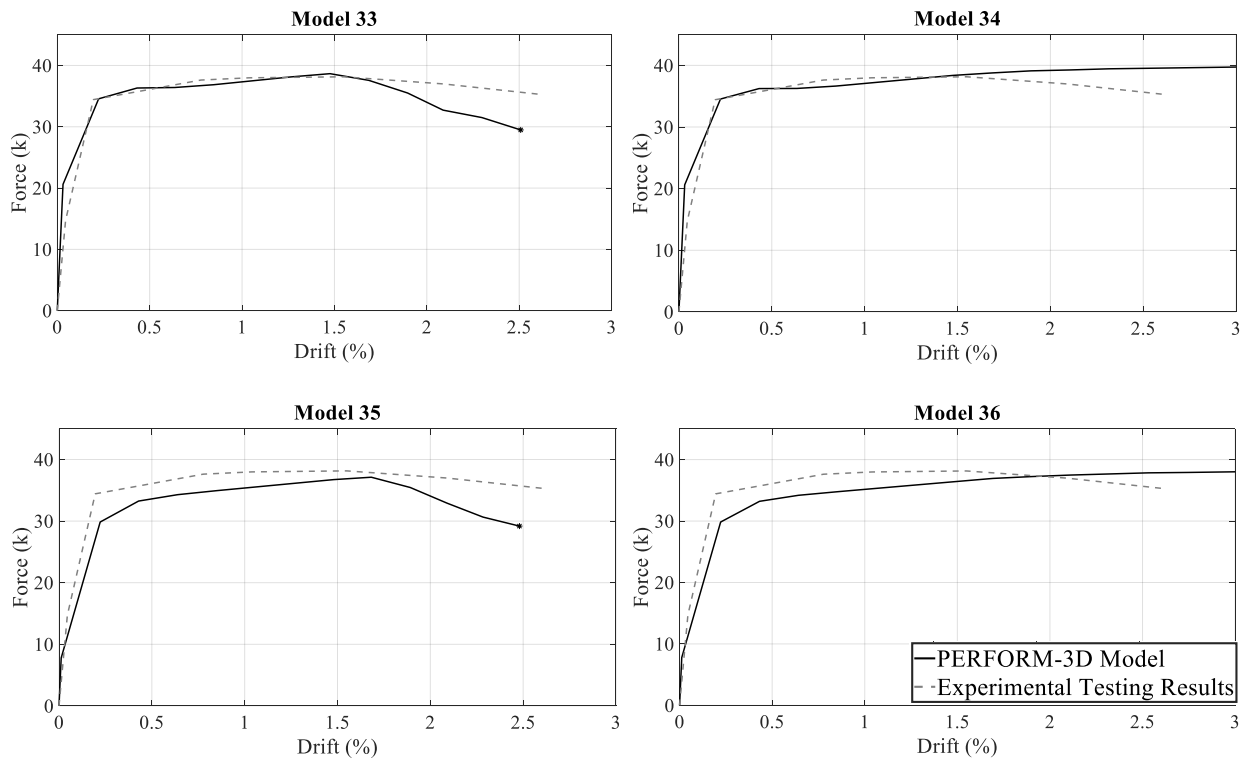


Figure 6.4 – 7x7 Mesh Models for Static Pushover Analysis

6.1.1.3 Strength Loss Rebar Model Investigation

To properly capture the wall degradation after peak strength was reached, calibrations were performed on the rebar with strength loss model. The original material model described in Figure 5.1 assumed a relatively steep strength loss therefore the value of DR in PERFORM-3D was utilized to decrease the rebar's post-peak negative stiffness slope, shown in Figure 6.5 and 6.6. The negative stiffness was incrementally decreased using DR = 0.07 (original value), DR = 0.08, DR = 0.09, and DR = 0.10 until the material degradation converged with the experimental results. DR = 0.10 was chosen as the final calibration for the rebar with strength loss model.

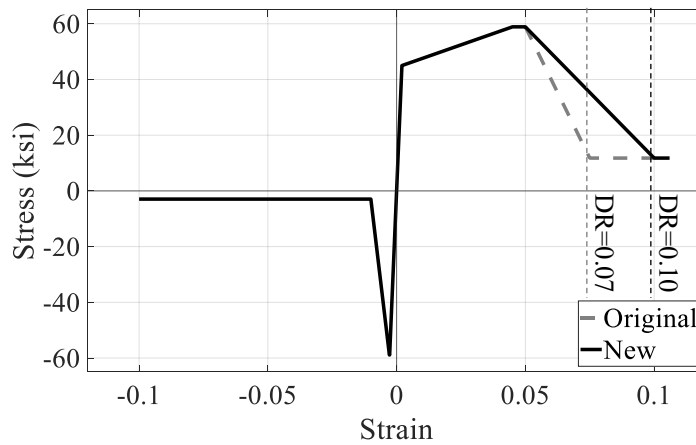


Figure 6.5 – Model 33 Strength Loss Rebar Model Investigation

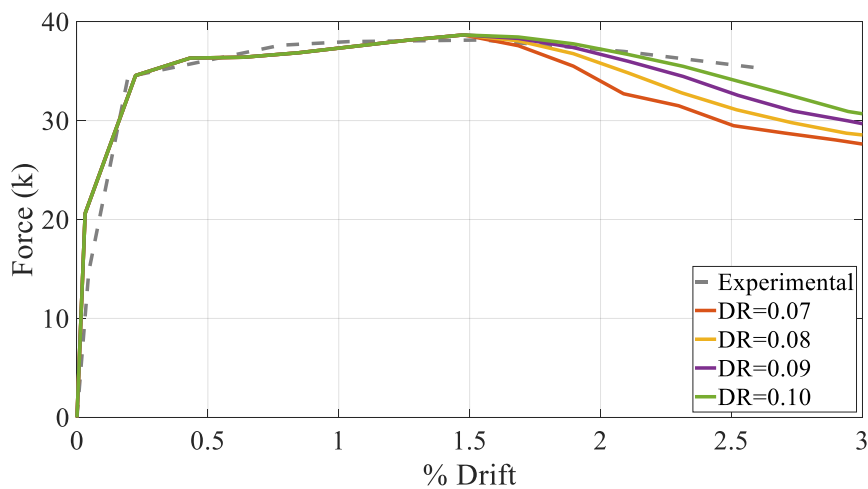


Figure 6.6 – Model 33 Strength Loss Rebar Model Investigation

6.1.1.4 Total Strength Loss at X Investigation

After finalizing the strength-loss definition for the rebar model, the authors explored the effect of strength-loss on the whole system from the definition of all materials. In a stress-strain envelope for any material model, point X is the final point of stress and strain a material can reach. This is the point of strain at which the cover concrete is considered to have completely spalled and ceased to carry any stress. In PERFORM-3D, there is no default point of strength-loss for the system. Point X is intended to be a point of maximum deformation, beyond which the component is severely deformed that the analysis ceased to have any further significance. Depicted in Figure 6.7, at 3% drift, the pushover showed the system exhibits lower strength and became unstable. Practicing engineers only focus on the strength of the system up to 3% drift.

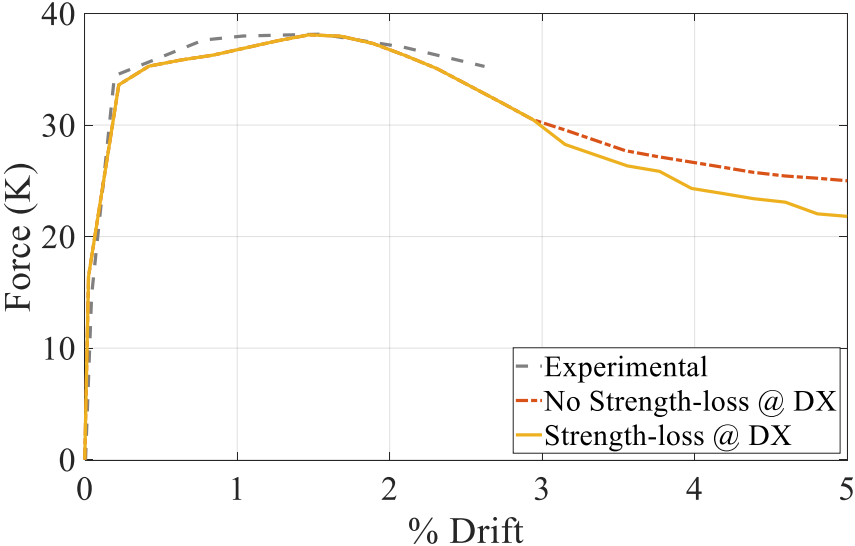


Figure 6.7 – Model 33 Total Strength Loss at X Investigation

6.1.1.5 P-Delta Investigation

Next, the authors investigated the effect of P-delta on the strength of the system. The P-delta involves the application of gravity load on laterally displaced walls and is associated with displacements of member ends. This condition contributes to the loss of lateral resistance, dynamic instability, magnification of story drift, and reduction of deformation capacity. The application of P-delta caused the system to drop in strength and the strength differences increased as higher displacements were reached while going through the pushover analysis as shown in Figure 6.8.

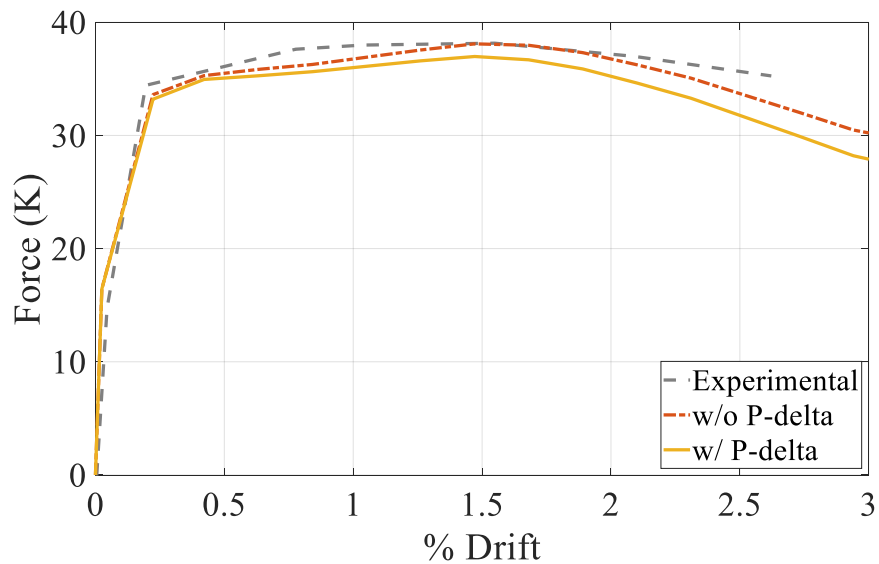


Figure 6.8 – Model 33 P-Delta Investigation

Although the inclusion of P-delta means lower strength for the system, the experimental procedure by De Sevilla et. al [11] and Lu et. al [24] convinced the authors that the P-delta effect should not necessarily be considered. Figure 6.9 (left) depicted the testing set up for walls C1-C3 by Lu et. al, which consisted of a loading jack pushing the wall laterally, and two additional actuators on the left and right of the wall to achieve the required combination of moment and axial load at the top of the wall. When lateral load was applied, the vertical actuators moved along with the loading beam, generating a self-centering axial load to the wall that does not create any eccentricity with respect to the wall's centerline. Due to this collective

motion, P-delta does not need to be considered for walls C1-C3. Similarly, for W1 shown in Figure 6.9 (right), the axial load was applied using a teeter beam placed at the top of the loading beam. This teeter beam was loaded in the center by a vertical actuator to transfer an axially applied reaction force to the wall. The absence of eccentricity eliminated the consideration of P-delta for all the walls as shown in Figure 6.10.

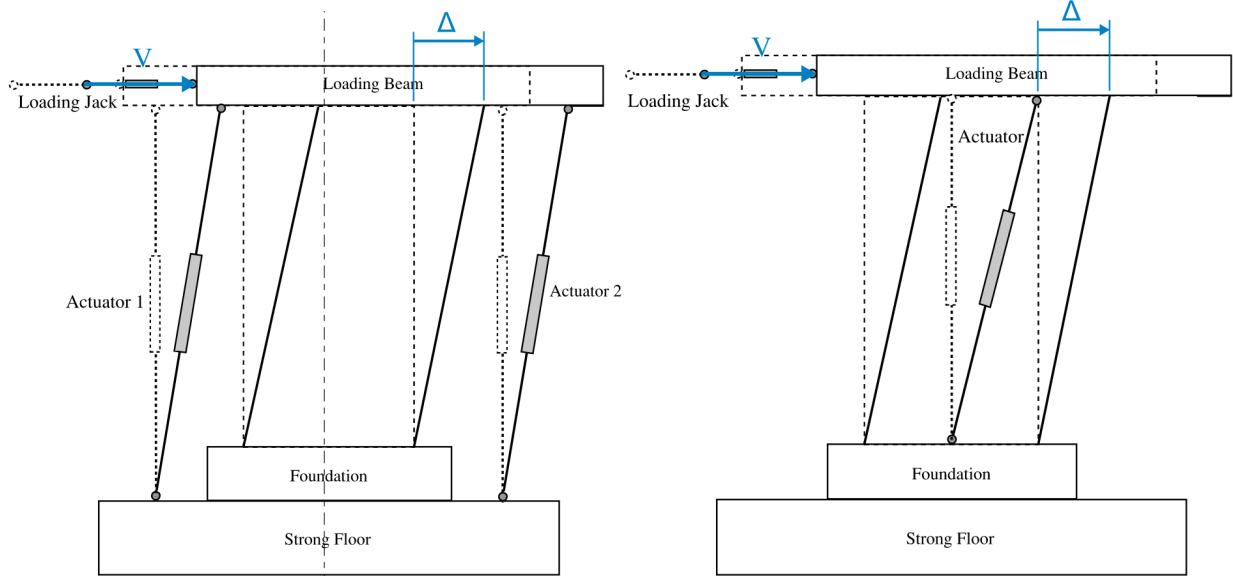


Figure 6.9 – Experimental Test Set-Up for (left) C1-C3 and (right) W1

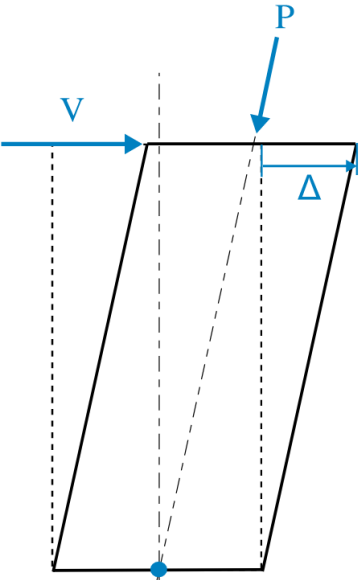


Figure 6.10 – P-delta Demonstration for C1-C3 and W1

6.1.1.6 Strain Limit Investigation

An important part of the final calibrations involved providing confidence that the PERFORM-3D model was predicting the correct behavior and performance pattern. As discussed in Chapter 5, the PERFORM-3D fiber strains were monitored for material behavior states and ASCE 41-17 strain limits. Also, the ASCE 41-17 rotational limits were monitored using 4-node rotation gages. Final failure of the wall was considered at 20% post-peak strength loss. All limit states are plotted on the final calibrated static pushover analysis curve of wall C1 in Figure 6.11.

Concrete cracking and concrete crushing limits were accurately predicted for the experimental test drifts, while rebar buckling and rebar fracture drift predictions were overestimated. This is due to the rebar fracture strain not being properly captured in the experimental test because the strain measurements were compromised when the reinforcement had previously buckled.

The ASCE 41-17 concrete compression and rebar tension strain limit states describe the maximum usable strains for calculating moment and axial strength. The rotation limits for Immediate Occupancy, Life Safety, and Collapse Prevention design are conservatively low when considering the true ductility that can be obtained if the wall performance to 20% post peak strength loss is considered.

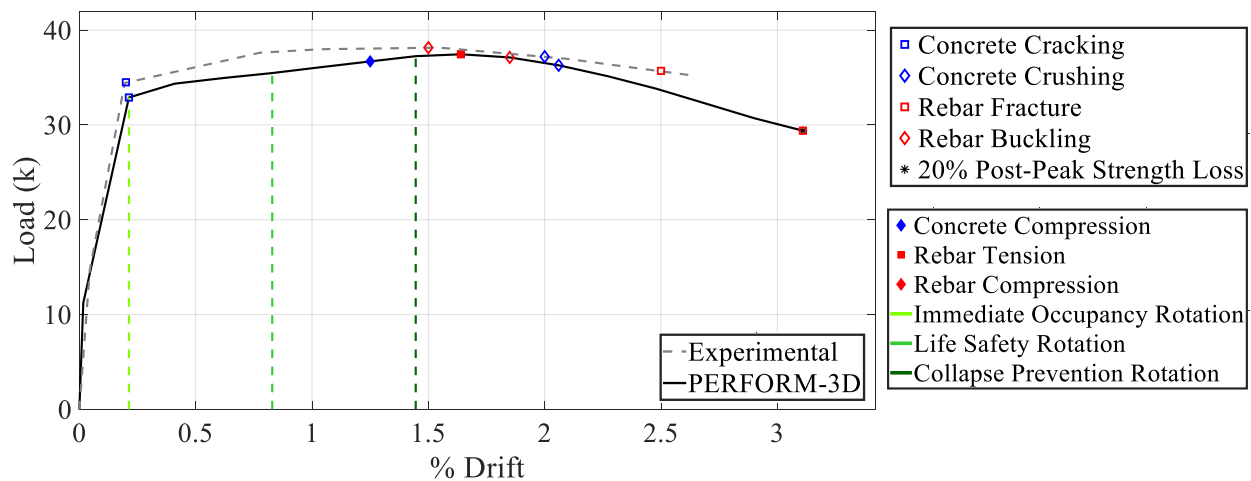


Figure 6.11 – Model 33 Strain Limit Investigation

6.1.2 Cyclic Load Analysis

Upon completing final calibrations on the static pushover curve, the authors explored a cyclic load analysis on the parametric study of 36 models and results can be found in Appendix A.2. It was determined the investigation would be narrowed down to Models 33-36 due to the improved accuracy of a 7x7 mesh observed in the static pushover analysis and subsequently in the cyclic load analysis. The global forces and displacements, global rotations, and extreme compression and tension fiber strains were post processed to complete the investigations in the following sections.

6.1.2.1 7x7 Mesh with Varying Material Model Investigation

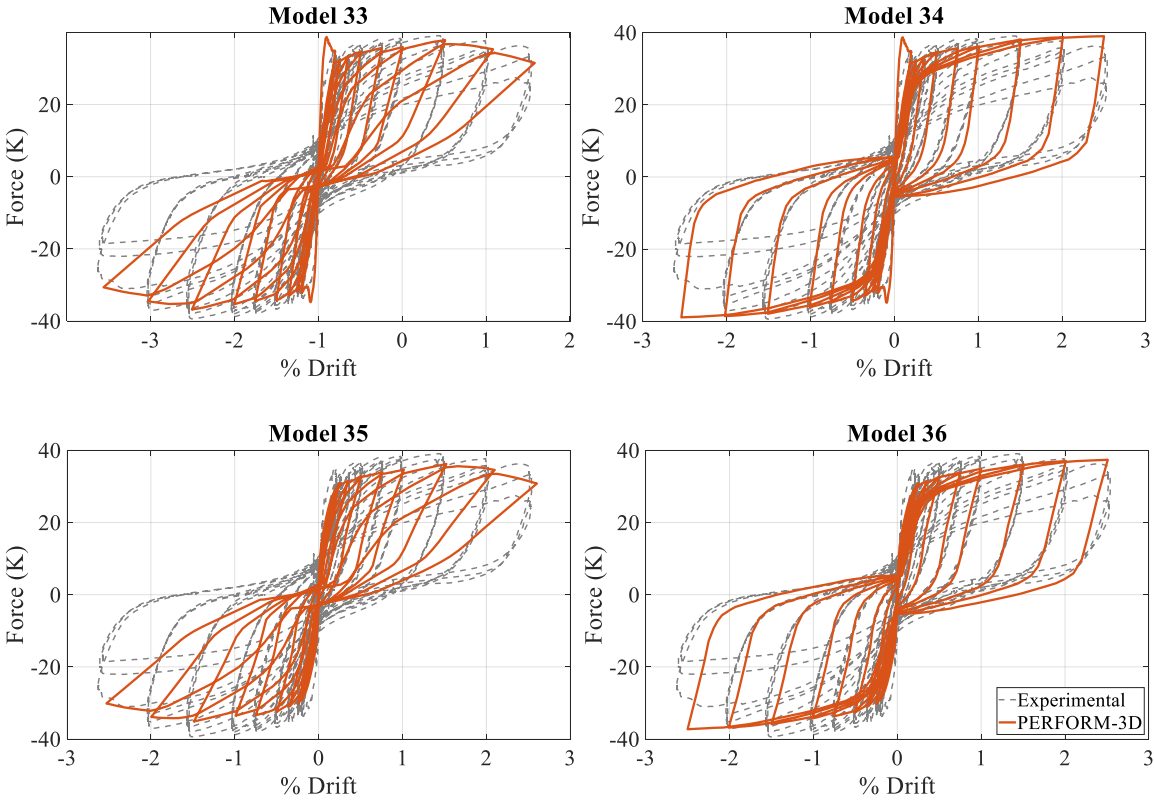


Figure 6.12 -7x7 Mesh Models for Cyclic Load Analysis

The first investigation of the 7x7 mesh models with varying materials provided insight on which should be maintained for the forthcoming investigations, shown in Figure 6.12. Model 35 and 36, neglecting tension strength, depicted significantly lower strength, in comparison to Model 33 and 34. Model 33 and 34 experienced a notable spike in strength during the initial cycle of loading due to the inclusion of concrete tension strength, yet the two models were able to reach the experimental strength quite closely. Model 33, with rebar strength-loss, showed a realistic depiction of the material's degradation at the final loops of the hysteresis. The issue of the energy dissipation represented by the volume of the loops will be further investigated by the authors. With these considerations, the authors proceeded the investigations using Model 33, with concrete tension and rebar strength-loss.

6.1.2.2 Concrete Tension Model Investigation

The authors investigated ways to manipulate the concrete tension model to reduce the spike in strength at the first loop. Initially, the authors defined the tensile stress of concrete from the tension material test presented by Lu et. al [24]. For this investigation, the authors explored a common rule in academia by taking a percentage of the modulus of rupture to define the peak tensile stress of concrete. The modulus of rupture, $f_r = 7.5\sqrt{f'_c}$ [1]. Various percentages of this value were used to define the ultimate (FU) and yield (FY) tensile stresses for the concrete in PERFORM-3D and the results were plotted in Figure 6.13. From visual observation, the spike was visible at $0.3f_r$ so the authors pursued the finalized model of using $0.2f_r$, shown in Figure 6.14.

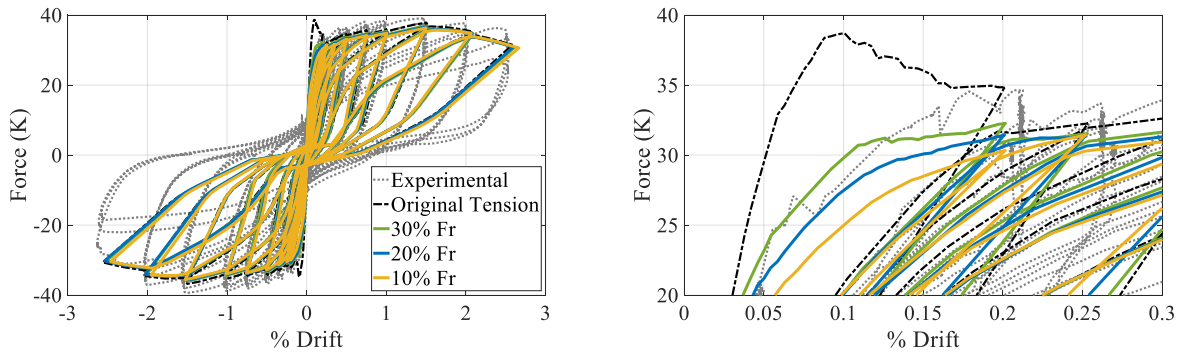


Figure 6.13 – Model 33 Tensile Strength Investigation (left) complete hysteresis and (right) zoom view

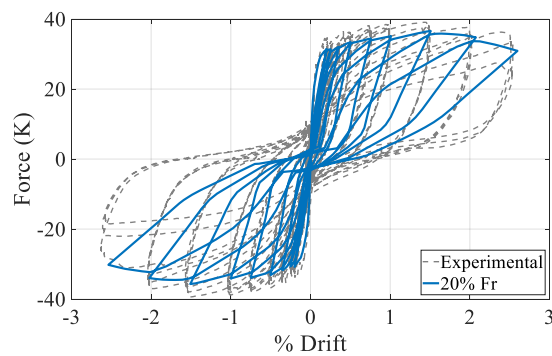


Figure 6.14 – Model 33 with Tensile Strength at 20% of Modulus of Rupture

ACI 318-14 [1] suggests that the tensile strength of concrete shall be conservatively neglected in flexural and axial strength calculations. Table 6.2 displays the accuracy between using a model that neglected tension, and a model that included $0.2f_r$, against the experimental results. For most of the behavioral characteristics of the system, the $0.2f_r$ model was slightly closer at capturing the experimental results and therefore retained in the calibration process.

Table 6.2 –Tension Models Quantitative Modeling Accuracy

Tension Model	Initial Stiffness	Nominal Strength	Yield Drift	Yield Moment	Ultimate Drift	Peak Moment	Legend (% error)
No Tension	0.66	0.93	1.18	0.88	1.03	0.93	>1 overestimate
20% Tension	0.91	0.94	1.03	0.90	1.04	0.94	<1 underestimate

6.1.2.3 Rebar Cyclic Degradation Investigation

Another calibration the authors explored to better match the experimental result was the effect of energy dissipation factors. Energy dissipation is a physical process by which energy becomes unavailable or irrecoverable in any form, that amount of energy is represented by the area enclosed in the hysteresis loops. Energy dissipation factors are related to the points of YULRX for the definition of each material model per Figure 5.4c. Values can be assigned for cyclic degradation at each of these points. Initially, identical values were used for rebar and concrete, yet further study indicated that these factors change the shape of the hysteresis loops and should be modified.

Defining the energy dissipation factor at any point as result in the system still has the absolute maximum amount of energy, 100% of energy remained. Conversely, defining any point as 0 indicated that at those points, the system has no energy left to dissipate. Y was defined as 1 since at the point of yield, the system still has full energy remained. The authors explored increasing point UL and RX, since rebar undergo strain hardening, it should be able to have more energy than concrete. The conclusive value to set ULRX was 0.75, indicated 75% of energy remaining in the rebar material. With this, the authors were able to create a model that better match the hysteresis shape of the experimental result shown in Figure 6.15.

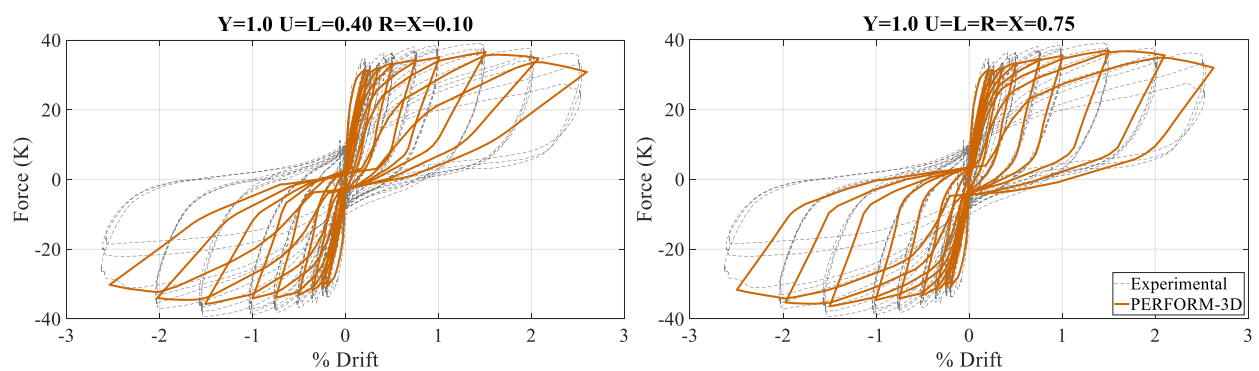


Figure 6.15 – Rebar Cyclic Degradation Factor Investigation

6.1.2.4 Stiffness Factors Investigation

To assist in matching the hysteresis loop shape, PEFORM-3D allows the user to specify unloading/reloading stiffness factors that control energy degradation. The authors investigated three different ways to capture the energy captured per hysteresis loop, shown in Figure 6.16 as the shaded orange area. The stiffness factor of -1 assumes the minimum stiffness for the largest elastic range per hysteresis loop. The stiffness factor of +1 assumes the maximum stiffness for the smallest elastic range per hysteresis loop. The default stiffness factor of zero assumes an average of the expected stiffness and elastic range per hysteresis loop [9]. The stiffness factor of +1 best fit the experimental data because a concrete wall is a relatively stiff lateral force resisting system and, therefore this calibration was utilized.

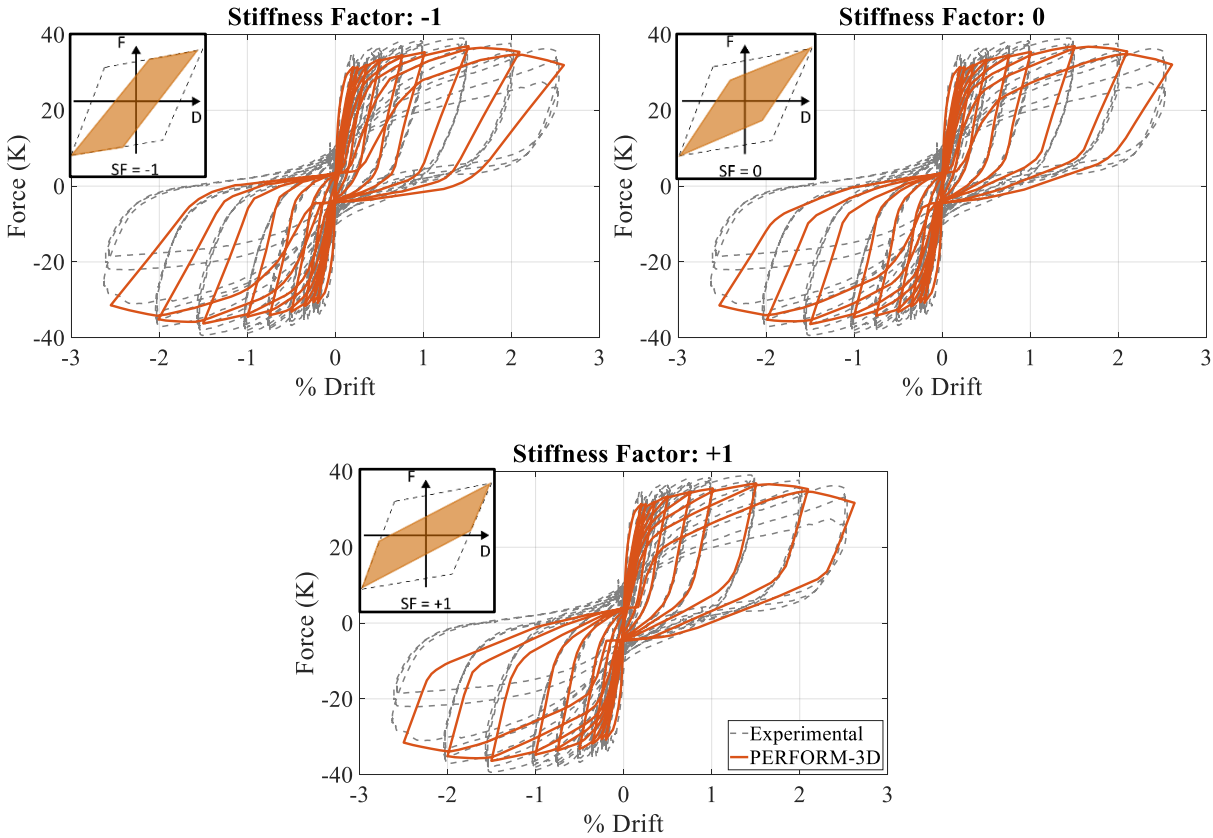


Figure 6.16 – Model 33 Stiffness Factors Investigation

6.1.2.5 Strength Loss Interaction Investigation

Another calibration pursued was defining the strength loss interaction for the rebar material model, shown in Figure 6.17. The initial assumption on the left plot was that strength loss in the one direction led to no strength loss in the opposite direction. In contrast, the right plot considered that strength loss in one direction was equal to the strength loss in the opposite direction. The PERFORM-3D manual [9] suggested that the equal strength loss assumptions may be useful if for example: a component was to fracture in tension, that the user may want to assume the strength in tension is also reduced. However, the interaction factor of zero was better suited for the model because the rebar material model is not symmetric in compression and tension, which would make it incorrect to assume equal strength loss. By visual inspection, the strength loss interaction factor of zero was slightly better at capturing the energy of the 2.5% drift loop, and therefore warranted inclusion in the final calibrated cyclic model.

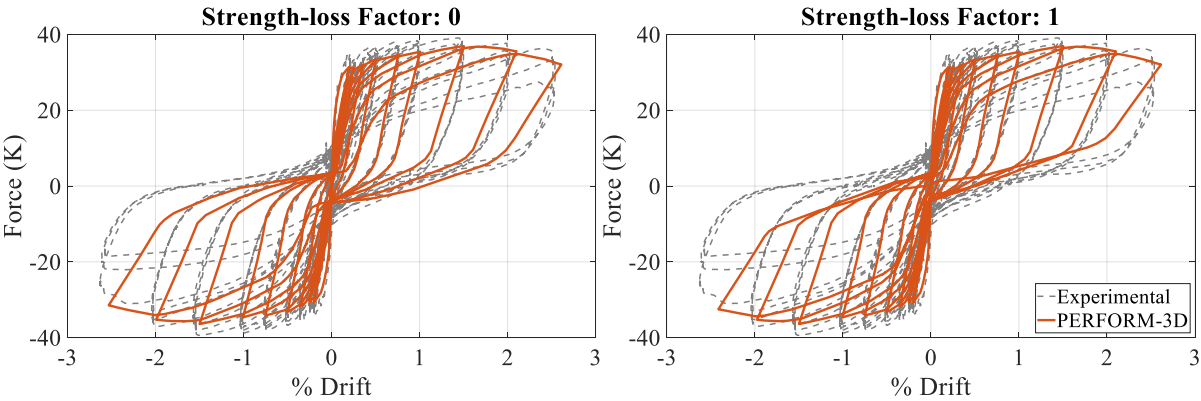


Figure 6.17 – Model 33 Strength Loss Interaction Investigation

6.1.2.6 Strain Limit Investigation

With the final calibrations of the cyclic load analysis complete, it was necessary to compare its behavioral limit states to those of the static pushover curve, shown in Figure 6.18. The ASCE 41-17 concrete compression limit, rebar limit, rebar fracture, concrete crushing, and ASCE 41-17 rotation limits states were all identical, verifying that the same behavior was occurring in the static pushover and cyclic load analyses. The only inconsistent limit state was for concrete cracking. The cyclic load analysis model had the benefit of smaller cyclic steps that led to an increased stiffness and earlier cracking state than the static, monotonic pushover. A lower initial stiffness in the pushover curve made the wall slightly more flexible than the cyclic load analysis, leading to later concrete cracking. Despite this one small difference, it was concluded that the limit states were consistent between the static pushover and cyclic load analyses.

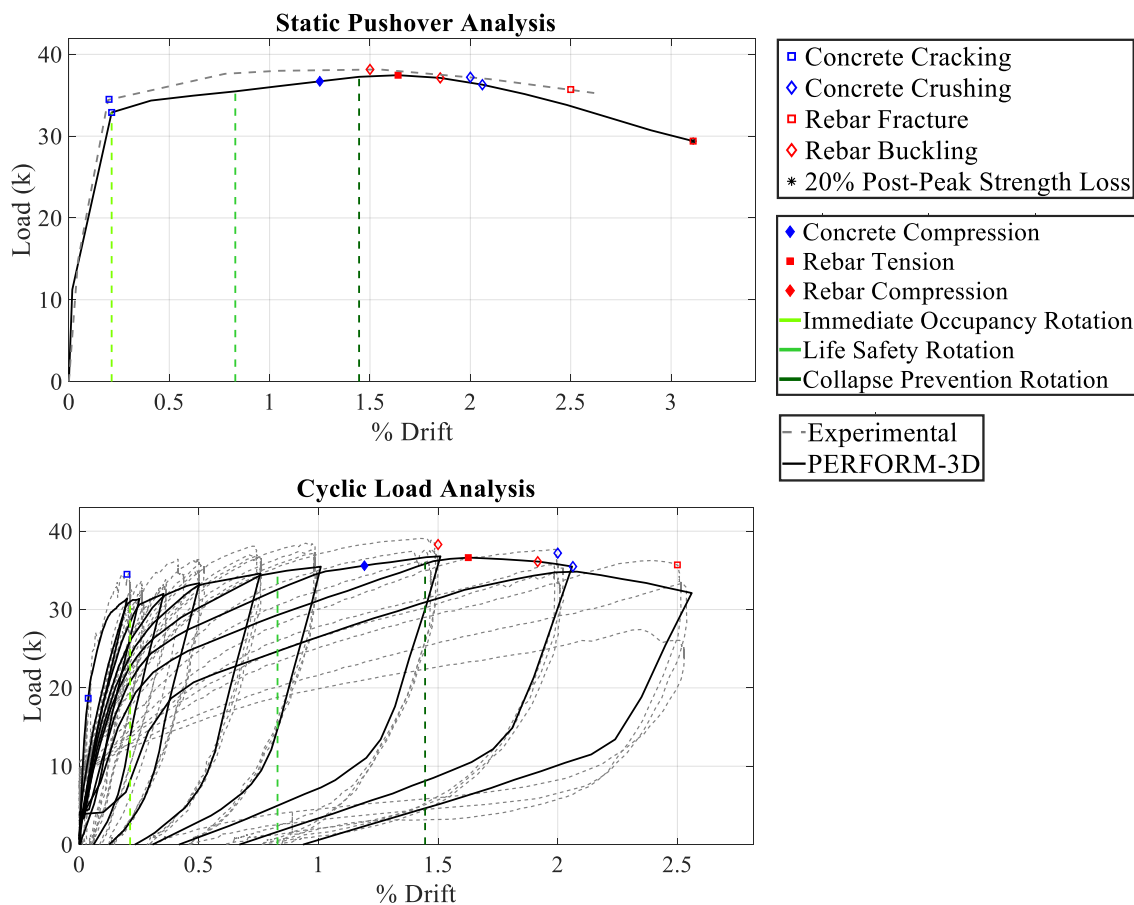


Figure 6.18 – Static Pushover and Cyclic Load Strain Limit Comparison

6.1.3 Final Calibrated Models Comparison

The final calibrated static pushover analysis model and cyclic load analysis model were compared to the experimental results in Table 6.3 and Figure 6.19 to provide conclusions on the accuracy for wall C1 from Lu et al. [24].

Table 6.3 – Static Pushover and Cyclic Load Analyses Comparisons

Method	Initial Stiffness	Nominal Strength	Yield Drift	Yield Moment	Ultimate Drift	Peak Moment	Legend (% error)
Pushover	0.87	0.98	1.09	0.96	1.06	0.98	>1 overestimate
Cyclic Load	1.07	0.94	0.85	0.90	1.04	0.94	<1 underestimate

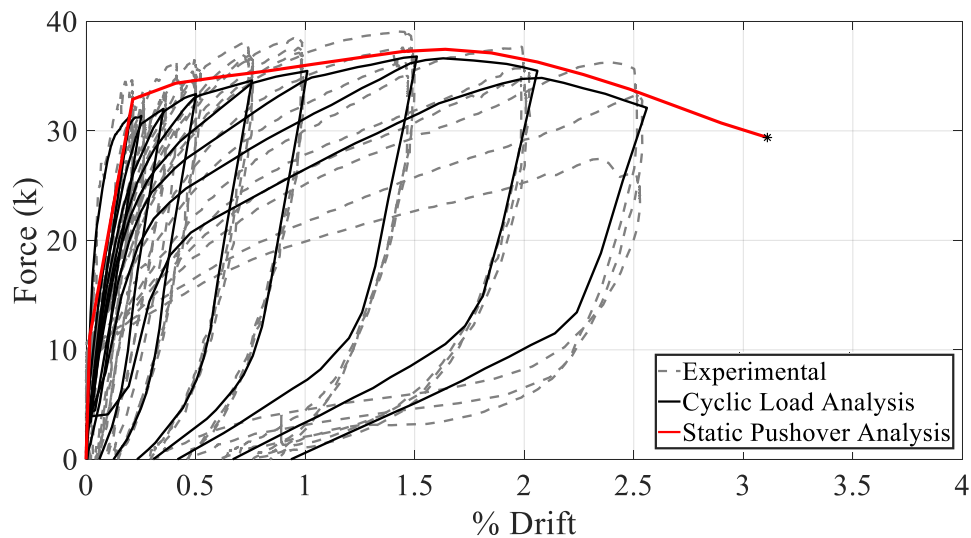


Figure 6.19 – Static Pushover and Cyclic Load Analyses Comparisons

The static pushover was slightly conservative in predicting the initial stiffness because it did not have the benefit of small cyclic steps that led to more accurate initial stiffness predictions by the cyclic load analysis. However, the cyclic load analysis was less accurate in predicting the yield drift than the pushover analysis. This means that the pushover analysis was able to self-correct an underpredicted initial stiffness with a more accurate yield strength. Another advantage to performing the static pushover is that the ultimate deformation can be determined at 20% post peak strength, as indicated with an asterisk in Figure 6.19, with

confidence since material degradation is being properly captured. The nominal strength, yield moment, and peak moment were all captured well.

Industry practitioners are left to choose what best fits their modeling needs. If a nonlinear time history is being performed where cyclic degradation and energy dissipation are important driving factors, the authors would suggest running the cyclic analysis. But if the objective is to perform a quick, relatively simple pushover analysis, the static pushover modeling calibrations can be utilized to find proper stiffness, strength, and displacement capacities.

6.2 Modeling Validation

With the confirmation of the PERFORM-3D results for C1 in comparison to the experimental for both pushover and hysteresis, the authors proceeded to validate the results for W1, C2 and C3. This section will discuss the differences between the PERFORM-3D and experimental results of each wall.

6.2.1 Model Verification with de Sevilla et. al Wall W1

Wall W1 by De Sevilla et. al [11] was modeled following the final calibrations of wall C1. The static pushover analysis and cyclic load analysis results are shown in Figure 6.20 and 6.21, respectively, and quantitative results are displayed in Table 6.4. Interestingly, the model of this wall predicts a higher strength than the experimental, but the stiffness was fairly accurate. For the cyclic load analysis, the energy dissipation and cyclic degradation were extremely well matched. The authors predicted the difference in strength and ductility for this wall was possibly due to construction issues during experimental testing and the potential overestimation of the concrete strength input in PERFORM 3D. The authors performed material testing from concrete cores of the outer left, outer right, and middle at the bottom and the middle of the wall. An average of the concrete core peak stresses was utilized for the concrete compressive strength in PERFORM-3D. These values may have included outliers which led to an overestimation of the wall strength.

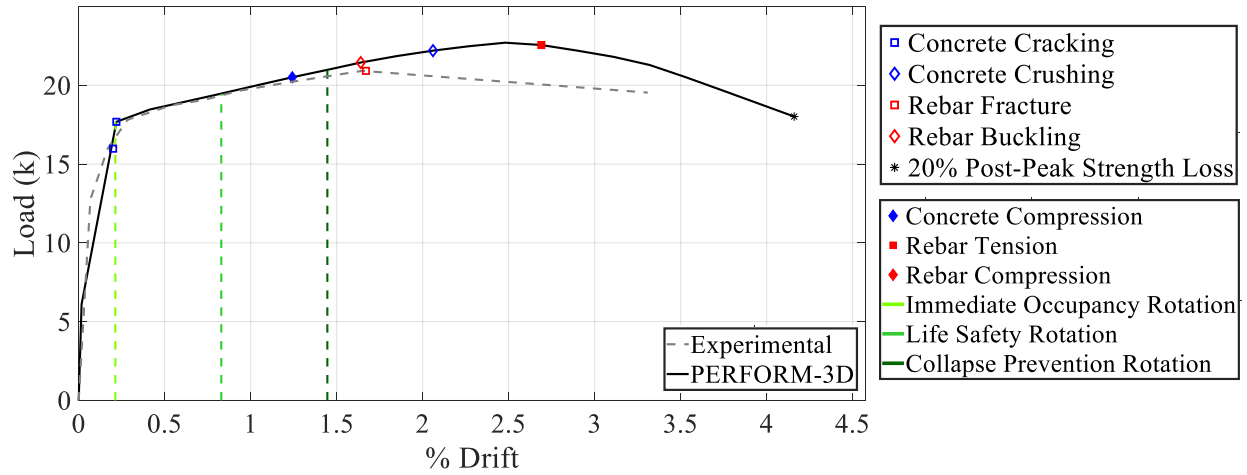


Figure 6.20 – W1 Static Pushover Analysis Results

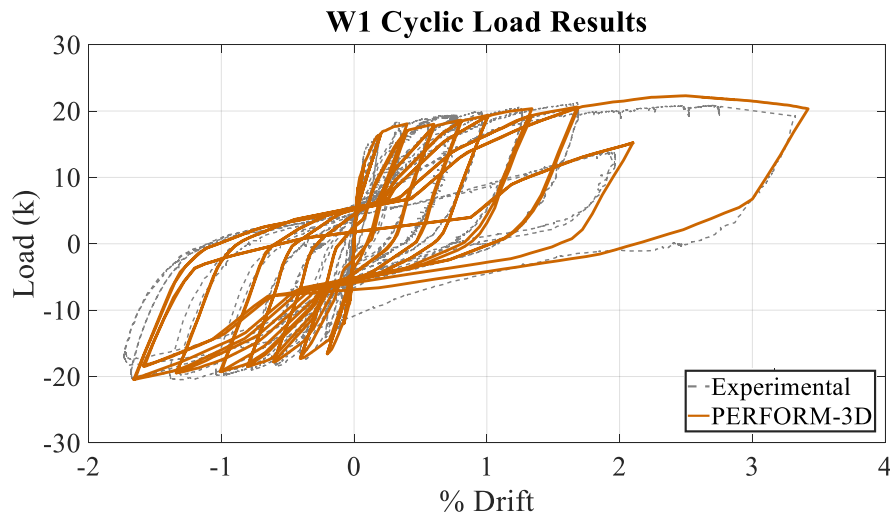


Figure 6.21 – W1 Cyclic Load Analysis Results

Table 6.4 – W1 Static Pushover and Cyclic Load Analyses Comparisons

Model	Initial Stiffness	Nominal Strength	Yield Drift	Yield Moment	Ultimate Drift	Peak Moment	Legend (% error)
Pushover	1.17	1.09	1.20	1.06	1.56	1.09	>1 overestimate
Cyclic Load	1.21	0.94	0.77	0.93	0.68	0.94	<1 underestimate

6.2.2 Strategy Verification with Lu et. al Wall C2 and C3

Prior to modeling wall C2 and C3, additional considerations were made for force couples that acted as the superimposed moments on the walls that are, respectively, two times and three times the height of C1. Two different modeling methods were implemented to simulate the loading protocol. The first was modeling both walls at the full respective height C2 at 220.5 in, C3 at 330.75 in. These models consisted of the finalized meshing configuration for C1 which was 7 horizontal meshes by 7 vertical meshes which did not produce accurate strength and displacement capacities for C2 and C3. The authors attempted other meshing configurations using combinations of lower and higher values for both horizontal and vertical meshes but no combination was quite capturing the experimental results.

The second modeling method consisted of C2 and C3 modeled at the testing height, 110.25 in, same as C1. This method required converting the lateral load applied at each wall's actual height into a force couple that applied the same moment as the experimental test.

Both methods using the 7x7 meshing configuration produced the same results. Even though there was an increase in moment gradients depicted on the cracking pattern, the PERFORM-3D results were not capturing this moment in the same way as the experimental test, as discussed in the following sections.

6.2.2.1 Wall C2

The main concerns for the C2 static pushover results were the strength, initial stiffness, and displacement capacity. The PERFORM-3D results showed a slight overestimation of the yield strength while underestimating the peak strength, shown in Figure 6.22 and Table 6.5. The displacements for yield and ultimate were also severely shifted indicating a poor prediction of the experimental wall's ductility. The pushover curve from PERFORM-3D was essentially shifting all the limit states.

The static pushover limit states occurred as predicted with respect to the strength of the C2 wall from PERFORM-3D, shown in Figure 6.23. The cyclic load results, however, still extremely underpredicted the strength of the experimental test. Stiffness, cyclic degradation, and energy dissipation were closely matched to the experimental result as well.

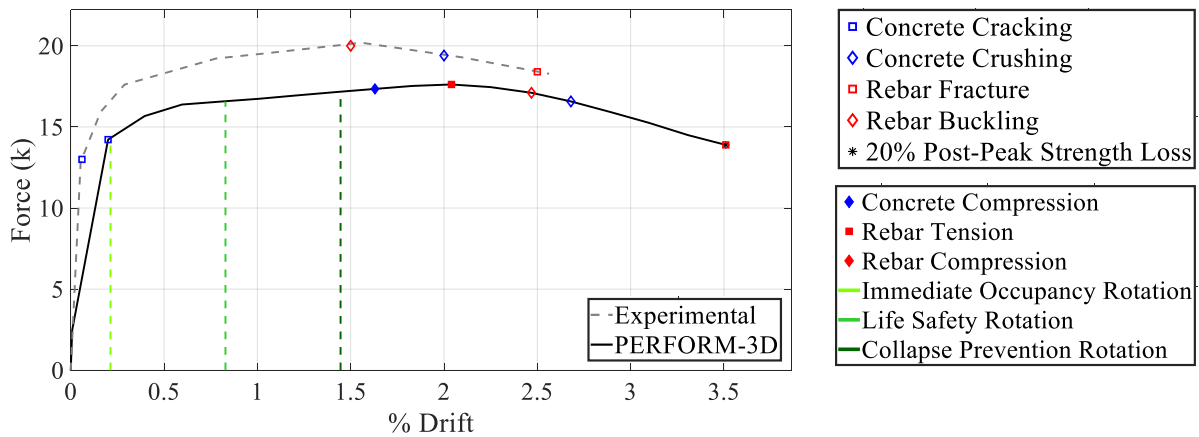


Figure 6.22 – C2 Static Pushover Analysis Results

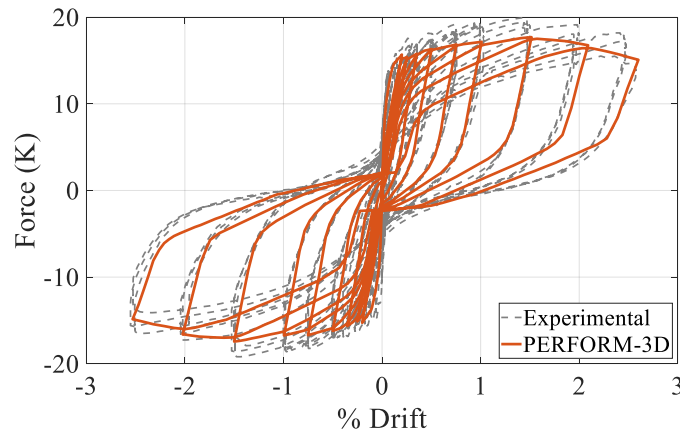


Figure 6.23 – C2 Cyclic Load Analysis Results

Table 6.5 – C2 Static Pushover and Cyclic Load Analyses Comparisons

Model	Initial Stiffness	Nominal Strength	Yield Drift	Yield Moment	Ultimate Drift	Peak Moment	Legend (% error)
Pushover	0.59	0.85	2.22	1.08	1.40	0.85	>1 overestimate
Cyclic Load	1.57	0.89	0.58	0.91	1.03	0.89	<1 underestimate

6.2.2.2 Wall C3

For the wall C3, there were similar concerns regarding strength, initial stiffness, and ductility. Quantitative values for these categories are shown in Table 6.6. The pushover showed a drastic underestimation in yield and peak strength, while overpredicting drift at yield and peak moments per Figure 6.24. However, the PERFORM-3D model for C3 more closely captured the experimental strength than C2. The drifts for C3, however, were more severely shifted, and the final drift for PERFORM-3D at 20% post peak strength-loss occurred much later than that of the experimental pushover, a discrepancy greater than that of C2. The PERFORM-3D cyclic load analysis for C3 was able to better capture the experimental strength than the static pushover, shown in Figure 6.25.

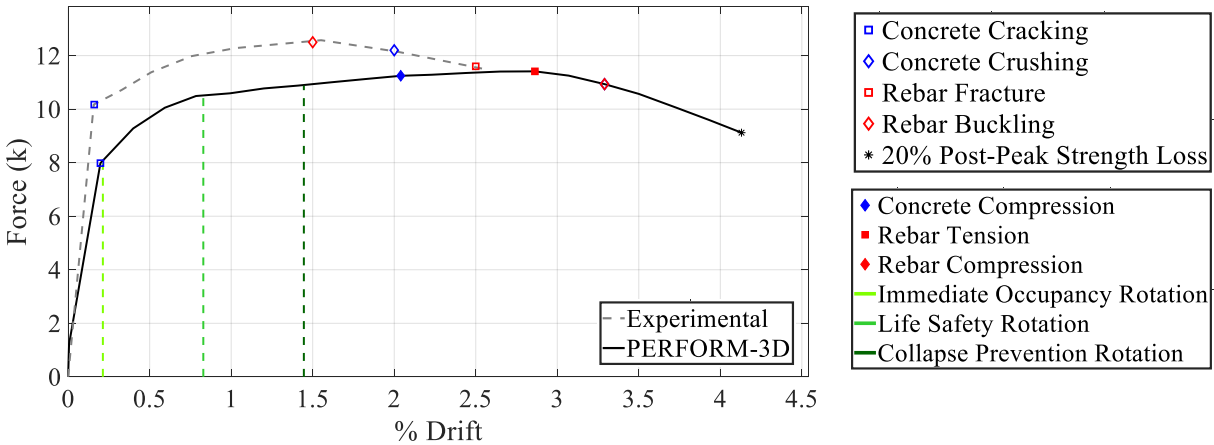


Figure 6.24 – C3 Static Pushover Analysis Results

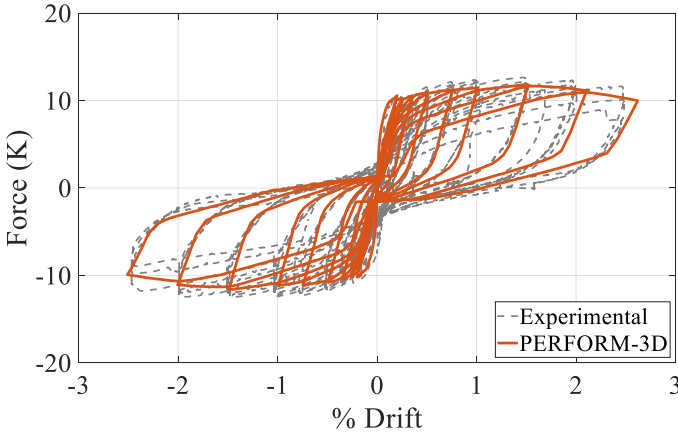


Figure 6.25 – C3 Cyclic Load Analysis Results

Table 6.6 – C3 Static Pushover and Cyclic Load Analyses Comparisons

Model	Initial Stiffness	Nominal Strength	Yield Drift	Yield Moment	Ultimate Drift	Peak Moment	Legend (% error)
Pushover	0.97	0.88	1.14	0.80	1.67	0.88	>1 overestimate
Cyclic Load	1.26	0.94	0.79	0.99	1.04	0.94	<1 underestimate

The PERFORM-3D results for both C2 and C3 indicate that the cyclic load analysis more adequately captured walls with moment gradients than the static pushover analysis. However, the results were still not able to sufficiently capture the strength and ductility of the experimental wall test. The PERFORM-3D results consistently underpredicted the wall’s resistance in comparison to the experimental test for these walls, leading the authors to believe the flaw was due to difficulty in applying and capturing the moment gradient. If the goal was to simulate walls C2 and C3 to be at twice and three times the height of C1, then the modeling method that considered the full wall height would have been able to capture the experimental results just as well as C1. Ultimately, due to the inconsistency in the trend of the cyclic results between C2 and C3 walls, the authors proceeded with using the pushover analysis results to compare the accuracy of the walls as these results are more consistent.

6.3 Modeling Recommendations

Conclusive modeling calibration on wall C1 and validation with walls C2, C3 and W1 led to the formation of the modeling recommendations in this section. General recommendations for meshing and materials modeling are provided, as well as suggestions specific to the completion of a static pushover analysis or a cyclic load analysis.

Meshing variation investigations conclusively proved that a finer mesh would converge on an accurate nominal strength prediction. The 7x7 mesh created elements with a 2:1 aspect ratio, height to width, respectively. Horizontal meshing should be determined by appropriately lumping curtains of rebar, but vertical meshing is dependent on the shear span ratio. While the 7x7 mesh was conclusive for walls C1 and

W1 in predicting strength, C2 and C3 were much more difficult to match to experimental results due to the additional moment gradient. The above recommendation of a 2:1 aspect ratio is suitable per story of wall.

Concrete and rebar material models were extensively investigated in this project, and the following conclusions were made based on the ability of these models to best replicate a wall's global strength, stiffness, and ductility of the experimental testing results. The concrete compression model should be based on Mander et. al [25]. The concrete tension model should be based on Hwang and Rizkalla [17] with the peak tension strength considered 20% of the modulus of rupture. The rebar tension model should be based on Menegotto and Pinto to peak tension strength and with the strength loss to 0.10 strain according to the rebar strength loss model investigation.

For a static pushover analysis, additional parameters were investigated to determine their necessity in an analysis. The inclusion of total strength loss at X did not change the pushover results out to 3% drift, indicating that it was unnecessary to include this factor. The inclusion of P-delta did not increase the accuracy of the pushover results and was not supported as a proper assumption for the testing set-up.

Investigations for the cyclic load analysis led to accurately capturing the energy dissipation and cyclic degradation found in the experimental test. The rebar cyclic degradation factors were set at $Y=1$ and $U=L=R=X=0.75$ to achieve accurate energy dissipation. The unloading and reloading stiffness factor of +1 was best suited for capturing the energy in the final hysteresis loops. The strength loss interaction factor of 0 found the best match to the observed cyclic degradation.

The meshing, concrete and rebar material model, static pushover analysis and cyclic load analysis modeling recommendations were determined to accurately capture the stiffness, strength, ductility, cyclic degradation, and energy dissipation of existing lightly reinforced concrete shear walls. The authors believe that more experimental testing of lightly reinforced concrete shear walls without boundary elements is necessary to further demonstrate that these PERFORM-3D recommendations are applicable for the common behavior and failure observed in past experimental tests of the aforementioned walls.

CHAPTER 7

WALL MODELING STRATEGY RESULTS

This chapter provides a summary of the different wall modeling strategies pursued. Simplified pushover analyses by Priestley [32] recommendations and ASCE 41-17 [4] guidelines were compared to the calibrated PERFORM-3D static pushover modeling results for each wall: W1, C1, C2, and C3. Then, the authors examined the effectiveness of each method as it relates to industry practitioners' goals. Finally, a set of modeling recommendations are provided to suggest a proper set of analyses to pursue for the analysis of lightly reinforced concrete shear walls.

7.1 Comparison of Results

After finalizing the static pushover analysis and the cyclic load analysis for each PERFORM-3D model, these results were compared to the simplified pushover methods of Priestley [32] and ASCE 41-17 [4]. Table 7.1a-d display the accuracy of each method to the experimental results with the most accurate method to match the experimental result for each criterion highlighted, and the final pushovers are plotted in Figure 7.1. The simplified pushover methods provided quick estimations of the wall behavior whereas the PERFORM-3D modeling method captured additional, detailed aspects of the wall.

Table 7.1a – W1 Quantitative Modeling Accuracy

Method	Initial Stiffness	Nominal Strength	Yield Drift	Yield Moment	Ultimate Drift	Peak Moment	Legend (% error)
Priestley	1.13	1.02	1.16	0.85	0.91	0.92	>1 overestimate
ASCE 41-17	2.29	0.97	0.73	1.09	0.45	0.91	=1 accurate
PERFORM-3D	1.17	1.09	1.20	1.06	1.56	1.09	<1 underestimate

PERFORM-3D = Best Match to Experimental Data

Table 7.1b – C1 Quantitative Modeling Accuracy

Method	Initial Stiffness	Nominal Strength	Yield Drift	Yield Moment	Ultimate Drift	Peak Moment	Legend (% error)
Priestley	1.06	0.98	1.16	1.01	0.65	0.92	>1 overestimate
ASCE 41-17	1.71	0.93	0.93	1.30	0.47	0.93	=1 accurate
PERFORM-3D	0.87	0.98	1.09	0.96	1.06	0.98	<1 underestimate

PERFORM-3D = Best Match to Experimental Data

Table 7.1c – C2 Quantitative Modeling Accuracy

Model	Initial Stiffness	Nominal Strength	Yield Drift	Yield Moment	Ultimate Drift	Peak Moment	Legend (% error)
Priestley	0.20	0.95	1.63	0.78	1.22	0.95	>1 overestimate
ASCE 41-17	0.30	0.91	1.40	1.00	0.64	0.96	=1 accurate
PERFORM-3D	0.59	0.85	2.22	1.08	1.40	0.85	<1 underestimate

PERFORM-3D = Best Match to Experimental Data

Table 7.1d – C3 Quantitative Modeling Accuracy

Model	Initial Stiffness	Nominal Strength	Yield Drift	Yield Moment	Ultimate Drift	Peak Moment	Legend (% error)
Priestley	0.33	0.93	2.46	0.82	1.65	0.92	>1 overestimate
ASCE 41-17	0.50	0.89	2.09	1.05	0.68	0.93	=1 accurate
PERFORM-3D	0.97	0.88	1.14	0.80	1.67	0.88	<1 underestimate

PERFORM-3D = Best Match to Experimental Data

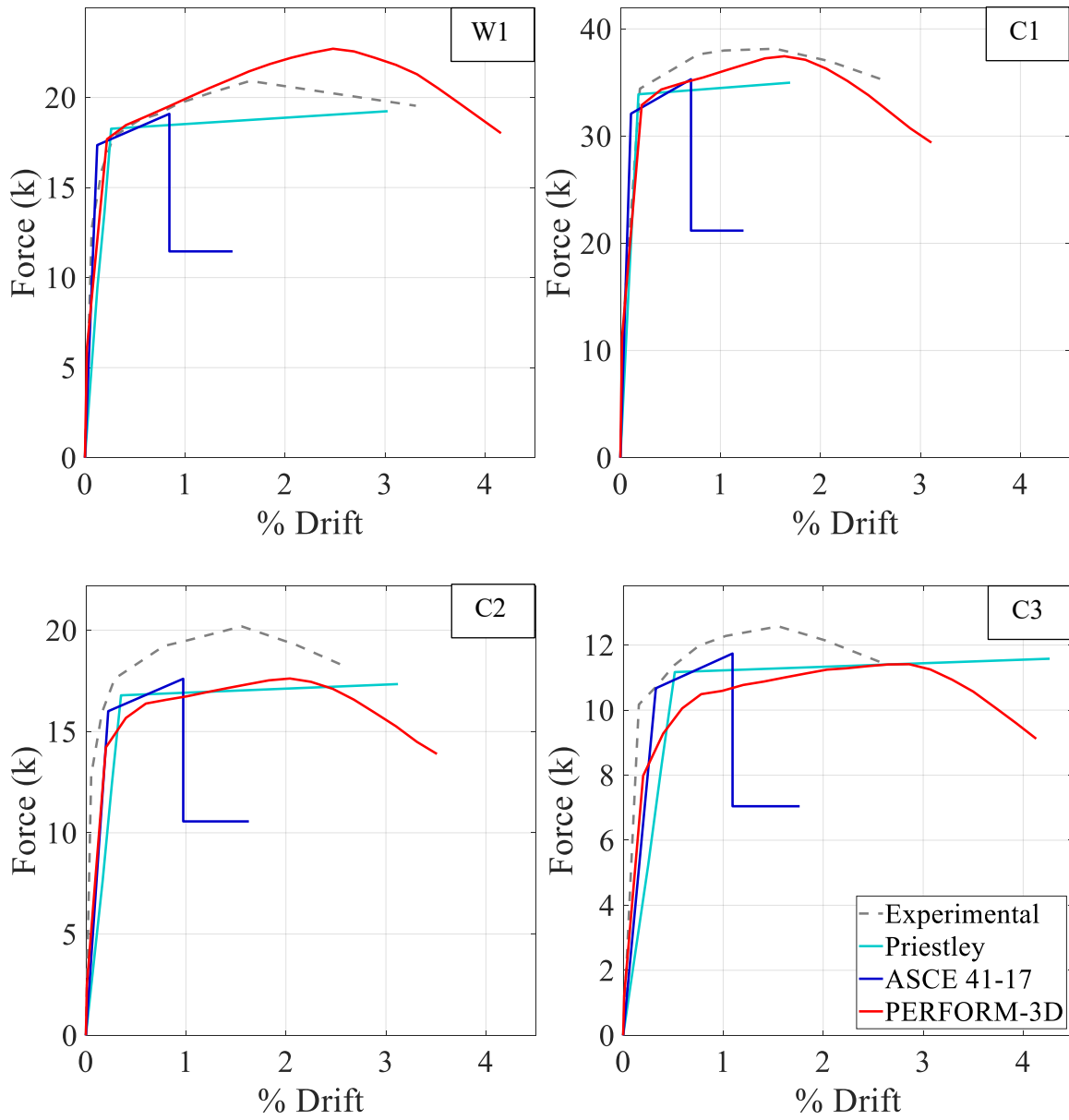


Figure 7.1 – Comparison of Wall Modeling Strategies

7.1.1 Wall W1

Priestley and ASCE 41-17 underestimated the strength of W1 by around 10% and PERFORM-3D was overestimating by a similar magnitude due to potential overestimation of the material properties input in PERFORM-3D. In terms of initial stiffness, the PERFORM-3D result seemed to match the Priestley quite well while ASCE 41-17 was severely overpredicting. The benefit of the PERFORM-3D result was the ability to capture ductility and the material's degradation, but it meant the drifts were largely overestimated in comparison to the simplified methods. Despite the discrepancies in the peak strength, the static pushover result from PERFORM-3D best captured the yield and peak moment. The Priestley method best captured the initial stiffness and nominal strength, and ASCE 41-17 method captured nominal strength and yield moment.

7.1.2 Wall C1

Wall C1 was the baseline calibration model for all other walls described in Section 7.1. Calibration parameters were made to this wall to capture the strength, initial stiffness, energy dissipation, and cyclic degradation of the experimental cyclic test result. As anticipated, the pushover generated from PERFORM-3D best matched the experimental results in comparison to the other walls. Similar to wall W1, the initial stiffness was more closely matched by PERFORM-3D and Priestley than with ASCE 41-17, which depicted a much stiffer wall. The peak strength predicted exactly by PERFORM-3D while the two simplified methods slightly underestimated the experimental results. Conclusively, the PERFORM-3D modeling most accurately captured the nominal strength, yield drift, peak drift, and moment of the experimental. Priestley best captured the initial stiffness, nominal strength, and yield moment. ASCE 41-17 closely captured the yield drift, while severely overpredicting and underpredicting other parameters.

7.1.3 Wall C2

The flawed implementation from the experimental protocol of a moment gradient for a wall twice the height of wall C1 led to unpredictable results for wall C2. Although the PERFORM-3D model was calibrated according to wall C1 and took into consideration the higher shear span ratio, the predictions for wall C2 were far from the experimental results. The authors experimented with various modeling techniques for C2 and C3 to best match the experimental results, as discussed in Chapter 6. The method that most closely captured the experimental result was to model C2 and C3 at the same height as C1 and applied a force couple to implement the superimposed moments. Not only was the strength severely underestimated, the stiffness and ductility were also not representative of the trending patterns prominent in C1 and W1. All three modeling strategies were depicting a wall significantly less stiff than the experimental shown to be. The nominal strength, yield moment, and peak moment were well captured by the three methods, while the other parameters remained incorrect. PERFORM-3D provided the most accurate initial stiffness. Priestley best captured nominal strength, peak drift, and moment. ASCE 41-17 best captured yield drift, yield moment, and peak moment.

7.1.4 Wall C3

The discrepancies in the results of wall C3 can be attributed to similar reasons as wall C2, specifically in the experimental protocol to model a wall three times taller than wall C1. The PERFORM-3D results for wall C3 strayed even farther from the experimental and simplified pushover results than C2 in terms of yield strength and moment. The initial stiffness was closely matched between PERFORM-3D, ASCE 41-17, and the experimental results. Other parameters seemed to be diverse, even between the two simplified methods, more so than the other walls. For initial stiffness and yield drift, PERFORM-3D best captured the experimental results. For nominal strength, Priestly slightly underestimated the experimental, while the other two remained close behind. ASCE 41-17, interestingly, captured yield moment, peak drift, and peak moment, best out of all three methods.

7.2 Analysis of Effectiveness

This section will summarize the usefulness of each wall modeling strategy as it relates to the results for wall W1 and C1 described in the previous section. Wall C2 and C3 were removed from this analysis due to the large variability in the methodology results that were due to an inability to replicate the moment gradient applied in experimental testing. The qualitative accuracy of each wall modeling strategy is displayed in Table 7.2 in relation to an average of the percent error calculated from wall W1 and C1 static pushover results. A summary of each methodology’s effectiveness is described in the following sections as it relates to initial, nominal, yield, peak, and ultimate performance.

Table 7.2 – Qualitative Accuracy for Wall W1 and C1

Method	Initial Stiffness	Nominal Strength	Yield Drift	Yield Moment	Ultimate Drift	Peak Moment	Legend (% error)	
Priestley								+20% and up
ASCE 41-17								+11% to + 20%
PERFORM-3D								0% to +/- 10%
								-11% to -20%
								-20% and up

7.2.1 Priestley

The Priestley method was conclusively accurate in capturing the nominal strength and ultimate moment. Small errors were found in predicting the initial stiffness, yield drift, yield moment, peak drift, and peak moment. The Priestley method was unsuccessful in capturing yield moment and ultimate drift. The Priestley method results were dependent on the plastic hinge length definition, which made it difficult to establish a condition that would apply to all lightly reinforced concrete shear wall cases. From the authors’ studies, regardless of generalized plastic hinge length definitions, the Priestley force-displacement bilinearization can be utilized for accurately predicting strength but not ductility. The authors advise that use of the Priestley method should be supplemented with an investigation of proper plastic hinge length assumptions.

7.2.2 ASCE 41-17

The ASCE 41-17 method was conclusively accurate in capturing the nominal strength. Small errors were found in predicting the peak moment. The ASCE 41-17 method was unsuccessful in capturing initial stiffness, yield drift and moment, peak drift, and ultimate drift and moment. The intent to be overly conservative in predicting peak and ultimate drift and moment are intentional for industry practitioners to design for a safety factor, but comparison to experimental results showed that these underestimations led to incorrectly predicting the wall behavior. The lack of accuracy captured by the ASCE 41-17 method proves that it would be difficult to have confidence in the accuracy of any of the predictions aside from nominal strength.

7.2.3 PERFORM-3D

The PERFORM-3D static pushover and cyclic load analyses results were conclusively accurate in capturing the nominal strength, yield moment, peak moment, ultimate drift, and ultimate moment. Additionally, the PERFORM-3D results were able to capture the cyclic degradation and energy dissipation that occurred. Errors were found in predicting the yield and peak drift. The abovementioned unsuccessful results on walls C2 and C3 require further investigation to prove that PERFORM-3D can be reliable for modeling the complete behavior of lightly reinforced concrete shear walls.

7.3 Methodology Recommendations

After evaluating the individual results of each method and utilizing the overall results obtained from wall W1 and C1, Table 7.3 describes the achievable results pertinent to accuracy and the required time. Based on this, PERFORM-3D is the best choice in terms of accuracy and ASCE 41-17 is the best choice in terms of required time.

Table 7.3 – Methodology Effectiveness for Wall W1 and C1

Method	Accuracy					Time	
	Stiffness	Strength	Ductility	Cyclic Degradation	Energy Dissipation	Analysis	Review
Priestley	✓	✓	-	N/A	N/A	moderate	slow
ASCE 41-17	+	✓	-	N/A	N/A	quick	quick
PERFORM-3D	✓	✓	✓	✓	✓	slow	moderate

Two different analysis options are recommended below: minimum accuracy and time versus maximum accuracy and time. It is the authors’ opinions that these methods can be used individually, but validation of nominal strength and code compliancy against computer simulation modeling can be obtained by running both analysis methods simultaneously.

1. *Minimum Accuracy and Time:* To achieve quick results on the nominal strength of a wall, the ASCE 41-17 simplified pushover analysis is the best choice. As the standard code method for analyzing existing walls, the analysis and review time for this method is the quickest of the three methods. However, caution should be taken in using this method to predict anything other than strength. If stiffness is overestimated and ductility is underestimated, the incorrect retrofit solution could be applied to the reinforced concrete shear wall under analysis. This risk combined with the inability to observe material degradation behavior does not make the ASCE 41-17 method appropriate for any prediction other than nominal strength.
2. *Maximum Accuracy and Time:* To achieve accurate results in stiffness, strength, ductility, cyclic degradation, and energy dissipation the PERFORM-3D analysis method is the best choice. This method does require more time to create and run an analysis model and an in-depth peer review. However, the authors believe that with the correct modeling parameters recommended in Chapter 6 and familiarity with PERFORM-3D that can be gained through tutorials, this is the superior wall modeling strategy.

CHAPTER 8

DESIGN-BUILD-TEST PREPARATIONS

After investigating various parameters to improve the accuracy of computer simulation and prediction of lightly reinforced concrete shear wall behavior, the authors recognized that the future of this project is to design, construct and test a typical lightly reinforced wall in the High Bay laboratory on the Cal Poly campus. The following chapter describes the preparations made by the authors for experimental for such a test. Reinforced concrete shear wall behavior studies by each author and an industry survey will provide guidance to the next students undertaking this research.

8.1 Reinforced Concrete Shear Wall Behavior Studies

While enrolled in an Engineering Risk Analysis course (CE 448) during Fall 2019, the authors conducted reinforced concrete shear wall behavior studies on the flexural capacity and failure mechanisms of planar lightly reinforced concrete shear walls. The purpose of these studies was to find basis for predicting the behavior and failures observed in large-scale experimental tests.

8.1.1 Flexural Capacity of Walls

To better study the behavior of lightly reinforced concrete walls, past experimental test programs have investigated the behavior of large-scale rectangular walls. A crucial aspect in a wall's ability to withstand these loading is the flexural strength in the wall. This is the amount stress the material can withstand such that it resists any bending failures. This study will focus on the effect of the uncertainty of components that go into the equation for flexural strength of rectangular shear walls. These shear walls contain uniformly distributed vertical reinforcement and subjected to an axial load smaller than that producing a balanced failure condition. The findings will allow the authors to identify variables that can significantly impact the strength of the wall and manipulate those variables to achieve the desired strength.

8.1.1.1 Flexural Strength Calculation

The flexural strength of rectangular shear walls containing uniformly distributed vertical reinforcement and subjected to an axial load smaller than that producing a balanced failure condition can be approximated as shown in Equation 1 [1].

$$Mu = 0.5A_sF_y\ell_w\left(1 + \frac{N_u}{A_sF_y}\right)\left(1 - \frac{c}{\ell_w}\right) \quad [\text{Equation. 1}]$$

Where M_u = design resisting moment at section, in-lbs.

A_s = total area of vertical reinforcement at section, in^2

F_y = specified yield strength of vertical reinforcement, psi.

ℓ_w = horizontal length of shear wall, in.

N_u = design axial load, positive if compression, lbs.

c = distance from extreme compression fiber to neutral axis, in

the distance from the extreme compression fiber to the neutral axis, c , can be described by Equations 2-4.

$$c = \frac{(\omega + \alpha)}{(2\omega + 0.85\beta_1)} \ell_w \quad [\text{Equation 2}]$$

$$\omega = \frac{A_s f_y}{\ell_w h f'_c} \quad [\text{Equation 3}]$$

$$\alpha = \frac{N_u}{\ell_w h f'_c} \quad [\text{Equation 4}]$$

β_1 is the ratio of depth of rectangular concrete stress block to the depth to the neutral axis of the wall, it can be described by Equation 5.

$$\beta_1 = 0.85 - \frac{0.05*(f'_c - 4000)}{1000} \quad [\text{Equation 5}]$$

Where

f'_c = specified compressive strength of concrete, psi

h = total thickness of shear wall

The following data was taken from the research of Cardenas et. al [7] on the testing of six rectangular reinforced shear wall specimens subjected to static loads, specifically focusing on wall SW-1. This test was the standard test to determine the strength of lightly reinforced concrete shear walls. The flexural strength of SW-1 using Equations 1-5 is shown in Table 8.1.

Table 8.1 – Summarized Dimension and Material Properties of Test Specimens

l_w (in)	h (in)	f'_c (psi)	f_y (psi)	N_u (lb)	A_s (in ²)	ω	α	β_1	c (in)	M_u (lb – in)
75	3	7420	60750	93375	0.675	0.0221	0.0559	0.679	9.419	4406420

8.1.1.2 Percent Relative Contribution to Variance

In this section, uncertainty in Equation 1 will be evaluated, the full Matlab script can be found in Appendix B.1.1. With this equation, each variable is being treated as a random variable with an unknown distribution so the first order second moment (FOSM) approach will be used to approximate each mean and standard deviation for their respective random variable [27]. The mean for each variable comes from the data in Table 8.1. To calculate the total mean, the Equation 6 below was implemented.

$$\mu_{Mu} = 0.5\mu_{As}\mu_{fy}\mu_{\ell_w}\left(1 + \frac{\mu_{Nu}}{\mu_{As}\mu_{fy}}\right)\left(1 - \frac{\mu_c}{\mu_{\ell_w}}\right) \quad [\text{Equation 6}]$$

To calculate the effect of the uncertainty of components in the equation for flexural strength of rectangular shear walls, a coefficient of variation will be assigned to investigate how variation in each parameter correlated to how much the contribution of each variable change. With that, the standard deviation Equation 7 was used in Matlab for the FOSM approach.

$$\sigma_{Mu}^2 = \sigma_{As}^2 \left(\frac{\partial Mu}{\partial As}\right)^2 + \sigma_{fy}^2 \left(\frac{\partial Mu}{\partial fy}\right)^2 + \sigma_{\ell_w}^2 \left(\frac{\partial Mu}{\partial \ell_w}\right)^2 + \sigma_{Nu}^2 \left(\frac{\partial Mu}{\partial Nu}\right)^2 + \sigma_c^2 \left(\frac{\partial Mu}{\partial c}\right)^2 \quad [\text{Equation 7}]$$

By assigning a coefficient of variation of 5%, the data can have a small variation in the result. With this, other values of coefficient of variations were assigned to see how much the contribution of each variable

change as the data varies. To perform this in Matlab, the equation being evaluated is the mean equation σ_{Mu}^2 , Table 8.2 shows the results from Matlab.

Table 8.2 – Differentials of Random Variables

	<u>As</u>	<u>Fy</u>	<u>Lw</u>	<u>Nu</u>	<u>c</u>
Differentials	1.992e+06	22.134	67191	32.79	-67191

A benefit to using the FOSM method is that it allows a sensitivity analysis to be implemented on the equation of interest and how the uncertainty of each individual variable impacts the resultant. Looking at the variance, the uncertainty from the input parameter propagates as the product of the variance and the squared partial derivative of σ_{Mu}^2 with respect to each random variable. The variance when divided by total resultant uncertainty, provides the percent relative contribution to variance (RCV%) from each random variable. Equation 8 was implemented for RCV%.

$$RCV\% = \frac{\sigma_{x_i}^2 \left(\frac{\partial Mu}{\partial x_i} \right)^2}{\partial Y^2} \quad [\text{Equation 8}]$$

The standard deviation calculation shown in Equation 8 calculated by component. To calculate the percent relative contribution to variance, each component of variable is divided by the total variance of all components. The results are shown in Table 8.3.

Table 8.3 – Percent Relative Contribution to Variance of Random Variables

	<u>As</u>	<u>Fy</u>	<u>Lw</u>	<u>Nu</u>	<u>c</u>
RCV%	4.6615	4.6615	65.474	24.17	1.0327

8.1.1.3 Results

Based on the results in Table 8.3, the most prominent contributor to the flexural strength equation of rectangular shear walls is the horizontal length of shear wall (ℓ_w) followed by design axial load (N_u). Therefore, in the design of a wall as a lateral force resisting member in a building, the length of the lateral

force resisting member in a building, the longer the wall, the greater load resistance or flexural strength. The greater the axial load applied to the wall, the lower the flexural strength. The FOSM process helps identify how much each variable contributes to the overall equation informing engineer how to best modify the design to maximize wall performance.

8.1.2 Fault Tree Analysis of Wall Failure Mechanisms

An unexpected tension-controlled failure in the de Sevilla et. al. [11] experimental test prompted the authors to seek an answer for why this happened instead of the intended compression-controlled failure . To ensure that the next large scale physical test at Cal Poly will produce a compression-controlled failure, the authors performed an engineering risk analysis on three variables that contribute to reinforced concrete shear wall response: axial load ratio, vertical reinforcement ratio, and presence of boundary elements.

The wall failures can be categorized as either flexure or shear, and further categorization of the former as either tension-controlled or compression-controlled. The investigation involved 56 wall tests from 12 different experimental testing programs, this analysis intended to capture a wide array of different testing outcomes. A summary table of the data set can be found in Appendix B.2.

8.1.2.1 Analysis Method

The fault tree analysis approach illustrated in Figure 8.1 can be implemented to effectively organize and evaluate the wall data set. The fault tree begins with dividing the data set as either flexure or shear failures, and then further divided specifically as either tension-controlled or compression-controlled.

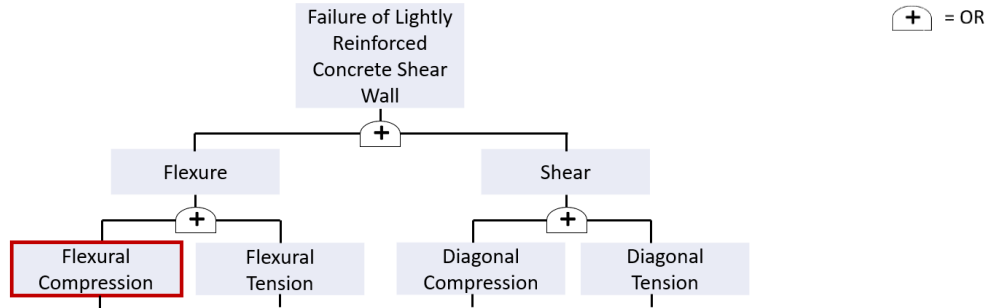


Figure 8.1 – Fault Tree Analysis Stem

Each of these specific failure modes are defined as:

- Flexural Compression: compression failure at wall ends due to concrete crushing
- Flexural Tension: tension failure due to fracture of multiple flexural rebar
- Diagonal Compression: web crushing
- Diagonal Tension: diagonal cracking along wall

From each of these specific failure modes, the data set is divided into wall specifications—axial load ratio, vertical reinforcement ratio, and boundary elements—shown for the Flexural Compression in Figure 8.2.

A detailed, complete fault tree with probabilities for each parameter can be found in Appendix B.2.

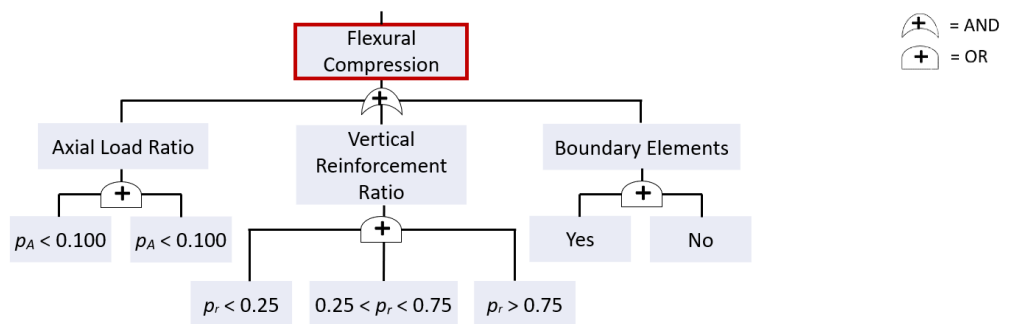


Figure 8.2 – Fault Tree Analysis Flexural Compression Branch

8.1.2.2 Results

Using the previously created fault tree analysis, it was possible to create a set theory that could find the probability associated with each wall specification and failure mode combination. Below is an example of the set theory that was implemented. All the set theory results can be found in Appendix B.2.

- Failure Mode: Flexure (E1)
 - Specific Failure Mode: Compression (E2)
 - Wall Specifications:
 - Axial Load Ratio: $p_A < 0.100$ (E4)
 - Vertical Reinforcement Ratio: $p_r < 0.25$ (E6)
 - Boundary Elements: Yes (E9)

In set theory this would look like: $P(E1 \cup E2 \cup (E4 \cap E6 \cap E9)) = E1 + E2 + (E4 \times E6 \times E9)$

One point of interest in the results were the wall specifications related to flexural tension failure:

- Axial Load Ratio: $p_A < 0.100$
- Vertical Reinforcement Ratio: $0.25 < p_r < 0.75$
- Boundary Elements: No

It is of little surprise that the wall specifications used by de Sevilla et. al [11] and Lu et. al [24] are in line with what the fault tree analysis predicted:

- Axial Load Ratio: $p_A < 0.100$
- Vertical Reinforcement Ratio: $p_r = 0.37$
- Boundary Elements: No

This gives further proof that the fault tree analysis is reliable. Now we can look at the wall specifications related to flexural compression failure:

- Axial Load Ratio: $p_A > 0.100$
- Vertical Reinforcement Ratio: $p_r > 0.75$
- Boundary Elements: Yes

From this fault tree analysis, the authors concluded that very lightly reinforced concrete walls without boundary elements are unlikely to fail in flexural compression as industry practitioners had predicted. These wall specifications will inform the wall specifications that will be chosen for future experimental tests.

8.2 Industry Survey on Existing Concrete Buildings

8.2.1 Survey Implementation

8.2.1.1 Survey Goals

Discovery of lightly reinforced concrete shear walls not performing as expected by de Sevilla et. al. [11] and Lu et. al. [24] led the authors to investigate the existing walls and wall modeling strategies that industry practitioners are using to determine wall capacity and failure. The authors reached out to industry practitioners to describe the typical properties of flexure dominated, lightly reinforced concrete structural walls found in existing buildings and subject to the Los Angeles Ordinance 183893, Non-Ductile Concrete Retrofit Program or a similar non-ductile concrete ordinance. The authors were seeking information from consulting engineers regarding their experiences analyzing and retrofitting these walls to develop realistic wall specimens for future large-scale testing at Cal Poly.

8.2.1.2 Survey Questions

The flowchart in Figure 8.3 highlights the layout for two different survey versions: a short form where survey takers submit drawing exhibits instead of filling out numerical entries and a long form for sensitive projects that required a higher level of confidentiality. The full length surveys can be found in Appendix C.

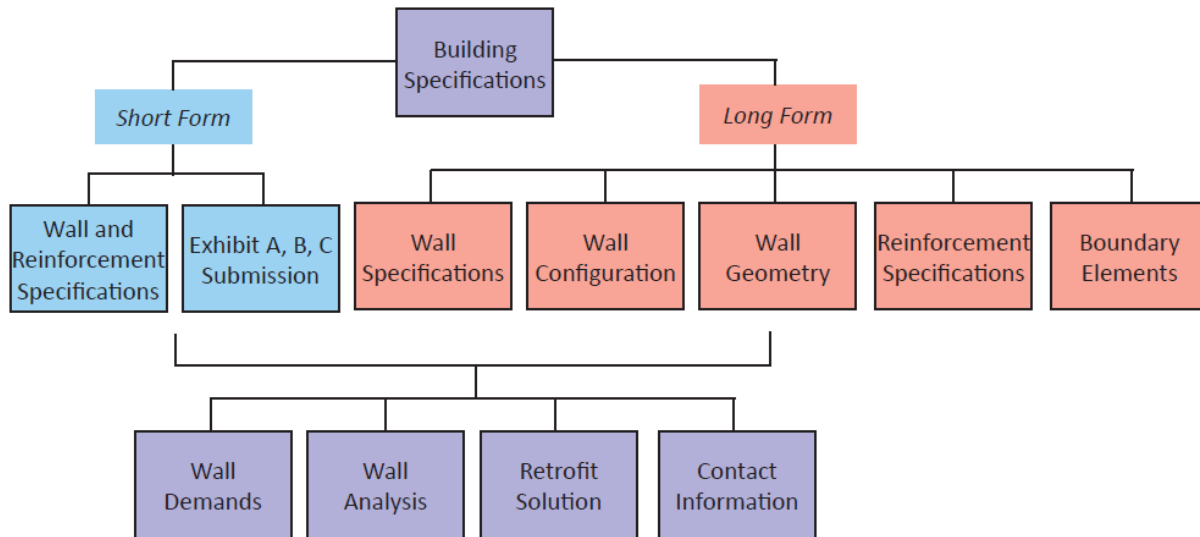


Figure 8.3 – Survey Flowchart

Both survey versions began with *Building Specifications* building sector, year constructed, location, and stories, then the survey was specific to the chosen version.

For the long form, the survey taker provided:

- *Wall Specifications*: concrete strength, full wall height, and first floor wall height
- *Wall Configuration*: planar; T-shaped; C-shaped; L-shaped; barbell
- *Wall Geometry*: wall length, wall and/or flange thickness(es), and wall openings/perforations.
- *Reinforcement Specifications*: reinforcement strength, vertical and horizontal bar sizes and spacing, layers of rebar in each direction, foundation conditions (hook and/or splice), and a description of any abnormal reinforcement types or configurations.
- *Boundary Elements*: length and height, and tie reinforcement strength, size, spacing, and configuration (should the survey taker specify the existence of boundary elements)

For the short form, the survey taker would complete *Wall and Reinforcement Specifications* to provide concrete and reinforcement details and then submit three exhibits to provide information that would otherwise be input for the long form version: (A) a wall elevation, (B) a wall cross section, and (C) a wall schedule.

Finally, survey takers of both versions are asked to provide:

- *Wall Demands*: gravity and lateral loads
- *Wall Analysis*: performance objective, analysis method, and modeling software.
- *Retrofit Solution*: wall retrofit options and final, pursued design.
- *Contact Information*: participate in further questions or to provide advice to the authors.

8.2.1.3 Survey Distribution

The survey was primarily distributed by email with the letter of investigation in Appendix C.1. In addition to emails, the authors presented their research progress to a panel of industry advisors to recruit survey takers and solicit feedback on the survey layout. Thirty-six industry practitioners were contacted, amongst which fifteen survey responses were collected, organized by building locations in Table 8.4. The survey contributors were past and current industry practitioners in California.

Table 8.4 – Survey Responses by City

City	# of Responses
Sacramento	1
San Francisco	3
Los Angeles	10
San Diego	1

8.2.2 Survey Results

8.2.2.1 Building Demographics

The building age and occupancy distribution, shown in Figure 8.4 and Figure 8.5, respectively, give insight on the typical building demographics for non-ductile concrete buildings. A majority reported were either hospital or commercial buildings and built in the 1950s-1960s. Previous discussions with industry suggest that hospitals that meet non-ductile concrete ordinances are often demolished instead of retrofitted due to current analyses indicating that the walls are inadequate for the code required performance levels. However, the research conclusions from Chapter 7 demonstrating the higher than anticipated ductility in experimental tests and replicated through PERFORM-3D modeling, it is possible that these buildings are being unnecessarily demolished.

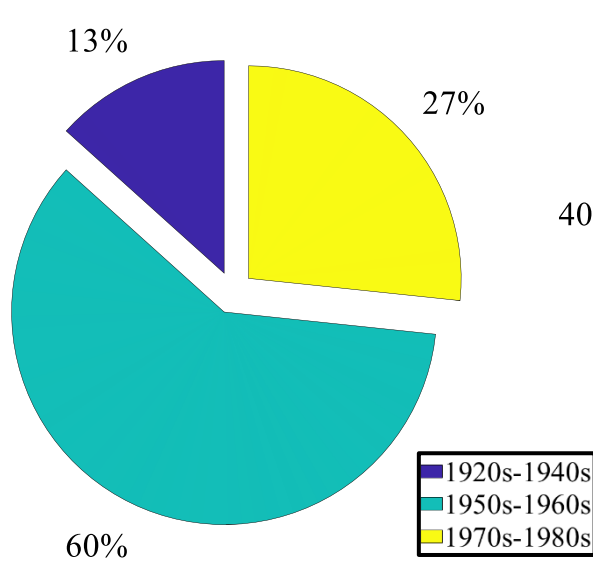


Figure 8.4 – Year Built

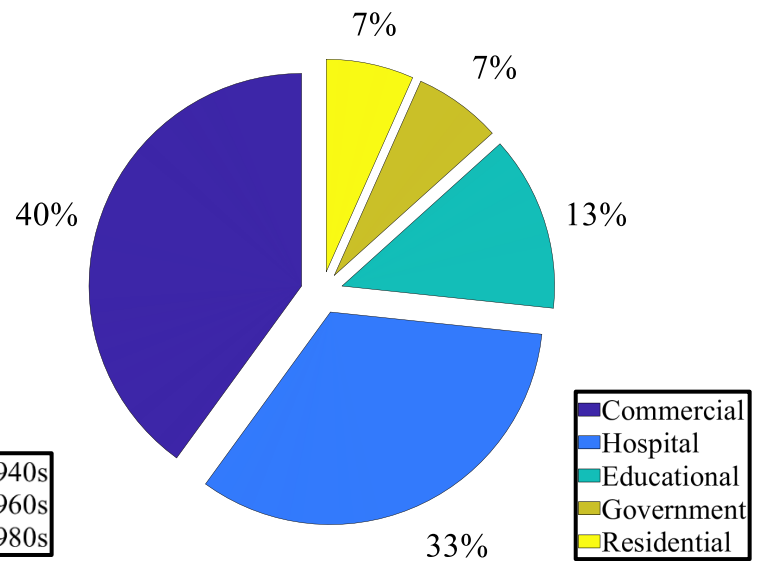


Figure 8.5 – Building Sector

8.2.2.2 Concrete Properties and Wall Geometry

Common wall characteristics are summarized in the bar chart per Figure 8.6 related to concrete strength and wall geometry. Responses to each survey are shown on the x-axis and frequency of the answer along the y-axis. Most of the engineers responded with 3 ksi concrete and planar shaped walls. The aspect ratio, the first story height to wall length ratio, was indicated to be 0.5-0.6 by most of the practitioners. Finally, as for wall thickness, most practitioners indicated to have 10 in walls, which are relative to the half-scaled testing of W1 (5 in) and C1-C3 (5.91 in).

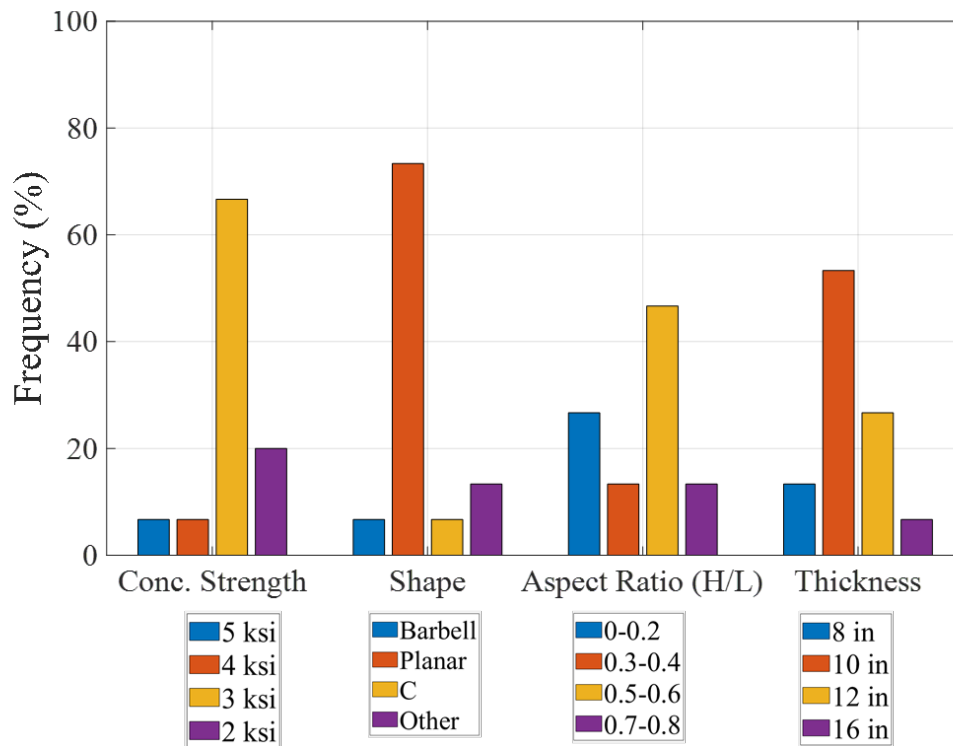


Figure 8.6 – Wall Characteristics

8.2.2.3 Rebar Properties

Reinforcement characteristics of the wall are shown in Figure 8.7. Most of the surveyors selected 40 ksi rebar strength along with 0.26-0.40% of vertical and horizontal reinforcement ratios. Further questions were asked regarding the detailing specifics of common wall are shown in Table 8.5.

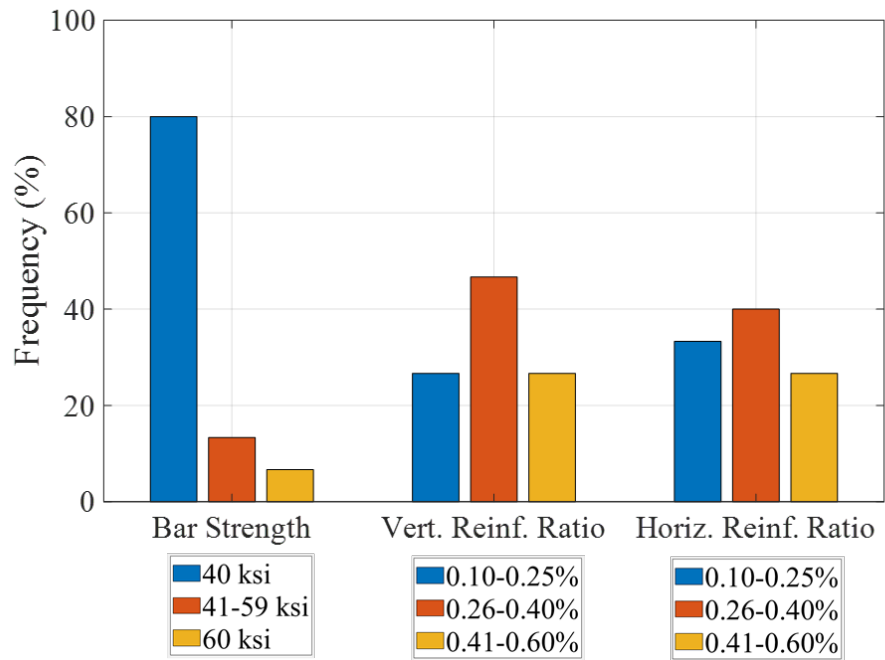


Figure 8.7 – Reinforcement Characteristics

Table 8.5 – Reinforcement Specifications

Vertical Reinf. Specification			Horizontal Reinf. Specification		Tie Specification		
Layer	Bar Spliced	Bars Hooked at Wall Base	Layer	Boundary	Strength	Configuration	Size
Double	Yes	Yes	Double	None	40 ksi	Rectilinear	#3

8.2.2.4 Analysis Method

In addition to wall characteristics, the engineers were asked to provide insight on the analysis stage of their projects. The results indicate that majority of analyses for existing concrete structures were triggered by local and state building ordinances, shown in Figure 8.8, but surprisingly many requests were made by owners themselves, suggesting there is increased interest by building owners to be proactive in creating earthquake resilient communities. However, this is not always the case in communities where retrofit ordinances leave building owners to increase tenant rents or provide large funds up front. Continued education to the community on the importance of building longevity is necessary.

The practitioners were also asked to describe the chosen wall analysis method, shown in Figure 8.9. Eighty percent specified the use of shell elements in ETABS and only twenty percent used shear wall elements in PERFORM-3D as the authors similarly pursued in Chapter 5. Despite being a more sophisticated program, PERFORM-3D lacks a user-friendly interface and limited resources are available to help users gain a deeper understanding of the program. For this reason, the authors have provided practitioners guidance on modeling assumptions in Chapter 6 on modelling walls in PERFORM-3D as well as a general wall tutorial video for this software [37].

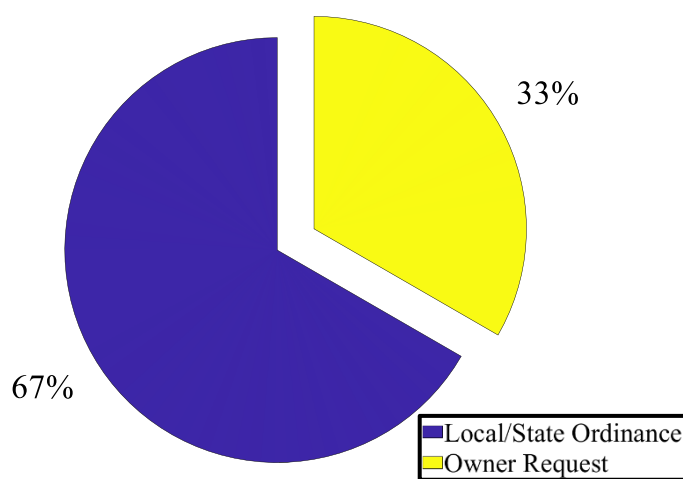


Figure 8.8 – Analysis Trigger

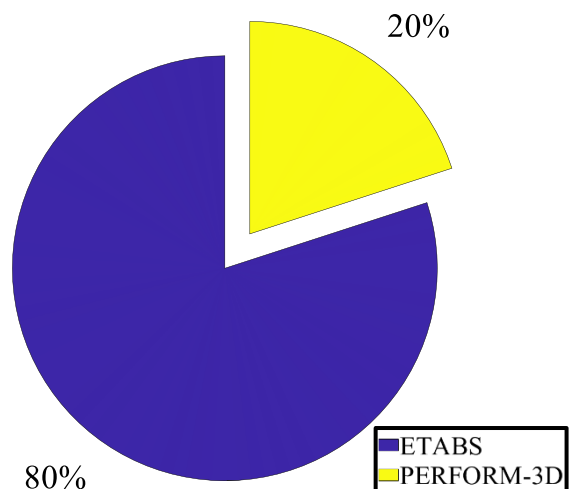


Figure 8.9 – Analysis Method

8.2.2.5 Retrofit Solution

When choosing retrofit solutions, shown in Figure 8.10, practitioners and their clients were more likely to choose to shotcrete walls or use FRP strengthening to protect against lightly reinforced concrete shear wall failure. Practitioners commonly specified that the solution they chose was for ease of construction and inexpensive cost, shown in Figure 8.11. The next team of Cal Poly researchers to physically test a wall retrofit will need to choose a solution that focuses on those driving decision factors – time and money.

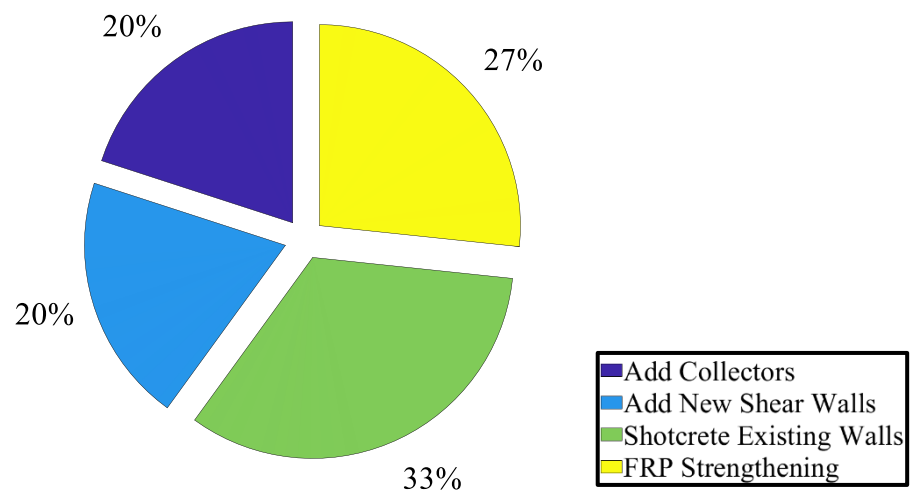


Figure 8.10 – Retrofit Solution Pursued

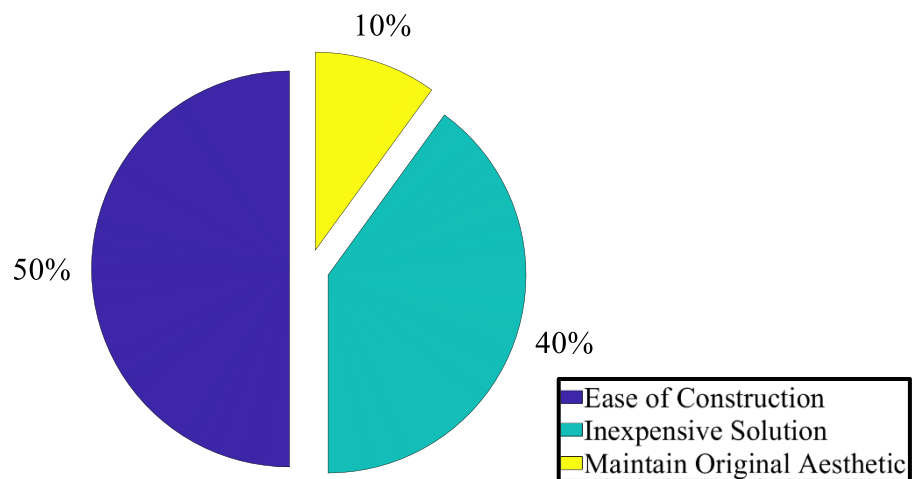


Figure 8.11 – Retrofit Solution Decision Factor

8.3 Future Design-Build-Test Recommendations

This chapter provides a basis for determining the design parameters that should be considered for the next large-scale physical baseline and retrofit tests of a lightly reinforced concrete shear walls at Cal Poly.

The independent study of the flexural capacity of walls concluded that the wall length and axial load will be the largest contributors to the ultimate moment strength of the wall. The students who design the next wall will be able to improve the behavior and performance of the wall design by increasing the wall length and decreasing the axial load.

The independent study on wall failure mechanisms provided key design parameters to implement if the goal of the test is to produce a flexural tension failure or a flexural compression failure. For a flexural tension failure, the study advised that the axial load ratio should be less than 0.100, the vertical reinforcement ratio should be between 0.25 and 0.75, and that boundary elements should not be included. For a flexural compression failure, the study advised that the axial load ratio should be less than 0.100, the vertical reinforcement ratio should be greater than 0.75, and that boundary elements should be included.

The industry survey determined the appropriate wall design parameters that will be most relevant to investigate via a large-scale to inform industry practitioners. The walls should be planar, have 3ksi concrete strength, have an aspect ratio of 0.5-0.6, and have a full-scale thickness of 10 inches. The most prominent reinforcement parameters were 40ksi rebar strength, double layers, and 0.26% - 0.40% horizontal and vertical reinforcement ratios. Vertical reinforcement should be spliced and hooked into the base, with minimal boundary element reinforcement – #3 rectilinear or u-hook ties, if any. As the next student designers pursue a retrofit solution for their wall, the industry practitioners indicated that ease of construction and inexpensive cost would be the driving decision factors.

These recommendations will provide guidance on the necessary next steps for a design, build, test, and retrofit of a lightly reinforced concrete shear wall that aligns with academic and industry experiences.

CHAPTER 9

REFERENCES

- [1] ACI 318-14, Building Code Requirements for Structural Concrete, American Concrete Institute, 2014.
- [2] Alarcon, C., M. A. Hube and J. C. de la Llera. 2014. Effect of axial loads in the seismic behavior of reinforced concrete walls with unconfined wall boundaries. *Engineering Structures*, 73: 13-23.
- [3] Applied Technology Council (ATC). “Modeling and acceptance criteria for seismic design and analysis of tall buildings,” Prepared by Applied Technology Council for the Pacific Earthquake Engineering Research Center, Redwood City, California, Tech. Rep. Report No. PEER/ATC-72-1, 2010.
- [4] ASCE 41-17, Seismic Evaluation and Retrofit of Existing Buildings, American Society of Civil Engineers, 2017.
- [5] Behrouzi, Anahid A., et al. “Impact of Cross Section, Web Reinforcement and Load History on the Seismic Performance of Slender Concrete Walls.” University of Illinois at Urbana-Champaign, 2016.
- [6] B. Scott, R. Park, and M. Priestley. Fiber element modeling for seismic performance of bridge columns made of concrete-filled frp tubes. *Journal of the American Concrete Institute*, 79(1):13{27, 1982.
- [7] Cardenas, Alex E. and Magura, Donald D. “Strength of High-Rise Shear Walls - Rectangular Cross Section.” 1972.
- [8] Chadwell, C.B., and R.A. Imbsen, “XTRACT: A Tool for Axial Force-Ultimate Curvature Interactions,” Proceedings for 2004 ASCE-SEI Structures Congress, 2004.
- [9] Computers and Structures, Inc. “User Guide PERFORM-3DTM: Nonlinear Analysis and Performance Assessment for 3D Structures”. CSI, June 2011.

- [10] Dazio, A., K. Beyer, and H. Bachmann. 2009. Quasi-static cyclic tests and plastic hinge analysis of RC structural walls. *Engineering Structures*, 31(7): 1556-1571.
- [11] De Sevilla et al., "Feasibility of a Fiber Reinforced Polymer Retrofit for Non-Ductile Concrete Walls," 2019 SEAOC Convention Proceedings, 2019.
- [12] Deng, K., Pan, P., Shi, Y., Miao, Q., Li, W., and Wang, T. "Quasistatic test of reinforced concrete shear wall with low concrete strength and reinforcement ratio." Hong Kong, 2012.
- [13] Greifenhagen, C., and Lestuzzi, P. "Static cyclic tests on lightly reinforced concrete shear walls." *Eng. Struct.*, 2005.
- [14] Hagen, Garrett. Personal Interview. 11 March 2020.
- [15] Hidalgo, P. A., Ledezma, C. A., and Jordan, R. M. "Seismic behavior of squat reinforced concrete shear walls." *Earthquake Spectra*, 2002.
- [16] Hube, M. A., A. Marihuén, J. C. de la Llera and B. Stojadinovic. 2014. Seismic behavior of slender reinforced concrete walls. *Engineering Structures*, 80: 377-388.
- [17] Hwang, L., and S. Rizkalla. "Effective Tensile Stress-Strain Characteristics for Reinforced Concrete." Department of Civil Engineering, University of Manitoba, Winnipeg.
- [18] Kent and Park. Flexural members with confined concrete. *ASCE Journal of Structural Division*, 97:1969-1990, 1971.
- [19] Kuang, J. S. and Y. B. Ho. 2007. Enhancing ductility of non-seismically designed RC shear walls. *Proceedings of the Institution of Civil Engineers: Structures and Buildings*, 160(3): 139-149.
- [20] Kuang, J. S. and Y. B. Ho. 2008. Seismic behavior and ductility of squat reinforced concrete shear walls with nonseismic detailing. *ACI Structural Journal*, 105(2): 225-231.
- [21] Lowes, Laura & Baker, Carson, "Recommendations for Modeling the Nonlinear Response of Slender Reinforced Concrete Walls Using PERFORM-3D", 2016 SEAOC Convention Proceedings, 2016.

- [22] Lowes, L. N., D. E. Lehman, A. C. Birely, D. A. Kuchma, K. P. Marley, and C. R. Hart. 2012. Earthquake response of slender planar concrete walls with modern detailing. *Engineering Structures*, 43: 31-47.
- [23] Lu, Yiqiu, et.al., “Cyclic Testing of Reinforced Concrete Walls with Distributed Minimum Vertical Reinforcement,” *Journal of Structural Engineering*, vol. 143, no. 5, 2017.
- [24] Lu, Yiqiu, et. al., “Seismic Design of Lightly Reinforced Concrete Shear Walls,” University of Auckland Research Repository, 2017.
- [25] Mander, J.B., et. al., “Theoretical Stress-Strain Model for Confined Concrete.” *Journal of Structural Engineering*, 1984.
- [26] Menegotto, M., and Pinto, P.E., “Method of Analysis of Cyclically Loaded RC Plane Frames Including Changes in Geometry and Non-Elastic Behavior of Elements Under Normal Force and Bending”. Preliminary Report IABSE, v. 13, 1973.
- [27] Moss, R. E. S. “Applied Civil Engineering Risk Analysis.” Springer Nature Switzerland AG, 2020.
- [28] Oh, Y. H., S. W. Han, and L. H. Lee. 2002. Effect of boundary element details on the seismic deformation capacity of structural walls. *Earthquake Engineering and Structural Dynamics*, 31(8): 1583-1602.
- [29] Park, R. “Evaluation of Ductility of Structures and Structures and Structural Assemblages from Laboratory Testing”. *Bulletin of the New Zealand National Society for Earthquake Engineering*, Vol. 22, No.3, September 1989.
- [30] Popovics, S., "A Numerical Approach to the Complete Stress-Strain Curves for Concrete." *Cement and Concrete Research*, v. 3, 583-599, 1973.
- [31] Powell, Graham. “Nonlinear Analysis and Performance Assessment for 3D Structures: Shear Wall Example”. CSI, January 2007.
- [32] Priestley, M. J. N., et. al., “Displacement-Based Seismic Design of Structures,” EUCENTRE, 2017.
- [33] Seymour, Emmett, et al. “Inventory of Non-Ductile Concrete Buildings in High Seismic Risk Areas of California.” Pacific Earthquake Engineering Research Center, 2009.

- [34] Thomsen Iv, J. H., and J. W. Wallace. 2004. Displacement-based design of slender reinforced concrete structural walls - Experimental verification. *Journal of Structural Engineering*, 130(4): 618-630.
- [35] Tran, T., and J. Wallace. 2014. Cyclic behavior of special reinforced concrete shear walls. Tenth U.S. National Conference on Earthquake Engineering 10NCEE, *Frontiers of Earthquake Engineering*, Anchorage, Alaska.
- [36] Tran, T. A. 2012. Experimental and Analytical Studies of Moderate Aspect Ratio Reinforced Concrete Structural Walls. 3541917 Ph.D., University of California, Los Angeles.
- [37] Williams, Jenna. "PERFORM-3D Concrete Shear Wall Tutorial". YouTube, 11 May 2020, <https://www.youtube.com/watch?v=dWwgRHLRLjY>.
- [38] NZS (Standards New Zealand). "Concrete structures standard (Amendment 2)." Wellington, New Zealand, 2006.

APPENDIX A

PERFORM-3D ANALYSIS

This appendix provides context to the PERFORM-3D parametric study performed in Chapter 5 and 6. Appendix A.1 details the PERFORM-3D modules and set up for one of the parametric study models: Model 36. Appendix A.2 includes the parametric study matrix on wall C1 with model information regarding mesh and material modeling as well as the static pushover results for each model. The limit states and PERFORM-3D curve can be visually compared to the experimental test results out to 3% drift.

A.1 Phase 1

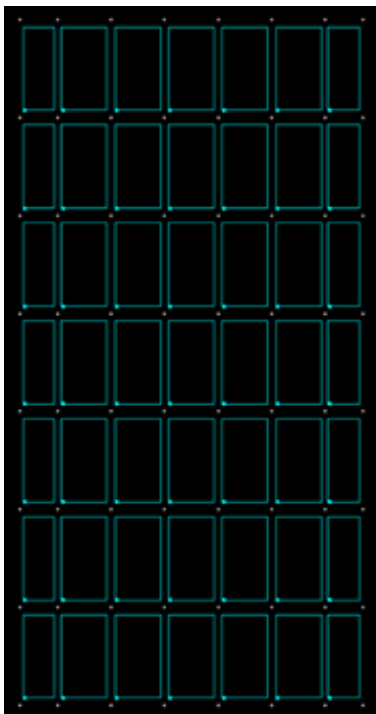


Figure A.1.1 – Node Set Up

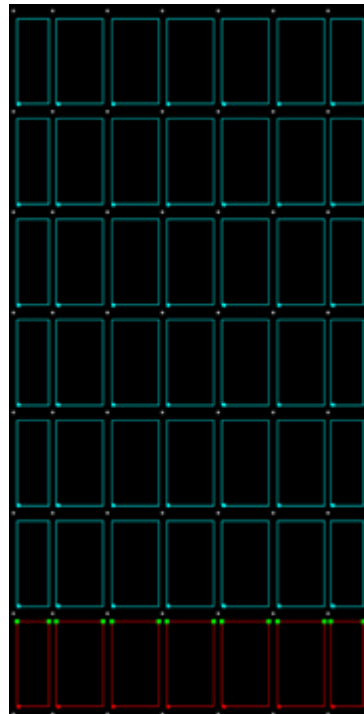


Figure A.1.2 – Structure Section Cut

LOAD CASES

Load Case Type: Gravity Status: Saved

Load Case Name: Gravity Save Save As Delete UnChange

Analysis Method

Linear (usual option)
Load applied in one step. Stops if there is a nonlinear event.

Nonlinear
See control information in box to right.

Control Information for Nonlinear Analysis

No. of Load Steps:
Max. Events in any Step:
Initial Step to First Event? Yes No

Limit State to Stop Analysis: Type:
Name:

Load is applied in equal steps, not counting optional initial step to first nonlinear event. Analysis stops when all load is applied or limit state is reached, whichever occurs first. Analysis aborts if the maximum number of nonlinear events is exceeded in any step.

Gravity Load Patterns for this Load Case

LOAD PATTERN TO BE ADDED OR CHANGED

Load Type: Nodal Element Self Weight

Pattern Name: Gravity Load

Scale Factor:

Add Insert Replace Delete

LOAD PATTERN LIST
Click to highlight for Insert, Replace or Delete

No.	Type	Name	Factor
1	Nodal	Gravity Load	1

A Gravity load case can be any combination of nodal, element and self weight load patterns, up to a maximum of 20 patterns.

LOAD CASES

Load Case Type: Static Push-Over Status: Saved

Load Case Name: Pushover Save Save As Delete UnChange

Analysis Method

Nonlinear (usual option)
See control information to right.

Linear (currently not allowed)

Control Information for Nonlinear Analysis

No. of Load Steps:
Max. Events in any Step:
Initial Step to First Event? Yes No

Limit State to Stop Analysis: Type: Drift
Name: Roof Drift
Reference Drift: Roof Drift

Maximum Allowable Drift (see Controlled Drifts):
The reference drift is usually the roof drift relative to the base. It is used as the main deformation measure for plotting push-over analysis results.

Load Type

Nodal Load Patterns
 Displacement Pattern
 Mode Shapes

Nodal Load Patterns

LOAD PATTERN LIST (MAX. 20) Click to highlight for Insert/Replace/Delete

No.	Type	Name	Factor
1	Nodal	Lateral Load	1

LOAD PATTERN TO BE ADDED OR CHANGED

Name: Gravity Load

Scale Factor:
The sign of the scale factor defines the load direction, and hence the push-over direction.

Add Insert Replace Delete

LOAD CASES

Load Case Type: Static Push-Over Status: Saved

Load Case Name: +0.20 Save Save As Delete UnChange

Analysis Method

Nonlinear (usual option)
See control information to right.

Linear (currently not allowed)

Control Information for Nonlinear Analysis

No. of Load Steps:
Max. Events in any Step:
Initial Step to First Event? Yes No

Limit State to Stop Analysis: Type: Drift
Name: Floor Drift
Reference Drift: Floor Drift

Maximum Allowable Drift (see Controlled Drifts):
The reference drift is usually the roof drift relative to the base. It is used as the main deformation measure for plotting push-over analysis results.

Load Type

Nodal Load Patterns
 Displacement Pattern
 Mode Shapes

Displacement Pattern


Specify horizontal displacement pattern. Load at any mass is proportional to Mass * Displacement.

V Coordinate	Point	V (in.)	d along H1	d along H2
V3	1	0	0	0
V2	2	116.25	1	0
V1	3			
	4			
	5			
	6			

Specify at least 2 points.
Displacements define only a pattern.
Length unit is not needed.

Figure A.1.3 – Load Case Set Ups for Gravity, Pushover, and Cyclic Load Cases

F = stress. D = strain.


Positive


Stiffness, K0	Tension Stresses	Compression Stresses
Modulus, E 29000	FY 45	FY 45
KH/K0 Pos = 0.011	FU 58.9	FU 58.9
KH/K0 Neg = 0.417	Tension Strains	Compression Strains
	DU 0.045	DU 0.0027
	DX 0.1	DX 0.1

Tension Strains	Compression Strains
DL 0.05	DL 0.0028
DR 0.07	DR 0.01
FR/FU 0.2	FR/FU 0.05

Figure A.1.4 – Stress-Strain Definition for Rebar Strength Loss Model

F = stress. D = strain.

Positive


Stiffness, K0	Tension Stresses	Compression Stresses
Modulus, E 29000	FY 45	FY 45
KH/K0 Pos = 0.010	FU 58.9	FU 58.9
KH/K0 Neg = 0.417	Tension Strains	Compression Strains
	DU 0.05	DU 0.0027
	DX 0.19	DX 0.05

Figure A.1.5 – Stress-Strain Definition for Rebar No Strength Loss Basic Relationship



Figure A.1.6 – 7 Horizontal Mesh (a) Outer Left and (b) Middle Cross Section Drawing

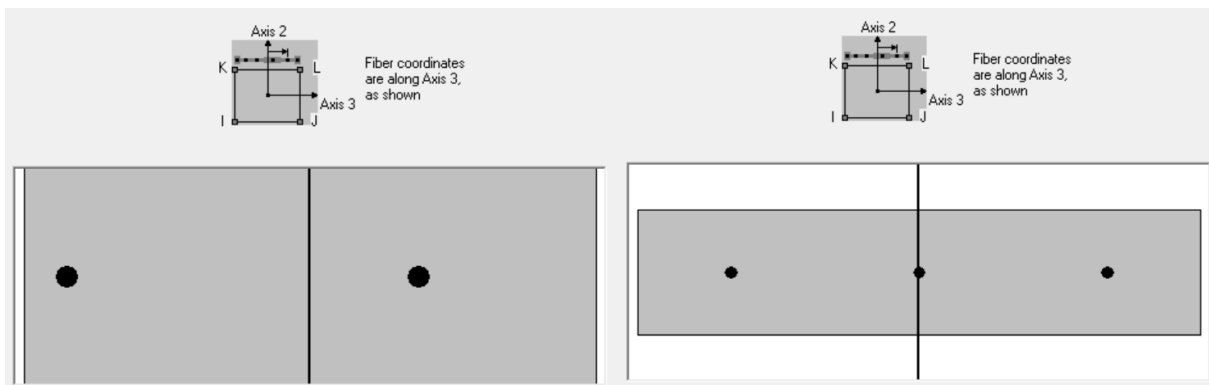


Figure A.1.7 – 3 Horizontal Mesh (a) Outer Left and (b) Middle Cross Section Drawing

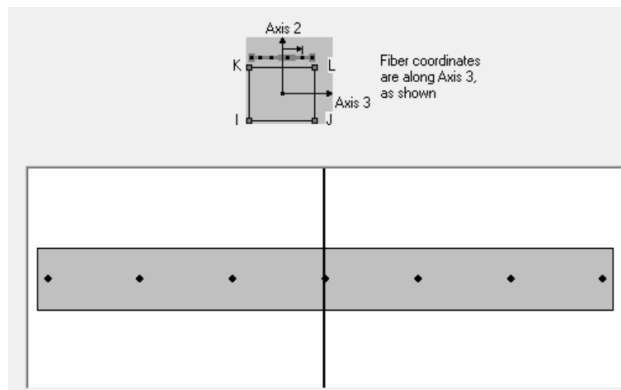


Figure A.1.8 – 1 Horizontal Mesh Cross Section Drawing

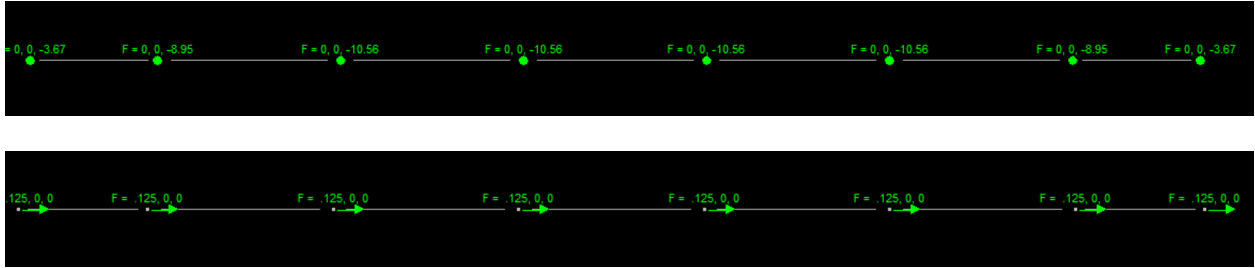


Figure A.1.9 – PERFORM-3D Plan View (a) Gravity Loading and (b) Lateral Loading for C1 7x7 Mesh

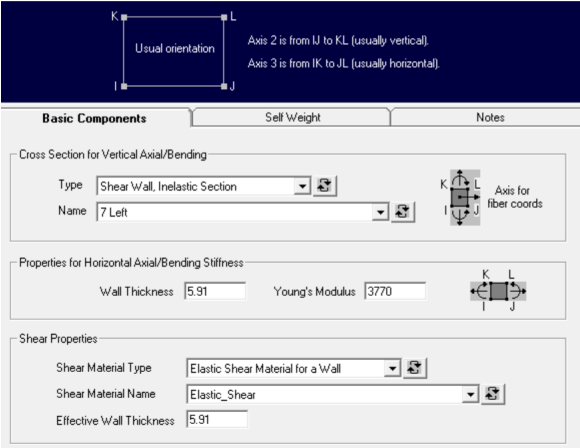


Figure A.1.10 – PERFORM-3D Shear Wall Compound Component Definition

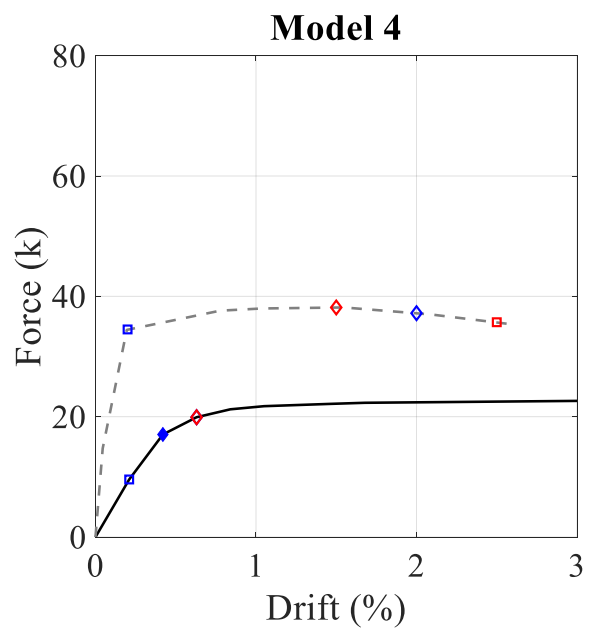
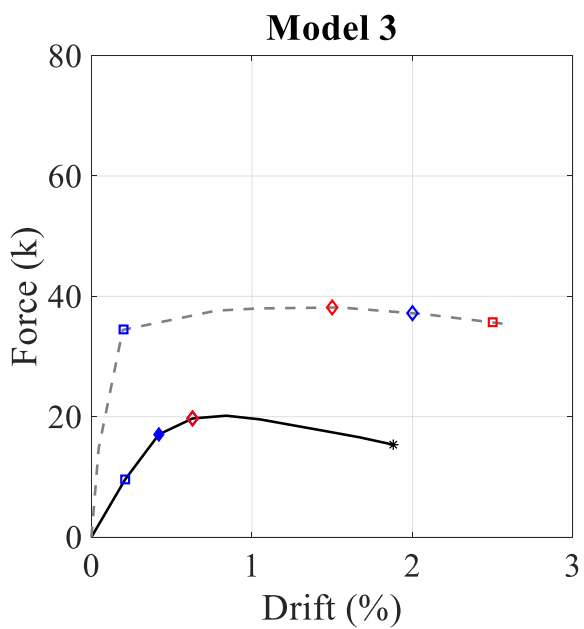
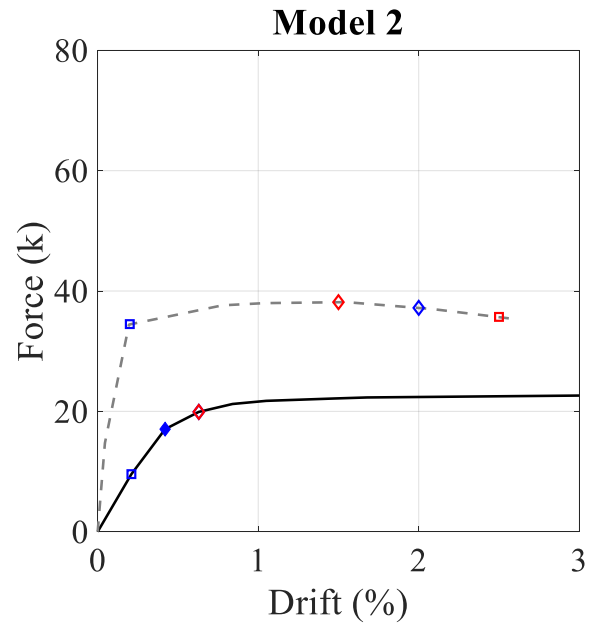
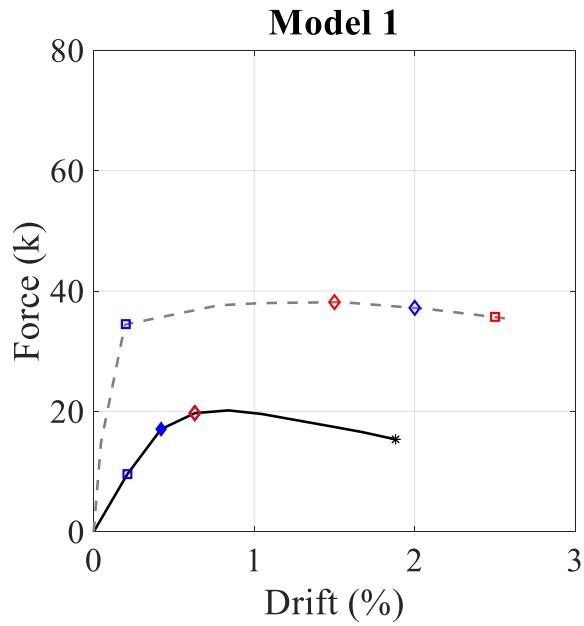
Table A.1.1 – Fibers Coordinate and Area Inputs for Horizontal Mesh Variations

7 Horizontal Meshes					
Description	Mat Type	Mat Name	Coordinate (in)	Area (in ²)	Tdraw (in)
7 Left	Concrete	Concrete	0	31.969	5.91
	Steel	Steel (cover)	-1.644	0.22	0
7 Mid	Concrete	Concrete	0	52.313	5.91
	Steel	Steel (middle)	0	0.22	0
7 Right	Concrete	Concrete	0	31.969	5.91
	Steel	Steel (cover)	1.644	0.22	0
3 Horizontal Meshes					
Description	Mat Type	Mat Name	Coordinate (in)	Area (in ²)	Tdraw (in)
3 Left	Concrete	Concrete	0	84.282	5.91
	Steel	Steel	2.707	0.22	0
	Steel	Steel (cover)	-6.073	0.22	0
3 Mid	Concrete	Concrete	0	156.93798	5.91
	Steel	Steel	-8.858	0.22	0
	Steel	Steel (middle)	0	0.22	0
	Steel	Steel	8.858	0.22	0
3 Right	Concrete	Concrete	0	84.282	5.91
	Steel	Steel	-2.707	0.22	0
	Steel	Steel (cover)	6.073	0.22	0
1 Horizontal Mesh					
Description	Mat Type	Mat Name	Coordinate (in)	Area (in ²)	Tdraw (in)
1 Main	Concrete	Concrete	0	325.501	5.91
	Steel	Steel (cover)	-26.496	0.22	0
	Steel	Steel	-17.717	0.22	0
	Steel	Steel	-8.858	0.22	0
	Steel	Steel (middle)	0	0.22	0
	Steel	Steel	8.858	0.22	0
	Steel	Steel	17.717	0.22	0
	Steel	Steel (cover)	26.496	0.22	0

A.2 Phase 2

Table A.2.1 – Parametric Study Model Matrix

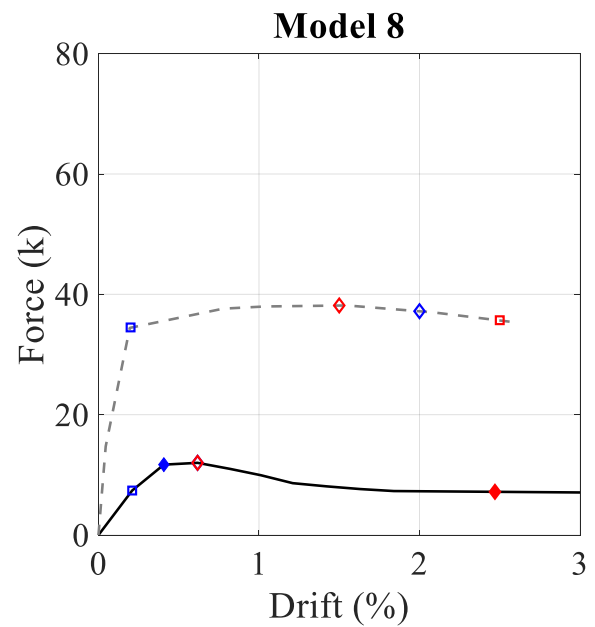
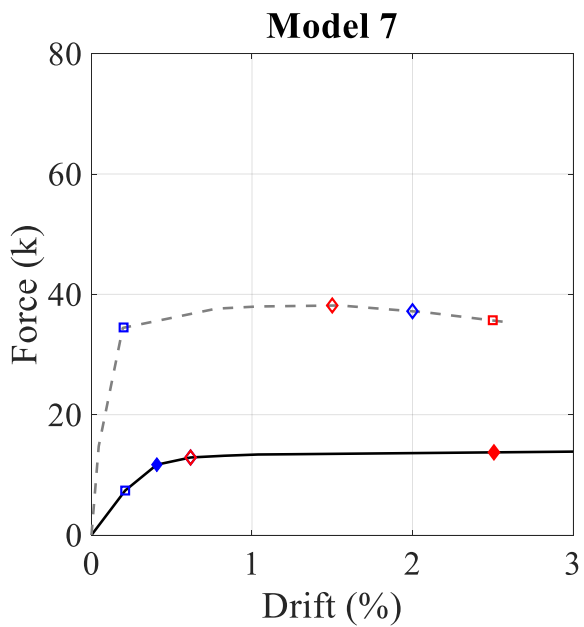
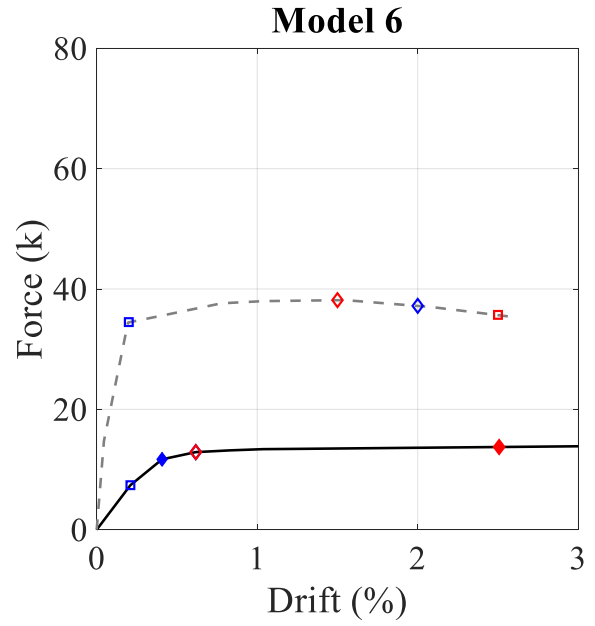
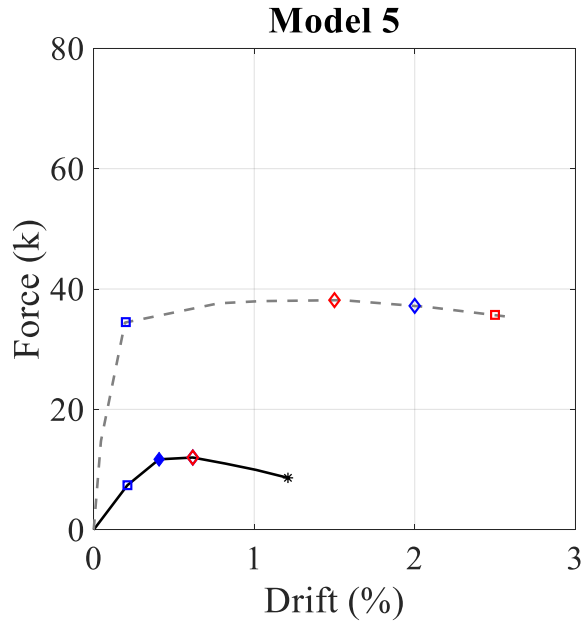
Model No.	Horizontal Mesh	Vertical Mesh	Concrete Tension?	Rebar Strength-loss?
1	1	1	✓	✓
2			✓	
3				✓
4				
5		3	✓	✓
6			✓	
7				✓
8				
9		7	✓	✓
10			✓	
11				✓
12				
13	3	1	✓	✓
14			✓	
15				✓
16				
17		3	✓	✓
18			✓	
19				✓
20				
21		7	✓	✓
22			✓	
23				✓
24				
25	7	1	✓	✓
26			✓	
27				✓
28				
29		3	✓	✓
30			✓	
31				✓
32				
33		7	✓	✓
34			✓	
35				✓
36				



- Concrete Cracking
- ◇ Concrete Crushing
- Rebar Fracture
- ◇ Rebar Buckling
- ◆ ASCE 41-17 Concrete Compression Limit
- ASCE 41-17 Rebar Tension Limit
- ◆ ASCE 41-17 Rebar Compression Limit
- * 20% Post-Peak Strength Loss

- PERFORM-3D Model
- - Experimental Testing Results

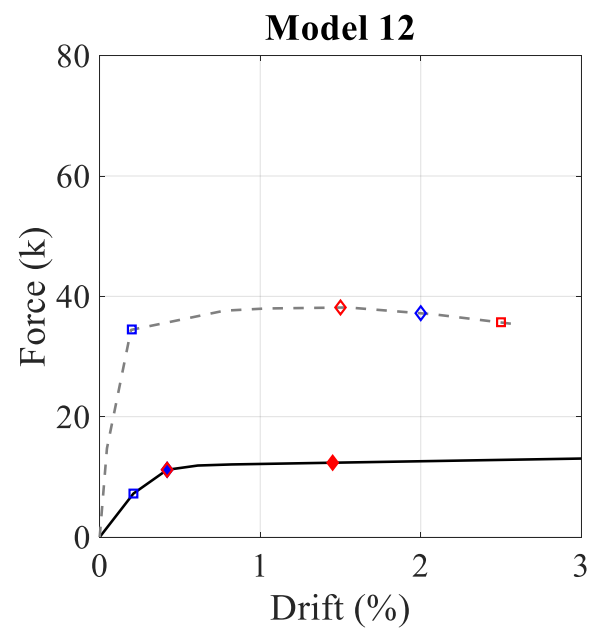
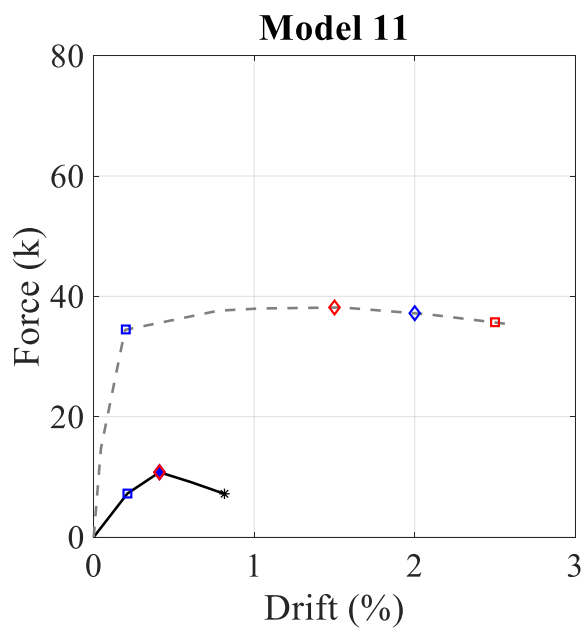
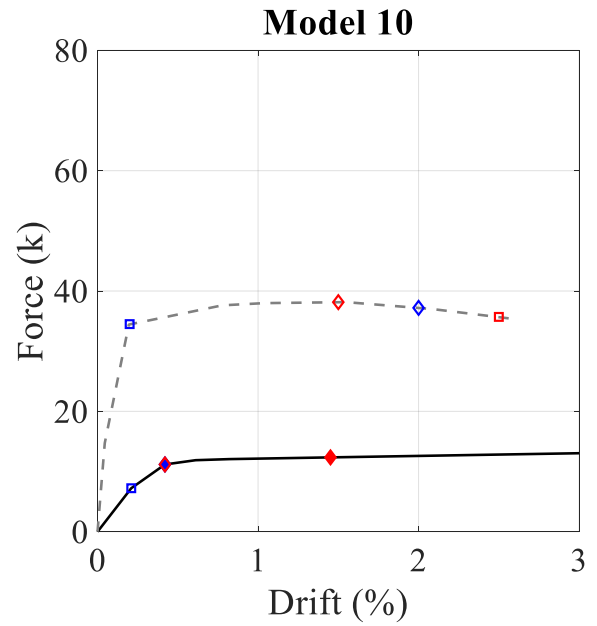
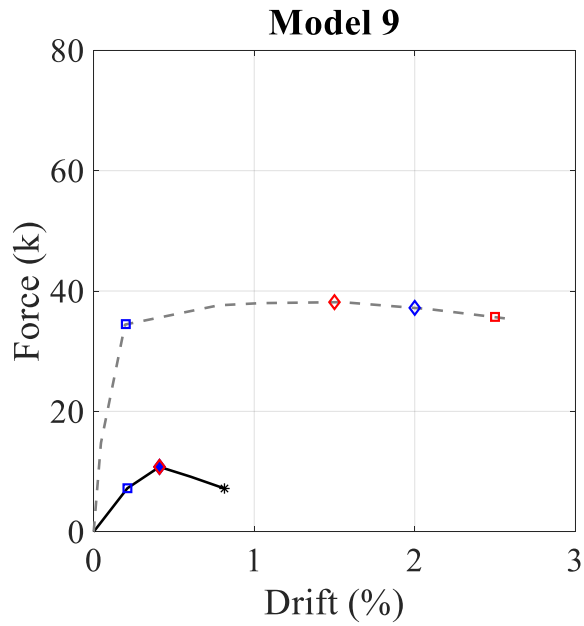
Figure A.2.1 Parametric Study Static Pushover Curves



- Concrete Cracking
- ◇ Concrete Crushing
- Rebar Fracture
- ◆ Rebar Buckling
- ◆ ASCE 41-17 Concrete Compression Limit
- ASCE 41-17 Rebar Tension Limit
- ◆ ASCE 41-17 Rebar Compression Limit
- * 20% Post-Peak Strength Loss

- PERFORM-3D Model
- - Experimental Testing Results

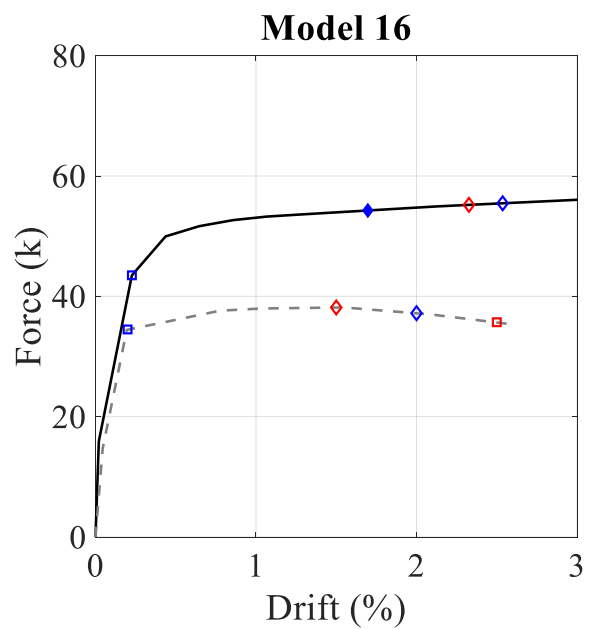
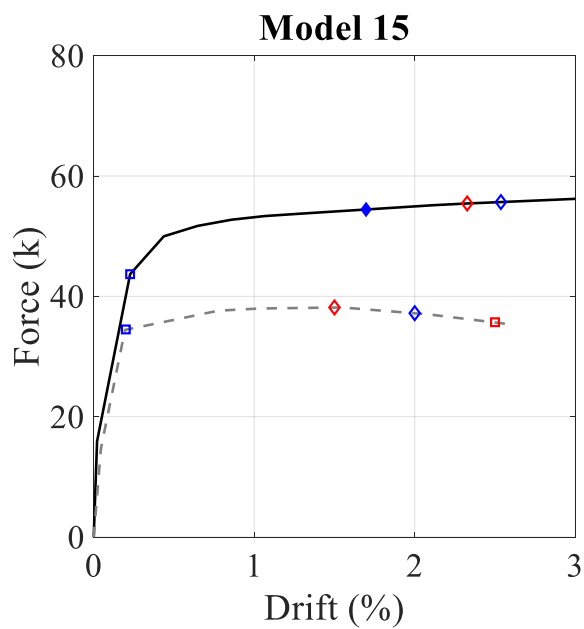
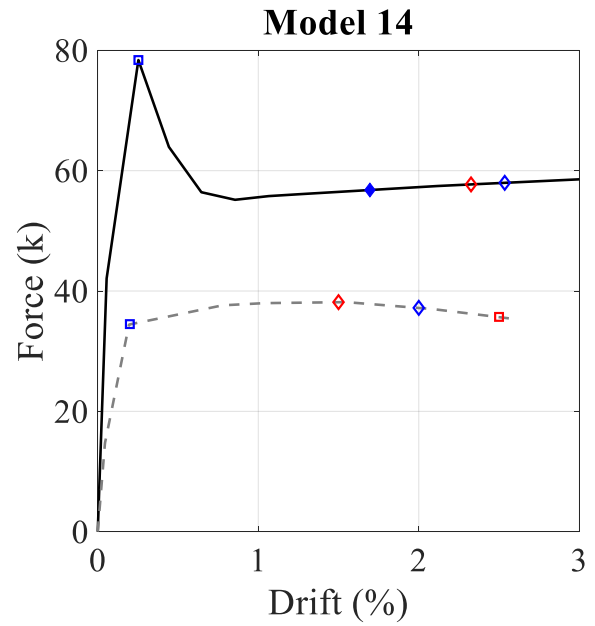
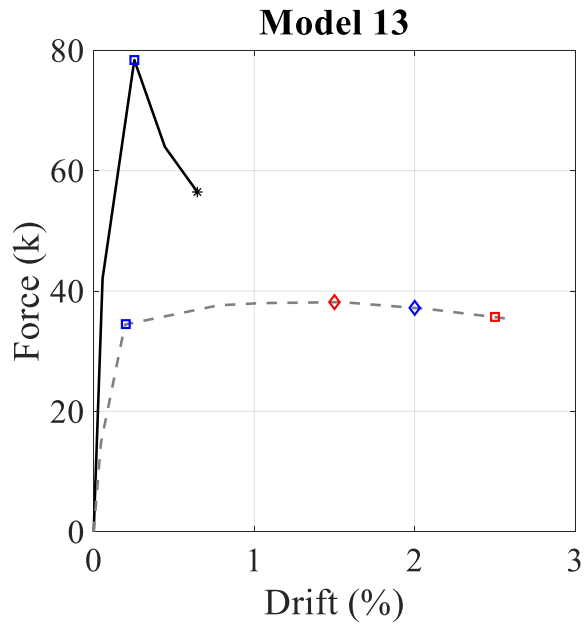
Figure A.2.1 Parametric Study Static Pushover Curves (cont.)



- Concrete Cracking
- ◇ Concrete Crushing
- Rebar Fracture
- ◆ Rebar Buckling
- ◆ ASCE 41-17 Concrete Compression Limit
- ASCE 41-17 Rebar Tension Limit
- ◆ ASCE 41-17 Rebar Compression Limit
- * 20% Post-Peak Strength Loss

- PERFORM-3D Model
- - Experimental Testing Results

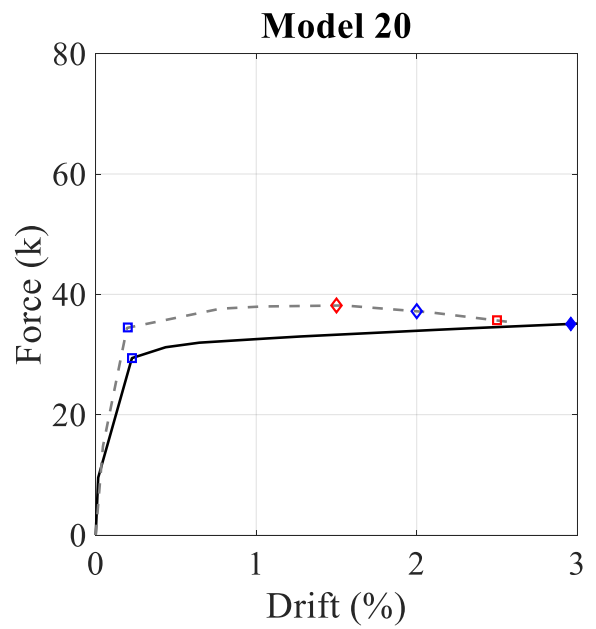
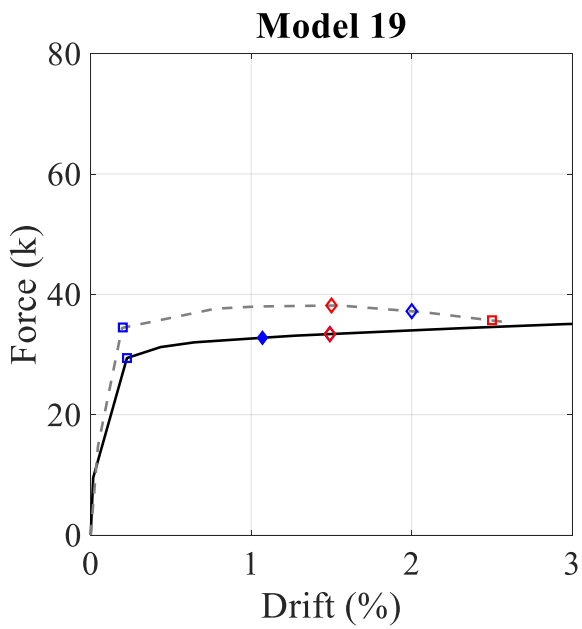
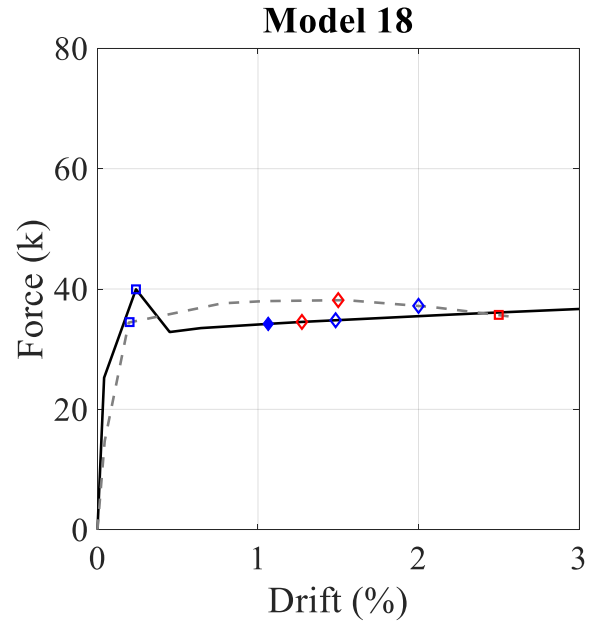
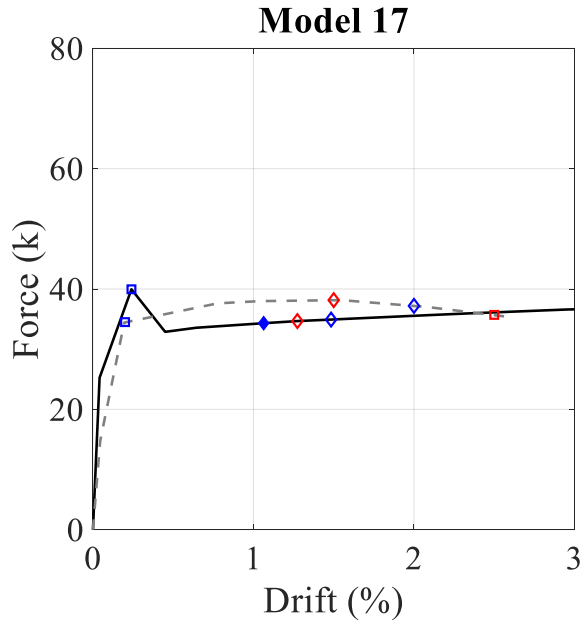
Figure A.2.1 Parametric Study Static Pushover Curves (cont.)



- Concrete Cracking
- ◇ Concrete Crushing
- Rebar Fracture
- ◆ Rebar Buckling
- ◆ ASCE 41-17 Concrete Compression Limit
- ASCE 41-17 Rebar Tension Limit
- ◆ ASCE 41-17 Rebar Compression Limit
- * 20% Post-Peak Strength Loss

- PERFORM-3D Model
- - Experimental Testing Results

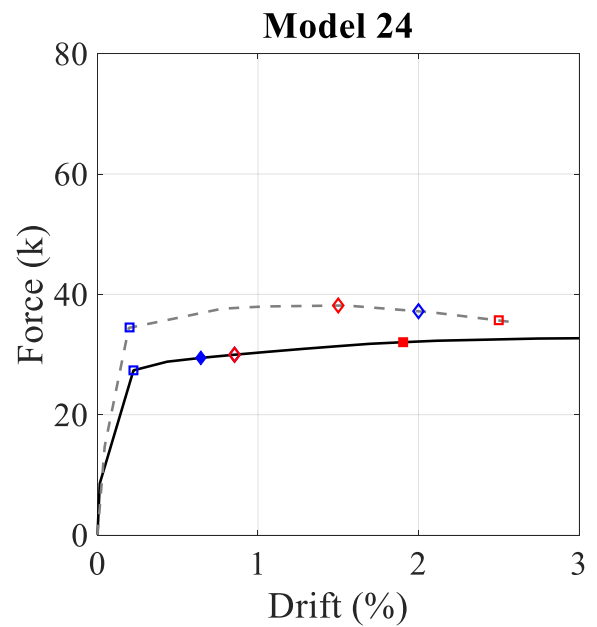
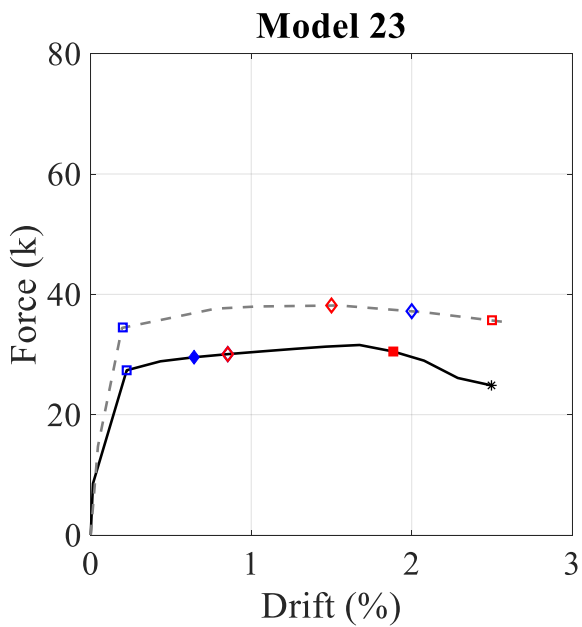
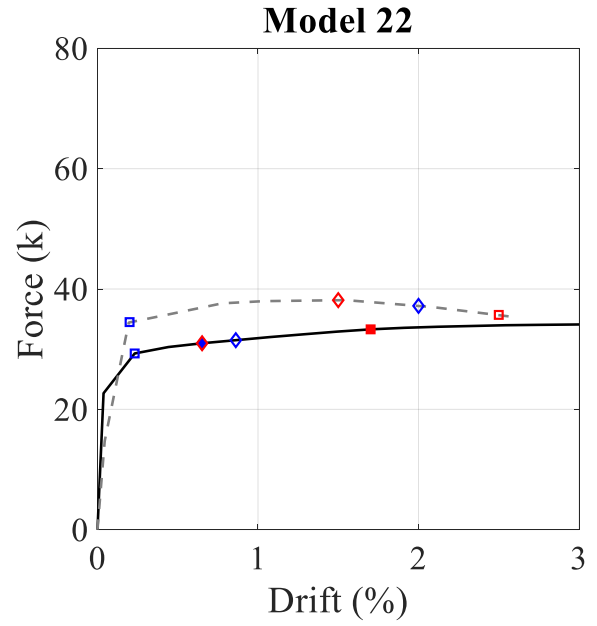
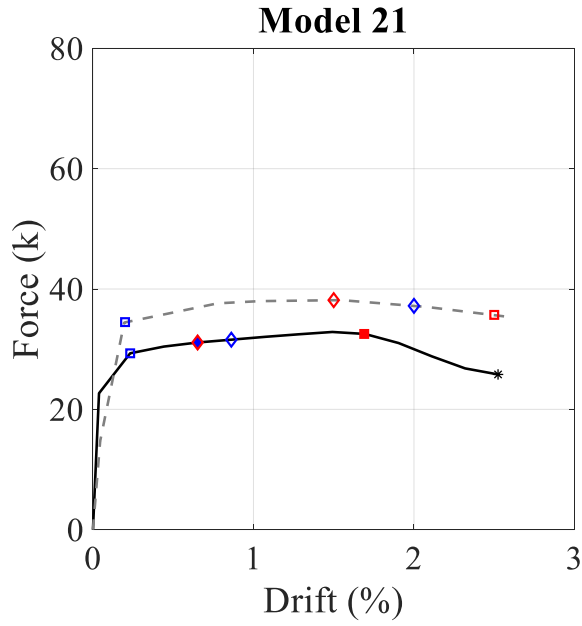
Figure A.2.1 Parametric Study Static Pushover Curves (cont.)



- Concrete Cracking
- ◇ Concrete Crushing
- Rebar Fracture
- ◇ Rebar Buckling
- ◆ ASCE 41-17 Concrete Compression Limit
- ASCE 41-17 Rebar Tension Limit
- ◆ ASCE 41-17 Rebar Compression Limit
- * 20% Post-Peak Strength Loss

- PERFORM-3D Model
- - Experimental Testing Results

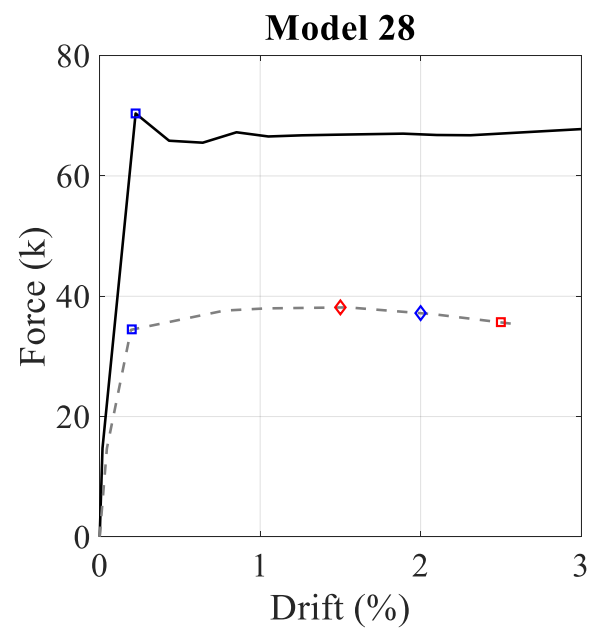
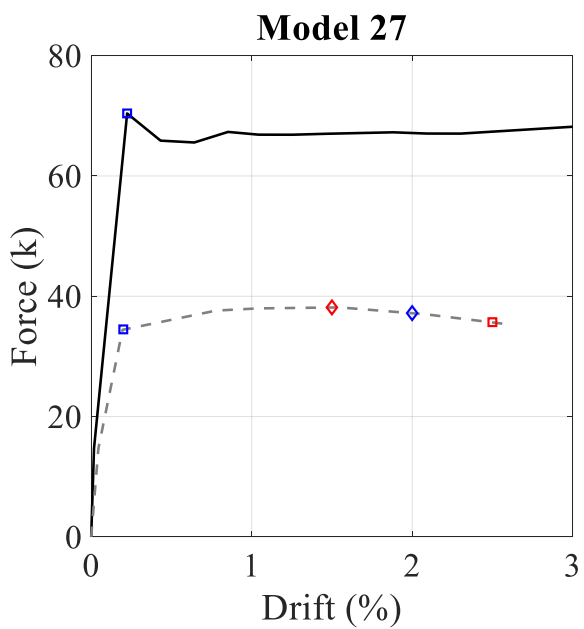
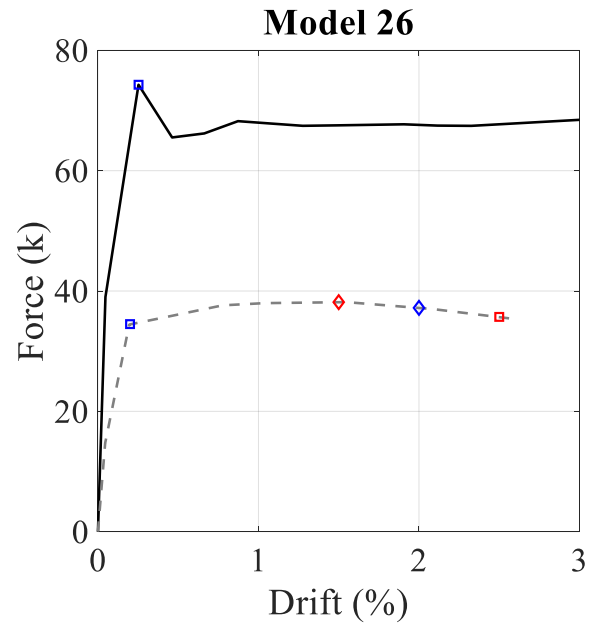
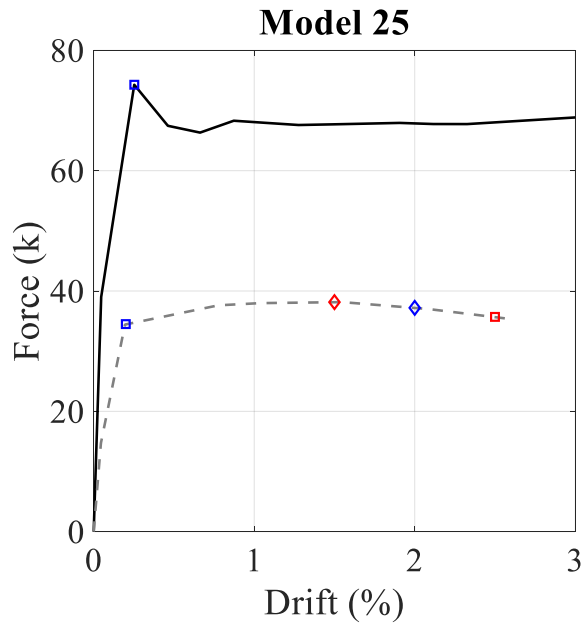
Figure A.2.1 Parametric Study Static Pushover Curves (cont.)



- Concrete Cracking
- ◇ Concrete Crushing
- Rebar Fracture
- ◇ Rebar Buckling
- ◆ ASCE 41-17 Concrete Compression Limit
- ASCE 41-17 Rebar Tension Limit
- ◆ ASCE 41-17 Rebar Compression Limit
- * 20% Post-Peak Strength Loss

- PERFORM-3D Model
- - Experimental Testing Results

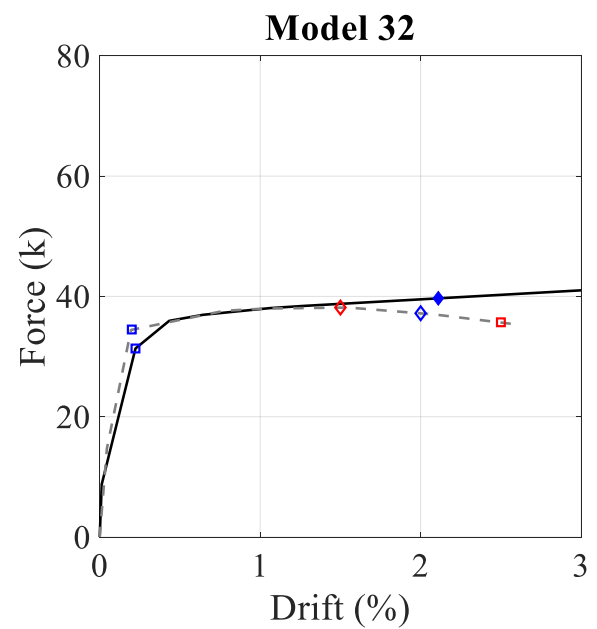
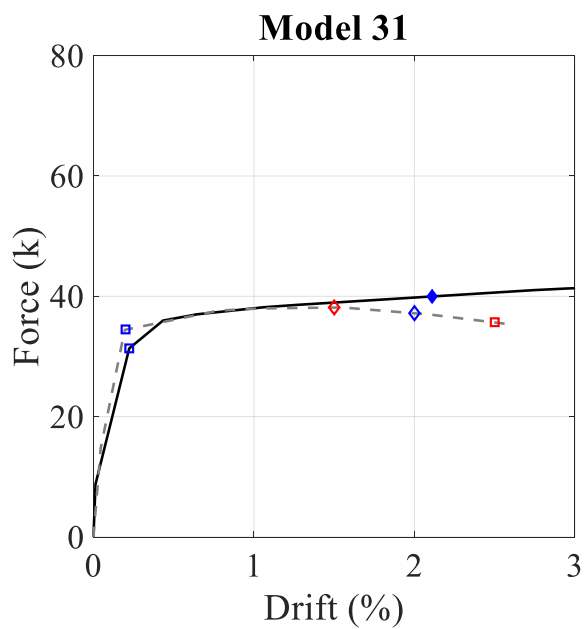
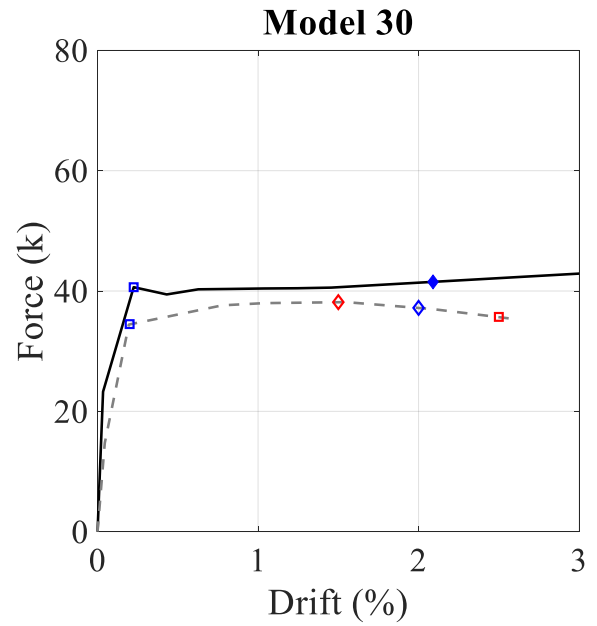
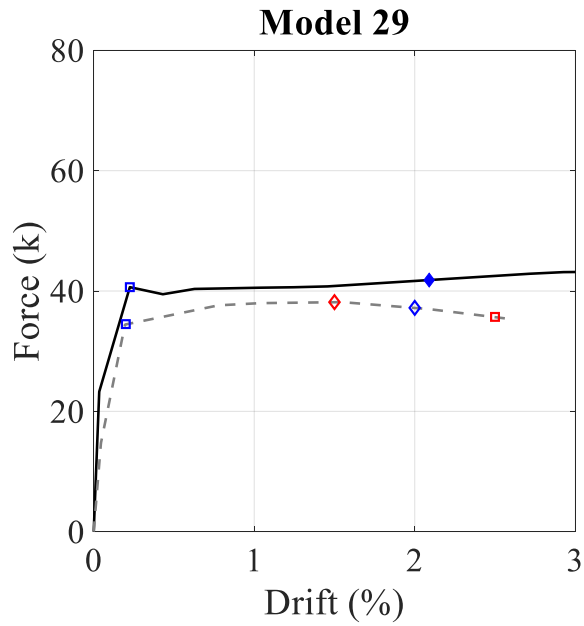
Figure A.2.1 Parametric Study Static Pushover Curves (cont.)



- Concrete Cracking
- ◇ Concrete Crushing
- Rebar Fracture
- ◆ Rebar Buckling
- ◆ ASCE 41-17 Concrete Compression Limit
- ASCE 41-17 Rebar Tension Limit
- ◆ ASCE 41-17 Rebar Compression Limit
- * 20% Post-Peak Strength Loss

- PERFORM-3D Model
- - Experimental Testing Results

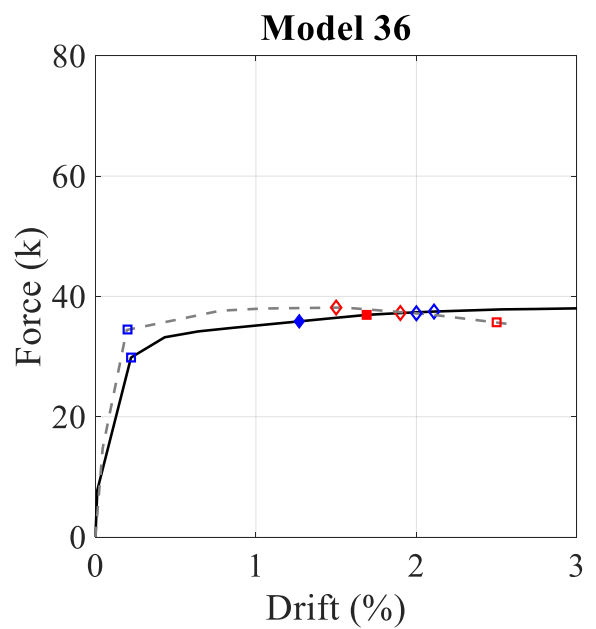
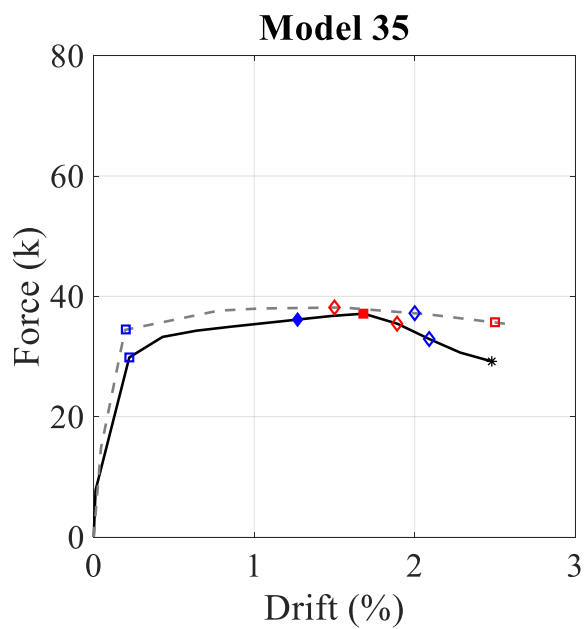
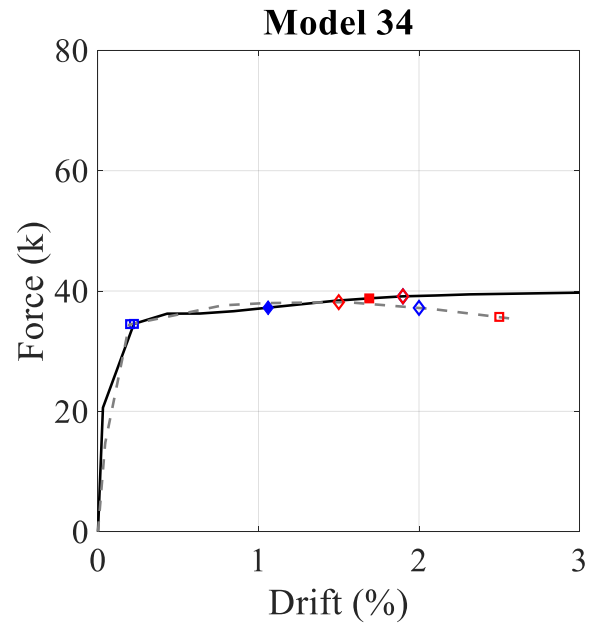
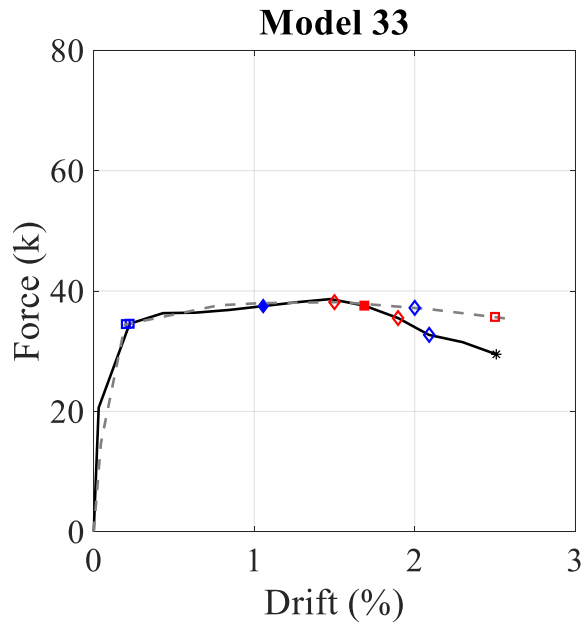
Figure A.2.1 Parametric Study Static Pushover Curves (cont.)



- Concrete Cracking
- ◇ Concrete Crushing
- Rebar Fracture
- ◇ Rebar Buckling
- ◆ ASCE 41-17 Concrete Compression Limit
- ASCE 41-17 Rebar Tension Limit
- ◆ ASCE 41-17 Rebar Compression Limit
- * 20% Post-Peak Strength Loss

- PERFORM-3D Model
- - Experimental Testing Results

Figure A.2.1 Parametric Study Static Pushover Curves (cont.)



- Concrete Cracking
- ◇ Concrete Crushing
- Rebar Fracture
- ◇ Rebar Buckling
- ◆ ASCE 41-17 Concrete Compression Limit
- ASCE 41-17 Rebar Tension Limit
- ◆ ASCE 41-17 Rebar Compression Limit
- * 20% Post-Peak Strength Loss

- PERFORM-3D Model
- - Experimental Testing Results

Figure A.2.1 Parametric Study Static Pushover Curves (cont.)

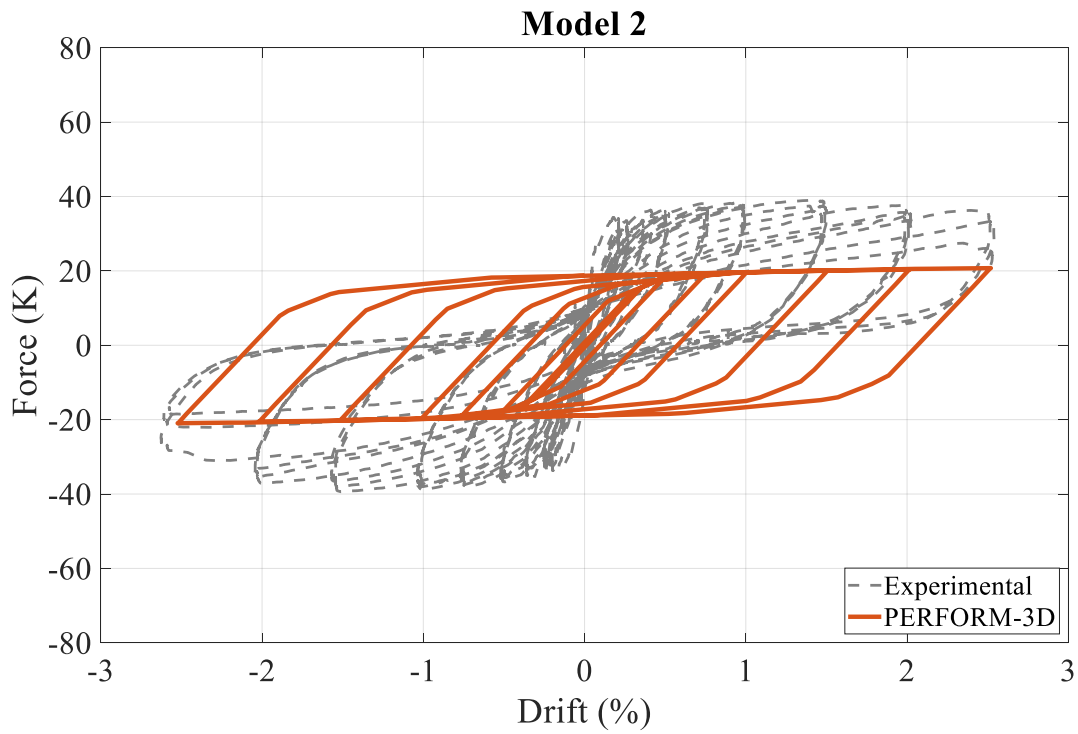
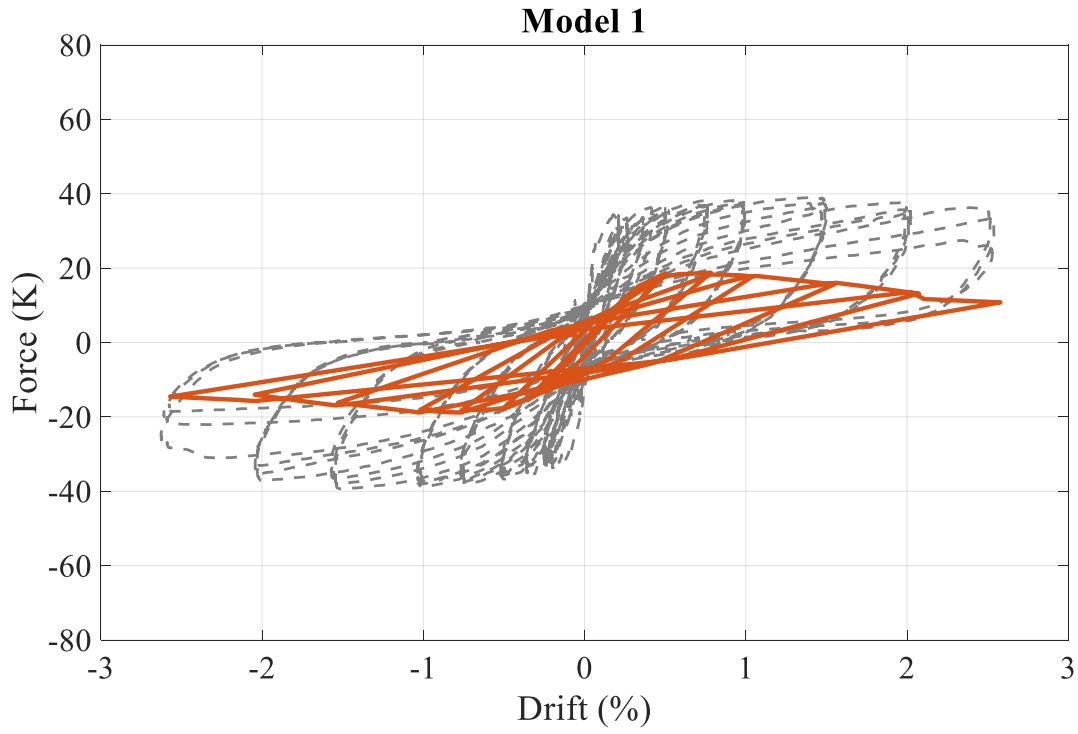


Figure A.2.2 Parametric Study Cyclic Load Analysis

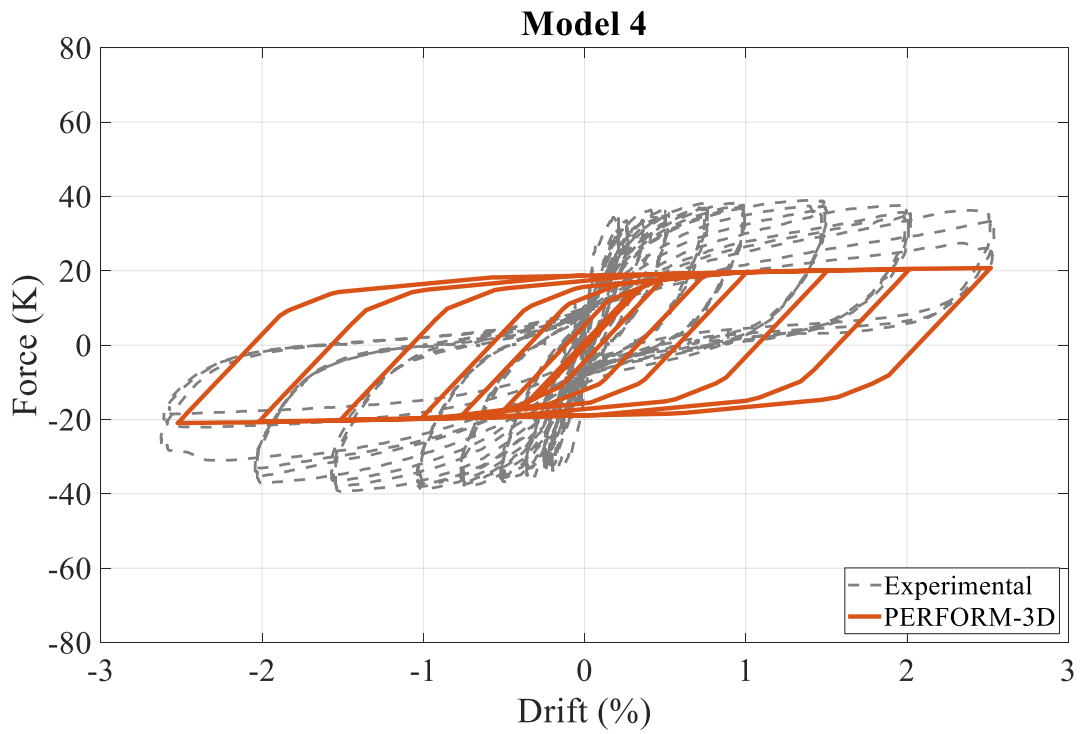
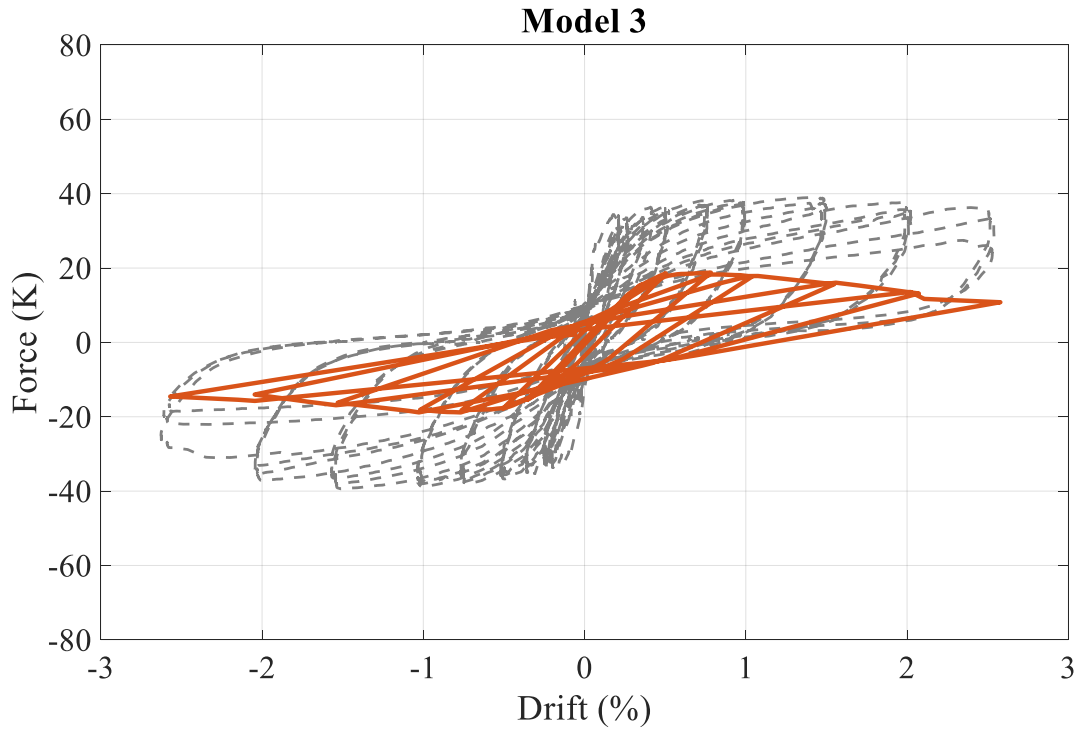


Figure A.2.2 Parametric Study Cyclic Load Analysis (cont.)

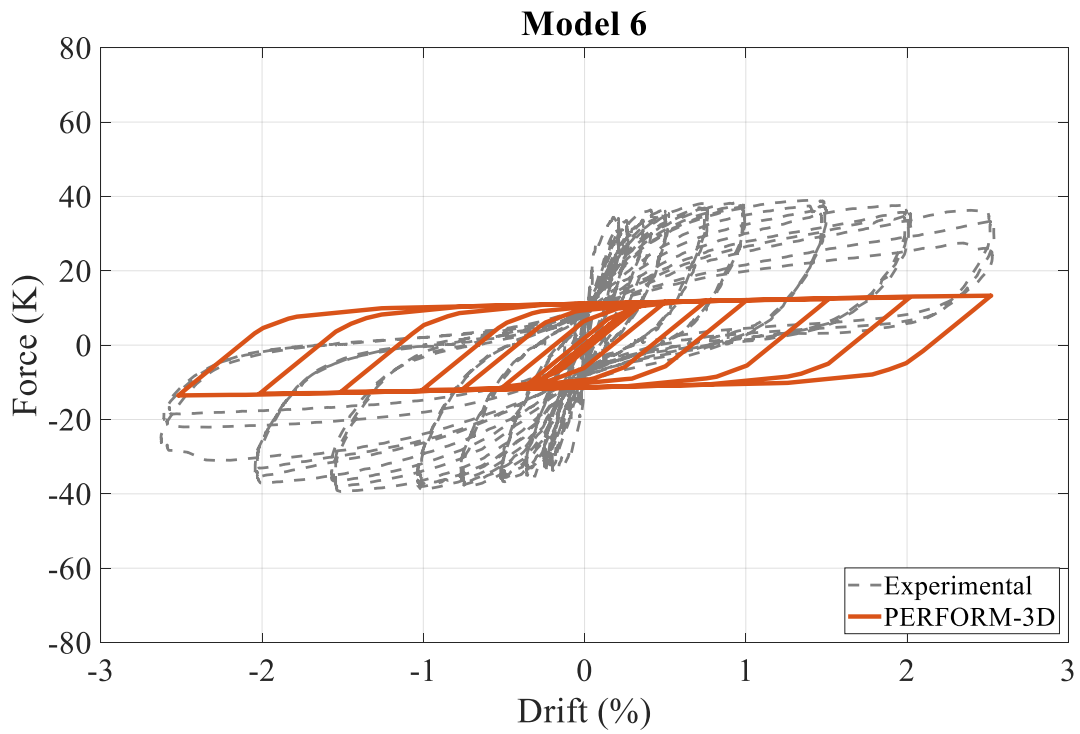
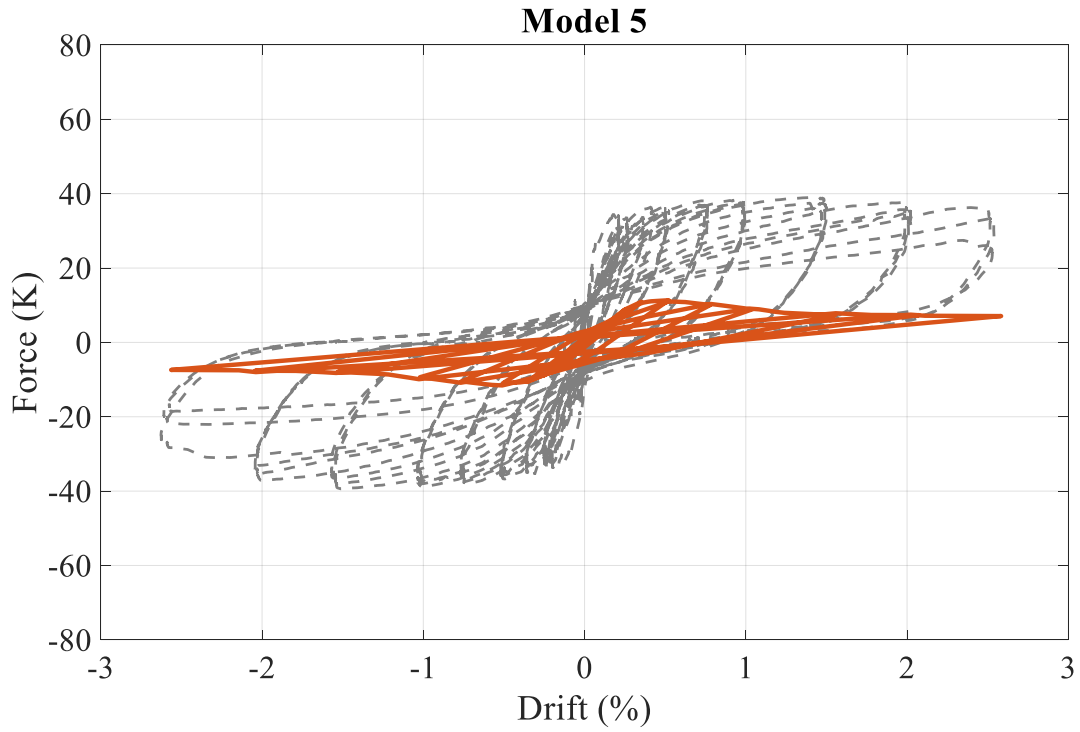


Figure A.2.2 Parametric Study Cyclic Load Analysis (cont.)

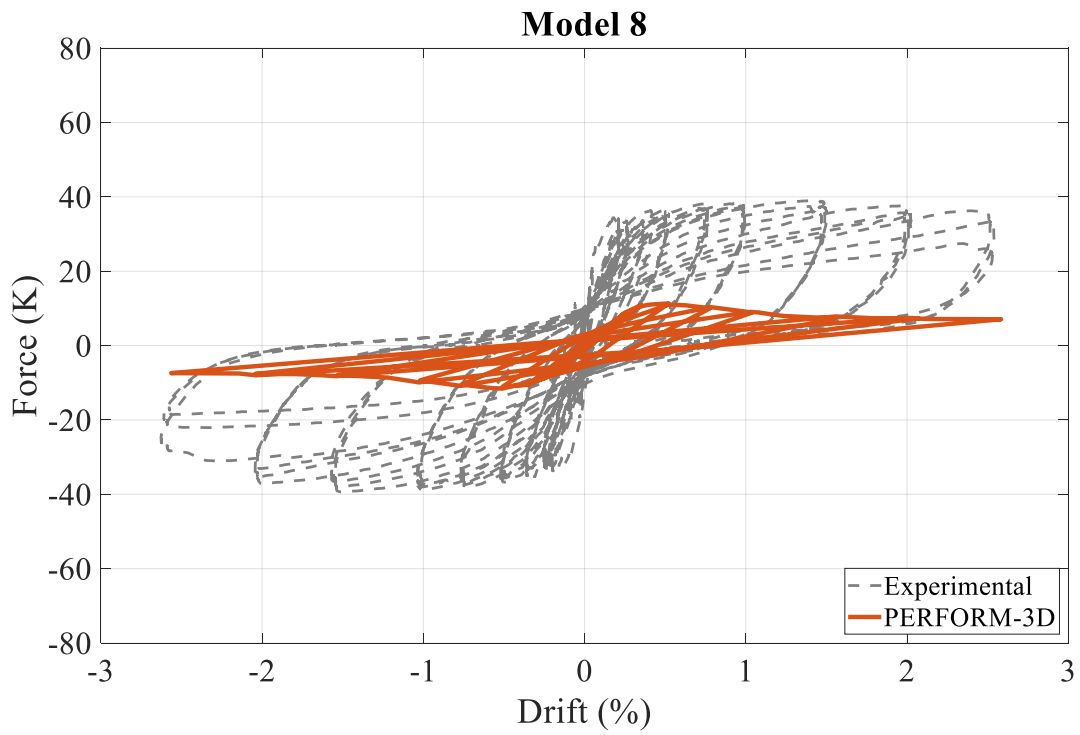
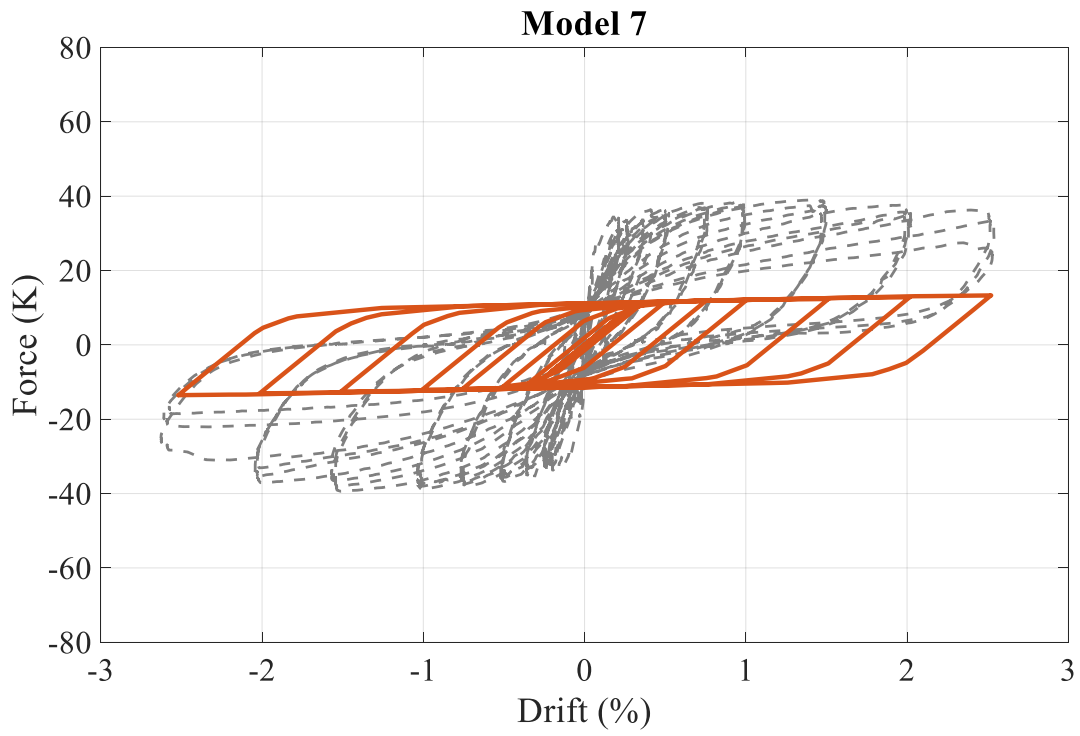


Figure A.2.2 Parametric Study Cyclic Load Analysis (cont.)

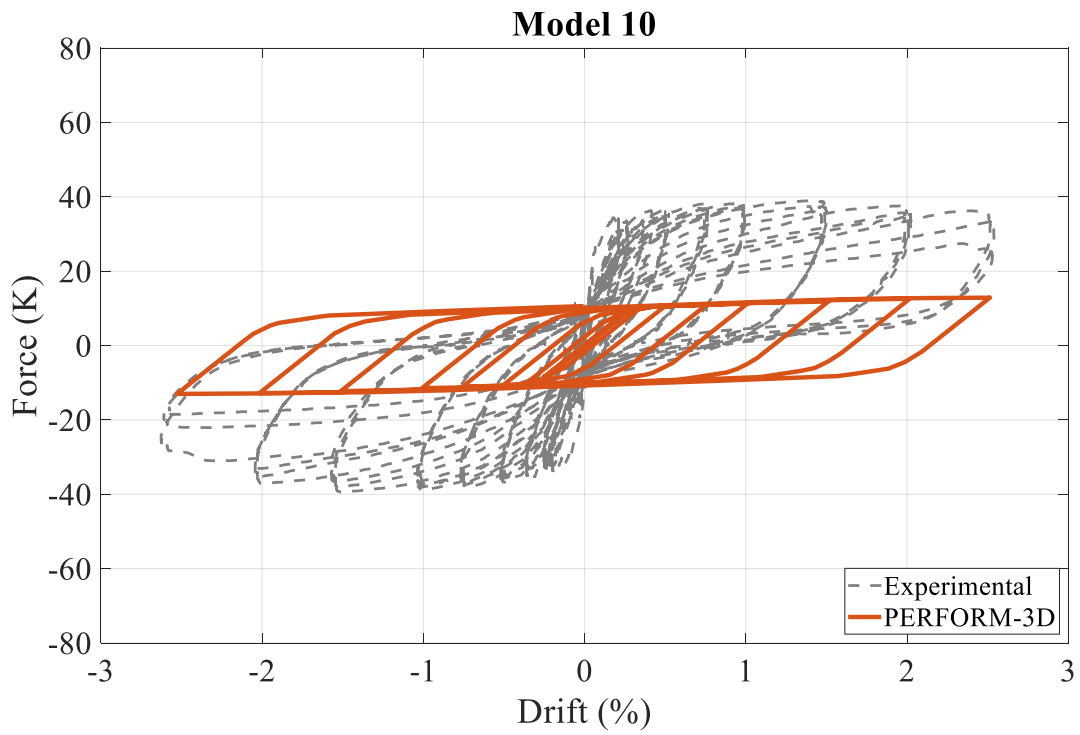
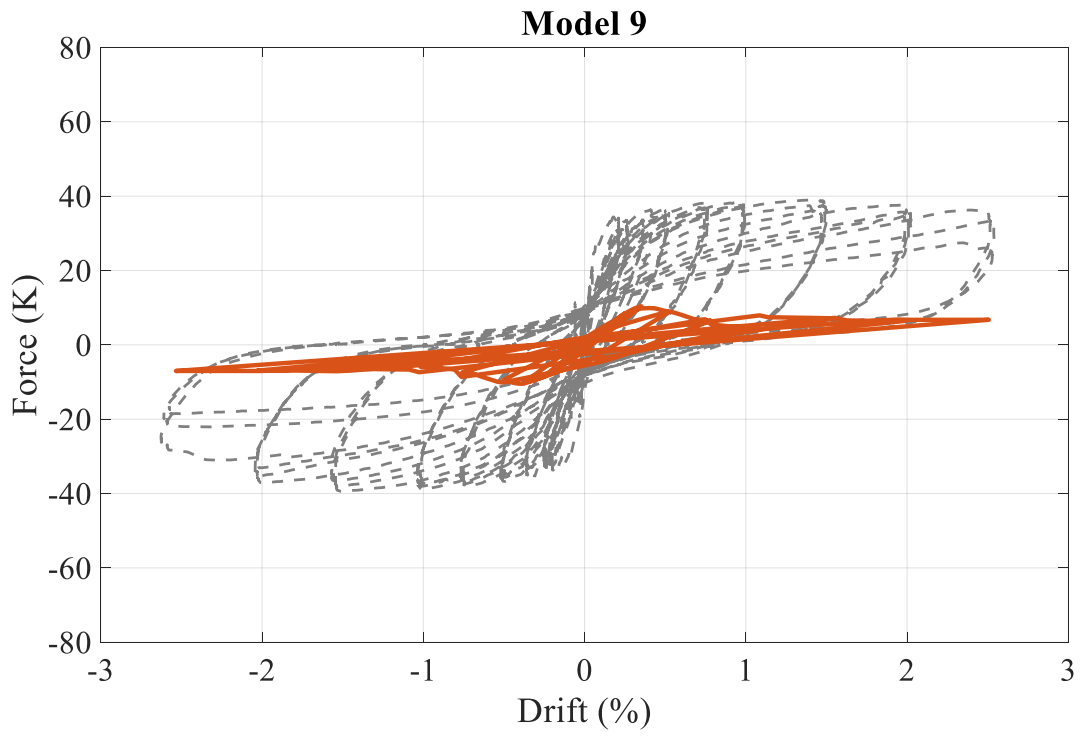


Figure A.2.2 Parametric Study Cyclic Load Analysis (cont.)

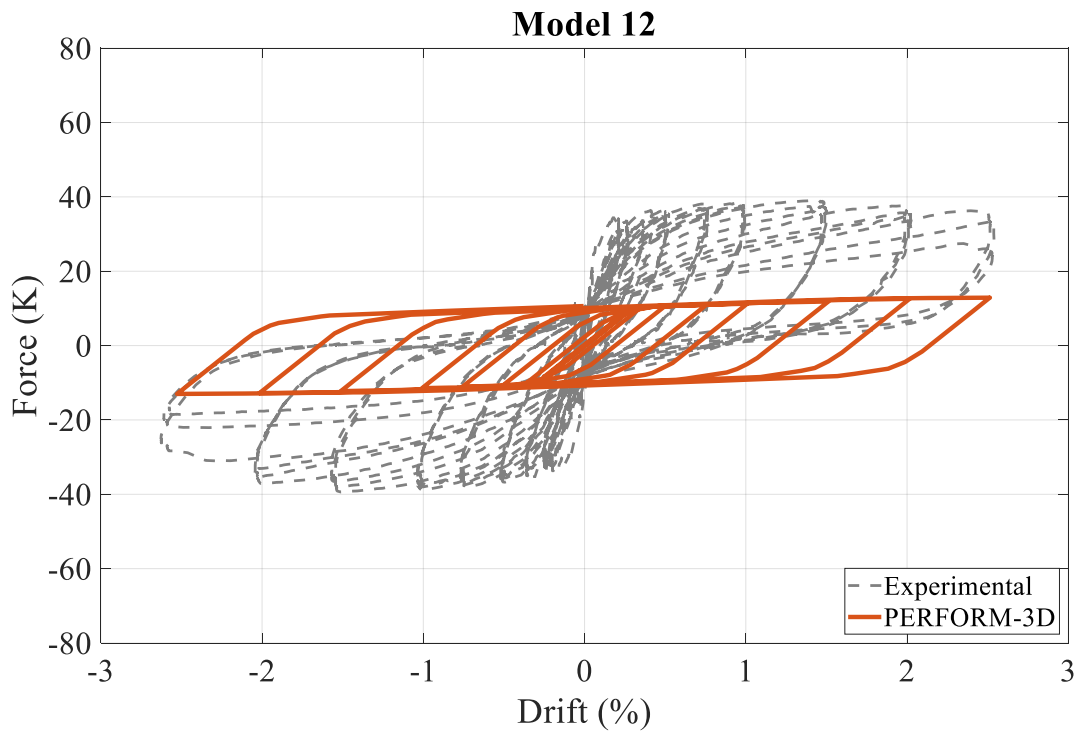
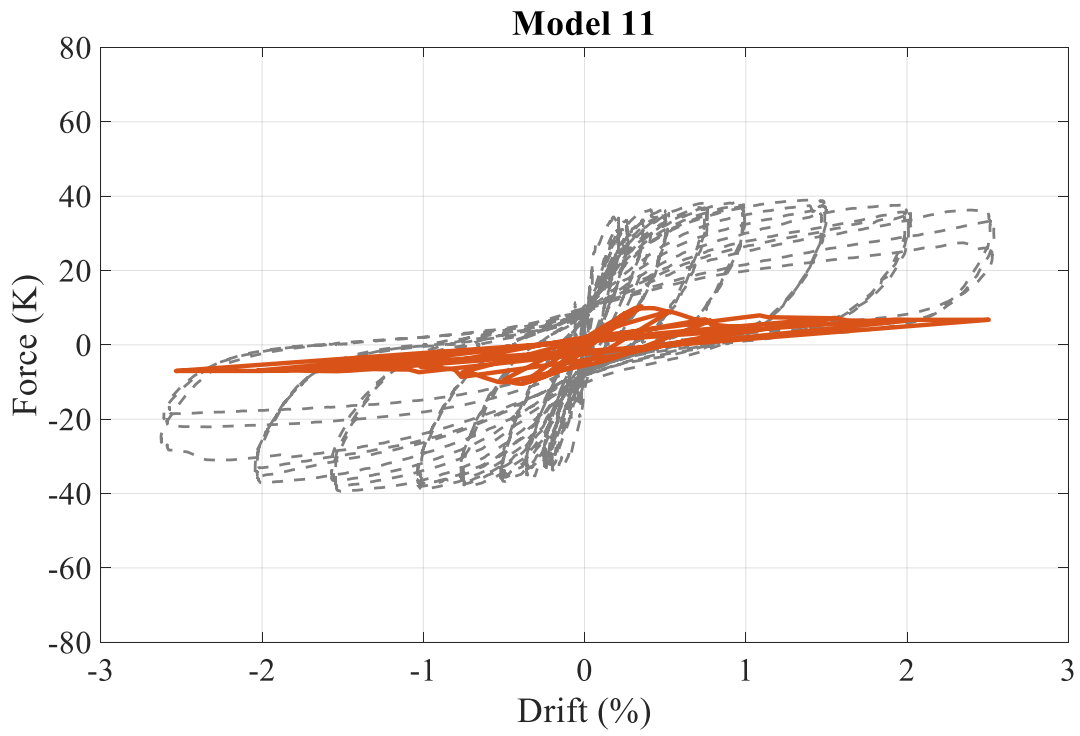


Figure A.2.2 Parametric Study Cyclic Load Analysis (cont.)

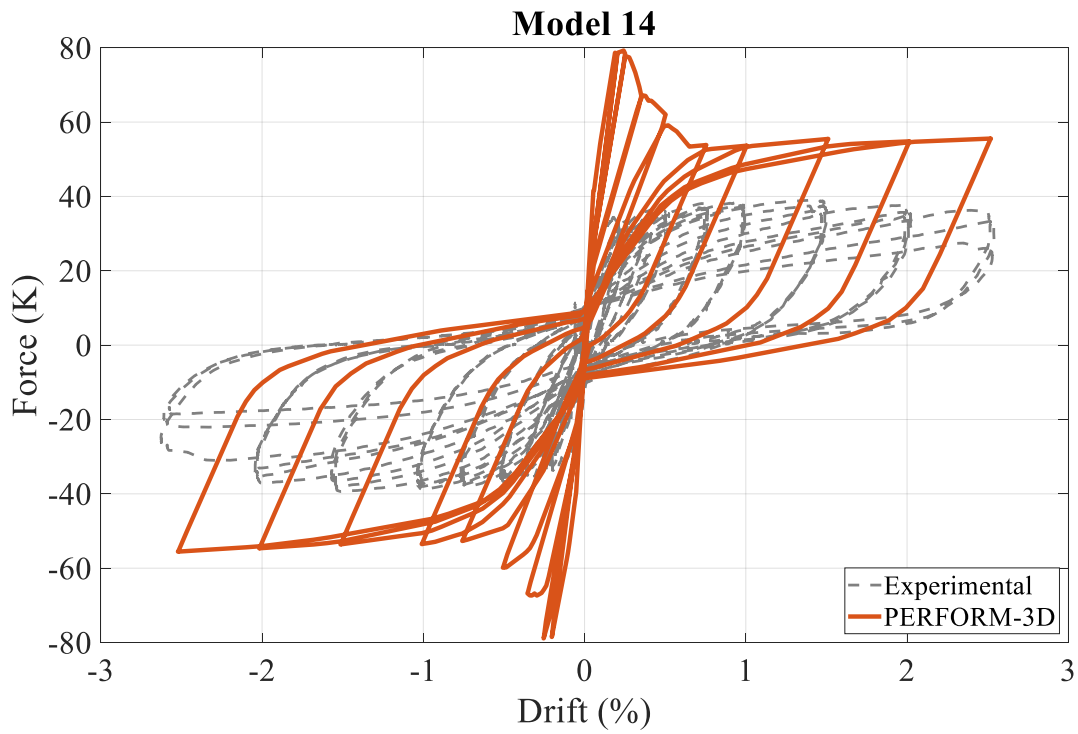
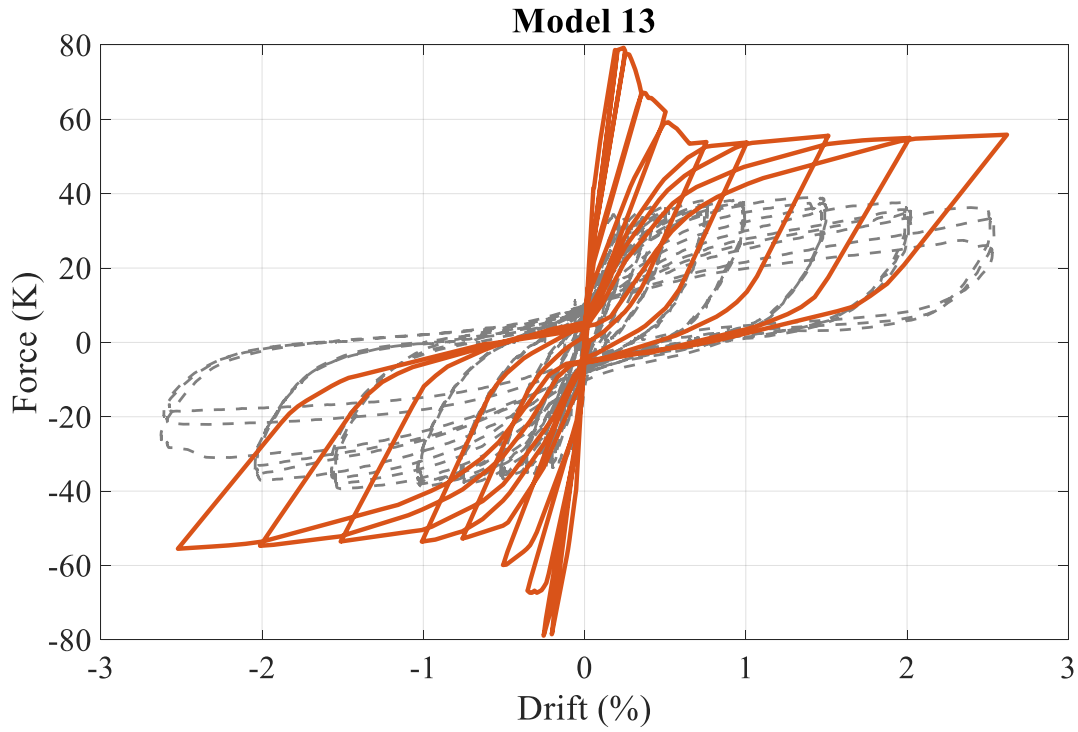


Figure A.2.2 Parametric Study Cyclic Load Analysis (cont.)

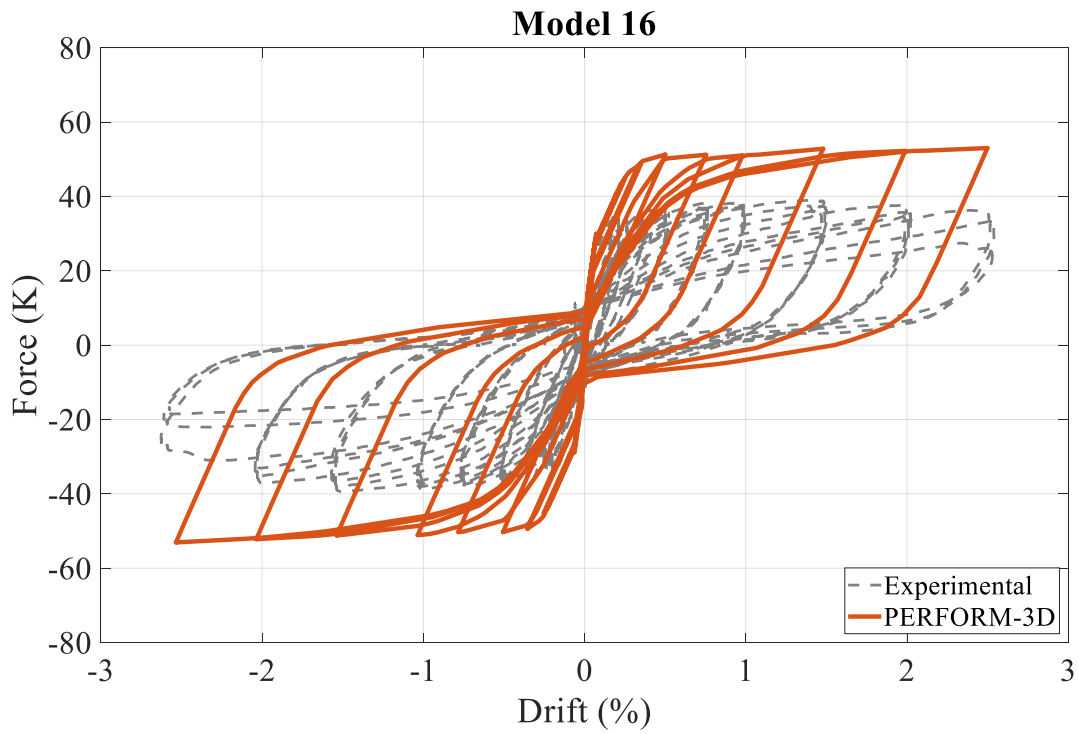
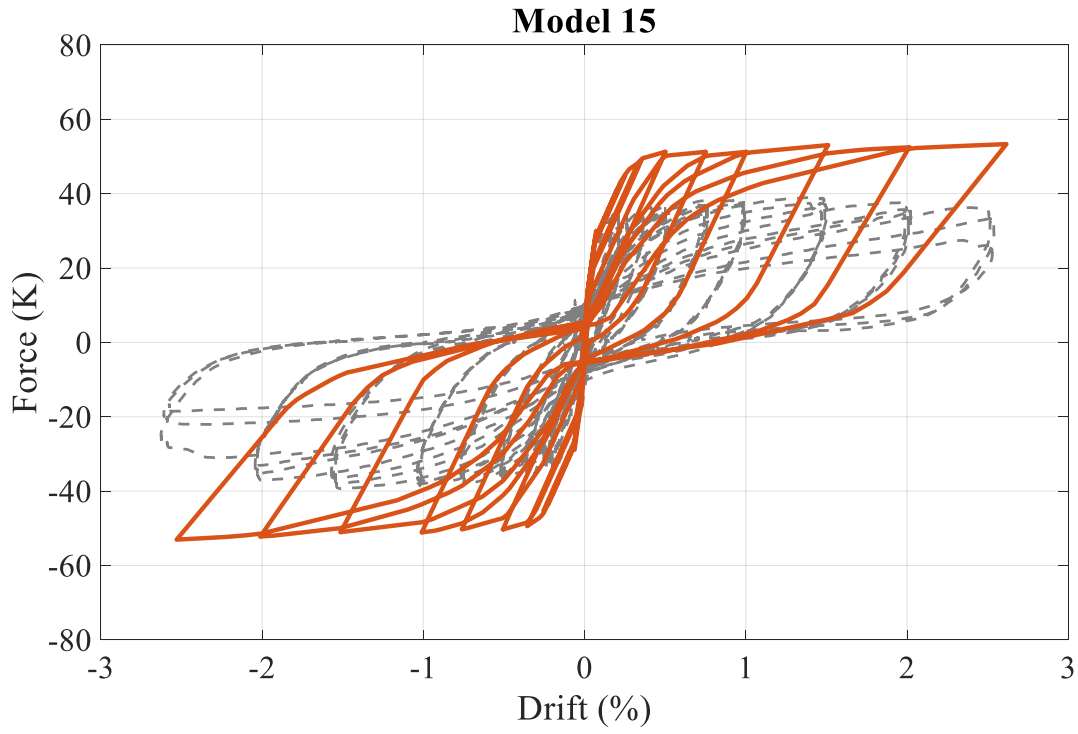


Figure A.2.2 Parametric Study Cyclic Load Analysis (cont.)

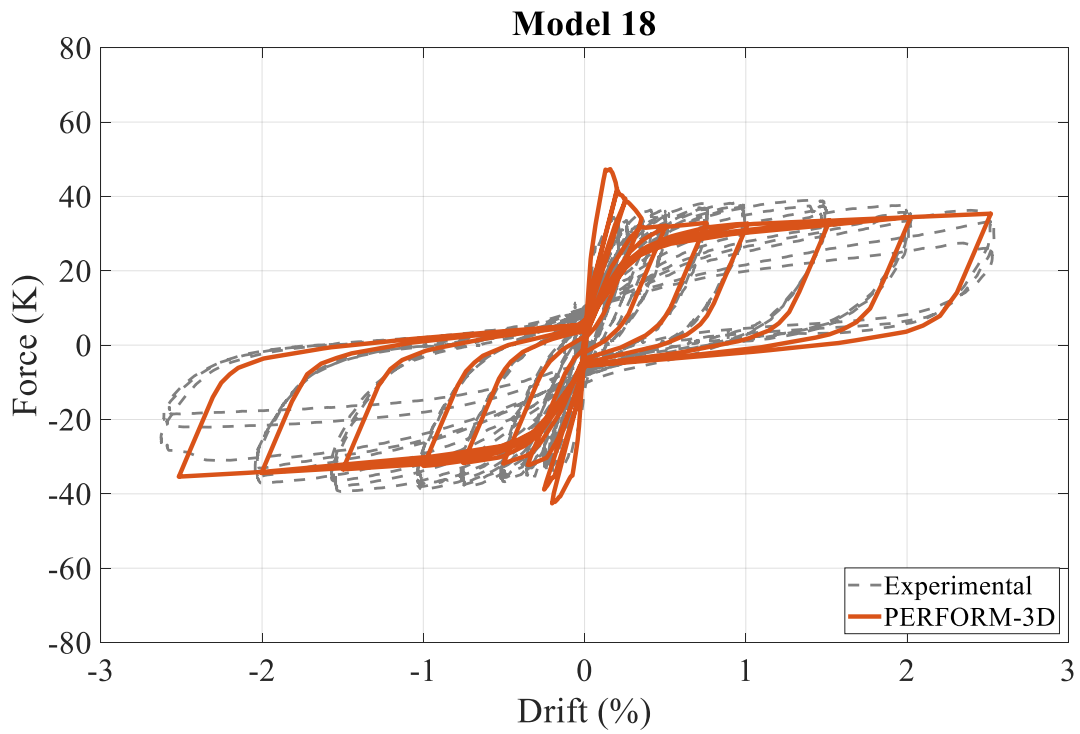
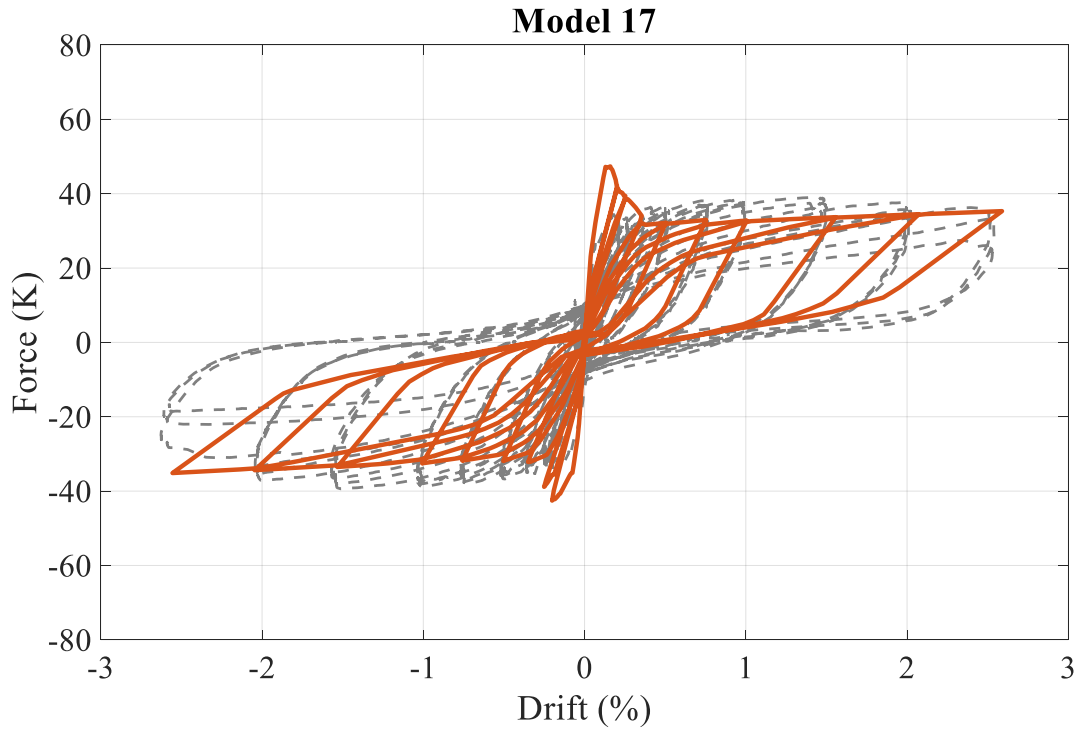


Figure A.2.2 Parametric Study Cyclic Load Analysis (cont.)

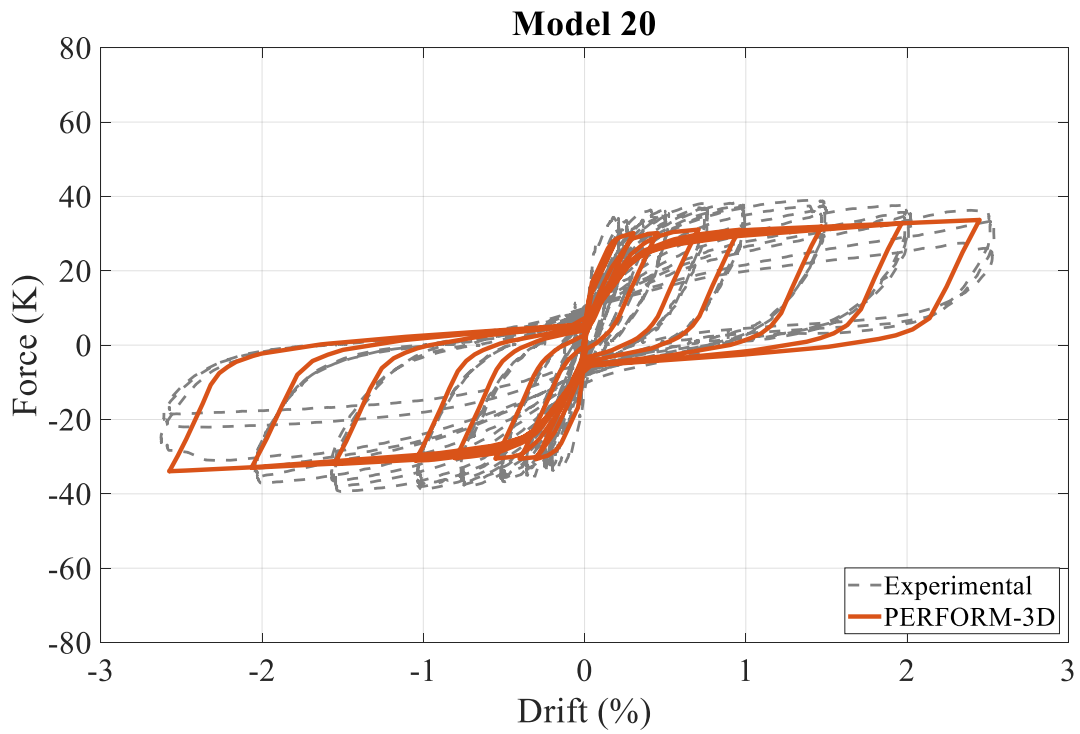
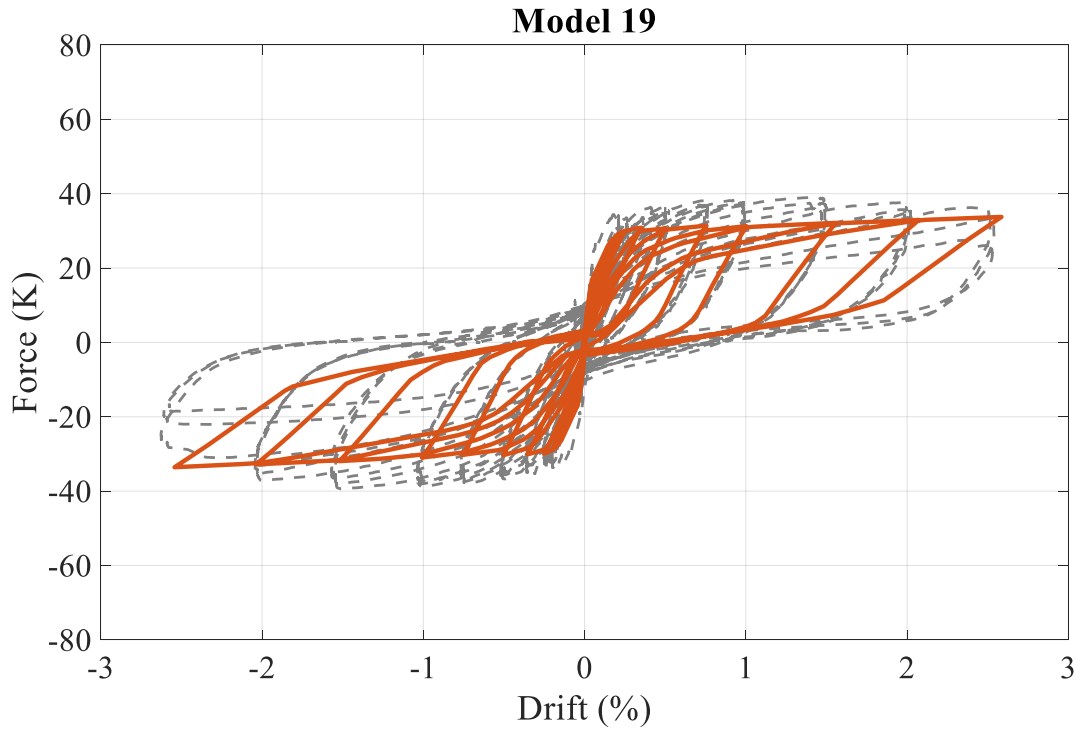


Figure A.2.2 Parametric Study Cyclic Load Analysis (cont.)

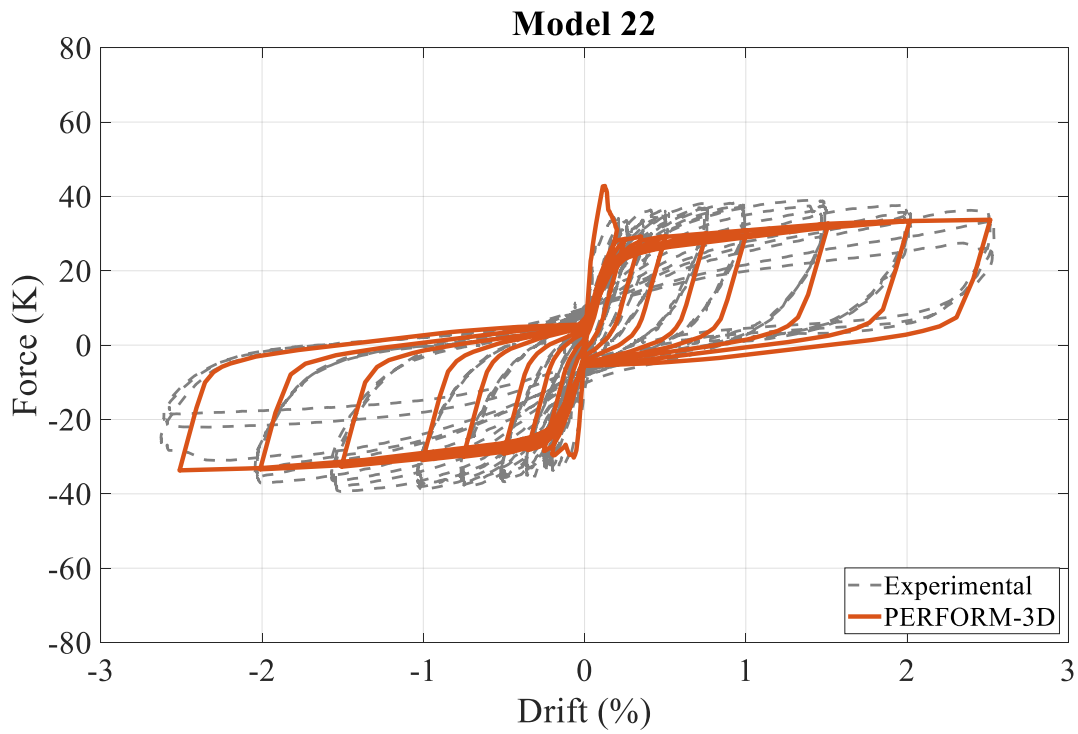
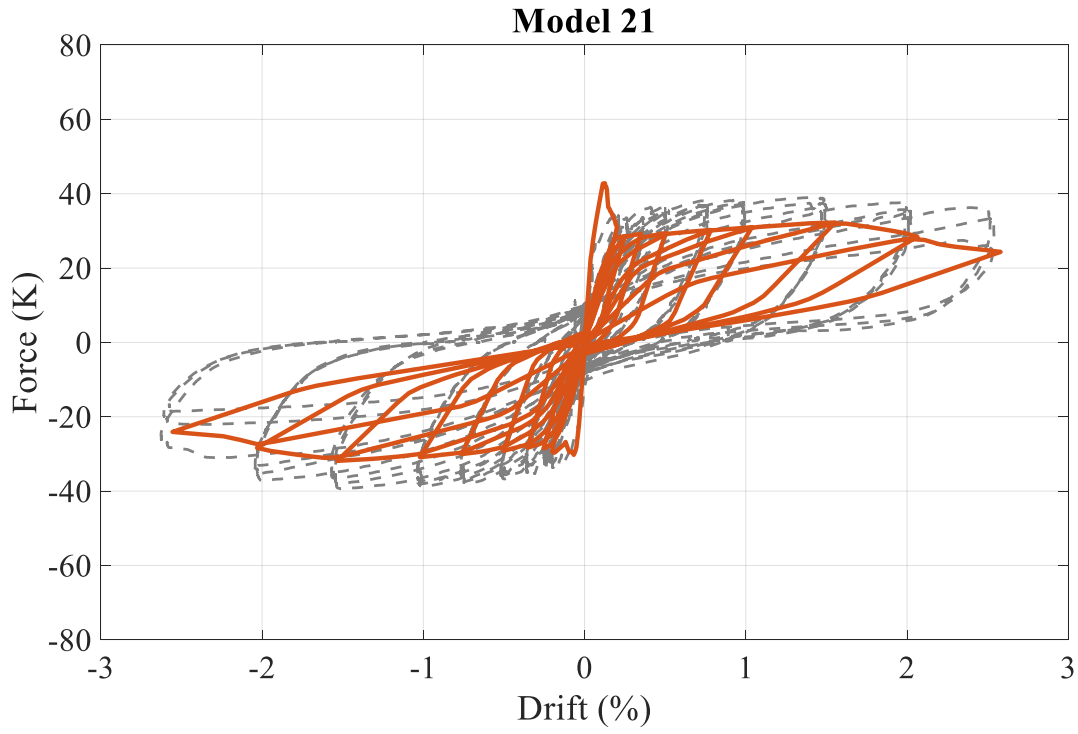


Figure A.2.2 Parametric Study Cyclic Load Analysis (cont.)

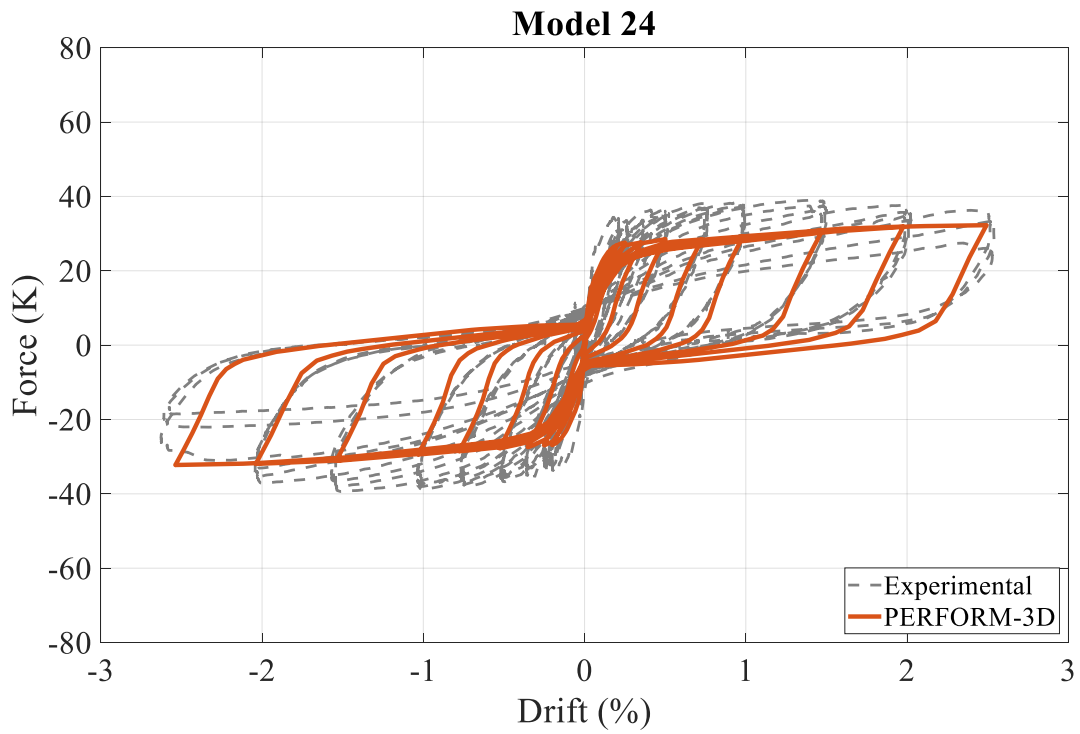
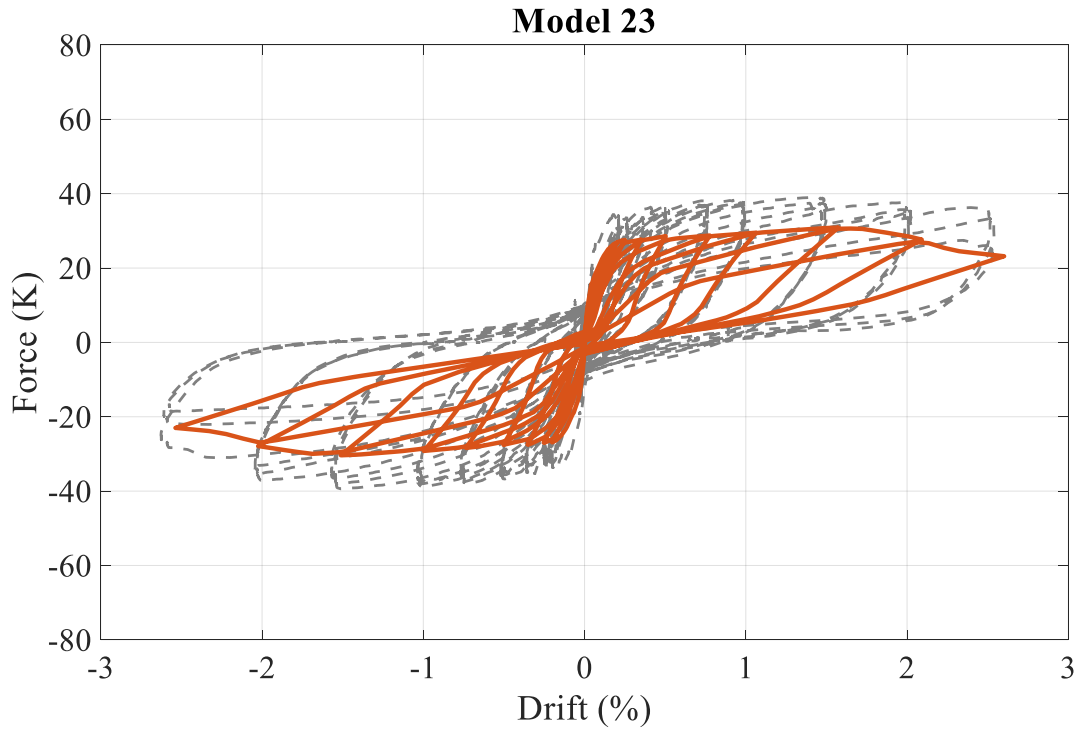


Figure A.2.2 Parametric Study Cyclic Load Analysis (cont.)

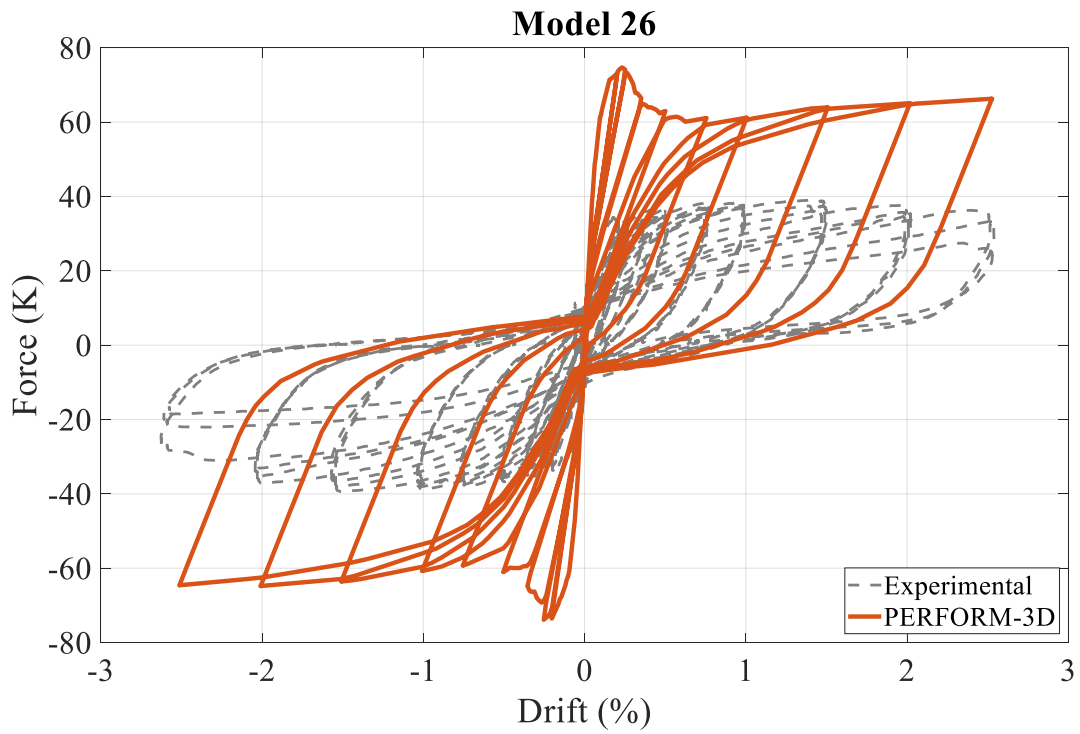
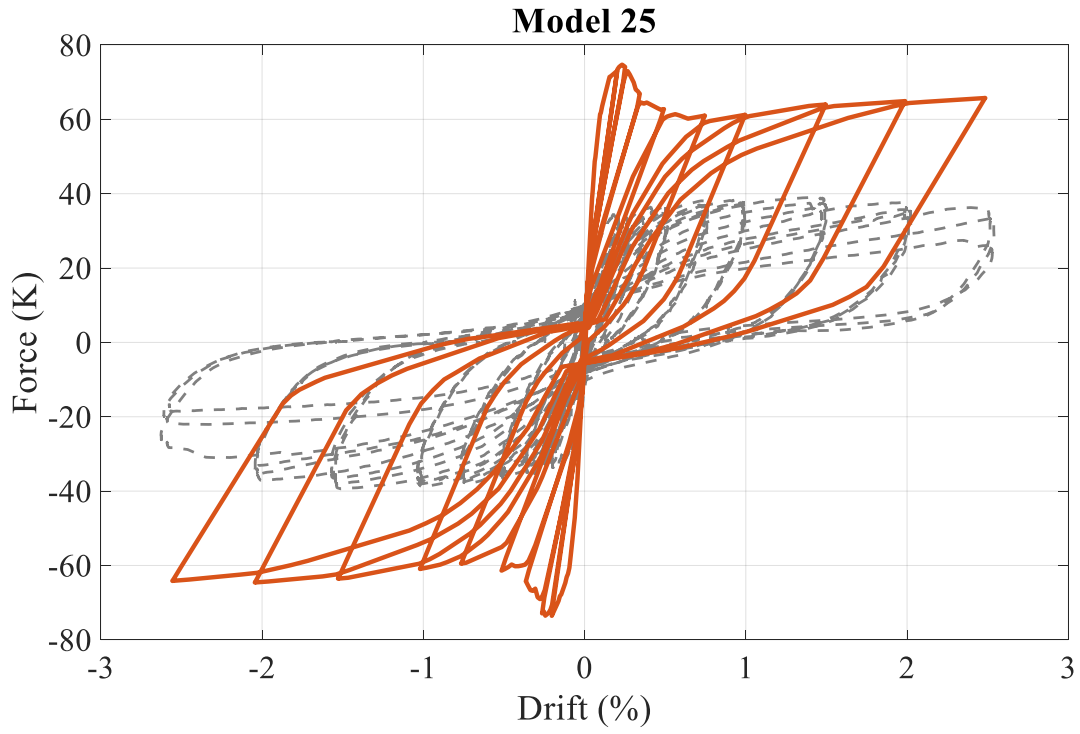


Figure A.2.2 Parametric Study Cyclic Load Analysis (cont.)

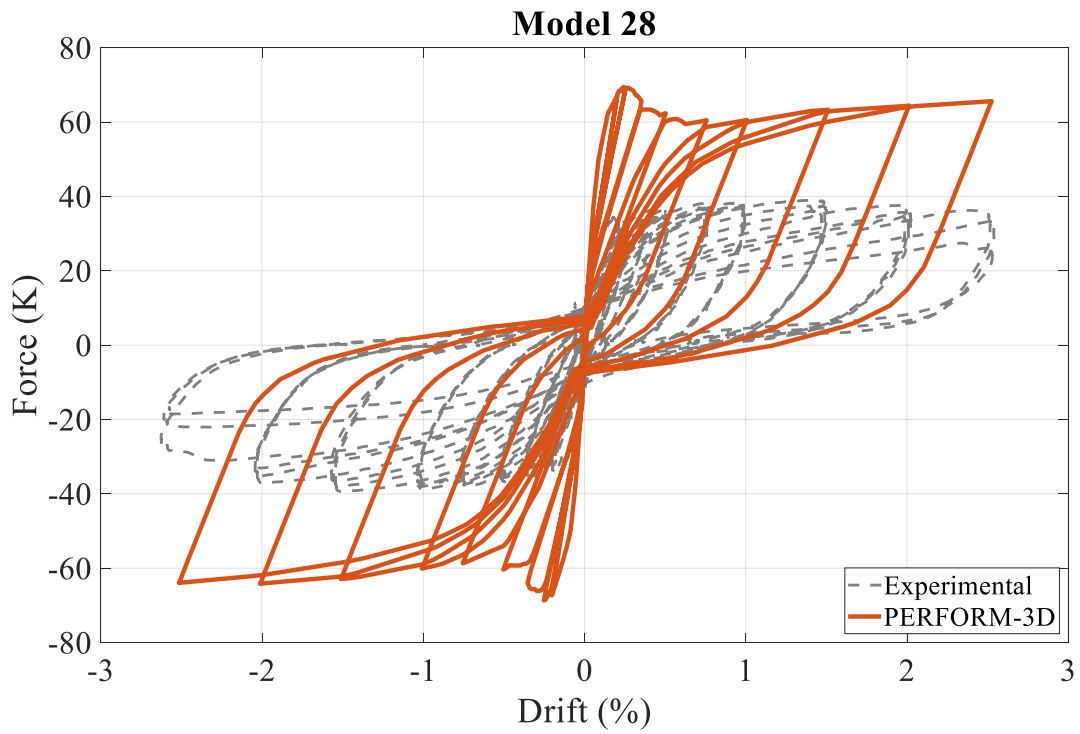
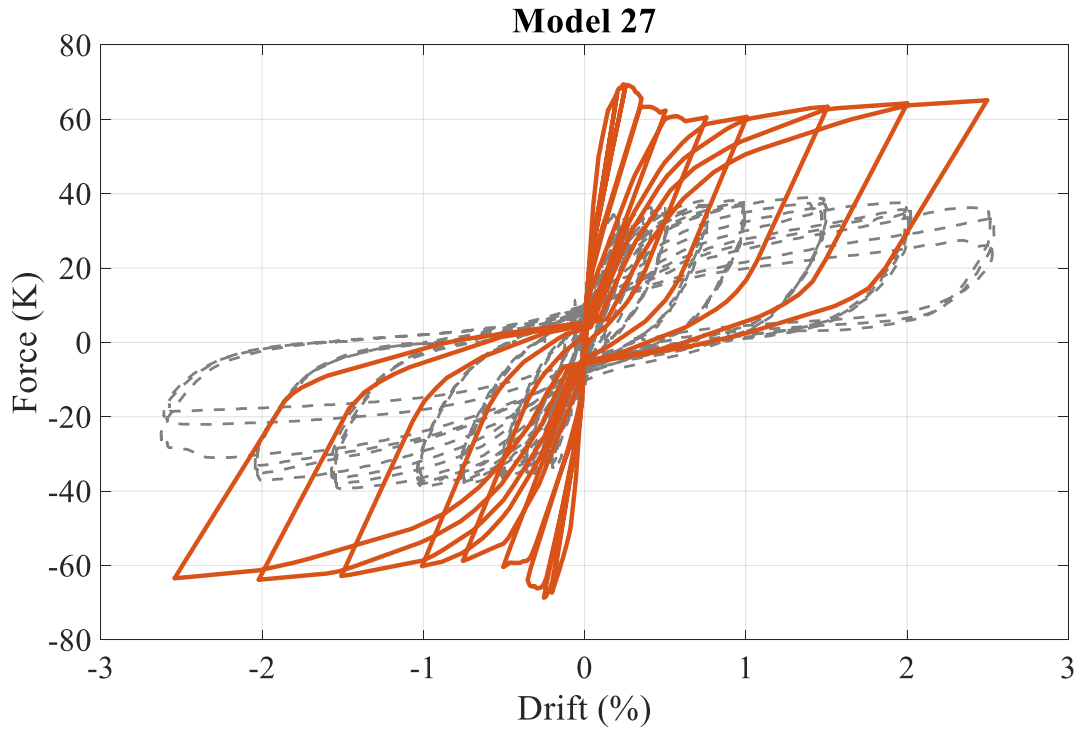


Figure A.2.2 Parametric Study Cyclic Load Analysis (cont.)

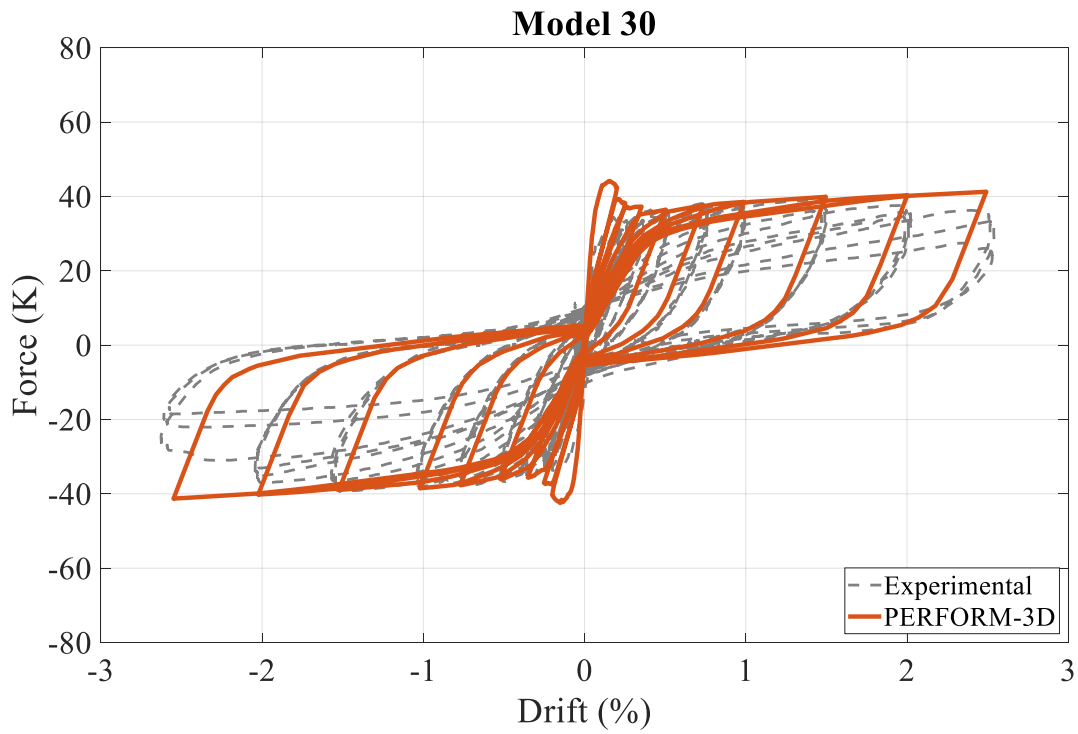
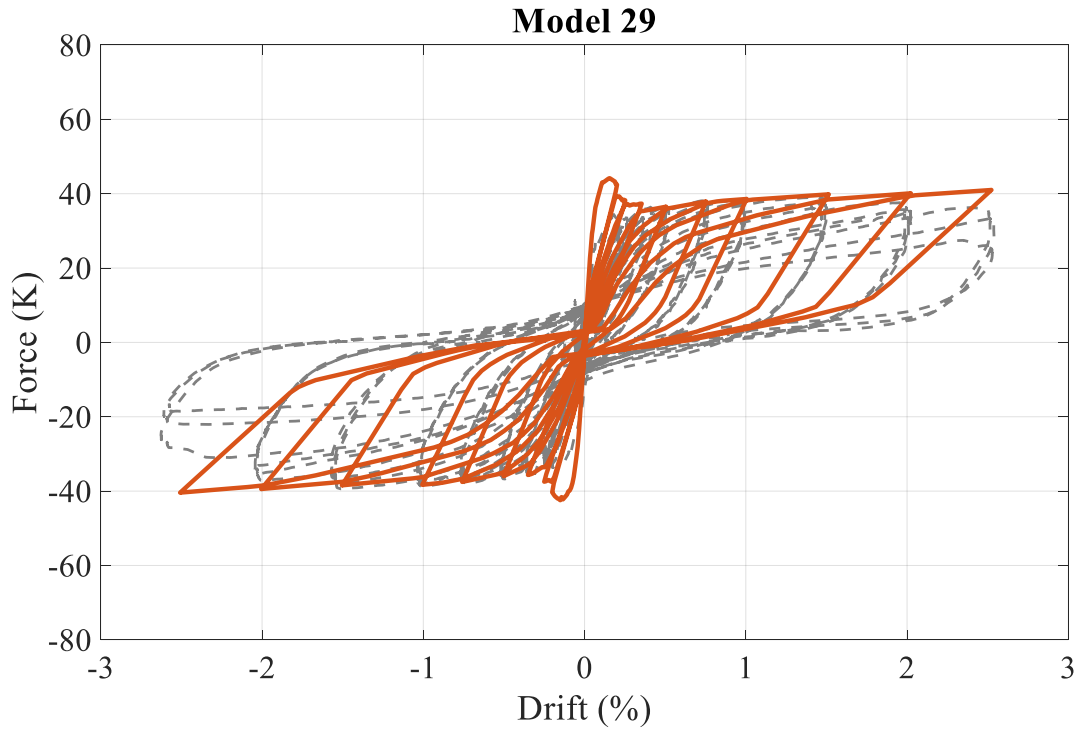


Figure A.2.2 Parametric Study Cyclic Load Analysis (cont.)

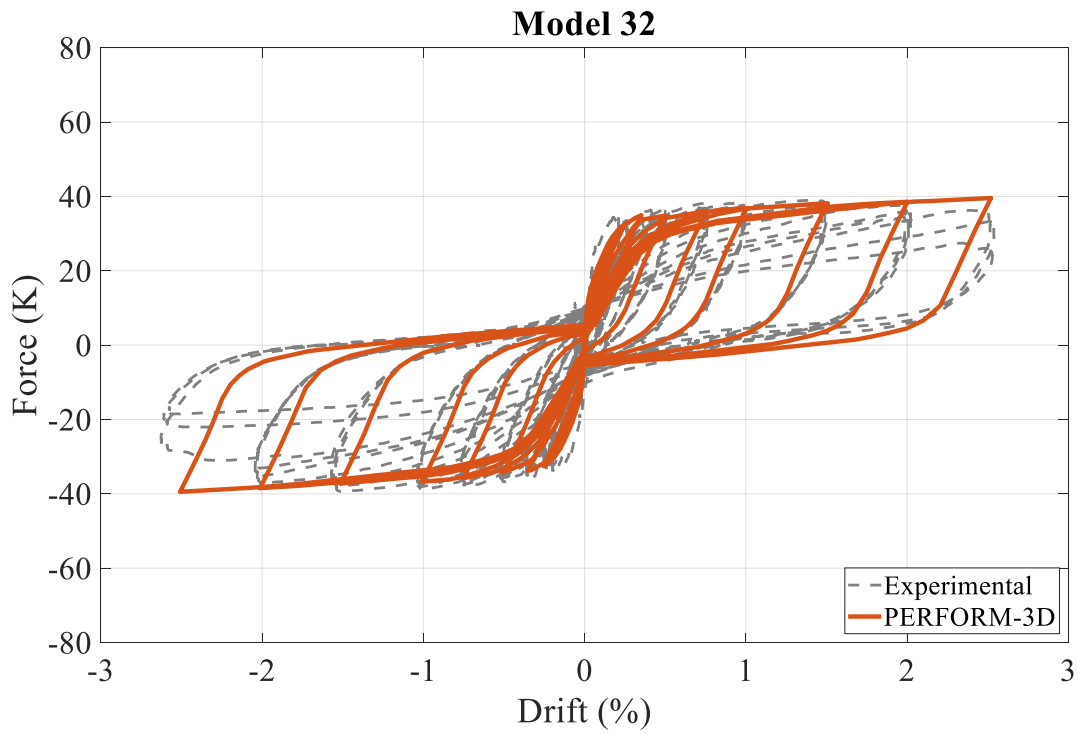
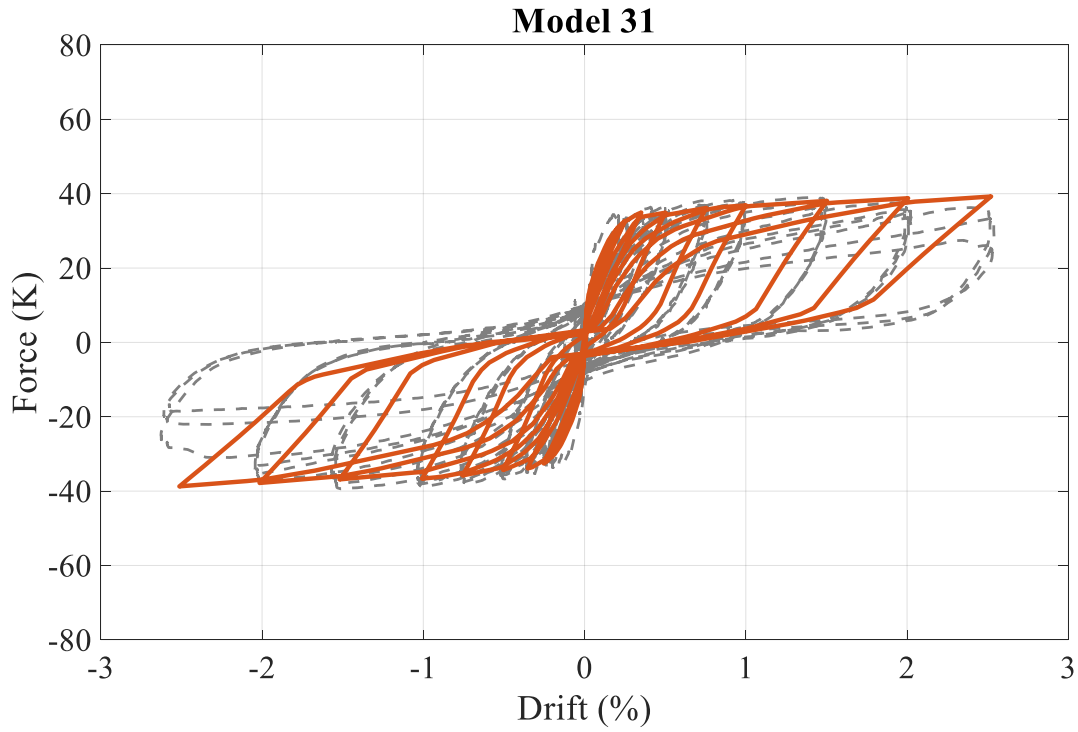


Figure A.2.2 Parametric Study Cyclic Load Analysis (cont.)

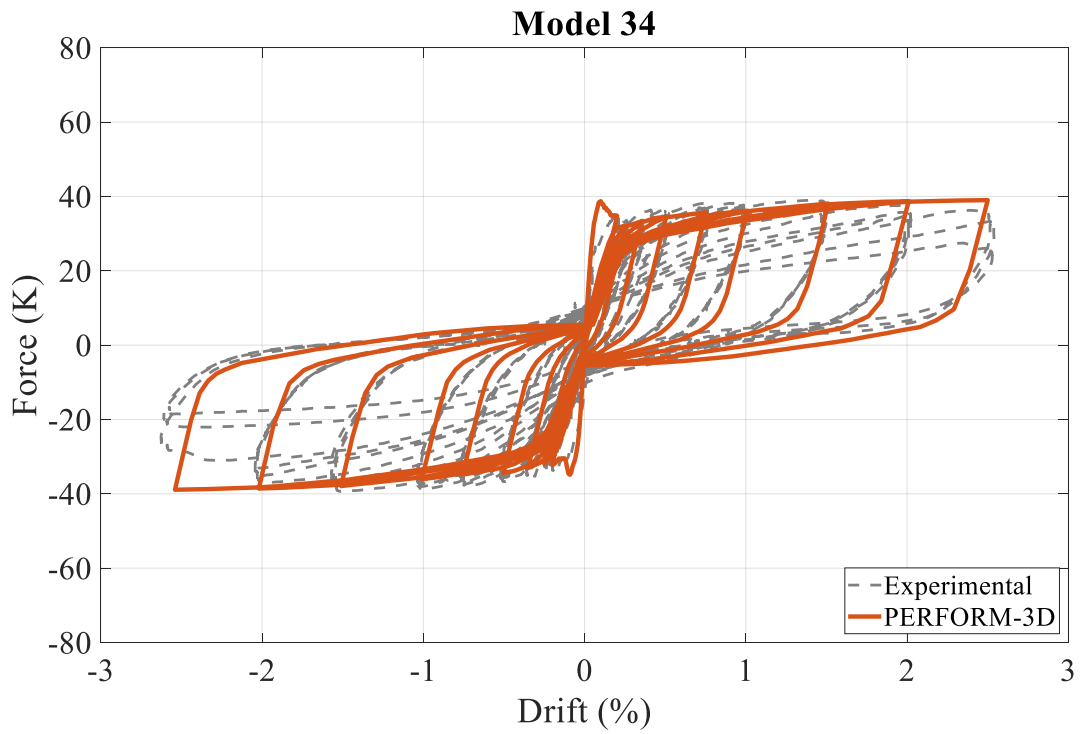
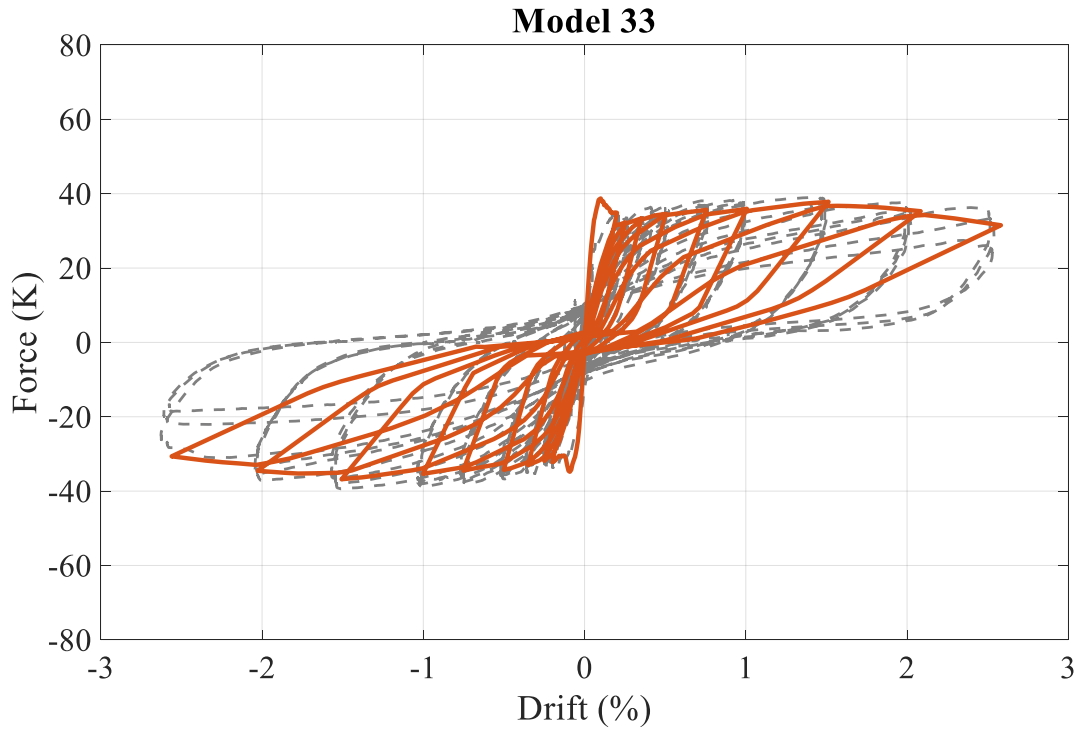


Figure A.2.2 Parametric Study Cyclic Load Analysis (cont.)

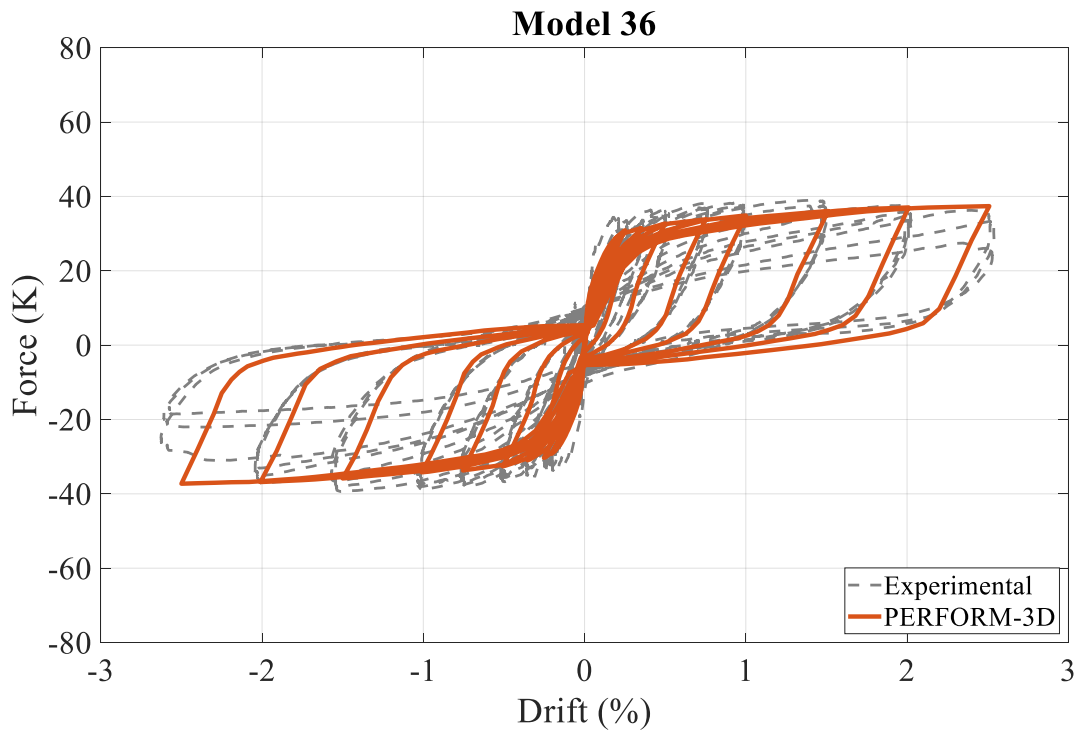
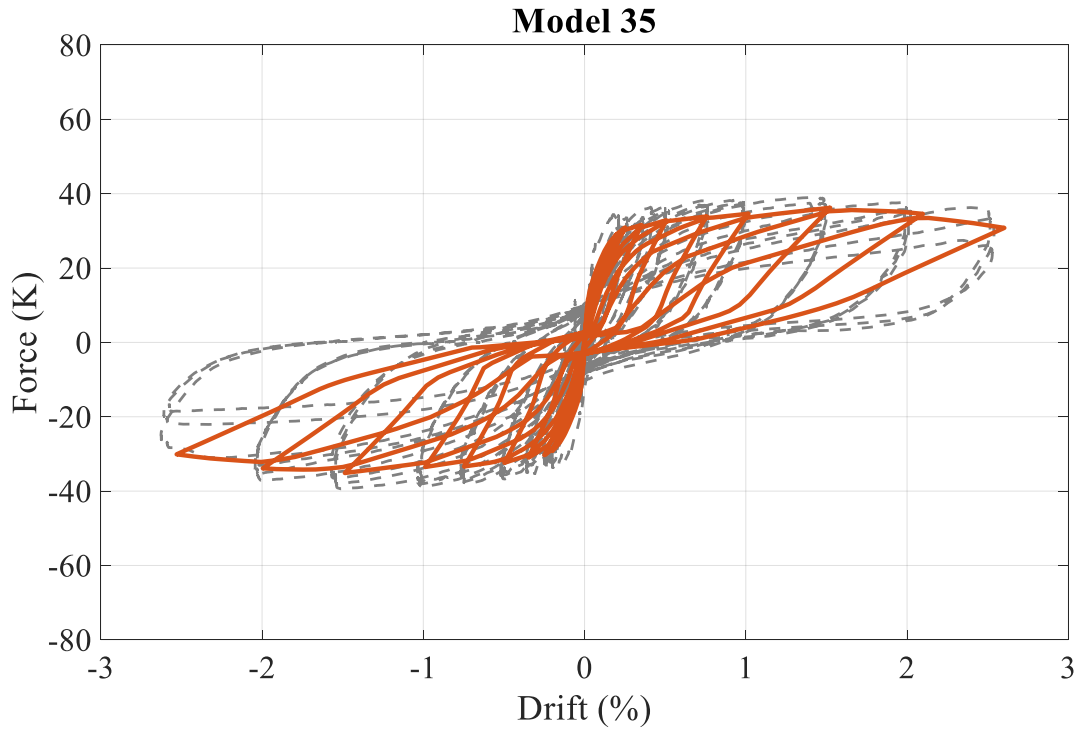


Figure A.2.2 Parametric Study Cyclic Load Analysis (cont.)

APPENDIX B

REINFORCED CONCRETE SHEAR WALL BEHAVIOR STUDIES

This appendix includes the details regarding independent studies described in Chapter 8. Appendix B.1 includes test specimen data and MATLAB data utilized in the flexural capacity of walls study. Appendix B.2 provides the fault tree analysis data set and data results for the wall failure mechanisms study.

B.1 Flexural Capacity of Walls

Table B.1.1 – Dimension and Material Properties of Test Specimens [X]

Mark	Height hw (ft)	Concrete		Reinforcement				Axial Stress Nu/lwh (psi)
		Comp Strength f _c (psi)	Tensile Splitting Strength f _{sp} (psi)	Vertical		Horizontal		
				Amount p _v	Yield Stress f _y (psi)	Amount p _h	Yield Stress f _y (psi)	
SW-1	21	7420	660	0.0027	60200	0.0027	61300	415
SW-2	21	6880	650	0.01	65400	0.0027	61000	430
SW-3	21	6780	615	0.03	66000	0.0027	60000	420
SW-4	12	6740	585	0.03	60000	0.0027	60000	430
SW-5	12	5900	565	0.023	60000	0.0027	60000	425
SW-6	21	5950	590	0.023	63000	0.0027	70000	430

Table B.1.2 – Summarized Dimension and Material of Specimen SW-1

Lw (in)	h (in)	fc' (psi)	fy (psi)	Nu (lb)	As (in ²)
75	3	7420	60750	93375	0.675
w	alpha	Beta	C (in)	Mu (lb-in)	
0.0221	0.0559	0.679	9.419	4406420	

B.1.1 Matlab Input

```
%FOSM
```

```
% Mean: M_Mu = 0.5*As*Fy*Lw*(1+(Nu/AsFy))*(1-(c/Lw))
```

```
% SD: S_Mu = S_As^2(dM_Mu/dM_As)^2 + S_fy^2(dM_Mu/dM_fy)^2 +
```

```
% S_Lw^2(dM_Mu/dM_Lw)^2 + S_Nu^2(dM_Mu/dM_Nu)^2 + S_C^2(dM_Mu/dM_C)^2
```

```

syms M_fc M_Pv M_fy M_Nu M_As M_Lw M_w M_c S_fc S_Pv S_fy S_Nu S_As S_Lw S_w
S_c

% Total Mean
M_Mu = 0.5*M_As*M_fy*M_Lw*(1+(M_Nu/(M_As*M_fy)))*(1-(M_c/M_Lw))

% Symbolically differentiate each term as Random Variable in terms of Mean
diff_As = (diff(M_Mu,M_As,1))
diff_fy = (diff(M_Mu,M_fy,1))
diff_Lw = (diff(M_Mu,M_Lw,1))
diff_Nu = (diff(M_Mu,M_Nu,1))
diff_c = (diff(M_Mu,M_c,1))

%% Assigning Variables
% Mean Values From Data
M_fy = 60750; % [psi]
M_Nu = 93375; % [lb]
M_As = 0.675; % [in2]
M_Lw = 75; % [in]
M_c = 9.419; % [in]
M_Mu = 0.5*M_As*M_fy*M_Lw*(1+(M_Nu/(M_As*M_fy)))*(1-(M_c/M_Lw)) % [lb-in]

% Standard Deviation Values
Cov = 0.05; % Assigning 5% coefficient of variation to each variable
S_fy = M_fy*Cov; % Sigma = Mean x CoV
S_Nu = M_Nu*Cov;
S_As = M_As*Cov;
S_Lw = M_Lw*Cov;
S_c = M_c*Cov;

% Numerically Differentiate each term as Random Variable in terms of Mean
diff_As = (M_Lw*M_Nu*(M_c/M_Lw - 1))/(2*M_As) - (M_Lw*M_fy*(M_Nu/(M_As*M_fy)
+ 1)*(M_c/M_Lw - 1))/2
diff_fy = (M_Lw*M_Nu*(M_c/M_Lw - 1))/(2*M_fy) - (M_As*M_Lw*(M_Nu/(M_As*M_fy)
+ 1)*(M_c/M_Lw - 1))/2

```

```

diff_Lw = (M_As*M_c*M_fy*(M_Nu/(M_As*M_fy) + 1))/(2*M_Lw) -
(M_As*M_fy*(M_Nu/(M_As*M_fy) + 1)*(M_c/M_Lw - 1))/2

diff_Nu = -(M_Lw*(M_c/M_Lw - 1))/2

diff_c = -(M_As*M_fy*(M_Nu/(M_As*M_fy) + 1))/2

T = table(diff_As,diff_fy, diff_Lw, diff_Nu, diff_c);
T.Properties.VariableNames = {'As', 'Fy', 'Lw', 'Nu', 'c'};
T.Properties.RowNames = {'Differentials'}

% Standard Deviation Calculation
% SD_Mu = S_As^2(dM_Mu/dM_As)^2 + S_fy^2(dM_Mu/dM_fy)^2 +
% S_Lw^2(dM_Mu/dM_Lw)^2 + S_Nu^2(dM_Mu/dM_Nu)^2 + S_C^2(dM_Mu/dM_C)^2
Var_mu_As = ((S_As^2)*(diff_As^2));
Var_mu_Fy = ((S_fy^2)*(diff_fy^2));
Var_mu_Lw = ((S_Lw^2)*(diff_Lw^2));
Var_mu_Nu = ((S_Nu^2)*(diff_Nu^2));
Var_mu_C = ((S_c^2)*(diff_c^2));
SD_mu = sqrt(Var_mu_As + Var_mu_Fy + Var_mu_Lw + Var_mu_Nu + Var_mu_C);
T = table([(Var_mu_As);sqrt(Var_mu_As)],[(
Var_mu_Fy);sqrt(Var_mu_Fy)],[(Var_mu_Lw);sqrt(Var_mu_Lw)],[(Var_mu_Nu);sqrt(
ar_mu_Nu)],[(Var_mu_C);sqrt(Var_mu_C)],[SD_mu^2;SD_mu]);
T.Properties.VariableNames = {'As', 'Fy', 'Lw', 'Nu', 'c', 'Total'};
T.Properties.RowNames = {'Variance'; 'Std Dev'}

% Percent Relative Contribution to Variance (RCV%)
% RCV% = [(S_x^2)*(dM_Mu/dM_x)^2]/SD_mu^2
RCV_As = (Var_mu_As/SD_mu^2);
RCV_Fy = (Var_mu_Fy/SD_mu^2);
RCV_Lw = (Var_mu_Lw/SD_mu^2);
RCV_Nu = (Var_mu_Nu/SD_mu^2);
RCV_C = (Var_mu_C/SD_mu^2);
tot = RCV_As + RCV_Fy + RCV_Lw + RCV_Nu + RCV_C;
T = table(RCV_As*100,RCV_Fy*100, RCV_Lw*100, RCV_Nu*100, RCV_C*100);
T.Properties.VariableNames = {'As', 'Fy', 'Lw', 'Nu', 'c'};

```

```
T.Properties.RowNames = {'RCV%'}
```

B.1.2 Matlab Output

```
M_Mu = -(M_As*M_Lw*M_fy*(M_Nu/(M_As*M_fy) + 1)*(M_c/M_Lw - 1))/2
diff_As = (M_Lw*M_Nu*(M_c/M_Lw - 1))/(2*M_As) - (M_Lw*M_fy*(M_Nu/(M_As*M_fy) +
1)*(M_c/M_Lw - 1))/2
diff_fy = (M_Lw*M_Nu*(M_c/M_Lw - 1))/(2*M_fy) - (M_As*M_Lw*(M_Nu/(M_As*M_fy) +
1)*(M_c/M_Lw - 1))/2
diff_Lw = (M_As*M_c*M_fy*(M_Nu/(M_As*M_fy) + 1))/(2*M_Lw) -
(M_As*M_fy*(M_Nu/(M_As*M_fy) + 1)*(M_c/M_Lw - 1))/2
diff_Nu = -(M_Lw*(M_c/M_Lw - 1))/2
diff_c = -(M_As*M_fy*(M_Nu/(M_As*M_fy) + 1))/2
M_Mu = 4.4064e+006
diff_As = 1.9920e+006
diff_fy = 22.1336e+000
diff_Lw = 67.1906e+003
diff_Nu = 32.7905e+000
diff_c = -67.1906e+003
```


B.2 Fault Tree Analysis of Wall Failure Mechanisms

Table B.2.1 – Fault Tree Analysis Data Set

Author	Specimen Name	BE?	V Reinf. Ratio	Axial Load Ratio	Failure
Deng et al. [12]	1	N	0.14	0.550	FC
	2	N	0.14	0.350	FC
	3	N	0.07	0.550	FC
	4	N	0.07	0.350	FC
Greifenhagen and Lestuzzi [13]	M1	N	0.30	0.027	FT
	M2	N	0.30	0.027	FC
	M3	N	0.30	0.094	FC
	M4	N	0.30	0.043	FT
Oh et al. [28]	WR-20	Y	0.51	0.100	FC
	WR-10	Y	0.51	0.100	FC
	WR-0	Y	0.51	0.100	FC
Dazio et al. [10]	SWH1	Y	0.54	0.051	FT
	SWH2	Y	0.54	0.057	FT
	SWH3	Y	0.82	0.058	FT
	SWH4	Y	0.82	0.057	FC
	SWH5	Y	0.39	0.128	FT
	SWH6	Y	0.82	0.108	FC
Thomsen and Wallace [34]	RW1	Y	1.10	0.100	FC
	RW2	Y	1.10	0.070	FC
Kuang and Ho [19,20]	U1.0	N	0.92	0.100	FC
	U1.5	N	0.92	0.100	FC
	C1.0	Y	1.05	0.100	FC
	C1.5	Y	1.05	0.100	FC
	U1.0-BC	N	0.92	0.100	FC
	U1.5-BC	N	0.92	0.100	FC
	U1.0-BC2	N	0.92	0.100	FC
	U1.0-CT	N	0.92	0.100	FC
Tran and Wallace [35]	RW-A20-P10-S38	Y	1.15	0.073	DT
	RW-A20-P10-S63	Y	2.54	0.073	FC
	RW-A15-P10-S51	Y	1.18	0.048	DT
	RW-A15-P10-S78	Y	2.31	0.064	DC
	RW-A15-P2.5-S64	Y	2.23	0.016	DC
Lowe et al. [22]	PW1	Y	1.32	0.096	FT
	PW2	Y	1.32	0.013	FC
	PW3	Y	1.81	0.101	FC
	PW4	Y	1.32	0.118	FC
Alarcon et al. [22]	W1	Y	1.30	0.150	FC
	W2	Y	1.30	0.250	FC
	W3	Y	1.30	0.350	FC
Hube et al. [16]	W4	Y	1.30	0.150	FC
	W5	Y	1.30	0.150	FC
	W6	Y	1.34	0.150	FC
	W7	Y	1.30	0.150	FC
	W8	Y	1.30	0.150	FC
	W9	Y	1.30	0.150	FC
Lu et al. [23]	C1	N	0.53	0.035	FT
	C2	N	0.53	0.035	FT
	C3	N	0.53	0.035	FT
	C4	N	0.53	0.000	FT
	C5	N	0.53	0.070	FT
	C6	N	0.53	0.035	FT
Lu et al. [24]	M1	Y	0.63	0.035	FT
	M2	Y	0.76	0.035	FT
	M3	Y	0.55	0.035	FT
	M4	Y	0.71	0.035	FT
	M5	Y	0.63	0.035	FT

Table B.2.2 – Fault Tree Analysis

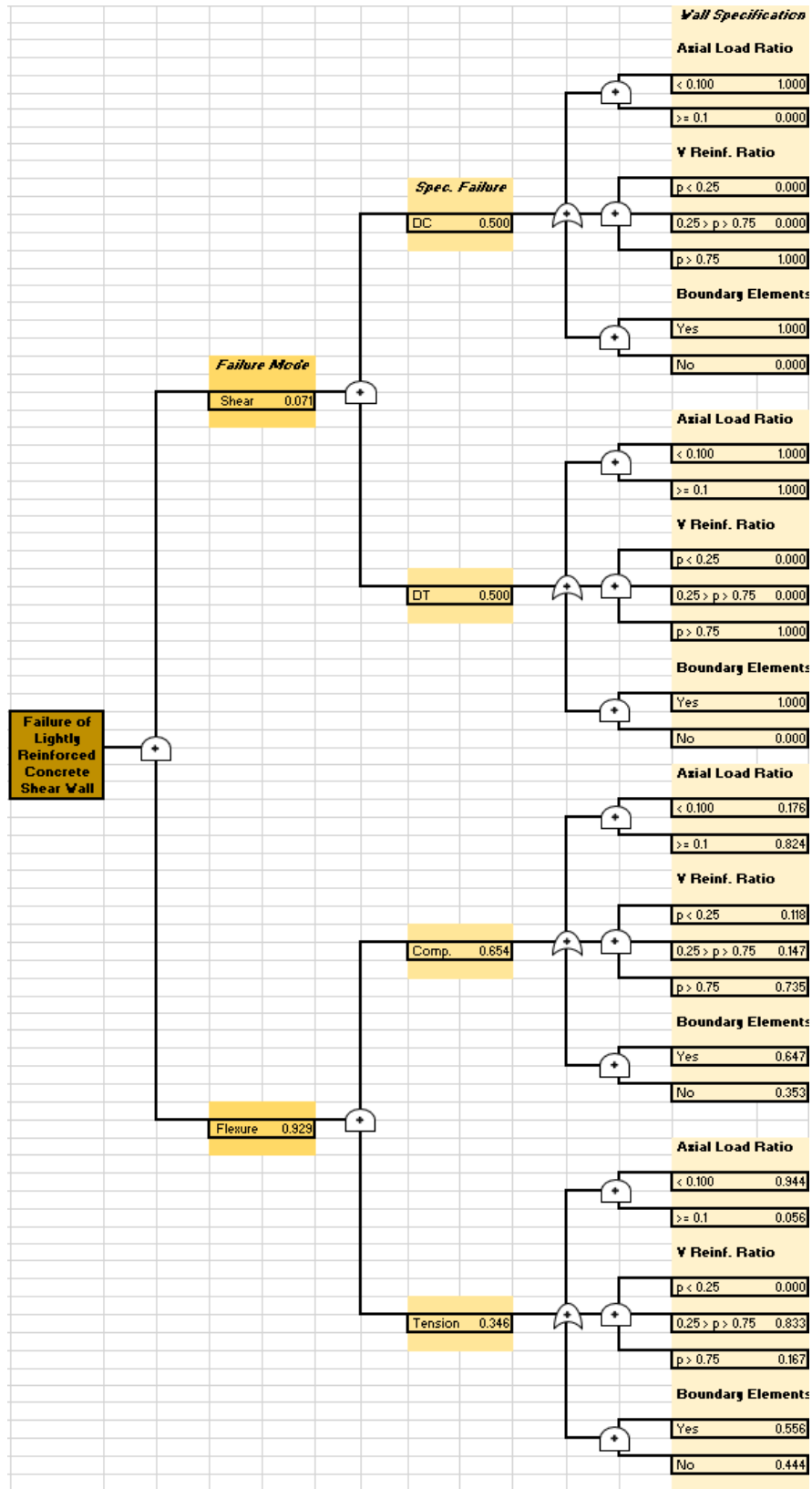


Table B.2.3 – Flexural Tension Failure Probabilities

0.008	Flexural Compression			0.038	Flexural Compression
	Axial Load Ratio < 0.100				Axial Load Ratio > 0.100
	V. Reinf Ratio < 0.25				V. Reinf Ratio < 0.25
	Boundary Elements				Boundary Elements
0.004	Flexural Compression			0.021	Flexural Compression
	Axial Load Ratio < 0.100				Axial Load Ratio > 0.100
	V Reinf. Ratio < 0.25				V Reinf. Ratio < 0.25
	No Boundary Elements				No Boundary Elements
0.010	Flexural Compression			0.048	Flexural Compression
	Axial Load Ratio < 0.100				Axial Load Ratio > 0.100
	V. Reinf Ratio 0.25 < p < 0.75				V. Reinf Ratio 0.25 < p < 0.75
	Boundary Elements				Boundary Elements
0.006	Flexural Compression			0.026	Flexural Compression
	Axial Load Ratio < 0.100				Axial Load Ratio > 0.100
	V. Reinf Ratio 0.25 < p < 0.75				V. Reinf Ratio 0.25 < p < 0.75
	No Boundary Elements				No Boundary Elements
0.051	Flexural Compression			0.238	Flexural Compression
	Axial Load Ratio < 0.100				Axial Load Ratio > 0.100
	V. Reinf Ratio > 0.75				V. Reinf Ratio > 0.75
	Boundary Elements				Boundary Elements
0.028	Flexural Compression			0.130	Flexural Compression
	Axial Load Ratio < 0.100				Axial Load Ratio > 0.100
	V. Reinf Ratio > 0.75				V. Reinf Ratio > 0.75
	No Boundary Elements				No Boundary Elements

Table B.2.4 – Flexural Compression Failure Probabilities

0.000	Flexural Tension			0.000	Flexural Tension
	Axial Load Ratio < 0.100				Axial Load Ratio > 0.100
	V. Reinf Ratio < 0.25				V. Reinf Ratio < 0.25
	Boundary Elements				Boundary Elements
0.000	Flexural Tension			0.000	Flexural Tension
	Axial Load Ratio < 0.100				Axial Load Ratio > 0.100
	V Reinf. Ratio < 0.25				V Reinf. Ratio < 0.25
	No Boundary Elements				No Boundary Elements
0.141	Flexural Tension			0.008	Flexural Tension
	Axial Load Ratio < 0.100				Axial Load Ratio > 0.100
	V. Reinf Ratio 0.25 < p < 0.75				V. Reinf Ratio 0.25 < p < 0.75
	Boundary Elements				Boundary Elements
0.112	Flexural Tension			0.007	Flexural Tension
	Axial Load Ratio < 0.100				Axial Load Ratio > 0.100
	V. Reinf Ratio 0.25 < p < 0.75				V. Reinf Ratio 0.25 < p < 0.75
	No Boundary Elements				No Boundary Elements
0.028	Flexural Tension			0.002	Flexural Tension
	Axial Load Ratio < 0.100				Axial Load Ratio > 0.100
	V. Reinf Ratio > 0.75				V. Reinf Ratio > 0.75
	Boundary Elements				Boundary Elements
0.022	Flexural Tension			0.001	Flexural Tension
	Axial Load Ratio < 0.100				Axial Load Ratio > 0.100
	V. Reinf Ratio > 0.75				V. Reinf Ratio > 0.75
	No Boundary Elements				No Boundary Elements

APPENDIX C

INDUSTRY SURVEY

This appendix contains the documents relevant to the industry survey performed in Fall 2019. Appendix C.1 includes the letter of investigation emailed to industry members. Appendix C.2 details the short form survey provided to industry practitioners who provided drawings via Dropbox. Appendix C.3 details the long form survey sent to engineers who did not want to disclose drawings from their sample projects.

C.1 Letter of Investigation



Good Morning,

We are reaching out to you to request assistance with a research project investigating the seismic behavior, analysis and design of flexure dominated reinforced concrete structural walls that fall under the Los Angeles Ordinance 183893, Non-Ductile Concrete Retrofit Program or a similar non-ductile concrete ordinance. The research team consists of ourselves, Architectural Engineering Graduate Students Tracy Doan and Jenna Williams, under the guidance of Assistant Professor Anahid Behrouzi, PhD and Professor Peter Laursen, PhD, PE at California Polytechnic State University of San Luis Obispo.

The primary objectives of this project are:

- To investigate existing condition seismic behavior, analysis and design of flexure dominated reinforced concrete structural walls and the effectiveness of retrofit approaches that can potentially increase wall displacement capacity without significantly increasing lateral strength.
- To experimentally determine the performance of planar walls considering wall reinforcement configuration, loading, and boundary conditions.
- To develop practical design recommendations and viable retrofit solutions for flexure dominated reinforced concrete structural walls.

To achieve these objectives, we are seeking information from consulting engineers regarding their experiences with flexure dominated reinforced concrete walls to develop experimental specimens that are representative of current practice and to create a better understanding of the issues related to design and construction of reinforced concrete wall systems. In this way, we will ensure that we are considering the behavior of typical walls and investigating issues that are of concern to practicing engineers. Specifically, we are seeking help to:

- Identify a typical flexure dominated reinforced concrete structural wall in a building that falls under a non-ductile concrete ordinance. Analysis of these prototype walls would provide a basis for defining the experiments and evaluating modeling tools.
- Identify inconsistencies and difficulties in current engineering procedures for walls, including design and analysis.
- Identify retrofit solutions implemented in practice given expected behavior found in analysis.

Given your expertise and experience working with reinforced concrete structural walls, we believe that you and your colleagues can provide valuable inputs to our project. To facilitate your efforts in providing inputs, we have developed [the survey at this link](#). We are hoping you and your colleagues can take some time (approximately 20 minutes) to fill out the questionnaire considering one of your recent projects that aligns with our objectives that we can use as one of our prototype buildings.

We thank you for your inputs and your assistance. We hope that your time will be rewarded by research results that address questions of concern to you regarding flexure dominated reinforced concrete structural walls. If you would like additional information about the project, please feel free to e-mail us.

Sincerely,

Tracy Doan and Jenna Williams
Architectural Engineering Graduate Students
California Polytechnic State University of San Luis Obispo
Email: tdoan04@calpoly.edu; jwill107@calpoly.edu

C.2 Short Form Survey

Reinforced Concrete Shear Wall Investigation (DropBox Option)

Please identify a typical flexure dominated wall that is part of a building that falls under the Los Angeles Ordinance 183893, Non-Ductile Concrete Retrofit Program or a similar non-ductile concrete ordinance to complete this survey.

Results from this survey will be anonymous; in the event of publication of this research, no personally identifying information related to the survey or focus group will be disclosed. Under no circumstances will the results be made public.

Section 1

...

Building Specifications

Please provide general information of the building that this wall is a part of.

1. Building Sector *

2. Year Built *

3. Location of Building (zip code) *

4. Number of Stories *

Wall and Reinforcement Specifications

Please input the material properties that were used for analysis.

5. Full Wall Height (ft) *

The value must be a number

6. Concrete Strength (psi) *

The value must be a number

7. Typical (Vertical and Horizontal) Reinforcement Strength (psi) *

The value must be a number

8. Boundary Element Tie Reinforcement Strength (psi) *

The value must be a number

9. Boundary Element Longitudinal Reinforcement Strength (psi) *

The value must be a number

10. Are there any abnormal reinforcement types (smooth bars, twisted bars) or configurations (inclined bars, unique detailing)? *

Enter your answer

11. Please submit a wall elevation (Exhibit A), a wall cross section (Exhibit B), and a wall schedule (Exhibit C) to the DropBox link below. The exhibits must include:

- 1) first floor wall height
- 2) wall length and thickness
- 3) boundary element length and height
- 4) vertical reinforcement sizes and spacing
- 5) horizontal reinforcement sizes and spacing
- 6) boundary element vertical reinforcement sizes and spacing
- 7) boundary element horizontal reinforcement sizes and spacing
- 8) wall to foundation reinforcement sizes, spacing, and lap splices
- 9) wall opening/perforation dimensions

Please upload files as "YourName_ExhibitA", "YourName_ExhibitB", and "YourName_ExhibitC" to:
<https://www.dropbox.com/request/LKWNpY7MBKqa6YbxjZRP>

By choosing "Yes" below, you are agreeing to sending Exhibit A, B, and C. *

Yes

Section 3

...

Wall Demands

12. What was the unfactored axial gravity load on the wall (kips)? *

Enter your answer

13. What was the unreduced lateral earthquake load on the wall (kips)? *

Enter your answer

Wall Analysis

The following questions relate to the existing condition analysis of the wall with respect to ASCE 41.

14. What performance objective (refer to ASCE 41-17 Table 2-1) was used to determine if the structure was deficient? *

Select your answer



15. Since ASCE 41 was not used, please describe the performance objective and associated standard for this building. *

Enter your answer

16. What triggered the analysis? *

- Change of tenant
- Change of building use
- Local Ordinance
-

Other

17. What was the target 1st story drift (inches) of the wall for Collapse Prevention? *

The value must be a number

18. What was the target 1st story drift (inches) of the wall for Life Safety? *

The value must be a number

19. Are the existing gravity elements in the structure modeled to account for the stiffness contribution? *

- Yes
- No

20. Were the existing drawings available to the SEOR at the start of the project? *

- Yes
- No

21. What type of analyses were performed to analyze the walls? *

- Linear Static: ELFP
- Nonlinear Static: Pushover
- Linear Dynamic: Response Spectrum
- Nonlinear Dynamic: Response History

22. What type of elements were used to model the walls? *

- solid
- shell
- beam-column
-

Other

23. What software programs were used to perform the analysis? *

SAP2000

ETABS

Perform 3D

OpenSees

Other

24. From the analysis results, what was the expected failure mechanism of the wall? *

Enter your answer

25. Was a retrofit solution considered? *

Yes

No

Retrofit Solution

If pursued, please answer the following questions related to the retrofit solution for the wall.

26. What were the proposed retrofit solutions? *

Enter your answer

27. What was the final retrofit solution? *

Enter your answer

28. Why was this solution chosen over the other proposed solutions? *

Enter your answer

29. Why was this solution chosen over the other proposed solutions? *

- Inexpensive
- Ease of Construction
- Lack of research/experimental data for other proposed solutions
-

Other

Contact Information

At a minimum, we are asking to collect your name and firm location for the research. If we have additional questions about your project, we would be interested in contacting you. Please provide your email if you consent to us reaching out to you in the future.

30. Your Name *

31. Your Firm

32. Your Firm Location *

33. Your Title *

34. Your Email

C.2 Long Form Survey

Reinforced Concrete Shear Wall Investigation



Please identify a typical flexure dominated wall that is part of a building that falls under the Los Angeles Ordinance 183893, Non-Ductile Concrete Retrofit Program, or a similar non ductile concrete ordinance to complete this survey.

Results from this survey will be anonymous; in the event of publication of this research, no personally identifying information related to the survey or focus group will be disclosed. Under no circumstances will the results be made public.

*** This survey requires inputting wall dimensions and properties. If you would prefer to upload wall sections and plans instead, please use the below link for a shorter survey that requires image uploads:

https://forms.office.com/Pages/ResponsePage.aspx?id=2wING578IUSVNx03nMoq55qbztjH_gRBks-1dYtFzAFUOUpJUjJlQzIRMTUwOEIVMVAwQzkwTUFCWS4u

Building Specifications

Please provide general information of the building that this wall is a part of.

1

Building Sector *

Select your answer



2

Year Built *

Enter your answer

3

Location of Building (zip code) *

The value must be a number

4

Number of Stories *

Select your answer



Wall Specifications

Please input the material properties that were used for analysis.

5

Concrete Strength (psi) *

The value must be a number

6

Full Wall Height (ft) *

The value must be a number

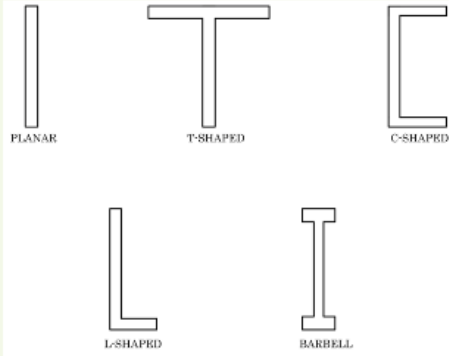
7

First Floor Wall Height (ft) *

The value must be a number

8

Wall Configuration *



Select your answer



9

Please describe the wall geometry (i.e. wall length and thickness, flange length and thickness, etc.) *

Enter your answer

Planar Wall Dimensions



10

Wall Length, L (feet) *

The value must be a number

11

Wall Thickness, t (inches) *

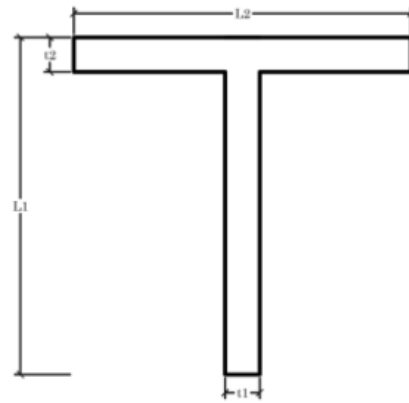
The value must be a number

12

Please describe any perforations or punched opening (dimensions and location) on the wall

Enter your answer

T-Shaped Wall Dimensions



13

Wall Length, L1 (feet) *

The value must be a number

14

Wall Thickness, t1 (inches) *

The value must be a number

15

Wall Length, L2 (feet) *

The value must be a number

16

Wall Thickness, t2 (inches) *

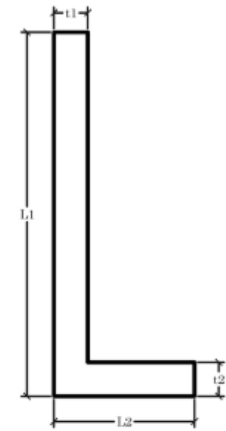
The value must be a number

17

Please describe any perforations or punched opening (dimensions and location) on the wall

Enter your answer

L-Shaped Wall Dimensions



18

Wall Length, L1 (feet) *

The value must be a number

19

Wall Thickness, t1 (inches) *

The value must be a number

20

Wall Length, L2 (feet) *

The value must be a number

21

Wall Thickness, t2 (inches) *

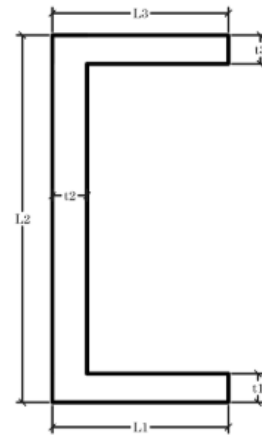
The value must be a number

22

Please describe any perforations or punched opening (dimensions and location) on the wall

Enter your answer

C-Shaped Wall Dimensions



23

Wall Length, L1 (feet) *

The value must be a number

24

Wall Thickness, t1 (inches) *

The value must be a number

25

Wall Length, L2 (feet) *

The value must be a number

26

Wall Thickness, t2 (inches) *

The value must be a number

27

Wall Length, L3 (feet) *

The value must be a number

28

Wall Thickness, t3 (inches) *

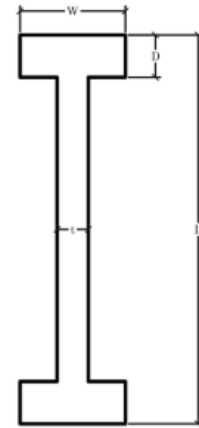
The value must be a number

29

Please describe any perforations or punched opening (dimensions and location) on the wall

Enter your answer

Barbell Wall Dimensions



30

Wall Length, L (feet) *

The value must be a number

31

Wall Thickness, t (inches) *

The value must be a number

32

Barbell depth, d (inches) *

The value must be a number

33

Barbell Width, w (inches) *

The value must be a number

34

Please describe any perforations or punched opening (dimensions and location) on the wall

Enter your answer

35

Is there any embedded structural steel within the ends of the wall?

Enter your answer

Reinforcement Specifications

Please answer the following questions with regards to the typical reinforcement and input the material properties that were used for analysis.

36

Reinforcement Strength (ksi) *

The value must be a number

37

Vertical Bar Size *

Select your answer

**38**

Vertical Bar Spacing (inches) *

The value must be a number

39

Layers of Vertical Rebar *

Select your answer



40

Are the vertical bars lap spliced at the base of the wall? *

- Yes
- No

41

Are the vertical bars hooked into the foundation? *

- Yes
- No

42

Horizontal Bar Size *

Select your answer 


43

Horizontal Bar Spacing (inches) *

The value must be a number

44

Layers of Horizontal Rebar *

Select your answer 

45

Are there any abnormal reinforcement types (smooth bars, twisted bars) or configurations (inclined bars, unique detailing)? *

Enter your answer

46

Are there boundary elements (i.e. confining reinforcement at wall end zones)? *

Select your answer



47

If there are no boundary elements, was another form of confinement used? *

U-hooks

Other

Boundary Elements

48

Length of the boundary element (inches) *

The value must be a number

49

Height of the boundary element (inches) *

The value must be a number

50

Tie reinforcement strength (ksi) *

The value must be a number

51

Tie Size *

Select your answer



52

Tie configuration *

Select your answer



53

Number of cross tie legs perpendicular to wall thickness *

The value must be a number

54

Number of cross tie legs parallel to wall thickness *

The value must be a number

55

Vertical spacing of ties (inches) *

The value must be a number

56

Longitudinal reinforcement strength (ksi) *

The value must be a number

57

Longitudinal reinforcement size *

Select your answer



Section 10



Wall Demands

58

What was the un-factored axial gravity load on the wall (kips)? *

Enter your answer

59

What was the unreduced lateral earthquake load on the wall (kips)? *

Enter your answer

Wall Analysis

The following questions relate to the existing condition analysis of the wall with respect to ASCE 41.

60

What performance objective (refer to ASCE 41-17 Table 2-1) was used to determine if the structure was deficient? *

Select your answer



61

Since ASCE 41 was not used, please describe the performance objective per associated standard. *

Enter your answer

62

What triggered the analysis? *

- Change of tenant
- Change of building use
- Local Ordinance
-

Other

63

Were the existing drawings available to the SEOR at the start of the project? *

- Yes
- No

64

Are the existing gravity elements in the structure modeled to account for the stiffness contribution? *

- Yes
- No

65

Which material properties were described in the previous sections and used for analysis? *

- Specified
- Assumed
- Measured

66

What was the target 1st story drift of the wall (inches) for Collapse Prevention? *

The value must be a number

66

What was the target 1st story drift of the wall (inches) for Collapse Prevention? *

The value must be a number

67

What was the target 1st story drift of the wall (inches) for Life Safety? *

The value must be a number

68

What type of analyses were performed to analyze the walls? *

- Linear Static: ELFP
- Nonlinear Static: Pushover
- Linear Dynamic: Response Spectrum
- Nonlinear Dynamic: Response History

69

What type of elements were used to model the walls? *

- solid
- shell
- beam-column
-

Other

70

What software programs were used to perform the analysis? *

SAP2000

ETABS

Perform 3D

OpenSees

Other

71

From the analysis results, what was the expected failure mechanism of the wall? *

Enter your answer

72

Was a retrofit solution considered? *

Yes

No

Retrofit Solution

If pursued, please answer the following questions related to the retrofit solution for the wall.

73

What were the proposed retrofit solutions? *

Enter your answer

74

What was the final retrofit solution? *

Enter your answer

75

Why was this solution chosen over the other proposed solutions? *

Enter your answer

76

Why was this solution chosen over the other proposed solutions *

- Inexpensive
- Ease of Construction
- Lack of research/experimental data for other proposed solutions
-

Other

Contact Information

At a minimum, we are asking to collect your name and firm location for the research. If we have additional questions about your project, we would be interested in contacting you. Please provide your email if you consent to us reaching out to you in the future.

77

Your Name *

78

Your Firm

79

Your Firm Location *

80

Your Title *

81

Your Email

Enter your answer